Functional Genetic Analysis of

Motor Neuron Disease

Dirk Bäumer

Oriel College

University of Oxford

Thesis submitted for the degree of Doctor of Philosophy.

Hilary Term 2010

Abstract

Functional genetic analysis of motor neuron disease

Dirk Bäumer, Oriel College, University of Oxford

Submitted for the degree of Doctor of Philosophy, Hilary Term, 2010

Amyotrophic lateral sclerosis (ALS) and spinal muscular atrophy (SMA) are the commonest motor neuron diseases of adult- and childhood onset. Alterations of the RNA binding protein TDP-43 are associated with most cases of ALS, while SMA is caused by deletion of the Survival Motor Neuron (*SMN1*) gene. SMN has been well characterised in its role in the assembly of the cellular machinery that carries out splicing of pre-mRNA, but is thought to have other functions in RNA metabolism unrelated to pre-mRNA splicing. It is conceivable that specific aspects of RNA handling are disrupted in both SMA and ALS.

A variety of genetic, molecular and neuropathological approaches were applied to investigate a potential common pathway in these diseases. The spectrum of genetic mutations underlying motor neuron disorders were explored by screening patient DNA. Cell culture and mouse models were used to test the hypothesis that altered pre-mRNA splicing causes motor neuron death. Human neuropathological specimens were examined for changes in proteins involved in RNA metabolism.

The results indicate that altered pre-mRNA splicing is a late occurrence in disease and more likely to be a consequence rather than the cause of motor neuron degeneration. However, the notion that RNA metabolism is highly relevant to motor neuron diseases was strengthened by the discovery of mutations in another RNA binding protein, FUS, in cases of ALS without TDP-43 pathology. Overall the findings highlight the need to consider disruption of mRNA transport and regulation of mRNA translation in future motor neuron disease research.

Declaration

The work presented in this thesis was carried out by the author in the Department of Physiology, Anatomy and Genetics, University of Oxford, during 2007-2010. Except where acknowledgement is made, all of the work reported in this thesis is my own. No part of this thesis has been submitted for any other degree or any other university or institute of learning.

Acknowledgements

Most of the work presented in this thesis was carried out in the MRC Functional Genomics Unit in the Department of Physiology, Anatomy and Genetics. I am grateful to Professor Dame Kay Davies for giving me this opportunity and for providing a well equipped and stimulating work environment. Dr. Kevin Talbot not only supervised this work, but sparked my interest in motor neuron disorders and in taking a basic science approach to investigating them at a time when I had already decided never to work in a lab. Combining the lab work with regular participation in the Oxford motor neuron disease clinic has been an enormously rewarding experience. Throughout this time, Kevin has been extremely encouraging and supportive, and allowed me to develop my own research interests. The neuropathological part of this thesis was carried out in the Department of Neuropathology at the John Radcliffe Hospital and supervised by Dr. Olaf Ansorge. “Up the hill” I found another incredibly friendly lab and much in terms of support, inspiration and ideas from Olaf.

The work presented in the final chapter was carried out in close collaboration with Dr. Sheena Lee, who runs the OXION microarray facility and performed the exon-array and splice-index analysis, as well as with Dr. George Nicholson and Joanna Davies from the Department of Statistics. George and Jo performed the Ensembl exon expression analysis.

Dr. Carmen Coxon not only provided the best cakes in Oxford, but also took a lot of time to read and correct this thesis.

Everyone in the Davies lab and the neuropathology department has been great, but none of this work would have been possible without the knowledge, help and

friendship of Dr. Esther Becker, Dr. Nicholas Parkinson, Dr. Bradley Turner, Justin Moore and Anna Dulneva. All of them made the last three years a really fantastic experience for me and I will miss their company wherever I go.

Table of Contents

List of figures and tables

Abbreviations

ADAR	Adenosine deaminase acting on RNA
ALS	Amyotrophic lateral sclerosis
ANG	Angiogenin
BAC	Bacterial artificial chromosome
BID	Basophilic inclusion disease
BSA	Bovine serum albumin
CaMKIIα	Ca2+-calmodulin-dependent protein kinase II
CPEB	Cytoplasmic polyadenylation element binding protein
CFTR	Cystic fibrosis transmembrane conductance regulator
DNA	Deoxyribonucleic acid
DNCT1	Dynactin
DHPLC	Denaturing high performance liquid chromatography
EDTA	Ethylenediaminetetraacetic acid
eIF2α	Eukaryotic initiation factor 2 alpha
ESE	Exonic splicing enhancer
ESS	Exonic splicing silencer
EV	Empty vector
FALS	Familial ALS
FL	Full length
FMRP	Fragile-X mental retardation protein
FUS	Fused in sarcoma
FTD	Frontotemporal dementia
FTLD-U	Frontotemporal lobar degeneration with ubiquitinated inclusions
FVT1	Follicular variant translocation protein 1
GARS	Glycyl-tRNA synthetase
GRN	Progranulin
GWAS	Genome wide association study

HMN	Hereditary motor neuropathy
hnRNP	Heterogeneous nuclear ribonucleoprotein
HRP	Horseradish peroxidise
ICC	Intraclass correlation coefficient
IGHMBP2	Immunoglobulin μ-binding protein 2
IP	Immunoprecipitation
LCCS	Lethal congenital contracture syndrome
mGluR5	Metabotropic glutamate receptor 5
MRI	Magnetic resonance imaging
mRNA	Messenger RNA
NFL	Neurofilament
NMDA	N-methyl-D-aspartic acid
PABP	Poly-A binding protein
PBS	Phosphate buffered saline
PCR	Polymerase chain reaction
q(RT)-PCR	Quantitative (RT)-PCR
RFLP	Restriction fragment length polymorphism
RISC	RNA induced silencing complex
RNA	Ribonucleic acid
RPM	Revolutions per minute
RRM	RNA recognition motif
RT-PCR	Reverse transcription PCR
SALS	Sporadic ALS
SETX	Senataxin
SDS	Sodium dodecyl sulfate
Sm protein	‘Smith’ protein (relates to Stephanie Smith, a patient with systemic lupus erythematosus)
SMN	Survival Motor Neuron
smA	Smooth muscle actin
SMA	Spinal Muscular Atrophy

SNP	Single nucleotide polymorphism
snRNA	Small nuclear RNA
snRNP	Small nuclear ribonucleoprotein
SOD1	Copper-zinc superoxide dismutase
SR proteins	Serine and arginine rich proteins
TARDBP	TAR DNA binding protein
TBS	Tris-buffered saline
TDP-43	TAR (trans-activating response region)-DNA binding protein of 43 kDa
TIA-1	T-cell intracytoplasmic antigen 1
TIAR	TIA-1-related protein
tRNA	Transfer RNA
UTR	Untranslated region
VEGF	Vascular endothelial growth factor
YARS	Tyrosyl-tRNA synthetase
ZBP1	Zip-code binding protein

1 Introduction

Various neurological disorders are characterised by degeneration of a relatively selective subset of neurons despite the presence of generalised environmental stressors. Examples include the vulnerability of Purkinje cells to hyperthermia, of hippocampal neurons to hypoxia, or basal ganglia neurons to manganese poisoning (Ropper and Brown 2005). Similarly, disease-related variants in ubiquitously expressed genes can lead to highly selective neuronal loss. Reduction in the level of the ubiquitously expressed Survival Motor Neuron (SMN) protein, for example, leads to loss of lower motor neurons from the anterior horn of the spinal cord, causing autosomal recessive spinal muscular atrophy (SMA), the prototypical motor neuron disease (Lefebvre et al. 1995). The recent discovery of the TAR-DNA binding protein TDP-43, a nucleic acid binding protein that is also ubiquitously expressed, at the core of neuropathology in most cases of ALS (Neumann et al. 2006; Mackenzie et al. 2007), as well as mutations in TDP-43 and a similar RNA binding protein, FUS (fused in sarcoma) (Sreedharan et al. 2008; Vance et al. 2009), have led to a shift in our approach to understanding motor neuron disease. It seems that abnormal RNA processing provides a possible link between SMA, ALS and other motor neuron disorders. This thesis will begin with a review of the genetic basis of SMA and ALS as well as the salient features of RNA metabolism relevant to their pathophysiology. It will then take a candidate gene approach to identify novel disease-related variants (chapter 3), which are functionally characterised in cell culture (chapter 4). Neuropathological aspects of ALS and SMA with a focus on SMN, TDP-43 and FUS expression in mouse models and human samples are described in chapter 5. Chapter 6 will then

examine one aspect of RNA metabolism, alternative pre-mRNA splicing, in more detail using a mouse model of SMA.

1.1 Motor neuron disorders

Motor neuron disorders are often classified according to the relative involvement of upper or lower motor neurons. Lower motor neurons comprise those in the ventral horn of the spinal cord and motor nuclei of the brainstem that synapse at the neuromuscular junction (alpha motor neurons) and muscle spindles (gamma motor neurons) forming the final common pathway for voluntary movement. On spinal cord sections, lower motor neurons are conspicuous by their large size, with somata up to 75 μm in diameter and abundant Nissl substance, indicating the presence of ribosomal RNA associated with the rough endoplasmatic reticulum (Kandel et al. 2000) (for an example see figure 5.8 in chapter 5).

Lower motor neurons are multipolar cells that innervate between 2 and 1000 individual muscle fibres, with axons that can be up to one metre long. The neurotransmitter at the neuromuscular junction is acetylcholine. Each cell has an extensive network of branching dendrites, estimated to form 97% of the surface area of the cell excluding the axon (Ulfhake and Kellerth 1981) and harbouring up to 10,000 synaptic terminals that receive input from spinal interneurons, predominantly mediated through glycine and gamma-aminobutyric acid (GABA), as well as from descending upper motor neurons using excitatory aspartate and glutamate receptors.

Upper motor neurons in the cerebral cortex modulate lower motor neurons in the contralateral spinal cord, either synapsing directly, or more commonly via interneurons. The large pyramidal Betz cells in layer V of the motor cortex are the

archetypal upper motor neurons, but more numerous in the direct cortical control of movement are smaller cortical pyramidal cells in both the motor and pre-motor cortex (Lemon 2008). Direct corticomotorneuronal connections to anterior horn cells appear to be a recent evolutionary development, unique to higher primates (Eisen 2009). Upper and lower motor neurons share the qualities of extreme polarity, long axons and extensive dendritic networks.

1.1.1 Spinal muscular atrophy

Lower motor neurons are selectively lost in the commonest inherited motor neuron disorder of childhood, autosomal recessive spinal muscular atrophy (SMA), which affects 1 in 10,000 live births (Pearn 1978) and is caused by disruption of the Survival Motor Neuron (*SMN1*) gene by deletions, gene conversion events or point mutations (Lefebvre et al. 1995; Campbell et al. 1997) with subsequent reduction in levels of the SMN protein (Lefebvre et al. 1997). SMN is highly conserved in evolution and ubiquitously expressed. Complete loss of SMN, which is incompatible with life (Schrank et al. 1997), is prevented by production of low levels of SMN from the *SMN2* gene, a near identical paralogue of *SMN1* which has arisen from a duplication event in recent evolution (Rochette et al. 2001). The presence of a translationally silent C-T transition in *SMN2* exon 7, however, leads to disruption of an exonic splicing enhancer (ESE) element (Cartegni et al. 2002), or creation of an exonic splicing silencer (ESS) (Kashima and Manley 2003), with subsequent exon 7 skipping in the majority of *SMN2* derived transcripts and reduces the level of expression of full length SMN to about 10% of that normally derived from the *SMN1* gene (Lorson et al. 1999; Monani et al. 1999). Disease severity is broadly proportional to residual SMN levels, which is a function of *SMN2* copy number, although other modifying factors are involved in some cases

(Wirth et al. 1997; Oprea et al. 2008). The clinical spectrum of SMA ranges from a severe infantile form with onset in the first 6 months of life and death from respiratory failure within the first 2 years (mean age of death 9.6 months) (Thomas and Dubowitz 1994) to an uncommon, adult onset form with normal life expectancy (Wirth et al. 2006b) (table 1.1).

Type I SMA (Werdnig-Hoffmann disease)	Onset within 6 months, death within 2 years, generalised muscle weakness, never able to sit
Type II SMA (intermediate form)	Can sit but not walk, live beyond 2 years of age
Type III SMA (Kugelberg-Welander)	Able to sit and walk. Normal life expectancy. Onset before (type IIIa) or after (type IIIb) 3 years of age.
Type IV SMA (adult form)	Onset in adulthood with normal life expectancy

Table 1.1 Clinical classification of SMA (International SMA consortium (Munsat and Davies 1992))

1.1.2 Amyotrophic lateral sclerosis

The most common adult onset motor neuron disorder, amyotrophic lateral sclerosis (also known as Lou Gehrig's disease or simply as 'motor neuron disease'), affects both upper and lower motor neurons, although some patients display predominantly features of either upper or lower motor neuron dysfunction. Primary lateral sclerosis (PLS) and progressive muscular atrophy (PMA) are terms used to describe conditions with only upper motor neuron or lower motor neuron clinical features respectively, but which are probably part of the aetiopathological spectrum of ALS. In addition to motor dysfunction, many patients show more widespread involvement of the CNS both clinically and pathologically, commonly in the form of mild cognitive dysfunction and less frequently in the form of frank dementia (Strong 2008). The latter is usually in the form of a focal dementia with personality change and breakdown in social conduct, while memory and

visuospatial skills are spared (Neary et al. 2000). A recent prospective study based in a referral centre estimated the prevalence of cognitive impairment in patients with ALS as 50%, and with 15% fulfilling criteria for frontotemporal dementia (Ringholz et al. 2005). There is now increasing genetic and neuropathological evidence that ALS and frontotemporal lobar degeneration with ubiquitinated inclusions (FTLD-U) are part of the same spectrum of disease (Neary et al. 2000; Mackenzie and Feldman 2005). Both share characteristic features of TDP-43 positive neuropathology (Arai et al. 2006; Neumann et al. 2006) and mutations in the TDP-43 encoding gene *TARDBP* (or *TDP-43)* can cause both ALS (Gitcho et al. 2008; Sreedharan et al. 2008) and FTD (Borroni et al. 2009).

In contrast to SMA, ALS is generally a disease of aging (Beghi et al. 2006), although there are important exceptions. The incidence of ALS is similar in all examined populations, and was given as 2.6/100,000 for women, and 3.9/100,000 for men in a recent study in the United Kingdom (Alonso et al. 2009), with a lifetime risk of 2.1/1000 and 2.9/1000, respectively, and a peak onset between 75 and 79 years of age.

In addition to SMA and ALS, a heterogeneous group of individually-rare genetic disorders cause selective loss of upper or lower motor neurons, collectively called hereditary spastic paraplegias and distal spinal muscular atrophies (also known as hereditary motor neuropathies) respectively (James and Talbot 2006). Despite phenotypic differences between different motor neuron diseases, it is tempting to speculate that there are common pathways that lead to motor neuron degeneration

1.2 Genetics of SMA and ALS

1.2.1 SMA

SMA is one of the most common autosomal recessive disorders of humans with a carrier frequency of 1:35 (Cusin et al. 2003). 96% of cases are caused by deletions of *SMN1* exons 7, 8 or both, or *SMN1* conversions into *SMN2 (*which means change of the nucleotide sequence without physical deletion of the SMN1 gene on its chromosomal locus) (Campbell et al. 1997; Wirth 2000; Wirth et al. 2006a), while 4% of patients harbour various point mutations, always as compound heterozygotes with SMN deletions on the other chromosome. About 3% of childhood onset (type I) patients with a clinical phenotype that is indistinguishable from SMN-related SMA have no *SMN* mutations, and this proportion increases with age of onset, to up to 18% in type III patients and even higher in adult-onset (type IV) patients (Zerres et al. 1997). The number of patients with no genetic diagnosis despite clear Mendelian inheritance of a motor neuron disorder is even higher in the distal spinal muscular atrophies and hereditary spastic paraplegias (James and Talbot 2006).

1.2.2 ALS

1.2.2.1 Familial ALS

About 5% of ALS is familial with mostly autosomal dominant patterns of inheritance (table 1.2) (Logroscino et al. 2005; O'Toole et al. 2008). Mutations in the *SOD1* gene constitute up to 20% of familial ALS (Rosen et al. 1993), while mutations in *TARDBP* (Sreedharan et al. 2008), *FUS/TLS* (fused in sarcoma/translocated in liposarcoma) (Kwiatkowski et al. 2009; Vance et al. 2009)

and *ANG*, coding for angiogenin (Greenway et al. 2006), can also cause classical ALS. These genes are described in more detail in chapter 3. Several other genes cause familial motor neuron disorders that can be classified as ALS but have atypical clinical features with regard to age of onset and rate of progression.

Disease	Chromosome	Gene	Inheritance	Onset
ALS1	21q22.1	SOD1	AD	Adult
ALS2	2q33	ALS2	AR	Juvenile
ALS3	18q21	Unknown	AD	Adult
ALS4	9q34	Senataxin	AD	Juvenile
ALS5	15q15.1-21.1	Unknown	AR	Juvenile
ALS6	16q12	FUS	AD/AR	Adult/Juvenile
ALS7	20p13	Unknown	AD	Adult
ALS8	20q13.33	VAPB	AD	Adult
ALS9	14q11	Angiogenin (ANG)	AD	Adult
ALS10	1p36.22	TAR DNA-binding protein (TDP-43)	AD	Adult
ALS	2p13	Dynactin (DCTN1)	AD	Adult
ALS-X	Xcen	Unknown	XD	Adult
ALS-FTD1	9q21-22	Unknown	AD	Adult
ALS-FTD2	9p13.3-21.3	Unknown	AD	Adult

Table 1.2: Mendelian forms of ALS. Adapted from (Dion et al. 2009)

1.2.2.2 Sporadic ALS

The vast majority of ALS cases occur without a family history. Nonetheless, genetic factors are thought to play an important role in its aetiology (Schymick et al. 2007b). Part of the evidence for a genetic basis of sporadic ALS stems from a twin study examining twins for disease concordance while excluding families with dominant ALS (Graham et al. 1997). This study estimated the heritability of sporadic ALS to be between 38 and 85%, but was limited by the fact that the analysis hinged upon only one twin pair that might possibly have represented familial disease (Beleza-Meireles and Al-Chalabi 2009). It is currently unknown what genetic model best describes sporadic ALS. One contender is the common-disease/common-variant hypothesis, which states that the risk of a common disease is made up of a combination of common variants with individually small

odds ratios (below say 1.5), which were invisible to evolutionary selection (Bodmer and Bonilla 2008). Disease associated variants can be detected in genome wide case control association studies using chip-based genotyping of several hundred thousand single nucleotide polymorphisms (SNPs). SNPs that are significantly overrepresented in cases compared to controls, after correcting for multiple testing, might themselves be disease relevant, or might be tagging pathophysiologically relevant variants with which they are in linkage disequilibrium. Several genome wide association studies (GWAS) have now been conducted on patients with ALS (Schymick et al. 2007a; van Es et al. 2007; Blauw et al. 2008; Cronin et al. 2008; Chio et al. 2009b; Cronin et al. 2009; Sha et al. 2009; van Es et al. 2009b), but so far, no consistent results have emerged. Several reported loci, such as *DPP6* or *ITPR2*, did not reach genome wide significance when stringent correction was applied, and could not be replicated in other studies using truly independent sample sets. In fact there seems to be little overlap in signal between different studies. Genes known to cause monogenic ALS have so far not been flagged in GWAS, although a recent study identified SNPs located in 9p21.2, a locus known from linkage studies in familial ALS (see table 1.2) (van Es et al. 2009b). Taken together, the GWAS published to date make it unlikely that an association with an odds ratio over 1.2 has been missed, and although larger studies might uncover robust associations, these might well be very difficult to interpret functionally given the low odds ratio for individual SNPs that can be expected. However, the overall value in GWAS may be in defining a number of SNPs with low odds ratios which, although they do not lend themselves to be studied functionally individually, might instead define pathways of pathogenic significance. Importantly, the common-disease/common-variant hypothesis also

assumes little allelic heterogeneity within cases. The fact that several different genes can cause clinically indistinguishable disease in familial ALS, however, points towards the possibility of marked allelic heterogeneity in ALS in general, which would be in keeping with a different underlying genetic model, that of rare variants (Pritchard 2001). Rare variants stand between highly penetrant familial mutations and disease-associated common variants. They have a higher odds ratio than common variants and are directly linked to disease. They are not in linkage disequilibrium with common SNPs and are thus unlikely to be detected by GWAS using the current SNP-Chip technology, but are discovered by direct sequencing of candidate genes (Bodmer and Bonilla 2008). Depending on penetrance, family size and disease onset, rare variants in families can produce the impression of seemingly sporadic disease (Beleza-Meireles and Al-Chalabi 2009). The rare variant model is also in keeping with the observation that in every gene so far identified to cause familial ALS, mutations are also found in patients with sporadic disease. It is thus conceivable that ALS is a disease of allelic heterogeneity where the majority of genetic variability is carried by multiple (private) rare variants in multiple genes that might be functionally linked. As discussed below, a potential functional link between multiple ALS causing genes is their role in RNA metabolism. A candidate gene approach to detect rare variants in patients with ALS and non-SMN SMA is described in chapter 3.

1.3 RNA metabolism in motor neuron disorders

1.3.1 Pre-mRNA splicing

Post-transcriptional processing of mRNA by exon skipping and the use of alternative 3' or 5' splice sites, 5' and 3' terminal exons and polyadenylation sites,

can produce numerous different mRNA isoforms per gene, thus increasing the cellular protein repertoire. This process is particularly prominent in the nervous system (Lee and Irizarry 2003), and there are numerous examples of a role for alternative splicing events in the physiological regulation of neuronal development and maintenance (Li et al. 2007). A switch between alternative mRNA isoforms is essential for neurite outgrowth (Wojtowicz et al. 2004; Matthews et al. 2007), synapse formation (Boucard et al. 2005; Chih et al. 2005; Chih et al. 2006), and membrane function (Raingo et al. 2007) during neuronal development and postnatal maturation.

Splicing is a high fidelity process that relies on the interaction of specific sequences in the pre-mRNA molecule (*cis*-acting elements) with a complex array of *trans*-acting factors, including various RNA binding proteins and the spliceosome (figure 1A, page 44). *Cis*-acting elements include not only the 3' and 5' splice site consensus sequences, but also less well characterised splicing regulatory elements in both introns and exons that can enhance or inhibit exon recognition (exonic or intronic splicing enhancers and silencers). The latter sequences are binding sites for protein factors that promote (mainly SR proteins, rich in arginine-serine (RS) repeats) or inhibit (hnRNPs, heterogeneous nuclear ribonucleoproteins) exon recognition and assembly of the machinery that removes introns and joins exons, the spliceosome. The major spliceosome consists of five small nuclear ribonucleoprotein complexes (snRNPs) which in turn consist of snRNAs (U1, U2, U4/6, U5) and hundreds of proteins including a core of Sm proteins (Wahl et al. 2009). A far less abundant minor spliceosome utilises different U snRNAs (U11,U12, U4atac/U6atac, U5) and has different splice site and branch point consensus sequences (Will and Luhrmann 2005).

A critical step in the biogenesis of snRNPs, the coupling of the Sm core to the correct snRNA, is catalysed in the cytoplasm by a protein complex consisting of SMN and several other proteins, gemin 2-8 and unrip (Meister et al. 2001; Pellizzoni et al. 2002). While snRNP biogenesis is a ubiquitous process, the stoichiometry of many other splicing factors is specific for developmental stage and tissue type. Several splicing regulating factors are specifically expressed in the nervous system (Li et al. 2007). Particularly well characterised are the RNA binding proteins Nova1 and Nova2 (Yang et al. 1998b; Jensen et al. 2000). Nova binds to YCAY clusters (Y=pyrimidine base, U or C) that, depending on their position in introns or exons, lead to exon skipping or exon inclusion (Ule et al. 2006). Nova targets were identified in an exon specific microarray screen of Nova knockout mice, and shown to be enriched for genes involved in synapse biogenesis, including agrin, a factor with an alternatively spliced (Z+) isoform important for acetylcholine receptor clustering at the neuromuscular junction (Ule et al. 2005). Nova double-knockout mice are born alive but have markedly reduced levels of Z+ agrin in the spinal cord, and virtually no intact neuromuscular junctions. Functional neuromuscular junctions could be re-established by crossing the Nova knockout mice with agrin Z+ over expressing mice, but only to uncover a more proximal, as yet unidentified, defect in motor neuron physiology (Ruggiu et al. 2009) suggesting that Nova is vital for motor neuronal physiology at multiple levels. Nova is an example of a *trans*-acting RNA binding protein, deficiency of which can cause specific motor neuronal defects in mice associated with splicing alterations.

Two proteins recently implicated in the aetiopathogenesis of ALS, TDP-43 and FUS/TLS, are RNA binding proteins with a function in splicing regulation. TDP-43

has strong affinity to sequences containing (UG)n repeats (Buratti and Baralle 2001) and has been extensively characterised in its role in CFTR exon 9 skipping (Buratti et al. 2001; Buratti et al. 2004; Ayala et al. 2006) and splicing of the apoAII gene (Mercado et al. 2005), which is probably mediated via an interaction with hnRNPA2 (D'Ambrogio et al. 2009). Other RNA targets of TDP-43 are not yet known, although the top hit in a microarray analysis of TDP-43 knockdown in HeLa cells was Cdk6, which contains multiple TDP-43 target sequences in its pre-mRNA (Ayala et al. 2008a).

FUS/TLS encodes a 526 amino acid, 53-kDa nuclear protein containing a RNA recognition motif (RRM) surrounded by Arg-Gly-Gly (RGG) repeats. In addition, it contains a zinc finger domain with RNA binding properties (Iko et al. 2004). FUS interacts with and modulates the splicing function of several SR proteins (Yang et al. 1998a) and other splicing factors (Meissner et al. 2003; Sato et al. 2005), which it binds via its C-terminal domain (Yang et al. 2000). One possibility is that FUS is necessary to direct SR proteins to the correct splice sites (Meissner et al. 2003). FUS preferentially binds RNA sequences containing GGUG motifs (Lerga et al. 2001), but little is known about specific human FUS RNA targets.

In most cases of ALS and FTLD-U, TDP-43 forms ubiquitinated cytoplasmic or nuclear inclusions, while the physiological nuclear protein is translocated to the cytoplasm (Neumann et al. 2006; Cairns et al. 2007; Davidson et al. 2007; Mackenzie et al. 2007). FUS has been shown to form ubiquitinated inclusions in the few autopsy cases of ALS with FUS mutations (Kwiatkowski et al. 2009; Vance et al. 2009), as well as in the uncommon form of FTLD-U without TDP-43 pathology (Neumann et al. 2009a). FUS mutants show increased cytoplasmic and reduced nuclear distribution in cell culture (Kwiatkowski et al. 2009; Vance et al.

2009), and there appears to be a degree of nuclear loss of FUS in motor neurons post-mortem, albeit to a lesser degree than that seen with TDP-43 (Neumann et al. 2009a). It is therefore conceivable that loss of nuclear splicing factors in cells affected by ALS leads to a shift in the splicing pattern of one or several genes that are crucial for (motor) neuronal function, and that this, rather than a primary toxic effect of neuronal inclusions, is disease determinant. In keeping with this, loss of TDP-43 in *Drosophila* leads to defective neuromuscular junctions (Feiguin et al. 2009).

In contrast to Nova, both TDP-43 and FUS are ubiquitously expressed proteins (Aman et al. 1996; Buratti et al. 2001; Andersson et al. 2008), while ALS and FTLD are diseases in which pathology is limited to the spinal cord and brain. However, loss of a ubiquitous splicing factor could in theory cause tissue-specific alterations by interacting with other cellular factors. Unlike TDP-43 or FUS, SMN does not regulate splicing by binding specific RNA sequences, but has indirect effects through the regulation of spliceosome assembly. This assembly capacity is markedly reduced in models of SMA, although steady state levels of spliceosome components seem to be only very mildly reduced (Gabanella et al. 2005; Gabanella et al. 2007). End stage SMA mice have differentially spliced transcripts in several tissues, including the spinal cord (Zhang et al. 2008), but the selective loss of lower motor neurons in response to SMN deficiency implies that, if splicing alterations are at the core of SMA pathophysiology, motor neurons are either particularly vulnerable to a global change in the cellular mRNA, or a crucial sub-set of motor neuron specific mRNAs are mis-spliced. The lesson learned from Nova and agrin, however, is that alternative splicing of even a single mRNA can have deleterious consequences for the cell, and a splicing alteration of one or a

few genes could be relevant for SMA. So far, no target mRNA has been identified that could explain the SMA phenotype.

A recent study utilised exon-specific microarrays to analyse mRNA from laser-capture micro-dissected residual motor neurons in post-mortem spinal cord samples of ALS patients with TDP-43 positive neuropathology and identified a large number of differentially expressed exons compared to control samples (Rabin et al. 2009). Of note, no changes were obvious in the remaining tissue of the anterior horn after the motor neurons had been removed. While it remains unclear whether or not the observed changes are primary or secondary, this study highlights the importance of considering alternative splicing events in addition to crude levels of transcript in diseases like ALS. Whether the changes demonstrated reflect a failure of splicing fidelity or a shift in expression to known physiological isoforms appropriate to the 'stressed' cell requires further study.

1.3.2 mRNA transport

Motor neurons are the extreme example of a polarised cell, and not only have different protein requirements in different cellular compartments, but also rapidly changing protein needs in response to synaptic stimulation. In addition to the complexity of gene expression brought about by tissue specific alternative splicing, there is mounting evidence that neurons regulate gene expression both spatially and temporally by localised protein translation in dendrites and axons. Local translation does not seem to be an exceptional mechanism important for only a few transcripts, but may involve hundreds of mRNA species (Martin and Zukin 2006). Since several proteins implicated in motor neuron disorders have roles in mRNA transport and translation, these pathways constitute points of motor neuron vulnerability beyond pre-mRNA splicing (figure 1B and C).

Targeting of mRNAs to specific sites in dendrites or axons is a function of *cis*-acting factors consisting of specific nucleotide sequences on the nascent mRNA that are often, but not exclusively, located in the 3'UTR (localization elements or "zipcodes"), as well as *trans*-acting protein factors that bind to these sequences. This association often begins during transcription and splicing in the nucleus (Gu et al. 2002; Oleynikov and Singer 2003; Giorgi and Moore 2007; di Penta et al. 2009). One of the best studied examples of this is the association of the zip code binding protein 1 (ZBP1) with a corresponding 54 nucleotide localisation sequence (the zipcode) in the beta-actin 3'UTR (Ross et al. 1997), which is essential for correct asymmetrical targeting of beta-actin mRNA in a variety of cell types including neurons (Zhang et al. 2001; Tiruchinapalli et al. 2003; Condeelis and Singer 2005). Upon nuclear export, mRNAs and their associated binding proteins are found in granules that contain a variety of other proteins and facilitate transport or further processing. RNA transport granules are present in neurons (Knowles et al. 1996) and contain part of the machinery needed for later translation of the mRNA (Krichevsky and Kosik 2001; Kiebler and Bassell 2006), but there is probably a heterogeneous population of different macromolecular complexes that contain distinct mRNAs and mRNA binding proteins (Elvira et al. 2006; Martin and Ephrussi 2009). While transport of RNPs can take place by passive diffusion, it is often actively mediated by microtubules and associated kinesin and dynein motors (Knowles et al. 1996; Kiebler et al. 1999; Kanai et al. 2004).

Several mutations in kinesins are associated with disorders of both upper and lower motor neurons (James and Talbot 2006), and variation in the kinesin-associated protein 3 (KIFAP 3) modulates survival in ALS (Landers et al. 2009). In

addition, mutations in dynactin have been reported in a few cases of ALS (Puls et al. 2003; Munch et al. 2004; Munch et al. 2005). Although there is no direct evidence that mutations lead to ALS through disruption of RNA transport granules, RNA transport does appear to be dependent on the integrity of axonal transport motors.

Both TDP-43 and FUS have been identified outside the nucleus in association with protein complexes likely to have a role in RNA transport. FUS was found to be a constituent of kinesin-associated RNA transport granules in hippocampal neuronal dendrites that contained CaMKIIα and Arc mRNAs (Kanai et al. 2004). Translocation of FUS to dendrites was shown to be dependent on intact microtubules, as well as mGluR5 stimulation. Mice deficient in FUS were generated in a large scale mutagenesis programme using gene trap retroviral vectors (Hicks et al. 2000). *Fus -/-* mice died perinatally and showed abnormal B-lymphocyte development. No obvious central nervous system defect was detected by routine histology (Hicks et al. 2000). However, primary hippocampal pyramidal neurons derived from *Fus -/-* mice were later found to have abnormal dendritic morphology and reduced number of dendritic spines (Fujii et al. 2005).

FUS was also shown to be transported by a myosin-Va motor, which is actin-based (Yoshimura et al. 2006), and binds not only beta-actin mRNA, but also mRNA encoding an actin stabilising protein, Nd1-L (Fujii and Takumi 2005). Transport of beta-actin mRNA is also a function of the SMN protein. In addition to its cytoplasmic and nuclear role in snRNP assembly and maturation, SMN has been shown to be present in axons and growth cones in cultured cells (Jablonka et al. 2001; Fan and Simard 2002; Rossoll et al. 2002), in rat motor neuronal dendrites (Bechade et al. 1999; Pagliardini et al. 2000) and axons (Pagliardini et

al. 2000) as well as in proximal axons in human neurons (Briese et al. 2006; Giavazzi et al. 2006). Reduction of SMN levels induces altered axonal morphology in zebra fish (McWhorter et al. 2003) and cultured mouse motor neurons (Rossoll et al. 2003), and altered axonal growth is associated with reduced beta-actin mRNA transport (Rossoll et al. 2003). This is mediated by an SMN binding partner, hNRNP-R (Rossoll et al. 2002), but apparently independent of other canonical members of the SMN complex such as gemin-2 (Jablonka et al. 2001), indicating that the SMN function in axons is distinct from its role in snRNP biogenesis. hnRNP-R was shown to bind to the beta-actin mRNA zipcode (Rossoll et al. 2003), and while it cannot be ruled out that this association is dependent on the zipcode binding proteins ZBP1 or ZBP2, the absence of these proteins in several proteomic studies on SMN binding partners (Meister et al. 2002) makes it possible that the SMN-hnRNP complex is unique in motor neuronal mRNA transport. Beta-actin is important in axonal and dendritic growth as well as synapse formation (Luo 2002) and an actin stabilizing protein, Plastin 3, was recently shown to be a modifier of SMA disease severity (Oprea et al. 2008), but it is unknown whether beta-actin mRNA, or other, as yet unidentified mRNAs are relevant to disease pathogenesis, though locally synthesized dendritic and axonal proteins are known to function in synaptic plasticity and neural repair.

TDP-43 has been shown to bind to the 3'UTR of low molecular weight neurofilament (NFL) mRNA (Strong et al. 2007) and as part of RNA transport granules enriched for beta-actin mRNA (Elvira et al. 2006), as well as hippocampal dendritic RNA granules containing beta-actin and CaMKIIα mRNA (Wang et al. 2008a), implicating it in mRNA stability and transport that could be disrupted by pathological TDP-43 aggregate formation in ALS.

Although much of the research on SOD1-related ALS has focussed on toxicity of SOD1 aggregates, oxidative stress and mitochondrial dysfunction, there are recent reports of binding of mutant SOD1 to the VEGF 3'UTR (Lu et al. 2007; Li et al. 2009) as well as the NFL 3'UTR (Ge et al. 2005; Volkening et al. 2009) implying a possible dysregulation of post-transcriptional mRNA regulation as the disease mechanism.

1.3.3 mRNA translation

Neuronal transport granules are generally not translationally competent (Krichevsky and Kosik 2001) and the transported mRNAs are translationally repressed until released to polysomes. Translational repressors can act by various means, including blocking the recruitment of ribosomal components, shortening of the poly (A) tail of mRNAs with resulting reduced affinity for poly A binding protein (PABP), and, most commonly, by inhibition of the cap-dependent translation initiation process (Besse and Ephrussi 2008). For example, one of the best known components of RNA granules, FMRP, disrupts translation initiation by targeting the eIF4F complex through a protein binding partner (Napoli et al. 2008), modulating dendritic maturation and synaptic plasticity. FMRP has been reported to bind to SMN providing indirect evidence that SMN could have a neuronal-specific function through regulating local translation, in addition to modulating RNA transport.

The release of mRNAs from translational repressors and subsequent translation has been well studied in dendritic compartments, where it is often the consequence of synaptic activity-dependent depolarisation and spatially restricted phosphorylation of RNA binding proteins. For example, beta-actin mRNA remains translationally repressed through binding of ZBP1, but phosphorylation of ZBP1 by a Src-kinase releases beta-actin mRNA onto polysomes (Huttelmaier et al. 2005).

Phosphorylation of the translational repressor CPEB in response to NMDA receptor mediated Aurora kinase activation leads to stimulation of polyadenylation of CPEB target mRNAs such as CaMKIIα (Huang et al. 2002). In turn, phosphorylation of general translation initiation factors such as eIF4e will lead to global changes of mRNA translational activity.

While local translation is currently best characterised for the dendritic compartment in hippocampal cell cultures, motor neurons are likely to utilise similar mechanisms in their extensive dendritic tree. In addition, there is increasing evidence that despite the absence of easily identifiable ribosomes beyond the axonal hillock, functional components of the protein synthesis machinery are present in the axon (Koenig and Martin 1996; Koenig et al. 2000; Merianda et al. 2009) and that local mRNA translation occurs in axons as in dendrites (reviewed in (Giuditta et al. 2008; Lin and Holt 2008). For instance, there is evidence that the local translation of beta-actin mRNA in the axonal growth cone takes place in response to external guidance cues (Leung et al. 2006; Lin and Holt 2007) during development, but local mRNA transport and translation is also thought to be a feature in mature neurons (Hanz et al. 2003; Yudin et al. 2008; Taylor et al. 2009). A recent study examining the axonal compartment of a dorsal root ganglion model system systematically for locally translated mRNA content, by a combination of proteomics and RT-PCR, identified more than a hundred proteins of diverse function (Willis et al. 2005), many of which overlapped with mRNAs identified in axonal preparations of mature cortical neurons (Taylor et al. 2009). In parallel to what is known from dendrites, axonal protein translation is activity-dependent (Jimenez-Diaz et al. 2008), and changes in the repertoire of axonally synthesised

protein are part of a neuronal injury response programme (Taylor et al. 2009; Yoo et al. 2009).

Mutations in tRNA synthetases GARS and YARS, enzymes that charge tRNAs with the cognate amino acid glycine and tyrosine, respectively, cause a motor-predominant form of peripheral neuropathy, also referred to as distal spinal muscular atrophy (Antonellis et al. 2003; Jordanova et al. 2006). GARS is present in axons suggesting a function in supporting local protein translation. GARS and YARS mutations do not consistently lead to loss of enzyme function or altered cellular localisation. The presence of these proteins in axons implies a potential role in axonal protein synthesis, failure of which could underlie the neuropathy (Antonellis and Green 2008; Motley et al. 2010), a view that is supported by findings in Drosophila (Chihara et al. 2007).

Mutations in *IGHMBP2*, the gene encoding the immunoglobulin μ-binding protein 2, cause a more severe type of distal spinal muscular atrophy (Grohmann et al. 2001). IGHMBP2 is a DNA/RNA helicase initially thought to be involved in transcription or pre-mRNA splicing, but there is now evidence that it is in fact an RNA helicase associated with ribosomes in the neuronal cytoplasm that is also present in axons and growth cones (Grohmann et al. 2004). IGHMBP2 mutants lose their enzymatic activity *in vitro*, suggesting that dysfunction of mRNA translation underlies distal SMA (Guenther et al. 2009). Senataxin, the gene mutated in a juvenile form of slowly progressive ALS (ALS4) (Chen et al. 2004), is a member of the same helicase superfamily. While it has functions in transcription, DNA repair, as well as pre-mRNA splicing (Suraweera et al. 2007; Suraweera et al. 2009), senataxin shows strong cytoplasmic staining in mature murine neurons (Chen et al. 2006) and might have a function in translation regulation like

IGHMBP2. Interacting partners identified by mass spectrometry include PABP and SMN, in addition to several hnRNPs (Suraweera et al. 2009).

1.3.4 Translation control: stress granules, P bodies, and micro-RNAs

Whereas local mRNA translation contributes to fine spatial resolution of protein synthesis, temporal control of translation after nuclear export of mRNAs is achieved by temporary storage of mRNAs in ribonucleoprotein granules that can be classified according to their key protein constituents into stress granules or processing bodies (P bodies), although a considerable degree of overlap exists.

Cells, including neurons (DeGracia et al. 2007; Tsai et al. 2009), respond to a variety of stressors with a change in gene expression partially mediated by translational arrest of some mRNAs, while specific proteins, such as heat shock proteins, continue to be synthesised (Kawai et al. 2004; Anderson and Kedersha 2006; Anderson and Kedersha 2008). In the stereotypic stress response, cap-dependent translation initiation is inhibited by phosphorylation of eIF2α and disassembly of polysomes from translating mRNAs, the majority of which are then stabilized and stored temporarily in stress granules (Anderson and Kedersha 2006; Anderson and Kedersha 2008) (figure 1C).

The phosphorylation of eIF2α is mediated by a number of kinases that respond to specific stressors, including heat and viral infections, but also factors implicated in the pathogenesis of ALS such as oxidative stress and endoplasmatic reticulum stress induced by the unfolded protein response (Harding et al. 2002; Harding et al. 2003; Kawai et al. 2004).

Stress granules are characterised by the presence of stalled initiation complexes containing small ribosomal subunits, eIF3, eIF4e and PABP (Kedersha et al.

2002). In addition, they contain a variety of proteins involved in various aspects of RNA metabolism including stabilization, translational repression and localisation. Several of the proteins involved in motor neuron disorders appear to be present in stress granules. TDP-43 and FUS are nuclear-cytosolic shuttling proteins (Zinszner et al. 1997; Ayala et al. 2008b), a function shared by many stress granule components (Taupin et al. 1995; Gallouzi et al. 2000; Kedersha et al. 2000). FUS has been shown to be part of stress granules induced by oxidative stress in cell culture (Andersson et al. 2008). Cytosolic redistribution of TDP-43 is a key feature of ALS (Neumann et al. 2006), and transient TDP-43 relocalisation is observed in motor neurons after axotomy (Moisse et al. 2009a; Moisse et al. 2009b), indicating that cytoplasmic TDP-43 might be a physiological response to injury. In addition, TDP-43 was shown to localise to stress granules in a motor neuronal cell line under oxidative stress (Colombrita et al. 2009a). While the cytoplasmic TDP-43 in ALS motor neurons was not found to co-localise with the known stress granule markers TIAR or HuR in autopsy material (Colombrita et al. 2009a), another study found increased expression of stress granule marker TIA-1 and co-localisation with cytosolic TDP-43 in ALS motor neurons (Volkening et al. 2009).

Stress granule proteins TIA-1 and PABP are key components of basophilic inclusions in a rare form of juvenile ALS (see chapter 5) (Fujita et al. 2008). Stress-induced translational repression can also occur independently from eIF2alpha phosphorylation (McEwen et al. 2005; Mazroui et al. 2006) in a pathway involving cleaved tRNAs (Yamasaki et al. 2009). This pathway depends on the ribonuclease activity of angiogenin, mutations of which are a rare cause of familial and sporadic ALS (Greenway et al. 2006; Gellera et al. 2008). The

ribonuclease activity of angiogenin is reduced by mutations (Crabtree et al. 2007), suggesting that a disturbance of protein translation repression or faulty stress response might underlie the pathogenesis of these types of ALS. In keeping with this, wild-type angiogenin has been shown to protect motor neurons from hypoxia induced stress, whereas mutant angiogenin lacks this function (Subramanian et al. 2008). The SMN protein has been identified in stress granules (Hua and Zhou 2004a; Hua and Zhou 2004b), although little is known about its function in the stress-response pathway.

P-bodies are RNA granules related to stress granules. Like stress granules, they are present in neurons (Cougot et al. 2008; Zeitelhofer et al. 2008a; Zeitelhofer et al. 2008b) and play a role in translation control by storing untranslated mRNAs (Brengues et al. 2005), but also function in 5' 3' decay (Cougot et al. 2004) and nonsense-mediated decay of mRNAs harbouring a premature stop codon (Cougot et al. 2004; Sheth and Parker 2006). mRNAs contained in P-bodies are generally linearised and deadenylated, and not found in association with PABP (Anderson and Kedersha 2009). They contain proteins necessary for deadenylating and decapping mRNAs well as a 5' 3' exonuclease, XRN1. There is evidence that mRNA recognition by the general machinery for mRNA decay is mediated by mRNA sequence-specific binding of microRNAs which in turn recruit specific regulatory proteins (Parker and Sheth 2007).

The understanding of translational regulation through microRNAs is in its early stages. Micro-RNAs are the result of a two-step processing mechanism comprising cleavage of pre-microRNA in the nucleus by the RNAse Drosha, followed by cytoplasmic export of the resulting pre-microRNA and further cleavage by another RNAse, Dicer, in the cytoplasm or neuronal processes. The resulting

microRNA is a ~21 nucleotide long RNA duplex that is unwound and incorporated into the 'RNA induced silencing complex', or RISC, which acts on complementary regions in the 3'UTR of target mRNAs that, depending on the degree of complementarity, are either degraded or translationally silenced (Bicker and Schratt 2008; Carthew and Sontheimer 2009).

microRNAs are abundant the nervous system and play an important role in both neuronal development and in the adult brain, where they are thought to regulate synaptic plasticity (Kosik 2006). In mice, conditional ablation of Dicer in Purkinje cells or the retina leads to cerebellar degeneration or retinal cell loss, respectively (Schaefer et al. 2007; Damiani et al. 2008), underlining the general importance of an intact microRNA system for neuronal survival. Altered microRNAs have been implicated in Parkinson's disease (Kim et al. 2007), fragile-X mental retardation syndrome (Li and Jin 2009), Tourette's syndrome (Abelson et al. 2005) and Alzheimer's disease (Lukiw 2007), and altered microRNA level can modify the disease phenotype of polyglutamine disease models (Bilen et al. 2006a; Bilen et al. 2006b). Despite this, a causal relationship between altered microRNA expression and disease pathogenesis remains hypothetical.

On the other hand, there is some evidence that genetic variation in *cis* can alter microRNA binding and lead to altered gene expression in the absence of coding mutations. For example, loss of function coding mutations in the progranulin gene (*GRN*) cause FTLD-U (Gass et al. 2006), but do not explain all cases of disease. The binding of microRNA-659 to the *GRN* 3'UTR is increased by a single nucleotide polymorphism (SNP) in the *GRN* 3'UTR, leading to reduced progranulin expression *in vitro* (Rademakers et al. 2008). The SNP, rs5848, is strongly associated with FTLD-U, adding another genetic mechanism to the spectrum of

GRN mutations. No direct role for microRNAs has been demonstrated in motor neuron disorders to date, but with increasing interest in this rapidly evolving field studies are likely under way.

1.3.5 RNA modification

To add another layer of gene expression regulation, post-transcriptional mRNA modifications in the form of base pair change can occur in the cytoplasm. For example, the adenosine deaminase acting on RNA (ADAR) enzyme family catalyses the exchange of selected adenosine residues to inosine on mRNAs, which is then translated like a guanosine residue (Bass 2002). The glutamate receptor subunit GluR-2 mRNA is edited in a way that leads to a channel property-determining amino acid change (Burnashev et al. 1992; Greger et al. 2003). There are some reports that in spinal motor neurons from patients with ALS, this physiological editing function is almost completely lost, leading to channels that are pathologically permeable for calcium, which could explain the glutamate toxicity observed in ALS (Kawahara et al. 2004; Kwak and Kawahara 2005).

As opposed to the physiological modifications of RNA introduced by A-I editing, oxidation of bases, in particular guanine to 8-hydroxy-guanosine (8-OHG) (Wamer et al. 1997), is a pathological event that leads to disruption of translation (Shan et al. 2007; Tanaka et al. 2007). An increase in oxidised RNA has been detected in a variety of neurodegenerative conditions including Alzheimer's disease (Nunomura et al. 2009). RNA oxidation, as assessed by RNA IP (immunoprecipitation) with an antibody specific to 8-OHG, was also a feature in affected post-mortem brain regions of patients with ALS, as well as in spinal cords from mutant SOD1 transgenic mice, even at the pre-symptomatic stage (Chang et al. 2008).

1.4 Aims of this work

This thesis will examine various molecular aspects of amyotrophic lateral sclerosis and spinal muscular atrophy that relate to RNA metabolism.

It will start with a genetic screen for rare variants in patients with both ALS and non-5q SMA, including *TARDBP*, *FUS* and *ANG*, ALS candidate genes with functions in RNA metabolism (chapter 3).

The next chapter (chapter 4) aims to elucidate the functional difference between *TARDBP* variant and wild-type sequences, analysing both coding and non-coding changes in experimental systems. The focus of the analysis is on pre-mRNA splicing and RNA granule formation in the cellular stress response.

Chapter 5 analyses neuropathological aspects of TDP-43 in human ALS as well as mouse models of ALS and SMA. In addition, it will characterise the neuropathology of *FUS* mutations in patients with young-onset ALS in detail.

A major aspect of RNA metabolism is pre-mRNA splicing. Alterations in splicing might underlie SMA. Chapter 6 will examine the global profile of mRNA expression including differential expression of splice variants in spinal cord taken from an SMA mouse model using an exon-specific microarray. This experiment is repeated at several time points to answer the question of whether a differential splicing pattern is cause or consequence of SMA.

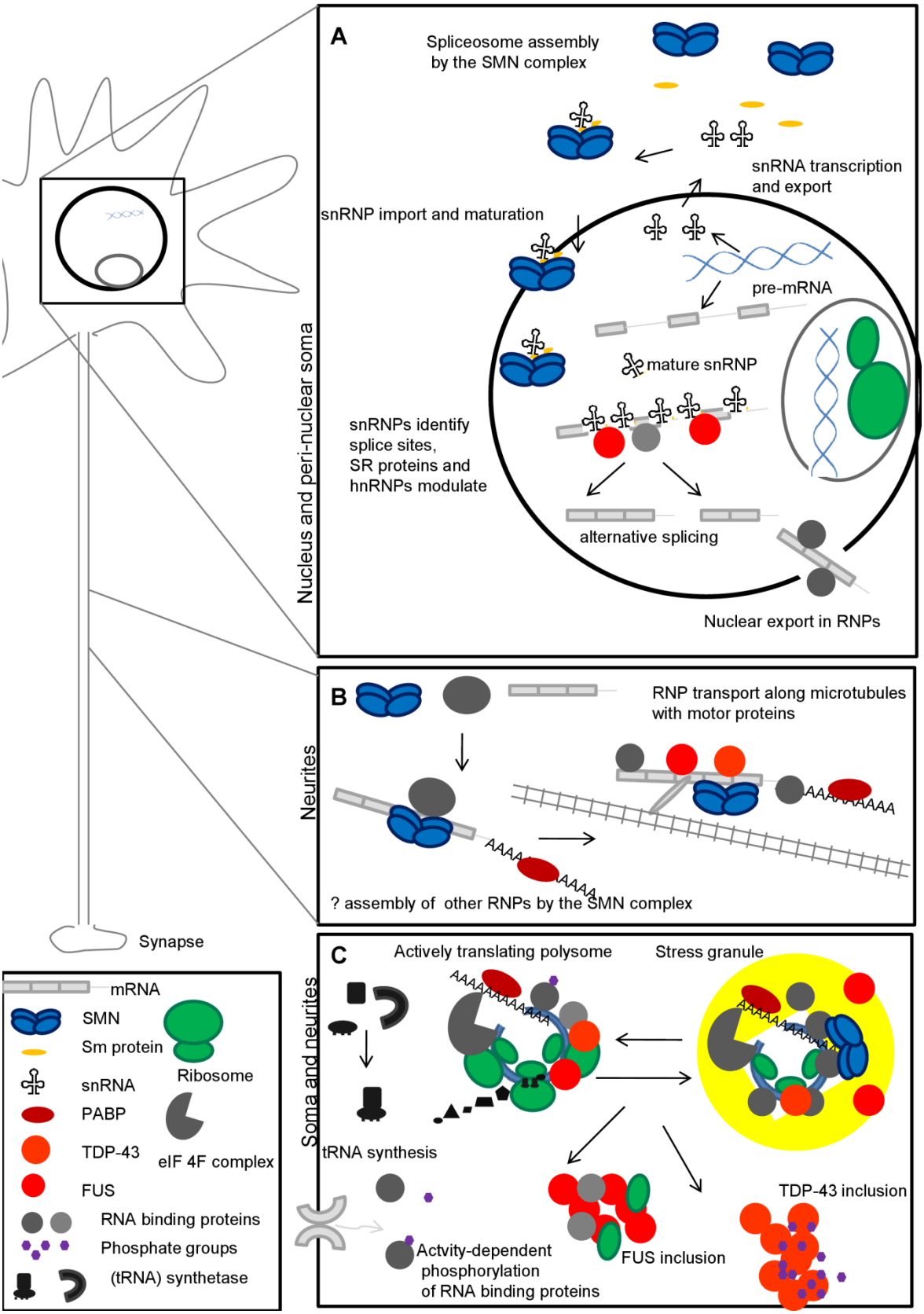
A
Spliceosome assembly
by the SMN complex
snRNA transcription
and export
snRNP import and maturation
pre-mRNA
mature snRNP
snRNPs identify
splice sites,
SR proteins and
hnRNPs modulate
alternative splicing
Nuclear export in RNPs
Nucleus and peri-nuclear soma
B
RNP transport along microtubules
with motor proteins
AAAAAAAAA
AAAA
AAAA
? assembly of other RNPs by the SMN complex
Neurites
Synapse
C
Actively translating polysome
Stress granule
AAAAAAAAAAA
AAAAAAAAAAA
tRNA synthesis
TDP-43 inclusion
FUS inclusion
Actvity-dependent
phosphorylation
of RNA binding proteins
Soma and neurites
mRNA
SMN
Sm protein
snRNA
PABP
TDP-43
FUS
RNA binding proteins
Phosphate groups
(tRNA) synthetase
Ribosome
eIF 4F complex

Figure 1.1 Key stages in neuronal RNA metabolism (A) Many alternative splice isoforms, some neuron specific, result from RNA processing. Small nuclear RNAs are transcribed and exported to the cytoplasm, where they are coupled with Sm proteins to form snRNPs, a reaction controlled by SMN, the protein depleted in spinal muscular atrophy. Nuclear export of mRNAs involves various mRNA binding proteins as well as GLE1, mutations in which cause LCCS1. (B) SMN is hypothesised to have a second, possibly motor neuron specific, function in neurites in complex with RNA binding proteins to target, stabilise and translationally repress the RNA cargo (C) Protein translation involves the complex interplay of mRNA, RNA binding proteins, ribosomes and tRNAs. Translation can occur in the soma, dendrites or axons and is dependent on the phosphorylation of RNA binding proteins and by local signalling. A variety of stressors can lead to disassembly of polysomes and aggregation of RNA, ribosomal subunits and various RNA binding proteins into stress granules that serve to temporarily store mRNA. Both TDP-43 and FUS forms aggregates in ALS and an active area of research is whether aggregation is related to stress granule formation and leads to loss of function.

2 Material and Methods

2.1 Genetic screening

2.1.1 Patient identification

Patients attending the Oxford Motor Neuron Disease Care & Research Centre (http://www.oxfordmnd.net/) were screened for participation in the genetic study. A clinical diagnosis of ALS was made by an expert neurologist in the field (Dr. Kevin Talbot) in accordance with the revised El Escorial criteria (Brooks et al. 2000). All patients had a progressive motor deficit with upper and lower motor neuron involvement in the absence of an alternative disease process that could explain these signs. Patients with upper motor neuron signs only for duration of at least four years were included with a diagnosis of primary lateral sclerosis.

A more heterogeneous group of patients with a range of motor neuron disorders not fulfilling diagnostic criteria for ALS were classified according to family history and clinical features into the following groups:

- distal dominant SMA
- distal sporadic SMA
- non-5q -recessive SMA
- sporadic SMA
- other pure motor neuron disorders

Patients in this group were not only ascertained in the Oxford Motor Neuron Disease Centre, but also referred on from clinicians throughout the UK.

2.1.2 Ethical approval, consent and storage of data

Ethical approval for the collection of DNA was obtained from the Oxfordshire Research Ethics Committee B (REC number 07/Q1605/60). All participants gave written informed consent prior to the DNA collection. Samples were anonymised and personal information was kept secure with access for the principal investigator only.

2.1.3 DNA extraction

2.1.3.1 DNA extraction from blood

Whole blood was collected into blood tubes containing 5ml EDTA. DNA was extracted from peripheral blood leukocytes within 24 hours of sample collection. Cell lysis, deproteinisation, DNA extraction and precipitation was accomplished with the use of a commercially available DNA extraction kit (Nucleon BACC, Amersham Biosciences), following the manufacturer's instructions. The precipitated DNA was recovered using a heat-sealed Pasteur pipette and resuspended in 100 µl nuclease free water.

2.1.3.2 DNA extraction from human brain and muscle tissue

DNA was extracted from post-mortem brain or skeletal muscle using a Qiagen DNeasy blood and tissue kit (Qiagen). Briefly, 10-20 mg of frozen tissue samples were homogenised in PBS using a rotor-stator homogeniser at maximum output for 20 seconds and then incubated in lysis buffer with proteinase K in a 55°C water bath overnight. DNA was then extracted following the manufacturer's instructions and eluted into dH_2O.

For extraction from formalin fixed, paraffin embedded samples, 3 separate 10 µm thick brain sections were freshly cut and dewaxed in xylene. Xylene was removed

by washing in 100% alcohol. DNA was extracted following an overnight incubation in lysis buffer with proteinase K at 55°C using QIAamp FFPE Tissue kit (Qiagen) following the manufacturer's instructions.

2.1.4 Polymerase chain reaction

2.1.4.1 Primer design

Genomic sequence and exon/intron boundaries of *SOD1*, *ANG, FVT1, FUS* and *TDP-43* were identified in Ensembl (http://www.ensembl.org/index.html). Primers were designed manually to yield amplicons of 300 to 500 base pair length, be of 20 to 21 base pairs in length, contain equal GC content of 40-80% and end in a GC clamp, while avoiding repeats of more than 4 nucleotides and self-complementary sequences. The following primer sequences were used:

AMPLICON	FORWARD PRIMER	REVERSE PRIMER	SIZE	AT
SOD1 EXON 1	GTGCGAGGCGATTGGTTTGG	TCGCAAACAAGCCTCCGTCC	264	59
SOD1 EXON 2	TGGCTAGAAAGTGGTCAGCC	GCATGAGGATCAATGGAGCC	447	59
SOD1 EXON 3	GTCAGCACTTTCTCCATGGG	GCATTCCAGCATTTGGGAGC	332	59
SOD1 EXON 4	TAGTGTGTAGACGTGAAGCC	CTGGATCTTTAGAAACCGCG	376	59
SOD1 EXON 5	CTTTTGGGTATTGTTGGGAGG	ACAGGGTTTTTATTCACAGGC	486	59
FVT1 EXON 1	ATTCGAGCTCCCGAAGAGCG	GACCGCGGCCTGGAAAAAGGG	638	59*
FVT1 EXON 2	AAACAGTCAAAGCAGCAGGC	CTCACATCAAGGAAGAAGCG	422	57
FVT1 EXON 3	ACTGTTTTGTGTGTTTTCTGG	GTAGATATGAATGTGTGTGGG	387	57
FVT1 EXON 4	GTTTTAACTCCAAAAGCTGCC	GAAAAATGTAGCAGAGCAGGC	459	57
FVT1 EXON 5	CTTGCCATTTTGCTATGTGGC	CAGATTAGAAGGTCCATTCCC	502	57
FVT1 EXON 6	CATTCAGCAAGCCTGTTGGG	GCAAAACTCAGGGTTGAGCC	486	57
FVT1 EXON 7	TGCAATTGGTGTAGTTCCCC	TCATCAGAAACCAGCTAGGC	396	57
FVT1 EXON 8	TCTAGAAATAGGAATCTGCCC	TACAATCAGTTTTCAGGAGGC	423	57
FVT1 EXON 9	CTCACTTGTTGAGAACTGCC	TTTCTCTATCTGCAAGGCCC	531	57
FVT1 EXON 10	TGTATCTGGGCTGTCCAGCG	TCTAGCCCCTTGCTTGCAGC	479	57
ANG EXON 1	AGCAGCAGCGAATAAGTACG	AGCAGGAGTGTGAACCTACC	587	59

ANG EXON 2	GTTCAAGAGCAGTGTCCTTGG	ATTCATGAGCTTGAGCCTGG	297	61
ANG EXON 3	TGTTCTTGGGTCTACCACACC	GAAATGGAAGGCAAGGACAGC	552	59
ANG 3'UTR	ATTTTCCGTCGTCCGTAACC	TCCTATGCAGTCCTCTCAGG	280	59
FUS EXON 1	GACCCTCTACCTGCCCTACG	CCCACTGAAAACGAAAAGCC	295	59
FUS EXON 2-3	CAAACTGCTGGGATTACAGG	ACATCTCAGTGCTGCTCAGG	795	59
FUS EXON 2	CAAACTGCTGGGATTACAGG	AGAAGAATAGCTGCTCTGGC	396	59
FUS EXON 3	AGTCCACGGACACTTCAGGC	ACATCTCAGTGCTGCTCAGG	443	62
FUS EXON 4	TGGGATTTGCCCCAAGGTCC GGTTGTCCTGTAGATACTGC	GCTGGTCCCTTTATCATTCC	584 543	59
FUS EXON 4A	TGGGATTTGCCCCAAGGTCC GGTTGTCCTGTAGATACTGC	CTATACTCATAAAGCCAGCC	286 245	59
FUS EXON 4B	AGTTGCAACATCACTAACAGC	GCTGGTCCCTTTATCATTCC	347	59
FUS EXON 5	GGGTACAGAGAATGGACTCC	CTCAGCAACAGAGACAGAGC	368	59
FUS EXON 6	TGCCTGGCACTTGTCAAACC	AACCATGCACTAGGGACTGG	422	59
FUS EXON 6A	TGCCTGGCACTTGTCAAACC	ACGGTCCTGCTGTCCATAGC	208	59
FUS EXON 6B	GGCAATCAAGACCAGAGTGG	AACCATGCACTAGGGACTGG	271	59
FUS EXON 7	AACACCTACCCATGTTTGGG	GTTCTGGACACCTCAAAACC	251	59
FUS EXON 8	TTCCTGTTGACTAACGGCTC	GTTTCAAAGAACATCCAGGC	178	59
FUS EXON 9	TGATACCAGTTGCTTGATGG	TGTTTTTACTGCTGGCAACC	304	59
FUS EXON 10	ATGGAGGTTTACATGTGAGG	AAGAACCCTCAAACTATGGC	363	59
FUS EXON 11	ACCATTTGAGAAAGGCACGC	AAGCCTTTACCATCTTCTGC	254	59
FUS EXON 12	GTGCAGAAGATGGTAAAGGC	TACCTAGGTAAGCTTTTGGC	359	59
FUS EXON 13	CTGTATCTCTAAAGTCACCG	TTCTTTGGTCCCAGCTCCC	235	59
FUS EXON 14	ATGGGTAAGAAAGGCAGACC	CCTAGCCCTCAAAATGAAACC	370	59
FUS EXON 15	TACTCGCTGGGTTAGGTAGG	GCCAACACTCATGACATCCC	533	59
FUS EXON 15 A	TACTCGCTGGGTTAGGTAGG	GGTGATCAGGAATTGGAAGG	232	59
FUS EXON 15 B	TGTACCCAGTGTTACCCTCG	GCCAACACTCATGACATCCC	352	59
TARDBP EXON 2	GAACTCTGACATGGTTTGGG	GGCAGAATGTCTCCTGAAAC	440	
TARDBP EXON 3	GAGCAAACATCACTTCTTGCC	TAGGGTACATAGTGATACCCC	411	
TARDBP EXON 4	AGTTTTAAGCCACTGCATCC	ATTCAGCATGCACTAAGGGC	415	
TARDBP EXON 5	CGTTACTCTTCACTGAAGCC	ATGGTCTTGATCTCCTGACC	469	
TARDBP EXON 6	ATTGCTTATTTTTCCTCTGGC	ATACTCCACACTGAACAAACC	778	

Table 2.1 Genetic screen primer sequences Amplicon length (size) in base pairs (bp) and annealing temperature (AT) in °C.

2.1.4.2 Reaction conditions

100 ng genomic DNA was used in a standard 50 µl PCR reaction using Taq polymerase (Sigma) and the following cycling conditions:

Step	Temperature	Duration
Initial denaturation	94°C	1 min
Denaturation	94°C	30 secs
Annealing	59°C	45 secs x35
Elongation	72°C	45 secs
Final elongation	72°C	7 mins

FUS exon 15 was amplified using Expand High Fidelity PCR system (Roche) and the following conditions:

Step	Temperature	Duration
Initial denaturation	95°C	2 mins
Denaturation	95°C	15 secs
Annealing	56°C	30secs x10
Elongation	72°C	45 secs
Denaturation	95°C	15 secs
Annealing	59°C	30 secs x15
Elongation	72°C	45 secs +5 secs/cycle
Final elongation	72°C	7 mins

Reactions were carried out in ABgene 96 well PCR plates (Thermo Scientific).

2.1.4.3 PCR purification

PCR reactions carried out in 96 well plates were purified by ethanol precipitation.

Ten microlitres of a reaction were visualised on a 1.5% agarose gel stained with SYBR safe DNA gel stain (Invitrogen). Four microlitres of sodium acetate (Sigma) were added to the remaining 40 µl and spun down at 500 g for 2 minutes. Ninety microlitres of 95% ethanol were added to each well, the plate was incubated at -20°C for 2 hours and then centrifuged at 3150 rpm for 60 minutes. The supernatant was removed by spinning the plate upside down at 500 rpm for 2

minutes before adding 100 µl 70% ethanol. A further 30 minute spin at 3150 rpm was carried out and the supernatant removed by an upside down spin. The plate was allowed to air dry and the DNA pellet was re-suspended in 20 µl nuclease-free water (Ambion). Individual PCR reactions were purified by gel extraction using a QIAquick Gel Extraction Kit (Qiagen) according to the manufacturer's instructions.

2.1.5 Copy number PCR

Gene copy number was assessed by quantitative PCR and comparative Ct ($\Delta\Delta$Ct) method using Fast SYBR Green chemistry (Applied Biosystems) and a StepOnePlus Real-time PCR machine (Applied Biosystems). Reactions were cycled as follows:

Step	**Temperature**	**Duration**
Initial denaturation	95°C	10 min
Denaturation	95°C	3 secs
Annealing/elongation	60°C	30 secs x40

All reactions were carried out in four technical replicates. Primers were designed using Primer Express software (Applied Biosystems). To avoid amplifying mRNA, primers were designed across an intron-exon boundary. Primer concentrations were optimised to yield low Ct values and minimal primer dimer formation. Optimal primer concentration was determined by triplicate reactions for combinations of forward and reverse primer concentrations at 50nM, 300nM and 900nM, respectively. Primer dimer formation, as well as non-specific amplification, was assessed by scrutinizing the melt curve analysis for additional peaks.

Primer efficiency was established by performing qPCR for the target gene and control gene on serial dilutions of genomic DNA. The dynamic range for the copy

number assay was identified by plotting the Delta Ct (target-reference) value against the log DNA input to create a semi-log regression line. A slope of less than 0.1 of this line indicates a valid primer set for the ΔΔCt method (figure 3.2 and 3.5)

Fold change was calculated as $2^{-\Delta\Delta Ct,}$ and gene copy number as CN=2xfold change.

2.1.6 Denaturing high performance liquid chromatography (DHPLC)

Mutation detection by DHPLC utilises differential retention on a chromatography column of homo- and heteroduplexes formed by denaturing and reannealing PCR products derived from two or more chromosomes (Xiao and Oefner 2001).

FVT1 amplicons were amplified by PCR as described above, denatured at 95°C for 5 minutes and allowed to reanneal gradually by reducing the temperature by 1°C per minute to 35 °C. 8 µl product was then injected into a DNAsep column of a WAVE DNA fragment analysis system (Transgenomics, Cheshire, UK) and exposed to a linear gradient of acetonitrile in 0.1M triethylamine acetate (TEAA) produced by mixing buffer A (5% TEAA) and buffer B (25% acetonitrile, 5% TEAA). Fragments bound the stationary phase DNAsep column in the presence of TEAA and were eluted by the acetonitrile gradient. Elution of DNA fragments was then detected by a spectrophotometer at a wavelength of 280 nm. Oven temperature (table 2.2) and acetonitrile gradient were adjusted for each amplicon depending on distribution and relative amount of A/T and G/C base pairs using WAVE Navigator software (Yu et al. 2006). For exon 6, two methods were designed to cover the entire coding region.

Samples with abnormal chromatograms were sequenced, unless amplicons contained a frequent SNP as in exon 4, and the chromatograms clearly resembled that of samples with known genotype.

FVT1 AMPLICON	WAVE TEMPERATURE
FVT1 EXON 1	66*
FVT1 EXON 2	57.5
FVT1 EXON 3	55.9
FVT1 EXON 4	55.4
FVT1 EXON 5	57.3
FVT1 EXON 6	59&62.8
FVT1 EXON 7	58.6
FVT1 EXON 8	56.2
FVT1 EXON 9	59.4
FVT1 EXON 10	57.7

Table 2.2 WAVE temperatures used in the *FVT1* screen Two methods were designed for exon 6. *The *FVT1* exon 1 PCR was carried out with 10% DMSO. Before injecting into the WAVE cartridge, sample was diluted to reach a final DMSO concentration of less than 7% compatible with the Transgenomic system.

2.1.7 DNA sequencing

Sequencing reactions were performed using ethanol precipitated PCR product re-suspended in dH_2O at a concentration of 10 ng/ µl as template. BigDye Terminator v3.1 chemistry (Applied Biosystems) was employed for all reactions. Reactions were set up in ABgene Thermo-Fast 96 Detection Plates (AB-1400) (Thermo Scientific) as follows:

BigDye	0.5µl
5x sequencing dilution buffer	1.75µl
dH2O	4.75µl
Primer (5uM)	1µl

DNA (10ng/ul)	2µl
Total volume	10µl

Primers used were the forward and/or reverse primers used for the PCR reactions. The sequencing reactions were cycled as follows:

Step	Temperature	Duration
Initial denaturation	96°C	1 min
Denaturation	96°C	10 secs
Annealing	50°C	5 secs x35
Elongation	60°C	4 min
Hold	10°C	variable

Sequencing reactions were ethanol precipitated after the addition of 2.5 µl 125 mM EDTA per well using 50 µl 95% alcohol and 100 µl 70% alcohol following the ethanol precipitation protocol outlined in 2.1.4.3.

Sequencing reactions were then run on an Applied Biosystems 3730 DNA Analyzer by Dr Teresa Street and Dr Rory Bowden in the Experimental Statistics laboratory, Department of Statistics, University of Oxford.

Sequencing of repeat individual samples was performed on ethanol precipitated, column purified or gel-extracted PCR products by Geneservice (Oxford, UK) or Beckman Coulter Genomics (Essex, UK).

2.1.8 Cloning of PCR product for sequencing

FUS exon 15 was amplified using *Taq* polymerase to create 3' deoxyadenosine overhangs and checked for non-specific amplification products or primer dimer by gel electrophoresis. Two microlitres PCR product were incubated for five minutes at room temperature with 1 µl each of linearised, activated pCR®2.1-TOPO® vector (Invitrogen) and salt solution to achieve insertion of the PCR insert into the plasmid. Two microlitres of the reaction were transformed into One Shot TOP

10 competent E.coli by heat shock, according to the manufacturer's instructions. Cells were then grown at 37°C in a shaking incubator for one hour after the addition of 250 µl SOC medium, and 50 µl were spread on ampicillin containing agarose plates. Plasmid DNA of ten colonies (see section 2.2) was analysed by direct sequencing.

2.1.9 Restriction digest

PCR-amplicons were scrutinised for the presence of differential restriction sites using NEBcutter v2.0 (http://tools.neb.com/NEBcutter2/). RsaI was identified to differentially cut the rs2003149 alleles. Five microlitres PCR product in *Taq* PCR buffer was incubated at 37°C overnight with 0.2 µl (2units) RsaI. Products were visualised on 1.5% agarose gels and scored according to the size of bands present.

2.1.10 Bioinformatical analysis

2.1.10.1 Sequence alignment

Sequences were identified in Ensembl (http://www.ensembl.org/index.html). For protein sequence alignment, homologues were identified in http://www.ncbi.nlm.nih.gov/homologene/ and aligned using the ClustalW2 algorithm using http://www.ebi.ac.uk/Tools/clustalw2/index.html . Results were then entered into Boxshade 3.21 (http://www.ch.embnet.org/software/BOX_form.html) to obtain shaded multiple alignment files.

2.1.10.2 Protein prediction

To predict the effect of sequence variants on protein function, three commonly used web based protein prediction algorithms were used. SIFT (Ng and Henikoff

2001; Ng and Henikoff 2003) uses position specific scoring based on sequence homologies to score substitutions as neutral (score=1) or damaging (score=0). Polyphen (http://genetics.bwh.harvard.edu/pph/) uses sequences conservation and structure to score a substitution as neutral (score=0) or damaging (positive value) (Ng and Henikoff 2006). SNAP (screening for non-acceptable polymorphisms) (http://cubic.bioc.columbia.edu/) combines several sequence analysis tools and includes predictions of solvent accessibility, secondary structure and flexibility (Rost et al. 2004; Bromberg et al. 2008). Exonic non-protein changing SNPs were examined for the presence of potential exonic splicing enhancer sites using ESE finder release 3.0 (Cartegni et al. 2003). Both wild-type and variant sequences were analysed and compared. To predict protein sequences from nucleotide sequences, the translate tool of the ExPASy Proteomics server (Swiss Institute of Bioinformatics, http://www.expasy.ch/tools/dna.html) was utilised. Domain structures for cartoons were identified on http://www.uniprot.org/uniprot/ for FUS with the reference sequence PRO_0000081591.

2.2 Cloning of constructs

2.2.1 *Cis*-splicing minigenes

2.2.1.1 A66A minigene

The A66A minigene was cloned on the basis of a pTB splicing reporter plasmid backbone kindly provided by Dr. Emmanuele Buratti and Professor Francesco Baralle (Molecular Pathology Group, International Centre for Genetic Engineering and Biotechnology, AREA Science Park, Padriciano 99, 34012 Trieste, Italy). The pTB plasmid is a pBluescript plasmid with added SV40 promoter followed by

alpha-globin exons 1-3, where exon 3 is fused to part of an EDB exon, followed by an intron that contains a unique NdeI site, and a 3' terminal exon consisting of fused EDB 1 and 3 sequences (figure 4.1).

TDP-43 exon 2 with 200 base pairs of adjacent 5' and 3' intron was PCR amplified from human genomic DNA with primers containing NdeI sites (TDP-43 exon 2 F/R NdeI, table 2.3). Both vector and PCR product were cut with NdeI (NEB) and ligated as described in 2.2.1. The correct orientation of the insert was assessed by direct colony PCR using the primers A66AOR_F and BRA_2 (table 2.3). Colonies containing the insert in the correct orientation were then directly sequenced. The 198T>C mutation, as well as mutations in position 2 and 3 of the 5' splice site were introduced by site directed mutagenesis (see 2.2.2.3).

2.2.1.2 A315A minigene

The A315A minigene was cloned in analogy to the A66A minigene using the primers TDP-43 exon 6 F NdeI/ TDP-43 exon 6 F NdeI (table 2.3) to amplify *TDP-43* exon 6 and 200 base pairs of adjacent intron 5 and 86 bases of the 3' UTR, and ligation of the cut vector and PCR product. Colonies were screened for correct orientation of the insert by PCR using the primers TDP_6BF and BRA_2 (table 2.3). The A315A mutation was introduced by site directed mutagenesis.

To test the splicing of exon 6 in a more realistic context, a second minigene was cloned that contained exon 6 as well as the entire 3' UTR. Because of the presence of multiple NdeI sites in the 3270 base pair long insert, this minigene was cloned using insertional mutagenesis in two steps, using two mega-primers generated by PCR of genomic DNA (see 2.2.2.3).

2.2.1.2.1 A315A ESE

To test the strength of the putative ESE sequence surrounding the A315A variant, a minigene devised to test exonic sequences in a beta-globin context was utilised. The 4.11.12muC plasmid was developed by Dr. Tom Cooper, Baylor College of Medicine, Houston, Texas, and was a gift from Dr. Esther Becker, University of Oxford. PAGE purified oligonucleotides were synthesised (Sigma) to contain the predicted SC-35 binding site for wild-type and mutant sequence as well as SalI/BamHI recognition sequences:

SC3-35 wild-type forward 5' TCGACTGGTGCGTTCAGCATTAATCTAGAG

SC-35 wild-type reverse 5' GATCCTCTAGATTAATGCTGAACGCACCAG

SC-35 A315A forward 5' TCGACTGGTGCATTCAGCATTAATCTAGAG

SC-35 A315A reverse 5' GATCCTCTAGATTAATGCTGAATGCACCAG

The synthetic oligonucleotides were resuspended in dH_2O to a final concentration of 100 µM and annealed by heating to 95°C in annealing buffer (10 mM Tris pH8, 50 mM NaCl) and gradual cooling to room temperature. The annealed oligonucleotides were then phosphorylated by incubation with T4 Polynucleotide Kinase (NEB) in T4 PNK Buffer (NEB) for one hour at 37°C.

The plasmid was cut using SalI and BamHI, purified and treated with CIP.

100 ng of plasmid DNA were ligated in a 1:4 molar ration with 2.5 ng of annealed synthetic oligonucleotide insert using T4 ligase (NEB) overnight at 16°C. Minipreps were screened for the presence of the insert by digest with XbaI and verified by direct sequencing.

2.2.2 Cloning of TDP-43 cDNA constructs

2.2.2.1 3xFLAG-TDP-43

Full length TDP-43 was PCR amplified from cDNA using oligonucleotide primers with added 5' prime HindIII and XbaI restriction sites (cTDP-43-HindIII_F/ cTDP-43_XbaI_R, table 2.3). The PCR product was cut in a double digest with HindIII and XbaI in NEB buffer 2 for two hours and column purified using a Qiagen PCR purification kit. Three micrograms of the p3XFLAG-CMV-7.1 vector (Sigma) were cut using the same enzymes, and treated with 1 µl of calf intestinal phosphatase (CIP) for one hour at 37°C after heat inactivation of the restriction enzymes for 20 minutes at 65°C, and purified by gel extraction using a Qiagen gel extraction kit. Eighty ng of cut and purified vector were ligated with an equimolar amount of insert using T4 ligase in a 20 µl reaction at 16 °C overnight.

Two microlitres of the ligation reaction were transformed into DH5α E.coli (NEB) using heat shock, and plated on agarose plates containing 100 µg/ml ampicillin.

Ligation and transformation efficiencies were monitored by transforming a control ligation reaction containing cut vector only.

Colonies were inoculated in 5 ml overnight cultures of LB broth (Invitrogen) with ampicillin, and plasmid DNA was purified using a Qiagen Miniprep kit.

Primer	**Sequence 5'-3'**
TDP-43 exon 2 F NdeI	GTCATATGAATGAACTGGCGAGGC
TDP-43 exon 2 R NdeI	GCCATATGATGTAACACCAAAAGG
TDP-43 exon 6 F NdeI	ATCATATGAGCCACCATGCCCAGCC
TDP-43 exon 6 R NdeI	CGCATATGAATTCTTTGCATTCAGGGC
cTDP-43-HindIII_F	5GCAAGCTTATGTCTGAATATATTCGGGTAACAG
cTDP-43_XbaI_R	AATCTAGAATTCTACATTCCCCAGCCAGAAGAC
A66AOR_F	GGATTTGATCATTGTCCTTTTGGTG
BRA_2	CAACTTCAAGCTCCTAAGCCACTGC
TDP_6BF	TCAAGGTAGTAATATGGGTGG
A315AR	CATATGCTGAATATACTCCACACTG

Table 2.3 Cloning primer sequences

2.2.2.2 3XFLAG-TDP-43-HA

A human influenza hemagglutinin (HA) tag (5'TAT CCT TAT GAT GTT CCT GAT TAT GCT 3') was added to the C-terminal end of the p3XFLAG-TDP-43 construct by insertional mutagenesis. After confirmation of the correct sequence, the A321G and M337V mutations were introduced by site-directed mutagenesis.

2.2.2.3 Site –directed mutagenesis

Site-directed mutagenesis was carried out using a QuikChange Site Directed Mutagenesis Kit (Stratagene/Agilent). Primers were designed using the QuikChange primer design program (http://www.stratagene.com/sdmdesigner/default.aspx) in the default setting. PAGE (polyacrylamide gel electrophoresis) purified primers were synthesised (Sigma) (table 2.4). For a standard mutagenesis reaction, 25 ng of plasmid template, 5 µl of buffer, 1 µl dNTP mix, 125 ng of each forward and reverse primer and 1 µl PfU Turbo enzyme were made up to 50 µl with dH20 and cycled for 12 times for point mutations and 18 times for the insertion of the HA tag as:

Step	**Temperature**	**Duration**
Initial denaturation	95^{o}C	30 secs
Denaturation	95^{o}C	30 secs
Annealing	55^{o}C	1 min
Elongation	68^{o}C	1 min/kb plasmid length

For the insertional mutagenesis of the TDP-43 3'UTR into the pTB-A315A vector, mutagenesis mega-primers were generated by PCR from genomic DNA using the primers TDP-43_Ins2F/ TDP-43_Ins2R and TDP-43_Ins3F/ TDP-43_Ins3R. The resulting PCR products (1204 and 1274 base pairs, respectively) contained 20 base pairs of sequence overlapping with the vector sequence at the 5' end and were used sequentially as primers in mutagenesis reactions utilising 50 ng of

vector, 400 ng of megaprimer and 1 µl of PfU Turbo. Reactions were cycled as follows:

Step	Temperature	Duration		
Initial denaturation	95°C	30 secs		
Denaturation	95°C	30	secs	
Annealing	52°C	5	min	x5
Elongation	68°C	15	min	
Denaturation	95°C	30	secs	
Annealing	55°C	5	min	x13
Elongation	68°C	15	min	

Resulting colonies were screened by PCR using the primers TDP_6BF/A315AR and sequence verified before proceeding to the next round of mutagenesis.

Mutagenesis primer	Sequence
A321G_mut_F	TTAGCATTAACCCAGGGATGATGGCTGCGGC
A321G_mut_R	GCCGCAGCCATCATCCCTGGGTTAATGCTAA
M337V_mut_F	GAGCAGTTGGGGTATGGTGGGCATGTTAGCC
M337V_mut_R	GGCTAACATGCCCACCATACCCCAACTGCTC
Q331K_mut_F	CTCAGGCAGCGTTGAAGAGCAGTTGGGGT
Q331K_mut_R	ACCCCAACTGCTCTTCAACGCTGCCTGAG
D169G_mut_F	GTCACAACGACATATGATAGGTGGGCGATGGTGT
D169G_mut_R	ACACCATCGCCCACCTATCATATGTCGTTGTGAC
TDP_262_STOP_F	GCGTGCATATATCCAATGCTGAACCTTAGCATAATAGCAATAG
TDP_262_STOP_R	CTATTGCTATTATGCTAAGGTTCAGCATTGGATATATGCACGC
TDP_HA_F	TCTTCTGGCTGGGGAATGTATCCTTATGATGTTCCTGATTATGCTTA GAATTCTAGAGGATCC
TDP_HA_R	GGATCCTCTAGAATTCTAAGCATAATCAGGAACATCATAAGGATACA TTCCCCAGCCAGAAGA
A66A_F	CATGCCCCAGATGCCGGCTGGGGAAATCT
A66A_R	AGATTTCCCCAGCCGGCATCTGGGGCATG
A66A_5ss2_F	GTATGTTGTCAACTATCCAAAAGGCTTGTTACCATTTGGTTTTTGTAA T
A66A_5ss2_R	ATTACAAAAACCAAATGGTAACAAGCCTTTTGGATAGTTGACAACATA C
A66A_5ss3_F	GTGTATGTTGTCAACTATCCAAAAGGTCTGTTACCATTTGGTTTTT
A66A_5ss3_R	AAAAACCAAATGGTAACAGACCTTTTGGATAGTTGACAACATACAC
A315A_mut_F	GGGATGAACTTTGGTGCATTCAGCATTAATCCAGC
A315A_mut_R	GCTGGATTAATGCTGAATGCACCAAAGTTCATCCC
A315A_3ss_mut_F	TCTTCTTTGTTTACATCCCTTATTTCTTATATATTGCGCAGTCTCTTTG
A315A_3ss_mut_F	CAAAGAGACTGCGCAATATATAAGAAATAAGGGATGTAAACAAAGAA GA
TDP-43_Ins2F	TGGTTGGTATAGAATGGTGGG
TDP-43_Ins2R	GCCACACAGCAAAGAGAAACATAGCAGCTCAGTCCATGTTCTCAGC
TDP-43_Ins3F	CTGATGGGCTGAGAACATGG
TDP-43_Ins3R	GCCACACAGCAAAGAGAAACATAGCATGCAGATTCAGATGCAG

Table 2.4 Mutagenesis primers

2.3 Cell culture

2.3.1 Cell lines

The cell lines NSC-34 (mouse motoneuronal), HeLa (human epithelial carcinoma) and HEK293T (human embryonic kidney) were maintained in Dulbecco's Modified Eagles Medium (DMEM-GlutaMAX, Invitrogen) supplemented with 10% fetal calf serum and 1% Penicillin-Streptomycin solution (Invitrogen). The human neuroblastoma cell line SH-SY5Y was maintained in DMEM F12 medium (Invitrogen). All cells were kept at 37°C and 5% CO_2 in a humidified incubator. When fully confluent, cells were washed in PBS, dissociated with trypsin-EDTA (Invitrogen), resuspended in medium and plated in 50% confluence in 24 well plates (Falcon) containing autoclaved coverslips for immunocytochemistry, 12 well plates for harvesting of RNA or 6 well plates for subsequent protein extraction.

2.3.2 Transfection

Cells were transfected when 50-80% confluent using FuGENE 6 transfection reagent (Roche) diluted in serum-free medium (Opti-MEM, Invitrogen) and endonuclease free DNA in a 3:1 ratio of FuGENE (µl) to DNA (µg) according o the manufacturer's instructions.

2.3.3 Cell Treatment

For proteasome inhibition, cells were treated with MG132 (Sigma) in DMSO at a final concentration of 20 µM for 6 hours. Cell stress experiments were performed with 1-10mM H_2O_2 or 1 µM staurosporine (InSolution Staurosporine, Calbiochem) for four hours and 1mM sodium meta-arsenite (Sigma) for one hour.

Translation arrest was achieved by treating cells with cycloheximide in DMSO (Sigma) for four hours at a final concentration of 37.5 µg/ml.

2.4 Splicing assays

The CFTR exon 9 splicing assay was performed using a previously published splicing reporter minigene (hCF-(TG)11T5, called CFTR minigene from here) (Pagani et al. 2000) kindly provided by Dr. Emmanuele Buratti and Professor Francesco Baralle. HeLa cells were co-transfected in 12 well plates with 1 µg of CFTR minigene as well as 1 µg of FLAG-TDP-43 constructs. The empty 3XFLAG vector was co-transfected with the CFTR minigene as a control. RNA was harvested using a Qiagen RNeasy Mini kit after 36 hours and 1 µg was reverse transcribed using random hexamer primers (Invitrogen). The RT-PCR was carried out using the primers MGF and MGR and *Taq* DNA polymerase (Sigma) at an annealing temperature of 59°C and 25 cycles. The cycle number was confirmed to be in the linear range of amplification by running product on an agarose gel after 10, 15, 20, 25, 30 and 35 cycles. Each transfection was performed on at least three separate occasions. Co-transfection with the TDP-43 constructs was monitored by RT-PCR for FLAG-TDP using the primers FLAG_TDP_F and FLAG_TDP_R, while reverse transcription efficiency was controlled by RT-PCR for GAPDH (table 2.5). Bands were quantified in Image J (NIH) and expressed as the fraction of transcript lacking the exon of interest to the total transcript. A One-way analysis of variance (ANOVA) with least significant difference (LSD) post-hoc test was performed in SPSS 16.0 (SPSS, Illinois, USA) to test for differences between genotypes, given a non-significant Levene's test for homogeneity of variances.

The effect on SMN splicing was examined by assessing the endogenous transcript in HeLa cells using the primers SMN 4F, SMN 6F and SMN 8R.

Cis-splicing assays for the A66A and A315A minigenes were carried out as above using SH-SY5Y cells and the MGF and MGR primers. The A315A-3'UTR minigene was analysed by RT-PCR with the primers MGF and TDP-43_3'UTR_R. Cells were co-transfected with pEGFP to control for equal transfection efficiency.

The 4.11.12muC-A315A minigene was transfected into SH-SY5Y cells and analysed in the same way using the primers ESE_MG_F/ ESE_MG_R.

Primer	**Sequence 5'-3'**
SMN Exon 4F	AACATCAAGCCCAAATCTGC
SMN Exon 6F	CCAGATTCTCTTGATGATGC
SMN Exon 8Ra	GAGTTACCCATTCCACTTCC
SMN Exon 8Rb	TACAACACCCTTCTCACAGC
FLAG_TDP_F	ACAAGGATGACGATGACAAGC
FLAG_TDP_R	CACTTTCACTGCAGAGGAAGC
MG_F	TAGGATCCGGTCACCAGGAAGTTGGTTAAATCA
MG_R	CAACTTCAAGCTCCTAAGCCACTGC
TDP-43_3'UTR_R	ATACTCCACACTGAACAAACC
ESE_MG_F	CTGAGGAGAAGTCTGCCGTTA
ESE_MG_R	GAGTGTGGTTGGCAAAGTGA
hGAPDH_6/7_F	CTCAAGATCATCAGCAATGCC
hGAPDH_8_R	GTCCACCACTGACACGTTGGC

Table 2.5 Splicing assay primers

2.5 Immunostaining of cells

24 hours after transfection, the medium was aspirated and cells washed in phosphate buffered saline (PBS), fixed with 4% paraformaldehyde (PFA) in PBS for 15 minutes at room temperature and permeabilised with 0.4% Triton-X 100 in PBS for 15 minutes. Coverslips were blocked with 5% milk in PBS for one hour at room temperature under gentle agitation. Coverslips were then carefully removed from the 24 well plate and transferred into a humidified incubation chamber for incubation with the primary antibody diluted in 5% weight per volume (w/v) milk in PBS at 4°C overnight. Coverslips were washed three times with PBS and incubated with the secondary antibody in PBS for two hours at room temperature,

washed with PBS and mounted in Vectashield mounting medium containing DAPI as the nuclear counterstain (Vector labs).

2.5.1 Image analysis

For counts of cells containing cytosolic TDP-43, cytosolic TDP-43 aggregates or stress granules, 3 low power (20x) field of view micrographs for each of three independent transfection experiments were analysed with the point picker function in Image J (NIH) marking all transfected cells as well as cells containing structures of interest. Counts of each field of view per transfection were summed, and average and standard deviation of the mean expressed for the total counts per transfection experiment. The fraction of cells containing granules was compared between groups using a Kruskal-Wallis test given a significant Levene's test for homogeneity of variances using SPSS version 16.0.

2.6 Cell viability assay

Cell viability was assessed using a colorimetric assay based on the reduction of yellow MTT (3-(4,5-Dimethylthiazol-2-yl)-2,5- diphenyltetrazolium bromide), to purple formazan in the mitochondria of living cells. Cells were grown to 80% confluence in 96 well plates (Falcon) and transfected with 3xFLAG-TDP-43 constructs (see 2.3.2) in triplicate. After 24 hours, 30µl of 5mg/ml MTT in PBS were added to each well followed by incubation at 37°C for one hour. Medium was removed by pipetting, and any formazan crystals were resuspended in 100 µl DMSO at 37°C. The assay was analysed by measuring absorbance at 590 nm in a FLUOstar OPTIMA plate reader (BMG labtech). Raw absorbance data were analysed in Microsoft Excel.

2.7 Western blotting

2.7.1 Human and mouse tissue protein extraction

Fresh frozen tissue was used for protein extraction. Depending on size, snap frozen whole spinal cords were extracted in 300-500 µl Radio Immuno Precipitation Assay (RIPA) lysis buffer (50 mM Tris-Cl, pH 7.5, 150 mM NaCl, 0.1% (w/v) SDS, 1% (v/v) sodium deoxycholate, 1% (v/v) TX-100) and 1% (v/v) protease inhibitors. Approximately 70 mg of human brain or spinal cord samples were extracted at 3 µl/mg in RIPA buffer. Samples were homogenised in buffer by sonication at 50% output for 30 seconds. Homogenates were chilled on ice for 30 minutes and clarified by centrifugation at 15,800 g for 30 min at 4°C.

RIPA insoluble fractions were obtained by re-extracting the resulting pellet in RIPA buffer as above, discarding the supernatant, and extracting the pellet in SDS buffer (50mM Tris-HCL pH 7.5, 2% SDS) at 3 µl/mg by sonicating.

The serial fractionation on SMNDelta7 and SOD1 mouse spinal cord was carried out by Dr. Bradley Turner as previously described (Neumann et al. 2006). Briefly, tissues were extracted at 200 mg/ml in low salt (LS) buffer by sonicating for 15 sec, incubating on ice for 30 min and centrifuging at 14,000 rpm for 30 min at 4°C. Pellets were sequentially extracted in high salt, Triton-X, sarkosyl and urea buffers as above. All buffers were supplemented with protease inhibitors (complete EDTA free protease inhibitor cocktail (Roche), Pepstatin A at 1µg/ml and 1 mM PMSF) and phosphatase inhibitors (5mM sodium fluoride and 1mM sodium orthovanadate).

Protein concentration in lysates was quantified using a colorimetric assay based on bicinchoninic acid (Pierce BCA Protein Assay Kit, Thermo Scientific) according to the manufacturer's instructions.

Protein samples (50µg/well) were separated by SDS polyacrylamide gel electrophoresis (SDS-PAGE) (7%-12%) and transferred to 0.2 µm nitrocellulose membranes (Millipore). Membranes were blocked with 5% (w/v) milk powder in TBS-T, pH 8.0, for 1 hr and incubated with the primary antibody (table 2.6) in 3% (w/v) BSA in TBS-T overnight at 4°C. Blots were probed with HRP-conjugated antibodies (1:10,000, Amersham) and developed using ECL reagents (Amersham).

Antibody	Manufacturer	Dilution
Mouse anti-SMN	BD Transduction lab	1:1000
Rabbit anti-TDP-43	Proteintech	1:500
Mouse anti-Actin	Abcam	1:1000
Rabbit anti-FUS	Sigma	1:500
Rabbit anti-FUS	Bethyl laboratory	1:10 000
Rabbit anti-tubulin	Abcam	1:500
Rabbit anti-LAP2	Abcam	1:500
Rabbit anti-SNRPA1	Abcam	1:1000
Goat anti-CHAT	Chemicon	1:500
Rabbit anti-USPL1	Santa Cruz	1:500
Rabbit anti-PCNA	Abcam	1:200
Mouse anti-FLAG	Sigma	1:500
Rabbit anti-HA	Sigma	1:500

Table 2.6 Antibodies used for Western blotting

2.7.2 Protein lysates from cells

Cells grown in monolayers in 6 well plates were washed in PBS and lysed in 200 µl ice-cold RIPA buffer using a cells scraper and incubated on ice for 30 minutes before clearing by centrifugation at 17, 000 g for 30 minutes. For soluble/insoluble preparations, cells were lysed in PBS containing 0.2% Triton-X 100 as above. The supernatant was kept as the soluble fraction, while the pellet was resuspended in PBS containing 3M urea and 2% SDS, cleared by centrifugation and kept as the insoluble fraction.

For nuclear/cytosolic fractionation, cells were harvested in 200 µl buffer A (10mM Hepes pH 7.9, 10mM KCl, 0.1 mM EDTA, 0.1mM EGTA), incubated on ice for 30

minutes and homogenised using 50 strokes of a Donnce homogeniser. After centrifuging for 5 minutes at 5000g, the supernatant was re-centrifuged and saved as the cytosolic fraction, while the pellet was washed in 200 µl buffer A plus 0.1% NP40 before being resuspended in buffer C (20mM Hepes, 400mM NaCl, 1 mM EDTA, 1 mM EGTA) as the nuclear fraction. The fractionation efficiency was assessed by probing the membrane with antibodies against the nuclear antigen LAP2B and the cytosolic beta-tubulin.

2.7.3 Dephosphophorylation assay

Protein was extracted in buffer without phosphatase inhibitors. Fifty micrograms of protein were supplemented with NEBuffer for Protein MetalloPhosphatases and 1 mM $MnCl_2$ and incubated with 2 µl of Lambda Protein Phosphatase (NEB) at 30°C for 1.5 hours.

For protein dephosphorylation of spinal cord lysates in urea buffer, extracts were dialysed against 50 mM Tris-HCl, pH 7.9, 100 mM NaCl, 10 mM $MgCl_2$ and 1 mM DTT using Slide-A-Lyzer mini dialysis units (Pierce). Dialysates (50 µg) were treated with 10 U calf intestinal phosphatase (New England Biolabs) for 1 hr at 37°C.

2.8 Immunoprecipitation

Cells were washed with ice-cold PBS and lysed in 0.5 ml IP lysis buffer (20mM Tris pH 7.5, 5mM EGTA, 1% Triton-X 100, 150 mM NaCl) supplemented with protease inhibitors on ice for 15 minutes and centrifuged at 14,000 g for 30 minutes. The supernatant was incubated with 10µl agarose beads coupled to anti-FLAG antibody (Sigma) at 4°C for 2 hours with constant agitation. Samples were then centrifuged at 5000g at 4°C for 5 minutes and washed three times with wash

buffer (20mM Tris pH7.5, 100 mM Na Cl, 0.1% Triton-X 100). The remaining pellet was resuspended in 20 µl 2X SDS sample buffer with 10% beta-mercaptoethanol and boiled for 5 minutes.

2.9 Immunohistochemistry

Six µm thick paraffin sections of formalin fixed, paraffin embedded spinal cord or brains were cut. Sections were dewaxed through serial baths of xylene and descending concentrations of ethanol and washed in tap water. For immunohistochemistry utilising a horseradish peroxidise detection system, sections were incubated in 3% hydrogen peroxide in PBS for 30 minutes followed by washes in tap and distilled water. For antigen retrieval, sections were either autoclaved for 10 minutes at 120°C or microwaved for 15 minutes at 800 Watt. 0.1 mM citrate pH6 was used as antigen retrieval buffer. Sections were then cooled to room temperature, washed in distilled water and two changes of of tris-buffered saline supplemeted with 0.1% Tween-20 (TBS-T). Sections were blocked with 10% fetal calf serum, 3% BSA in TBS-T for one hour at room temperature and incubated with the primary antibody (table 2.7) in block at 4°C overnight. Antibody-binding was visualised using a Dako REAL EnVision kit (Dako) according to manufacturer's instructions and counterstained with haematoxylin for 40 seconds.

Antibody	**Manufacturer**	**Dilution**	**Antigen retrieval**
Mouse anti-SMN	BD Transduction lab	1:320	AC
Rabbit anti SMN	Santa Cruz	1:50	AC
Rabbit anti TDP-43	Proteintech	1:500	AC or MW
Mouse anti TDP-43	Abcam	1:200	AC
Rabbit anti PABP	Abcam	1:800	MW

Rabbit anti FMRP	Abcam	1:600	MW
Rabbit anti HuR	Abcam	1:500	-
Mouse anti TIA1	Abcam	1:50	MW
Rabbit anti TIAL1	Abcam	1:250	MW
Rabbit anti FUS	Sigma	1:25-1:250	MW
rabbit anti-Uspl1	Santa Cruz	1:600	MW
mouse anti-Chodl	Abcam	1:200	MW
rabbit anti-PCN	Abcam	1:2500	MW
goat anti-Chat	Chemicon	1:400	MW
Mouse anti-P62	BD Transduction lab	1:800	MW/AC
Rabbit anti-coilin	Dundee Cell products	1:500	MW
Rabbit anti-ubiquitin	Dako	1:500	MW

Table 2.7 Antibodies used for immunohistochemistry MW, microwave; AC, autoclave.

Each immunostain was performed with a negative control by omitting the primary antibody.

All sections of human material used were selected by Dr Olaf Ansorge on the basis of the pathology identified on routine stains.

2.10 Immunofluorescence

Immunofluorescent studies were carried out on sections prepared as above. Pre-treatment with hydrogen peroxide was omitted. Following antigen retrieval, sections were blocked in 4% normal goat serum, 2% BSA in PBS-T for 30 minutes prior to primary antibody incubation in block. Primary antibody binding was visualised by incubation with Alexa Fluor 488 or 594 goat anti-rabbit and Alexa Fluor 488 or 594 goat anti-mouse secondary antibodies (Invitrogen) at 1:500 in

PBS-T for 2 hours at room temperature. Human sections with strong autofluorescence were counterstained with 0.1% Sudan Black B in 70% ethanol for 5 minutes followed by jet washes with PBS-T. Sections were mounted in Vectashield Hardset mounting medium with DAPI (Vector labs). Double labelling experiments were controlled by establishing specificity of both primary antibodies individually as well as including stains with the first or second antibody only while applying both secondary antibodies.

2.11 Microscopy

Fluorescent microscopy was carried out on a Zeiss Axioplan 2 fluorescent microscope with 20x, 40x or 63x oil immersion optics, an AxioCam MR camera and AxioVision software (Zeiss). The TDP-43 and SMN double labelling experiments on mouse sections were assessed using images captured on a Zeiss LSM 510 laser scanning microscope with a 63x oil immersion objective and 2x digital zoom. All images were compiled using NIH Image J software.

2.12 Animal work

2.12.1 Breeding of mice

2.12.1.1 SMNΔ7

2.12.1.1.1 Breeding

Transgenic $Smn^{+/-}$;SMN2;SMNΔ7 (Le et al. 2005) mice were maintained as heterozygous breeding pairs on an FVB/N background in standard animal facilities in Oxford . Homozygous $Smn^{-/-}$; SMN2; SMNΔ7 mice reached the disease end-point by post-natal day 13 (P13). Five mice of each genotype were sacrificed at

age P1, P3, P5, P7, P9, P11 and P13 for motor neuron counts, and 4 mice of each genotype at P1, P7 and P 13 for RNA and protein extraction.

All animal breeding and procedures were performed in accordance with Home Office and University guidelines.

2.12.1.1.2 Genotyping

For genotyping, mice were either tattooed and a small tail biopsy was taken, or an ear punch biopsy was obtained that served as the identifier depending on site and location of the biopsy.

Tissue biopsies were digested with 5 µl proteinase K (20µg/ml, Roche) in 200 µl DNA extraction buffer (100mM Tris-HCL pH 7.5, 0.2% SDS, 200 mM NaCl, 5mM EDTA pH 8.0) at 55 °C overnight, and DNA was precipitated by adding equal volume of isopropanol. DNA pellets obtained by centrifugation at 13,000 rpm in a bench top centrifuge were washed in 70% ethanol, air dried, and resuspended in 50 µl dH_2O.

Genotyping was performed by multiplex PCR with primers annealing either with the endogenous Smn (WT_SMNR, CTGTTTCAAGGGAGTTGTGGC), the mouse knock-out allele (βGAL_RN, GTGCATCTGCCAGTTTGAGGG), or both, in addition to a universal forward primer (SMN_Comm_F, GATGATTCTGACATTTGGGATG). 50 ng genomic DNA was used in a standard PCR reaction using *Taq* polymerase (Sigma) and the following cycling conditions:

Step	**Temperature**	**Duration**		
Initial denaturation	94°C	1	min	
Denaturation	94°C	30	secs	
Annealing	59°C	45	secs	x35
Elongation	72°C	45	secs	
Final elongation	72°C	7	mins	

Resulting PCR products were resolved on 1.5% agarose gels containing either 0.5 µg/ml ethidium bromide (Sigma) or SYBR safe DNA gel stain (Invitrogen) and scored according to size.

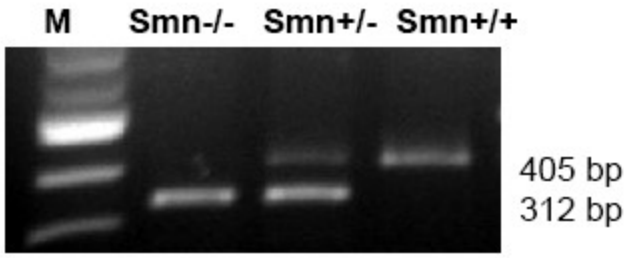

Figure 2.1 SMNΔ7 genotyping Multiplex PCR with expected bands of 312 base pairs for the wild-type allele and 405 base pairs for the knock-out allele. Heterozygous animals show two bands. M, 100 base pair molecular weight marker.

2.12.1.1.3 Weight analysis

Six animals of each genotype were weighed daily for 15 days starting at post-natal day 1 one to obtain weight curves.

2.12.1.2 SOD1

Transgenic SOD1^{G93A} mice derived from the B6SJL-TgN (SOD1-G93A) 1Gur line (Jackson Laboratory, Bar Harbor, ME) were backcrossed onto a pure C57BL6 background and generously provided by Prof. Pam Shaw (University of Sheffield). Mice were maintained by mating heterozygous transgenic males with C57BL6 females. Disease endpoint mice and age-matched wild-types at 4 months were

killed by lethal injection (pentobarbitone, IP) in accordance with Home Office regulations. The SOD1 colony was maintained by Dr. Bradley Turner.

2.12.2 Timed matings

Timed matings were set up by breeding heterozygous Smn+/-;SMN2;SMNΔ7 mice and observing the presence or absence of mating plugs. The day the mating plug was discovered was referred to as E 0.5. Pregnant mice were killed at E 16.5 by exposure to a rising concentration of carbon dioxide and embryos were dissected and rapidly killed by decapitation according to Schedule 1 to the Animals (Scientific Procedures) Act 1986 (Wolfensohn 2003).

2.12.3 Harvesting of tissues

2.12.3.1 RNA and protein

Mice were killed by intraperitoneal injection of at least 140 mg/kg body weight pentobarbitone (200 mg/ml). Whole spinal cord was rapidly dissected by laminectomy, rinsed in PBS (Sigma) and snap frozen on dry ice. Kidneys were dissected and snap frozen on dry ice. For muscle analysis, both gastrocnemius muscles were carefully dissected and frozen on dry ice. Total RNA was extracted using the Qiagen RNeasy Mini kit according to manufacturer's instructions (Qiagen). Genomic DNA was removed by on-column treatment with DNase (Qiagen).

2.12.3.2 Spinal cord samples for histology

Spinal cord specimens for histology of mice older than P5 were obtained after perfusion with paraformaldehyde. Mice were terminally anaesthetized with intraperitoneal pentobarbitone. The thoracic cavity was opened to expose the heart and the left ventricle catheterized with an 18-gauge butterfly needle.

Following the laceration of the right atrium, mice were perfused with approximately 30 ml of room temperature PBS until the liver was observed to become pale. Mice were then perfused with 25 ml of 4% PFA in PBS, pH 7.4.

Spinal cords were then carefully dissected by laminectomy and divided into cervical, thoracic and lumbar segments using the cervical and lumbar enlargements as landmarks.

For paraffin embedding, specimens were fixed in 4% PFA in PBS at 4°C overnight and then stored in 70% ethanol until embedding.

For motor neuron counts, specimens were post-fixed in 4% PFA at 4°C for 2 hours, and then cryoprotected in 30% sucrose in PBS overnight. Following cryoprotection, samples were embedded in optimal cutting temperature embedding medium (OCT) and flash frozen in liquid nitrogen cooled isopentane.

2.13 Motor neuron and nuclear body counts

2.13.1 Tissue processing

Snap frozen spinal cord specimens were stored at -80 °C, and equilibrated to -20°C in a cryostat. Twenty µm thick horizontal sections were cut, and every third section was collected on superfrost slides. Sections were then air dried for ten minutes, washed in PBS, stained with 0.5% Cresyl Violet (Sigma), 0.04% acetic acid for 30 seconds, dehydrated and coverslipped. Slides were numerically labelled without indication of the genotype, and labels were decoded only after the motor neuron counts had been performed.

2.13.2 Identification of motor neurons

2.13.2.1 ChAT immunohistochemistry

Ten air dried sections per genotype were washed in PBS, blocked in PBS, 3% normal goat serum (NGS), 10% bovine serum albumin (BSA) and 0.1% Triton-X 100 for 1 hour at room temperature, incubated with goat anti-ChAT (Chemicon, 1:400) antibody in block at 4°C overnight, washed in PBS, incubated with a rabbit anti-goat biotinylated secondary antibody (1:1000) in PBS and washed again in PBS. Antibody binding was visualized by a Vector ABC Elite kit and dab staining (Vector laboratories).

2.13.2.2 Cresyl violet stain

On Cresyl violet stained sections, motor neurons were identified by their location in the ventral horn of the spinal cord, large size, polygonal shape, large nucleus with prominent nucleolus and intense cytoplasmic staining. This correlated well with cells identified by ChAT immunohistochemistry in both control and SMA animals. For counting, only cells clearly identifiable as motor neurons on the Cresyl violet stain according to these criteria were included.

All counts were performed blinded to genotype by labelling all specimens and slides numerically according to when samples were obtained, and only unblinding after completion of the entire counting process.

2.13.3 Counting paradigm and statistical analysis

Motor neurons were identified in both ventral horns per spinal cord sections, and an average number per ventral horn was obtained by dividing the raw count by the number of sections x 2. All counts were performed twice on separate days and blinded to genotype.

2.13.3.1 Reliability testing

To establish the reliability of the motor neuron counts, samples derived from 11 animals (3=control, Smn+/+;SMN2;SMNΔ7, 3=het, Smn+/-;SMN2;SMNΔ7, 5=SMA, Smn-/-;SMN2;SMNΔ7) at P13 were counted twice one week apart, and an intraclass correlation coefficient (ICC) (Shrout and Fleiss 1979) was calculated according to the formula

ICC=(MS(between) - MS(within))/MS(between) + MS(within))

where MS is mean square (the total sum of squares divided by the degrees of freedom) derived from a single factor ANOVA.

The ICC was calculated using the reliability function in SPSS version 16.0.

2.13.3.2 Establishing motor neuron count differences according to region, genotype and time point

Between 30 and 34 non-consecutive lumbar spinal cord sections were used for counts for each of five animals per genotype and time point. At P13, sections were also cut from thoracic and cervical spinal cord to test for regional differences in motor neuron numbers.

2.13.3.3 Statistical analysis

The mean of two motor neuron counts was used for further analysis. After unblinding, motor neuron counts between control, heterozygous and SMA animals were compared using a univariate analysis of variance followed by the least significant difference (LSD) test. Counts between genotypes in different spinal cord regions were compared using a two way ANOVA and LSD test for “region”, while differences between genotypes at different time points were compared using

unpaired two-tailed t-tests in addition to a one way ANOVA on motor neuron counts in SMA animals. All statistical analyses were performed in SPSS 16.0.

2.13.4 Nuclear body count

Two spinal cord sections were analysed for each of 3 animals of each genotype. Per section, five large alpha motor neurons were examined per ventral horn (20 per animal). Motor neurons were identified by their location in the ventral horn, large nucleus, prominent nucleolus, polygonal shape and relatively large size. Only cells with clearly visible nucleolus were chosen for analysis. Images were captured using a Zeiss LSM 510 laser scanning microscope with a 63x oil immersion objective and 2x digital zoom. Image analysis was performed using Image J software (NIH). For TDP-43 body counts, images of motor neuron nuclei were displayed in Image J with automatic setting of brightness and contrast. Nuclear TDP-43 bodies were then counted manually using the point picker function. Cajal and TDP-43 body counts were performed blinded to genotype. Statistical analysis was performed using Microsoft Office Excel.

2.14 Microarray

2.14.1 Assessment of RNA quality

RNA quantity was assessed using a microvolume spectrophotometer (Gallagher and Desjardins 2008) (Nanodrop, Thermo Scientific) and samples with a concentration <300 ng/µl were discarded. RNA integrity was then assessed using an Agilent Bioanalyzer.

2.14.2 Hybridization

One ug starting RNA was ribosome depleted using the Ribominus Human/MouseTranscriptome Isolation kit (Invitrogen). Labelled sense single

stranded DNA (ssDNA) for hybridization was generated with the Affymetrix GeneChip Whole Transcript sense target labelling and control reagents kit (Affymetrix, UK) according to the manufacturer's instructions. Sense ssDNA was fragmented and the distribution of fragment lengths was measured on the BioAnalyser. The fragmented ssDNA was labelled and hybridized to the Affymetrix GeneChip Mouse Exon 1.0 ST Array (Affymetrix). Chips were processed on an Affymetrix GeneChip Fluidics Station 450 and Scanner 3000.The microarray was performed by Dr. Sheena Lee, Department of Physiology, Anatomy and Genetics, University of Oxford

2.14.3 Gene level analysis

2.14.3.1 Core probe set analysis

The core genes on the arrays (Core: RefSeq transcripts and full-length mRNAs (17,800 transcript clusters) were RMA (Robust multi-array analysis) (Irizarry et al. 2003) normalized in GeneSpring GX 10.1.02 (Agilent) and differentially expressed genes were identified using an unpaired t-test with an arbitrary p-value cut off of $p \leq 0.05$ and a fold change difference between SMA and control of ≥ 1.5.

2.14.3.2 Ensembl gene based analysis

Twenty-four CEL files (4 control mice plus 4 SMA mice, at each of three time points) were preprocessed concurrently using RMA without background correction (i.e. quantile normalization followed by robust probe-set summarization). For this analysis, as opposed to the core probe set analysis described above, RMA background correction was omitted because it had an empirically undesirable effect on the data, as is now described. RMA background applies a smooth,

monotonic transformation from raw probe intensities to corrected probe intensities (see figure 2.2 for the data-based mapping for a single array).

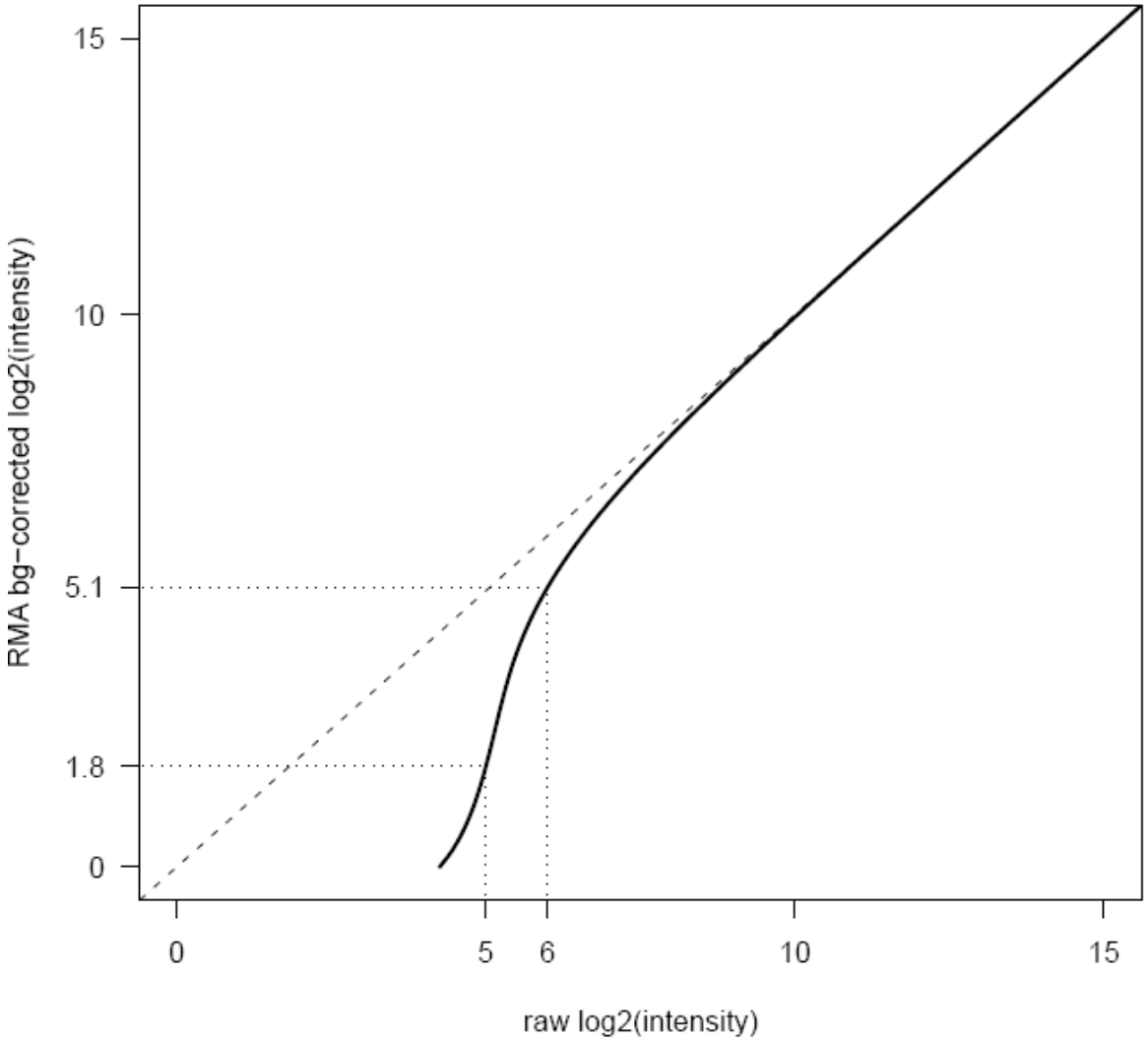

Figure 2.2 Effect of RMA background correction Data-based mapping for a single array. RMA background applies a smooth, monotonic transformation from raw probe intensities to corrected probe intensities. The function is linear for medium-to-high intensities, but tends to stretch out the low-intensity range (the figure is annotated with a two-fold interval that is mapped to a ten-fold interval).

The function is linear for medium-to-high intensities, but tends to stretch out the low-intensity range (the figure is annotated with a two-fold interval that is mapped to a ten-fold interval). Publicly available custom chip-definition files (CDFs)

(http://brainarray.mbni.med.umich.edu/Brainarray/Database/CustomCDF/CDF_download.asp) were used to group probes into sets. Parallel analyses, based on two different CDFs were performed. The first CDF, referred to as ENSG, defines a probe set for each Ensembl gene. The second, ENSE, defines a probe set for each Ensembl exon (see below) (Dai et al. 2005).

There were 21,911 probe sets for the ENSG analysis. At each probe set, a linear model was fit using the limma package, version 2.16.5 (Smyth 2004; Smyth et al. 2005). The fitted model comprises estimates of seven parameters, of which $\gamma_{P1}, \gamma_{P7}, \gamma_{P13}$ are of primary interest, representing case/control differences within a time point. For each γ_t, a p-value was calculated for the t-test of the null hypothesis $\gamma_t = 0$ against the two-sided alternative.

2.14.4 Exon level analysis

2.14.4.1 Splicing Index

At the exon level, core probe sets were PLIER (Probe Logarithmic Intensity Error) normalised in GeneSpring GX 10.1.02 (Agilent). Probe sets that had detection above background (DABG) p-value ≤ 0.05 in both SMA and control groups were retained. An ANOVA test was used to identify significant differences between exon-level signal and transcript level signal. As recommended in the Affymetrix White Paper (Affymetrix 2005; Affymetrix 2009), exon level probe sets exhibiting large exon-to-transcript intensity ratios (i.e. $\log_2$(exon-to-transcript ratio) = $\log_2$(exon expression) -$\log_2$(transcript expression) > 5) were excluded from the ANOVA. This filter removed probes with high background and cross-hybridisation potential. The p-value threshold for the ANOVA was selected to control for a false discovery rate of 0.05 using the Benjamini-Hochberg multiple testing procedure (Benjamini and Hochberg 1995). For exons selected on the basis of the ANOVA,

the splicing index, SI, i.e. the $\log_2$(exon-to-transcript expression ratio), was calculated and used as a measure of differential splicing between genotypes. See (Affymetrix 2005; Affymetrix 2009) for further details. A significantly differentially spliced exon was defined to be one having both an FDR-controlled ANOVA p-value ≤ 0.05 and |SI|≥0.5 (on the log scale, corresponding to a fold change up or down of approximately 1.4 in the exon-transcript ratio between genotypes).

2.14.4.2 Ensembl exon based analysis

In parallel to the Ensembl gene based analysis (see above), a second set of CDF was defined for each Ensembl exon, referred to as ENSE. There were 211,567 probe sets for ENSE, and the analysis was performed as for ENSG

2.14.5 False discovery rate

To assess the number of false positives, a permutation-based analysis was conducted. Each permutation of the data randomly permuted the case/control labels of the subjects within each time point. The data were permuted in this way 200 times. Each permuted data set was statistically analysed in the same way as the actual data set, giving three p-values (one for each time point) for each probe set. For a particular p-value cut-off, the false discovery rate (FDR) was estimated as ratio of number of false positives to number of significant probe sets. P values were chosen as 10^{-4} for ENSE, and 10^{-3} for ENSG, as these choices controlled the FDR at a reasonably low level. Statistical analyses were performed using R (Team 2008), version 2.8.1. The Ensemble gene and exon based analysis was performed by Joanna Davies and Dr. George Nicholson, Department of Statistics, Oxford University.

2.14.6 Pathway analysis

To detect pathways altered between genotypes or time points, genes as defined by core probe sets were sorted according to their gene ontology using GenMAPP's GO-Elite software (http://www.genmapp.org/go_elite/go_elite.html) MAPPFinder ontologies with ≥3 genes changed and a permuted p-value ≤0.05 were selected.

2.14.7 Validation of expression changes

2.14.7.1 Primer design

Gene expression changes identified in the exon-array were validated by RT-PCR and/or quantitative RT-PCR. cDNA sequences of targets were identified in Ensembl release 55 (http://www.ensembl.org/Mus_musculus/Info/Index). For splicing events, differentially expressed exons were identified by comparing probe set IDs with individual Ensembl exon numbers in Ensembl release 49 (http://mar2008.archive.ensembl.org/Mus_musculus/index.html). RT-PCR primers were designed manually to contain 20 or 21 bases, have equal GC content and to contain a 3'GC clamp. For validation of splicing events, primers were designed to flank differentially expressed exons as identified in the ENSE analysis (table 2.8). qRT-PCR primers were designed using Primer Express software and default settings (Applied Biosystems) (table 2.9).

Target	Forward primer 5'-3'	Reverse primer 5'-3'
Uspl1 1-3	CTGTATGCGAAGAAGGAGCG	TTTCGCTCTACAAGCAGGGC
Uspl1 5-10	CTTCAACCGAAGCTTAGATGC	TTCCGAGGCTGATTCTGTGC
Chodl	AGCTCCCAGTTCCGAAACTGG	CCACAGTGTAGACTGATTCGG
Mccc2-201	CAGGAGCTGCAGAACCGAGC	GGGTTACATCCTGAAGATGCC
Mccc2-203	GAGGTGAAGGCAGCTACAGG	AGCGGTAAGATGGGACATCC
Keratin 7	AGCTCCTGAACACCAAGCTGG	CACTGAAGCTCAGAGCATTGC
Cdkn1a	TGGCCTTGTCGCTGTCTTGC	GGCAGCGTATATACAGGAGACG
Wdr21	TGGAAGAGTAGGAGAAGACG	CGAAACAGTACAGGTCCTGC
Snrpa1	TGACAATGAGATCCGGAAACTG	CACCTATACGGCAAATTCTGTTGTT

Table 2.8 Primers used for semi-quantitative RT-PCR

Target	Forward primer 5'-3'	Reverse primer 5'-3'	Cf (nM)
GAPDH	TGTGTCCGTCGTGGATCTGA	CCTGCTTCACCACCTTCTTGA	300/300
Chodl 1-2	GGTCAGTGGTCAAAAGGTGTGTT	AAGCTCACCCGGCTAGACAGT	300/300
Chodl-001 5/6	TGCTTTGGGAACCTGCTGTT	CGGGCTAGTTTTTGATCTTCCTT	900/900
Chodl-002 5/6	GTTTCCAGATGTTGCATAAAAGGA	AGATGATAATGGAGTGGAGTCTTTGA	900/900
Snrpa1	TGACAATGAGATCCGGAAACTG	CACCTATACGGCAAATTCTGTTGTT	300/300
Mccc2	CAGAGCATACAGTCCAAGGTTTCTC	GCCTGCTCTCCTCCCATCA	300/300
Cdkn1	GGCAGACCAGCCTGACAGAT	TTCAGGGTTTTCTCTTGCAGAAG	300/300
Uspl1-2	AGAGGAGTTCGGGTCCACTGT	CAATGAACCCCTCCCGAAGT	300/300
Uspl1 9-10	CTTCCATGCATGAAGCCAAA	GGCAGCAACTGTGTCTGAGAGT	900/900
ChAT	AATGGCGTCCAACGAGGAT	CGGTTGGTGGAGTCTTTTAAGAG	300/300
mTardbp	TCCCCTGGAAAACAACAGAG	CCAGACGAGCCTTTGAGAAG	900/900

Table 2.9 Primers used for Fast SYBR Green qRT-PCR Final primer concentration, Cf.

2.14.7.2 RT-PCR

One µg of RNA was reverse transcribed into cDNA using Expand Reverse Transcriptase (Roche), Random Hexamer primers (Applied Biosystems) or oligodT primer (Invitrogen) in 20 µl reactions. cDNA was diluted 1:5, and 5 µl were used as RT-PCR template. Expand High Fidelity PCR system (Roche) was used in the PCR step using the following cycling conditions:

Step	Temperature	Duration
Initial denaturation	95°C	2 mins
Denaturation	95°C	15 secs
Annealing	56°C	30secs x10
Elongation	72°C	45 secs
Denaturation	95°C	15 secs
Annealing	59°C	30 secs x15
Elongation	72°C	45 secs +5 secs/cycle
Final elongation	72°C	7 mins

PCR products were visualised on 1.5% agarose gels with SafeSYBR DNA stain (Invitrogen).

2.14.7.3 qRT-PCR

Real-time PCR was performed using Fast SYBR Green chemistry (Applied Biosystems) and a StepOnePlus Real-time PCR machine (Applied Biosystems). Primer concentrations were optimised to yield low Ct values and minimal primer dimer formation. The effect of primer concentration was assessed by performing triplicate reactions for combinations of forward and reverse primer concentrations of 50nM, 300nM and 900nM, respectively. Primer dimer formation, as well as non-specific amplification, was assessed by scrutinizing the melt curve analysis for additional peaks and visualising PCR product on 2.5% agarose gels.

Reactions were cycled as follows:

Step	**Temperature**	**Duration**		
Initial denaturation	95°C	10	min	
Denaturation	95°C	3	secs	
Annealing/elongation	60°C	30	secs	x40

Glyceraldehyde 3-phosphate dehydrogenase (Gapdh) was chosen as the endogenous control because it was published as a suitable endogenous control in qRT-PCR experiments on spinal cord of the same mouse model used here (Zhang et al. 2008) and was not shown to be differentially expressed in the array data. In addition, Ct values for Gapdh between SMA and control mice were compared and found not to differ (independent sample two tailed t-test) (table 2.10):

Time point/ Average Ct value	**Control**	**SMA**	**P**
P1	18.6439	18.4603	0.121
P7	18.1347	17.935	0.391
P13	18.6580	18.7037	0.53.9

Table 2.10 Gapdh Ct values for SMA and control P value of t-test between genotypes

After optimising primer concentration, primer efficiency was assessed by performing qPCR reactions on serial, 4 log dilutions of cDNA. Primer efficiency was estimated as

$$E = (10^{-\frac{1}{slope}} - 1) \times 100$$

where *slope* is the slope of the linear regression line fitted through the mean Ct values plotted against the log cDNA input (figure 2.3 A, B).

Primer efficiencies of different targets were compared by plotting mean Ct values against cDNA input, as well as plotting the Delta Ct values against log cDNA input and observing a slope of a fitted line to be smaller than 0.1.

Primers were considered unsuitable when this slope was larger than 0.1.

Relative expression was calculated using the ΔΔCt method, where

$\Delta C_T = C_{T\ target} - C_{T\ GAPDH}$ and

$\Delta\Delta C_T = \Delta C_{T\ sample} - \Delta C_{T\ calibrator}$

where “calibrator” is the first control sample. Four biological and four technical replicates were used in every experiment. At P13, an additional four animals per genotype were used for array validation to rule out litter specific effects. Relative expression was then displayed as the mean expression of four biological replicates per genotype plus the standard deviation of the mean. Significance was tested using an unpaired two-tailed t-test in Microsoft Excel (figure 2.4).

A

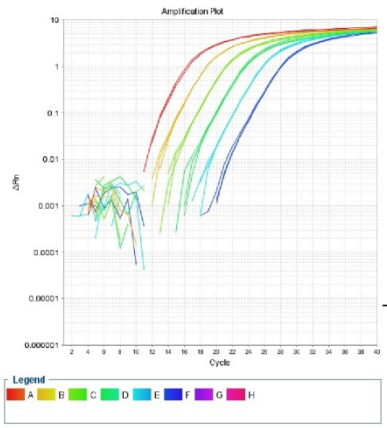

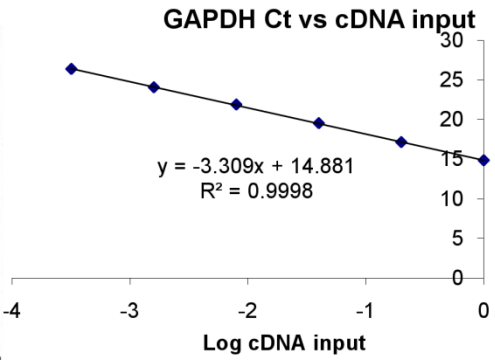

$E=(10^{-1/-3.309}-1)x100=100.5424$

B

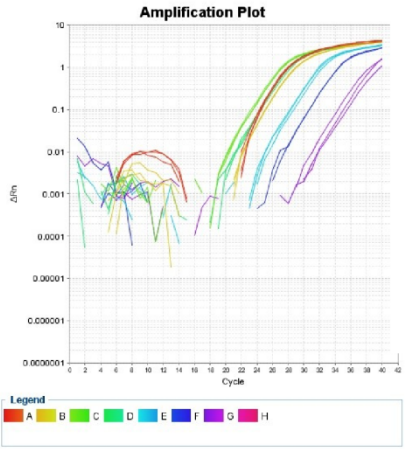

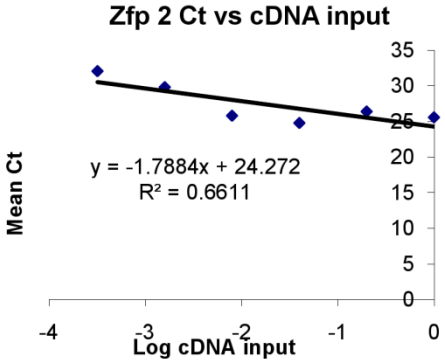

$E=(10^{-1/-1.7884}-1)x100= 262.3757$

C

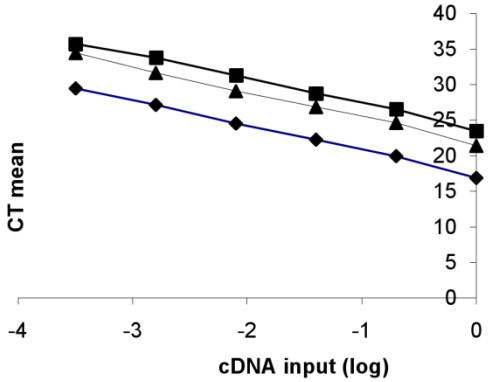

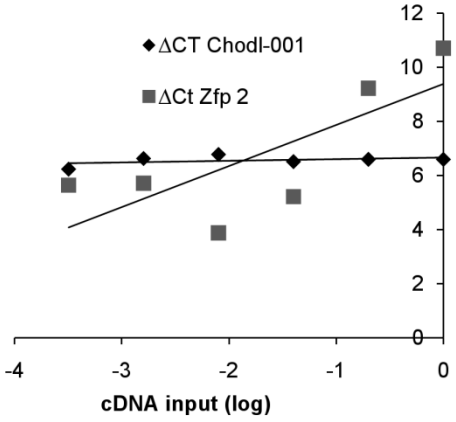

Figure 2.3: qRT-PCR primer validation (A) Amplification plot of ΔRn versus cycle for GAPDH dilution series (different colours) showing increasing cycle number with every cDNA dilution. When Ct values are plotted against log cDNA input, the linear regression shows a high R^2 value and a slope of -3.309, corresponding to a primer efficiency of 100%. (B) Primers used to amplify Zfp2 are unsuitable for the ΔΔCt method – the amplification plot shows that decreasing template concentration leads to unpredictable changes in Ct value, the R^2 value is low and the primer efficiency artificially high. (C) Three primer pairs with equal efficiency have identical slopes (left) and can be used for the ΔΔCt method. When plotting the ΔCt values for two primer pairs against cDNA input, Chodl-001 shows a slope of 0.06, indicating almost identical primer efficiency to GAPDH, whereas Zfp2 ΔCt values show no correlation with cDNA input in keeping with (B).Primers for Zfp2 had to be discarded.

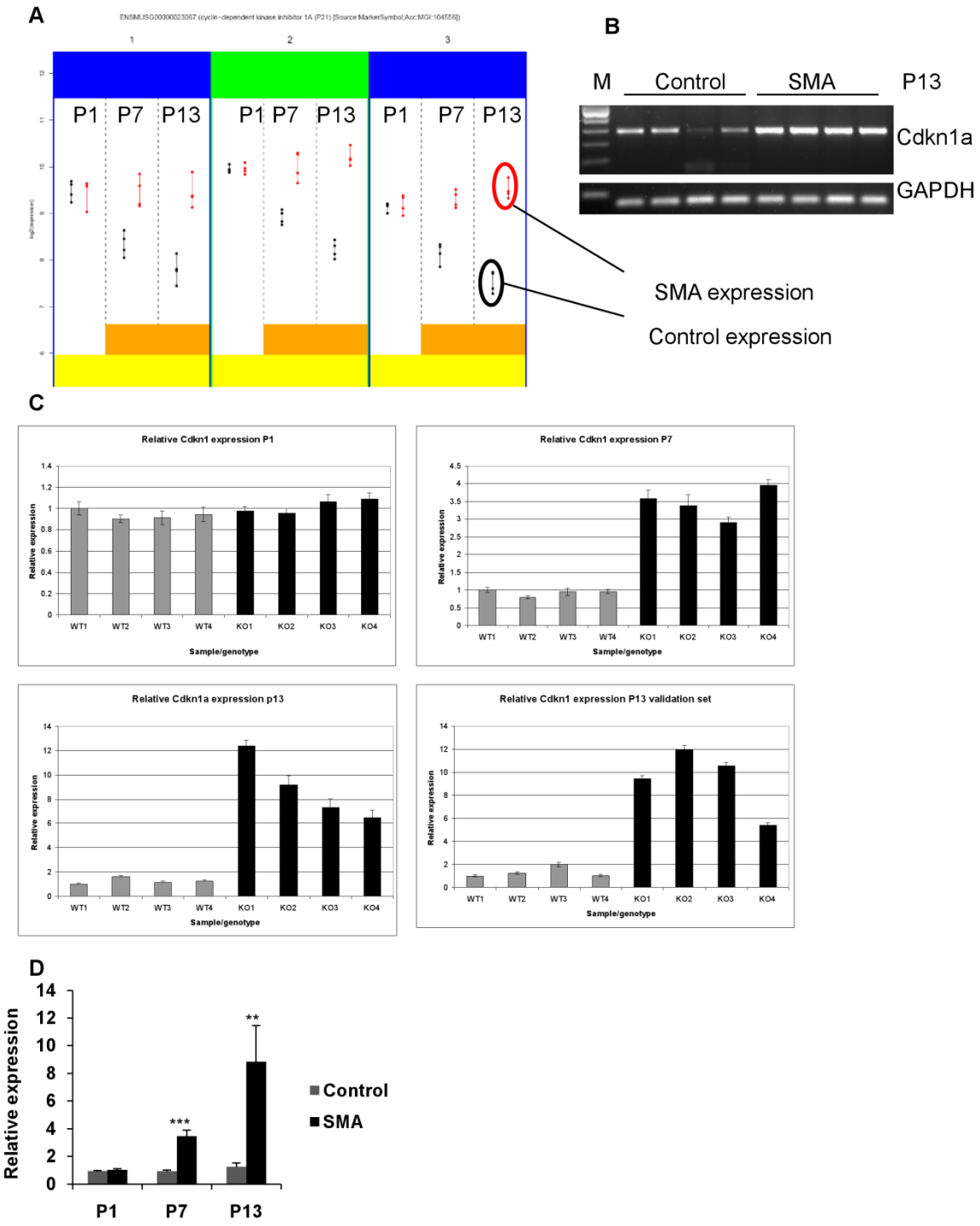

Figure 2.4: Exon array validation by semi-quantitative and quantitative RT-PCR (A) Example of graphical output for the ENSE analysis for Cdkn1a. Each column, delineated by bold black lines, corresponds to the pre-processed data from a single Ensembl exon. The vertical axis displays $\log_2$ expression for control (black) and SMA (red) animals, with each point corresponding to an individual animal. Each column is subdivided by vertical dashed lines into time points P1, P7, and P13 (left to right). Orange boxes mark those (exon, time point)

combinations that exhibit significant differential expression between cases and controls. Progressively Increasing expression of all three Cdkn1a exons is shown. (B) Semi-quantitative exon boundary spanning RT-PCR for Cdkn1a and GAPDH (M=100 base pair ladder) is in keeping with array finding at P13 and does not show any splice variants. (C) qRT-PCR results for P1, P7, P13 and a second set of animals at P13 was performed for four biological replicates, and data were then displayed as in (D), where **=$p<0.01$ and ***=$p<0.001$ in an unpaired two tailed t-test.

3 Candidate gene approach to SMA and ALS

3.1 Introduction

The genetic basis of motor neuron disorders is incompletely understood. Only a minority of causative genes have been identified in families with autosomal dominant ALS or distal dominant SMA, despite clear Mendelian inheritance. The vast majority of ALS cases occur without a family history, but are likely to have at least a strong genetic contribution ((Graham et al. 1997; Simpson and Al-Chalabi 2006; Schymick et al. 2007b)(chapter 1). The assumption for the work in this chapter is that this genetic contribution is largely in the form of rare variants and low penetrance mutations, which are difficult or impossible to detect in genome wide association studies (see chapter 1), and require a candidate gene approach for identification.

Four candidate genes were chosen for the purpose of this work. The first gene, *FVT1,* is implicated in motor neuron disease in cattle (see section 3.1.1.2) and is a novel candidate for human motor neuron disorders. Mutations in the other three genes, *ANG*, *FUS* and *TARDBP* have recently been described in patients with both familial and sporadic ALS. They were chosen because the spectrum of mutations is incompletely understood, and because they appear to be functionally involved in related pathways of RNA metabolism, which will be a further focus of this thesis.

3.1.1 FVT1

3.1.1.1 The FVT1 gene

FVT1 (follicular variant translocation protein 1 (ENSG00000119537)) is a 39 kb gene located on the minus strand of chromosome 18q21. The gene is located 5' to

the proto-oncogene BCL-2, which is frequently involved in translocation events in Non-Hodgkin lymphomas. The name is derived from its identification as a new gene in a translocation event with atypical break points in a follicular lymphoma (Rimokh et al. 1993).

FVT1 encodes the 332 amino acid, 36 kDa 3-ketodihydrosphingosine reductase precursor protein that is widely expressed in various tissues including the central nervous system (AceView ; EntrezGene). The mature protein functions as a pivotal enzyme in the sphingolipid metabolism. It catalyses the reduction of 3-ketodihydrosphingosine (KDS) to dihydrosphingosine, in the second step of the *de novo* sphingolipid synthesis pathway. In keeping with this function, it is localised to the endoplasmatic reticulum (Kihara and Igarashi 2004).

3.1.1.2 The involvement of FVT1 in bovine SMA

A disease similar to human spinal muscular atrophy occurs as a recessive trait in cattle (Nielsen et al. 1990; Pumarola et al. 1997). Red Danish, Horned Hereford, Holstein-Friesian and Swiss Brown cattle calves are affected by early onset motor neuron disorders with some subtle phenotypic differences (el-Hamidi et al. 1989; Stocker et al. 1992; Troyer et al. 1993; Pumarola et al. 1997). The neuropathology of bovine SMA is characterised by swollen or chromatolytic anterior horn cells with neurofilament accumulation, anterior horn cell loss and the presence of empty cell beds, thinning of the anterior roots and neurogenic muscle atrophy. Calves die a few weeks after birth of bronchopneumonia and respiratory muscle weakness. In addition to the lower motor neuron involvement, there is also a degree of upper motor neuron disease (Troyer et al. 1992).

Bovine SMA, together with two other autosomal recessive neurological diseases, progressive degenerative myeloencephalopathy and spinal dysmyelination, creates an immense disease burden in an increasingly inbred cattle population, which has led to efforts to map the disease (Medugorac et al. 2003). Given the striking resemblance to human SMA, initial mapping focussed on regions carrying the bovine orthologue of human *SMN* on bovine chromosome BTA 20 (Pietrowski et al. 1998), but linkage to this region was excluded (Pietrowski et al. 1999; Medugorac et al. 2003). A whole genome scan established linkage to BTA 24 (Medugorac et al. 2003) and further fine mapping with additional markers established a region containing three genes, *FVT1*, *BCL2* , and *VPS4B*. Of these, only *BCL2* and *VPS4B* were regarded as plausible candidate genes for SMA, given a putative interaction of BCL2 with SMN (Iwahashi et al. 1997), the motor neuron loss observed in *Bcl2* knockout mice (Michaelidis et al. 1996), and the functional role of VPS4B in the endosomal sorting complex required for transport (ESCRT III), dysfunction of which has been linked to hereditary spastic paraplegia and recessive ALS (Krebs et al. 2006). However, involvement of *BCL2* in bovine SMA was excluded by extensive sequence analysis, and the development of additional SNP and microsatellite markers established linkage to *FVT1,* followed by identification of a G to A transition in the *FVT1* coding region in affected animals *(Krebs et al. 2007).* The mutation leads to an alanine to threonine substitution in an evolutionary conserved residue in the cytosolic domain close to a substrate binding serine residue (Kihara and Igarashi 2004; Krebs et al. 2007). The protein carrying the A175T mutation showed reduced KDS reductase activity in an *in vitro* assay, but was still able to rescue the deletion of the yeast *FVT1*

homologue *in vivo*, suggesting that residual function is maintained by the mutant protein (Krebs et al. 2007).

The high degree of similarity between human and bovine SMA make *FVT1* an excellent candidate gene for mutation screening in patients with SMA and no causative SMN mutations.

3.1.2 ANG

Angiogenin (*ANG* (ENSG00000214274)) is a 10kb gene located on the plus strand of chromosome 14q11.2. It shares two 5' untranslated exons with another gene, RNase 4.

Angiogenin encodes a 147 amino acid, 16.5 kDa protein containing an N-terminal 24 amino acid signal peptide that is cleaved to result in a mature protein with ribonuclease A activity. The ribonuclease activity is thought to be tRNA specific (Saxena et al. 1992), thereby contributing to translational arrest and reduced protein synthesis, particularly under conditions of cell stress, indicating that angiogenin might play a role in cellular stress response pathways (Yamasaki et al. 2009).

Angiogenin is a secreted protein that is taken up by cells via receptor mediated endocytosis followed by nuclear import mediated by a nuclear localisation signal (Xu et al. 2002). In the nucleus, angiogenin can stimulate transcription of ribosomal RNA (rRNA), but may have more widespread functions in transcription regulation by binding to CT repeat elements (Xu et al. 2003). At organ level, angiogenin is best characterised functionally for its role in angiogenesis (Strydom 1998).

Angiogenin evolved as a candidate gene for ALS through a combination of genetic studies showing allelic association with a SNP marker on 14q11 (Hayward et al. 1999; Greenway et al. 2004), and theoretical considerations based upon the functional similarity between angiogenin and another angiogenic protein, vascular endothelial growth factor, VEGF. Deletions in the *VEGF* promoter cause a motor neuron disease-like phenotype in mice (Oosthuyse et al. 2001), and an association between certain haplotypes of the *VEGF* promoter region were shown to be associated with ALS (Lambrechts et al. 2003). The identification of *ANG* as a candidate gene was closely followed by the demonstration of altered serum levels of angiogenin in ALS patients (Cronin et al. 2006). Several groups have now reported missense mutations in *ANG* in patients with both familial and sporadic ALS. Known mutations are summarised in table 3.1.

Base position	**Amino acid position**	**Disease**	**Author**	**N (cases)**	**N (control)**
A191T	K40I	SALS	(Greenway et al. 2004)	169	171
A107T	Q12L	SALS	(Greenway et al. 2006)	1629	1264
A122T	K17I	SALS			
A121G	K17E	SALS			
G164A	R31K	SALS			
C189G	C39W	FALS			
A191T	K40I	SALS			
A208G	I46V	FALS			
A208G	I46V	SALS Control	(Corrado et al. 2007)	262	415
G155A	S28N	SALS	(Wu et al. 2007)	298	0
C58T	P-4S	SALS			
A122T	K17I	SALS			
C407T	P112L	SALS			
G3A	M1I	SALS	(Conforti et al. 2008)	163	332
None	None	SALS	(Del Bo et al. 2008)	210	306
G3A	M-24I	SALS	(Gellera et al. 2008)	737	515
T35C	F-13S	SALS			
T61C	P-4S	SALS			

C132T G409A A413A Gg446T	G20G V113I H114R NA	SALS SALS SALS SALS			
A208G G434A	I46V R121H	SALS SALS	(Paubel et al. 2008)	855	232
A122T	K17I	FALS-FTD	(van Es et al. 2009a)	39 unrelated FALS	275

Table 3.1 Summary of genetic studies on *ANG* in ALS. A total of 4362 ALS patients were screened for ANG mutations, yielding 20 different protein changing mutations that were absent in 3510 controls, with the exception of I46V, which was also found in 2 healthy Italian controls.

Overall, the *ANG* mutation frequency is low (0.6% in reported cases). A synonymous SNP rs11701 has been shown to be associated with ALS in Irish and Scottish patients (Greenway et al. 2004; Greenway et al. 2006), but not in patients from England, Sweden, the USA (Greenway et al. 2006), Italy (Conforti et al. 2008; Del Bo et al. 2008; Gellera et al. 2008) or France (Paubel et al. 2008).

Characterisation of angiogenin mutants has shown that most mutations have reduced ribonuclease activity in functional assays, which is accompanied by a reduction in their angiogenic potential (Crabtree et al. 2007; Wu et al. 2007). Overexpression of wild-type, but not mutant, angiogenin in primary neuronal culture as well as neuronally differentiated cell lines was shown to have a protective effect on cells against a variety of insults, while various angiogenin mutations have been shown to be cytotoxic and lead to reduced neurite outgrowth (Kieran et al. 2008; Subramanian et al. 2008). At present it is unknown how the diverse molecular functions of angiogenin, including ribonuclease activity and transcriptional activation, are related to disease pathogenesis.

Little is known about the pathology of *ANG* related ALS. An unusual autopsy case of rapidly progressive ALS (with unknown family history) characterised by tau negative, ubiquitin positive intranuclear eosinophilic inclusions in neuronal cells (Seilhean et al. 2004) was later found to be positive for the ANG K17I mutation (Seilhean et al. 2009). The neuropathology was characterised by p62 positive, TDP-43 negative neuronal intranuclear inclusions that stained positive for smooth muscle alpha-actin (smA), as well as TDP-43 and p62 positive neuronal and glial cytoplasmic inclusions. Both nuclear and cytoplasmic inclusions were negative for alpha-synuclein and tau, but also for angiogenin. The significance of the smA positive inclusions could be related to the role of smA as a cell surface protein important in the endocytosis of angiogenin (Hu et al. 1993). It remains to be seen whether the features described in this case are specific for ALS caused by *ANG* mutations.

3.1.3 FUS

FUS (ENSG00000089280) (fusion (involved in t(12;16) in malignant liposarcoma) is a 11.6 kb gene located on the forward strand of chromosome 16p11.2. The locus is complex and gives rise to 6 splice variants in a conservative estimate (Ensembl), although more than 25 mRNAs have been described in cDNA libraries (Aceview)(Thierry-Mieg and Thierry-Mieg 2006).

FUS encodes a widely expressed 526 amino acid, 53 kDa nuclear protein containing a RNA binding domain (Aman et al. 1996). Together with the EWS and TAF 15 proteins, it belongs to the FET group of RNA binding proteins (Bertolotti et al. 1996). It was first described as part of a fusion gene with the negative transcription factor CHOP resulting from a translocation event in malignant myxoid liposarcoma (Crozat et al. 1993; Rabbitts et al. 1993). In the fusion protein, the

FUS RNA binding domain is replaced by the DNA binding domain of CHOP (Crozat et al. 1993). Another translocation event involving *FUS* and *ERG* is implicated in myeloid leukaemia (Ichikawa et al. 1994), and several other translocation events in cancers have been described that involve FUS (Storlazzi et al. 2003; Goransson et al. 2005)

The FUS C-terminal domain contains a RNA recognition motif (RRM) surrounded by Arg-Gly-Gly (RGG) repeats. In addition, it contains a zinc finger domain with RNA binding properties (Iko et al. 2004) (figure 3.3). In interspecies heterokaryon assays, where human and mouse cells are merged in the presence of cycloheximide, thus blocking new protein synthesis, human FUS can be demonstrated in mouse nuclei, demonstrating the shuttling of the protein between the nucleus and the cytoplasm (Zinszner et al. 1997). Nucleo-cytoplasmic shuttling is a feature that FUS shares with many hnRNPs (Pinol-Roma and Dreyfuss 1992).

FUS interacts with and modulates the function of several splicing factors (Yang et al. 1998a; Meissner et al. 2003; Sato et al. 2005), which it binds via its C-terminal domain (Yang et al. 2000). In the cytoplasm, FUS has been identified as part of RNA transport granules in mouse brain (Kanai et al. 2004) and as part of the NMDA receptor protein complexes in neuronal dendrites (Husi et al. 2000). It is localised to dendritic spines in hippocampal pyramidal cells dependent upon metabotropic glutamate receptor stimulation (Kanai et al. 2004; Fujii et al. 2005; Yoshimura et al. 2006). These reports indicate that FUS has a role beyond splicing in mRNA transport and local protein translation control in neuronal compartments (see chapter 1).

FUS was identified as an ALS candidate gene through a linkage study of a large British family with ALS identifying a 42Mb region on chromosome 16 (Ruddy et al. 2003) that was further refined to a haplotype containing 400 genes when more affected family members were included (Vance et al. 2009). A mutation in *FUS* (1561 C>T, R521C) was identified in all affected family members after this gene was prioritised for sequencing because of its similarity to the recently discovered TDP-43. At the same time, Kwiatkowski et al reported 15 mutations in *FUS* patients with familial ALS (Kwiatkowski et al. 2009). Interestingly, the genetic approach in this study was based on loss of heterozygosity mapping in a family of Cape Verdean origin with a potentially autosomal recessive pedigree. Linkage was established to chromosome 16 and a recessive *FUS* mutation was found. Further *FUS* mutations were then identified in 2 families with linkage to chromosome 16, as well as in 15 other families without prior knowledge about linkage (Kwiatkowski et al. 2009). A summary of FUS mutations described is given below in table 3.2. Of note, one report identified a FUS mutation in a patient with pure frontotemporal dementia (Van Langenhove et al.)

Base position	**Amino acid position**	**Disease**	**Author**	**N (cases)**	**N (control)**
1561C>T	R521C	FALS	(Vance et al. 2009)	198	400
1562G>A	R521H	FALS			
1540A>G	R514G	FALS			
C1551G	H517Q	FALS (AR)	(Kwiatkowski et al. 2009)	84 FALS 293 SALS	1446
C1561G	R521G	FALS			
insGAGGTG523	insGG	FALS			
del GAGGTG523	delGG	FALS			
C730T	R244C	FALS			
G1542T	R514S	FALS			
G1543T	G515C	FALS			
C1561T	R521C	FALS			
C1561G	R521G	FALS			
G1562A	R521H	FALS			

A1564G G1571C G1572C C1574T	R522G R524T R524S P525L	FALS FALS FALS FALS			
G1542C GC1547T G15566A	R514S P525L Synonymous	FALS FALS FALS	(Chio et al. 2009a)	52 FALS	280
C169_171delTCT 1561C>T 1562G>A c188A>G C676_684delGGCGGCGGC C684_685GGC	S57del R521C R521H N63S G226_G228del G228_G229insG	SALS SALS FALS,SALS SALS, controls SALS, control Schizophrenia/autism	(Belzil et al. 2009)	80 FALS 120 SALS 285 SALS (exon 15 only)	190 age matched healthy controls 285 schizophrenia/autism
G571A C646T G674T G676A G688T C700T G1520A C1561T	G191S R216C G225V G226S G230C R234C G507D R521C	FALS SALS SALS Control SALS SALS SALS FALS	(Corrado et al. 2009a)	45 FALS 964 SALS	500 healthy controls
G467A	G156E	FALS	(Ticozzi et al. 2009)	94 FALS	376 healthy controls
G701T	R234L	FALS			
C1561T	R521C	FALS			
C1561G	R521G	FALS			
G1562A	R521H	FALS	(Damme et al. 2009)	28 FALS	-
c.760A>G	M254V	FTLD	(Van Langenhove et al.)	122 FTLD 47 ALS 15 FTD-ALS	180 healthy controls
G1562A	R521H	FALS			

Table 3.2 Summary of genetic studies on FUS in ALS

The majority of mutations are located in the C-terminal domain of FUS, encoded by exons 14 and 15 (see figure 3.3). In addition, a few variants were identified in exon 6. These variants included changes found in healthy controls as well as a number of small deletions or insertions in repetitive poly-glycine tracts known to be polymorphic in the human population (Corrado et al. 2009a).

Four cases of FUS related ALS were submitted to autopsy (Kwiatkowski et al. 2009; Vance et al. 2009). There was a paucity of the typical ubiquitin positive inclusions, and no TDP-43 pathology was found. One case demonstrated increased cytoplasmic FUS immunoreactivity, and the other three cases contained FUS positive cytoplasmic inclusions.

3.1.4 TARDBP

TARDBP (*TAR* DNA binding protein, TDP-43) (ENSG00000120948) is a 12.8 kb gene located on the forward strand of chromosome 1. *TARDBP (TDP-43)* is ubiquitously expressed and highly conserved (Ayala et al. 2005) and encodes a 414 amino acid, 43 kDa nuclear protein. It was initially identified in a screen for binding proteins of the HIV1 *TAR* sequence and was shown to repress HIV transcription *in vitro* (Ou et al. 1995). In addition, it was well characterised as a nuclear protein involved in splicing regulation of the cystic fibrosis transmembrane conductance regulator (CFTR) gene (Buratti and Baralle 2001; Buratti et al. 2001; Buratti et al. 2004) as well as other genes containing a (UG)n repeat (Mercado et al. 2005; Acharya et al. 2006) (chapter 1).

TDP-43 became relevant for ALS with the landmark discovery in two independent proteomic studies of human post mortem material in 2006 that it is the major protein constituent of ubiquitinated neuronal inclusions in ALS and FTLD (Arai et

al. 2006; Neumann et al. 2006). The initial skepticism with regard to the aetiological role of TDP-43 in ALS (Rothstein 2007) was strengthened by early genetic studies of patients with both ALS and FTLD that did not identify mutations or copy number variation in *TARDBP* (Gijselinck et al. 2007; Rollinson et al. 2007; Schumacher et al. 2007). A series of publications identifying *TARDBP* mutations in 2008 changed this view, however. Gitcho et al demonstrated segregation with disease of the A315T mutation in a family with ALS (Gitcho et al. 2008). Sreedharan and colleagues identified a locus on chromosome 1 containing *TARDBP* in a genome wide scan of a British family with ALS (Sreedharan et al. 2008), and ruled out other regions of linkage. Sequencing of *TARDBP* in this family then revealed a mutation that segregated with disease. This study showed unequivocally that *TARDBP* mutations can be the genetic cause of ALS. Further *TARDBP* mutations have since then been identified in patients with both familial and sporadic ALS of European, North American and Chinese descent, including the study described in this chapter. Published mutations in *TARDBP* are summarized in table 3.3 below.

Base position	**Amino acid position**	**Disease**	**Author**	**N (cases)**	**N (control)**
Negative study (sequencing, copy number, SNP association study)		FTD/SALS	(Gijselinck et al. 2007)	173 FTD 237 SALS	459
Negative association study		FTD	(Rollinson et al. 2007)	259 FTD	286
Negative single SNP and haplotype association study		FTD	(Schumacher et al. 2007)	194 FTD	184
C1077G>A	A315T	FALS	(Gitcho et al. 2008)	8 families ALS 5 families FTLD-MND 25 families FTLD-U	1505 (RsaI digest)
A1028G	Q343R	FALS	(Yokoseki et al.	16 FALS	267

			2008)	112 SALS	(digest)
1009A>G 991 C>A 881G>C	M337V Q331K G294A	FALS SALS SALS	(Sreedharan et al. 2008)	154 FALS 372 SALS	872
1077G>A 1278G>A 640A>T 993G>A 1176G>T 1217G>T 1302A>G 1303A>G 945G>A	A315T A382T D169G G287S G348C R361S N390D N390S A315A A66A A90V	FALS FALS SALS SALS SALS SALS SALS SALS SALS FALS Control	(Kabashi et al. 2008b)	180 FALS 120 SALS	360
869G>C 892G>A	G290A G298S	FALS FALS	(Van Deerlin et al. 2008)	104 FALS 108 SALS 47 FTD	1127
c269C>T	A90V	FTLD-ALS, control	(Winton et al. 2008b)	148 FTLD	1385
c198C>T	A66A	SALS, control	(Guerreiro et al. 2008)	279 SALS	979
C945G>A	A315A D65E A90V P225P N352N	control control control control control			
1176G>T 1189A>G	G348C N352S	FALS FALS	(Kuhnlein et al. 2008)	31 FALS 134 SALS	400
c.198C>T c.1009A>G c.1035C>A c.1147A>G	A66A M337V N345K I383V	ALS FALS FALS FALS	(Rutherford et al. 2008)	92 FALS 24 SALS 180 other (FTD, AD, LBD)	185 640 (Taqman)
1176G>T 1226C>G	G348C P363A	SALS SALS	(Daoud et al. 2008)	285 SALS	360

1255_1256insA	Y374X	SALS			
1278G>C	A382P	SALS			
C198C>T	A66A	SALS			
*1462T>C	NA	SALS			
800A>G	N267S	SALS	(Corrado et al. 2009b)	541 SALS 125 FALS	771
859G>A	G287S	SALS			
881G>T	G294V	FALS			
883G>A	G295S	SALS			
883G>C	G295R	SALS			
995G>A	S332N	FALS			
1009A>G	M337V	FALS			
1004G>A	G335D	SALS			
1135T	S379P	FALS			
1136C>G	S379C	SALS			
1144G>A	A382T	FALS/ SALS			
1178C>T	S393L	SALS			
931A>G	M311V	FALS	(Lemmens et al. 2009)	31 FALS families	601
881G>T	G294V	SALS	(Del Bo et al. 2009)	16 FALS 298 SALS	181
883G>A	G295S	SALS			
1144G>A	A382T	FALS			
1042G>T	G348C	FALS			
945G>A	A315A	FALS (but absent in affected relative!	(Benajiba et al. 2009)	71 familial FTD-MND 78 sporadic FTD-MND	400
c.*1453G>A	NA (3'UTR)	Familial FTD-MND, controls			
883G>A	G295S	Familial and sporadic FTD-MND			
	K263E	FTD and	(Kovacs et al.	Case	530

		chorea	2009)	report	
2076G>A	3'UTR	FTD-U	(Gitcho et al. 2009)	Case report	982
C800A>G	N267S	FTD	(Borroni et al. 2009)	Case report	106
1-562T>C		SALS	(Luquin et al. 2009)	46 SALS (Brain DNA)	115
1-100C>T		SALS, control			
170C>T	N12N	SALS			
198C>T	A66A	SALS, control			
881G>C	G294A	SALS			
1178C>T	S393L	FALS	(Origone et al. 2009)	20 FALS 27 SALS 70 FTD	158
859G>A	G287S	SALS	(Kirby et al. 2009)	42 FALS 9 ALS-FTD 474 SALS 45 PMA	499
962C>T	A321V	SALS			
1009A>G	M337V	FALS			
1043G>T	G348V	FALS			
269C>T	A90V	SALS, control			
-69C>T	5'UTR	SALS			
-66G>T	5'UTR	SALS			
-12-54G>A	Intron 1	SALS			
81G>A	L27L	FALS			
198T>C	A66A	SALS			
312C>T	S104S	SALS			
411A>G	L137L	SALS			
403-80G>A		SALS			
543+112C>A		SALS			

Table 3.3 Summary of genetic studies on *TARDBP* in ALS

Several general remarks can be made about *TARDBP* mutations. Mutations have been identified in both familial and seemingly sporadic cases of ALS, implying reduced penetrance for some mutations. They occur in patients with ALS, MND-FTD and also, albeit less commonly, in seemingly pure FTD without any evidence

of motor involvement, thus strengthening the assumption that ALS is a spectrum disorder that includes pure motor neuron disorders on one side, but also pure dementia on the other side. Apart from a generally earlier age of onset, no distinctive clinical phenotype has emerged to be associated with *TARDBP*, and early speculation that lower motor neuron involvement might be more prominent, and that cognitive impairment is absent, have been premature in the light of more recent reports. Almost all mutations are located in exon 6 of the gene, which encodes the C-terminal, glycine rich domain of the protein, implying a common disease mechanism. Protein changing genetic variation is virtually absent in this exon in healthy controls. Exceptions to this clustering in exon 6 are the D169G mutation in exon 4 detected in a patient with SALS (Kabashi et al. 2008b) as well as the interesting report of a rare variant in the 3'UTR that was shown to lead to allele specific increased expression of *TARDBP* mRNA in a patient with FTLD (Gitcho et al. 2009).

3.2 Results

3.2.1 FVT1 mutation screen

3.2.1.1 Patient Identification

A panel of patient DNAs was assembled consisting of patients with a variety of different motor neuron disorders without known genetic cause. Given the limitations of extrapolating disease phenotypes across species barriers, disorders other than classical SMA were included in the *FVT1* screen. The panel comprised patients with familial and sporadic ALS, proximal non-5q SMA, distal SMA and other pure motor neuron disorders (table 3.4). Phenotypically classical SMA patients had previously been screened for SMN deletions and mutations. Patients

with familial ALS were screened for mutations in *SOD1* by direct sequencing, which revealed one case with the I113T mutation, which was excluded from the screen.

Disorder	Number of DNA samples
Distal dominant SMA	45
Distal sporadic SMA	9
Non-5q recessive SMA	6
Sporadic SMA	20
Sporadic ALS	98
Familial ALS	13
Primary lateral sclerosis	8
Other pure motor neuron disorders	16
Total	215

Table 3.4 Overview of patients included in the *FVT1* screen

3.2.1.2 WAVE screen

Principles and methods of the DHPLC screening are described in chapter 2. Briefly, PCR products spanning all 10 *FVT1* exons and splice sites were denatured and reannealed to allow formation of homo- and heteroduplexes. Samples were then injected into a WAVE cartridge containing beads with an affinity for double stranded DNA fragments. In the following elution step, DNA heteroduplexes with mismatched base pairs eluted off the cartridge first, allowing the differentiation of these fragments by a UV detector in form of a chromatogram. Samples with abnormal elution patterns were examined by direct sequencing.

Several sequence variants were identified by sequencing samples with abnormal peak patterns. These included 4 novel intronic SNPs (ss86236577, intron 3, ss86236578, intron 5, ss86236579, intron 8, ss86236580, intron 9) as well as the previously reported non-protein changing SNPs rs2003149 and rs1809319, which are located in exon 4 and intron 4, respectively. No protein changing variants or

splice site changes were detected. No variants were present in the amplicon of exon 6, which harbours the A175T mutation in cattle with SMA.

3.2.1.3 PCR-RFLP and SNP genotyping

SNPs rs2003149 and rs1809319 are also present on the HapMap SNP chip set (International HapMap 2003) and therefore allowed direct comparison of allele frequencies in this patient panel to those published for the HapMap CEU panel of 30 mother-father-child Utah resident trios with ancestry from northern and western Europe (Table 3.5). Due to the close proximity of rs2003149 and rs1809319 (160 base pairs), samples were screened for genotype frequency of rs2003149 only. SNP rs2003149 is a synonymous coding SNP in exon 4 and could be typed by a restriction enzyme digest assay using RsaI.

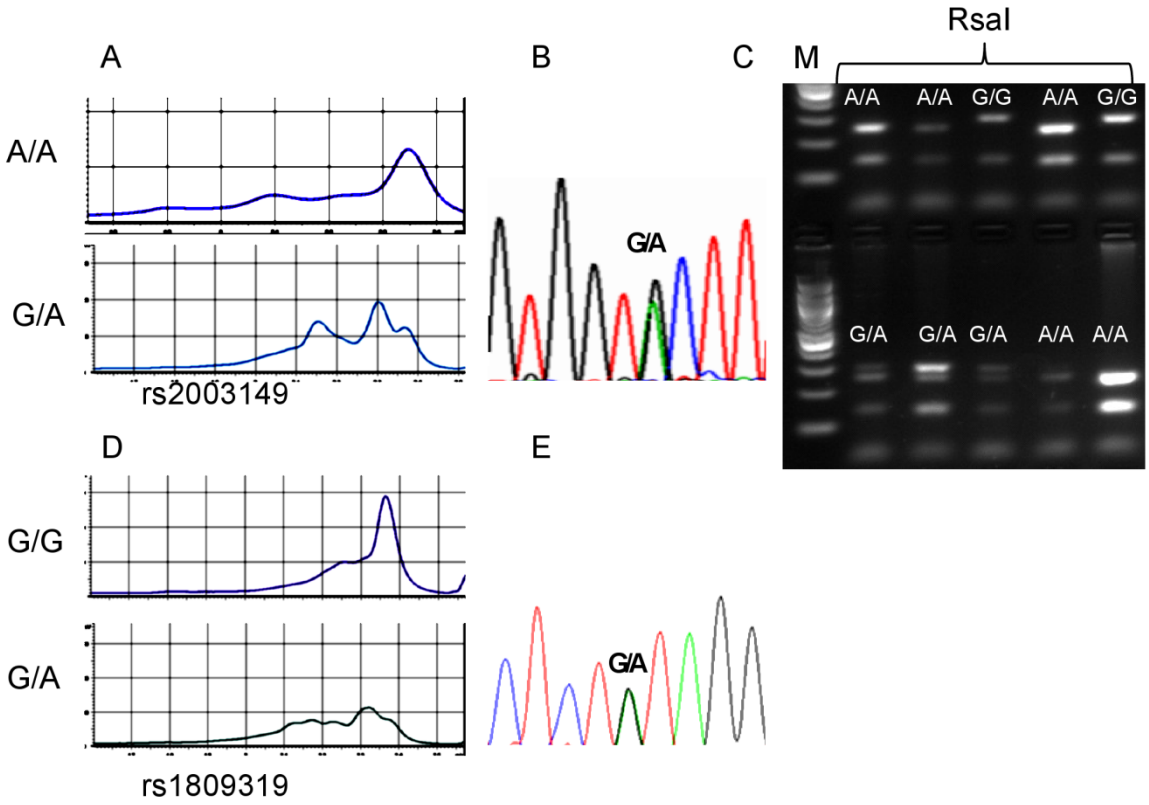

Figure 3.1 DHPLC mutation screen (A) DHPLC chromatogram for amplicon 4 showing elution curve for a homozygous A/A sample at SNP rs2003149 (top) and a heterozygous G/A sample (bottom) characterised by multiple elution peaks

caused by heteroduplex formation. (B) Direct sequencing of the heterozygous sample in A. (C) Agarose gel illustrating the genotyping of rs2003149 by RsaI digest and PCR-RFLP yielding fragments of 148 and 299 base pairs for G/G, 148, 255 and 44 for A/A, and 148, 255 and 299 for G/A. (D) DHPLC chromatogram for amplicon 5 showing rs1809319 with homozygous G/G alleles (top) and heterozygous G/A alleles.

As could be expected, neither allele nor genotype frequencies differed significantly between the HapMap population and the heterogeneous SMA patient cohort.

The C/T genotype was overrepresented in the ALS patient cohort, which just reached statistical significance in the Chi square test, indicating a possible association between this locus and ALS susceptibility.

Patient cohort	**rs2003149**						
	Allele frequencies			Genotype frequencies			
	C	T	X^2 *p*	C/C	C/T	T/T	X^2 *p*
SMA	46(0.280)	118 (0.720)	0.951	7 (0.085)	32 (0.390)	43 (0524)	0.551
ALS	74 (0.330)	150 (0.670)	0.364	9 (0.080)	56 (0.500)	47 (0.420)	0.038
HapMap	51 (0.284)	129 (0.716)	-	11 (0.121)	29 (0.328)	50 (0.552)	-

Table 3.5 rs2003149 genotyping. Allele and genotype frequencies as assessed by PCR-RFLP in patients with SMA and ALS were compared with the HapMap dataset.

3.2.2 Angiogenin

3.2.2.1 ANG mutation screen

A total of 160 patients were included in the *ANG* mutation screen (see table 3.6).

Diagnosis	**N**	**Male (average age)**	**Female (average age)**
Sporadic ALS	132	95 (61)	65 (70)
Familial ALS	18		
Primary lateral sclerosis	10		
Total	160		

Table 3.6 Patients included in the ANG mutation screen

Rather than using the DHPLC approach as for the *FVT1* screen, direct sequencing was used to screen for *ANG* mutations. The PCR amplicon used as the sequencing template included 40 base pairs of the preceding intron and 50 base pairs of the 3'UTR.

No mutation was identified in the coding region. The amplicon contained three known SNPs, rs17560 and rs222865, which were non-polymorphic in all patients, as well as rs11701, which has previously been described to be associated with ALS in the Irish and Scottish population (see 3.1.2). The allele and genotype frequency of rs11701 was compared to the HapMap CEU dataset and found not to be statistically different (table 3.7). Interestingly, the G and T allele frequency was almost identical to frequencies of both cases and controls of other published series, but differed from the frequency described in the control cohort used by Greenway et al (Greenway et al. 2004).

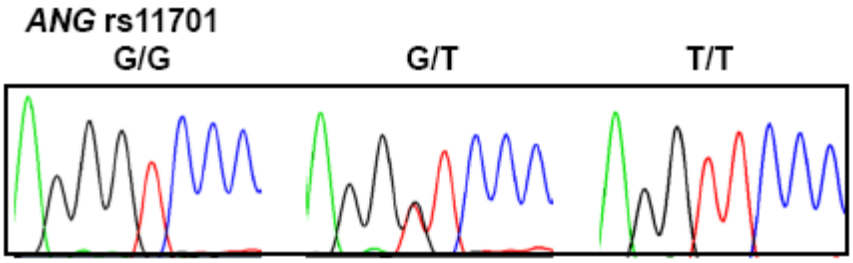

rs11701	Allele		Genotype		
	G	T	G/G	G/T	T/T
Oxford samples (frequency)	48 (0.1714)	232 (0.828)	3 (0.0214)	42 (0.3)	95 (0.678)
HapMap CEU (frequency)	0.192	0.808	0.033	0.317	0.67
Chi-square	0.764 (p=0.382)		0.872 (p=0.647)		

Table 3.7 Frequency of rs11701 alleles and genotypes in the study population compared to the HapMap CEU dataset. Results are based on direct sequencing.

3.2.2.2 ANG copy number

All described *ANG* mutations lead to loss of function and *ANG* haploinsufficiency is a conceivable genetic mechanism of disease. In addition to loss of function mutations, heterozygous gene deletion could lead to similar effects. One case included in the mutation screen had neuropathological features reminiscent of the previously published case report of the ANG K17I mutation (Seilhean et al. 2009).

No coding mutation was identified in this case. In addition to the coding exon, the non-coding exons 1 and 2 as well as the entire 3'UTR were sequenced for this case. No variant was identified. However, heterozygous gene deletion could not be ruled out as the common SNP rs11701 showed a single T peak and no other polymorphisms were present.

A qPCR based copy number assay was designed and validated, with a dynamic range of DNA input between 50 ng and 1.5 ng. As a calibrator, a genomic DNA sample with heterozygous rs11701 was used, indicating a gene copy number of at least 2. No evidence for a heterozygous ANG deletion was detected in this assay.

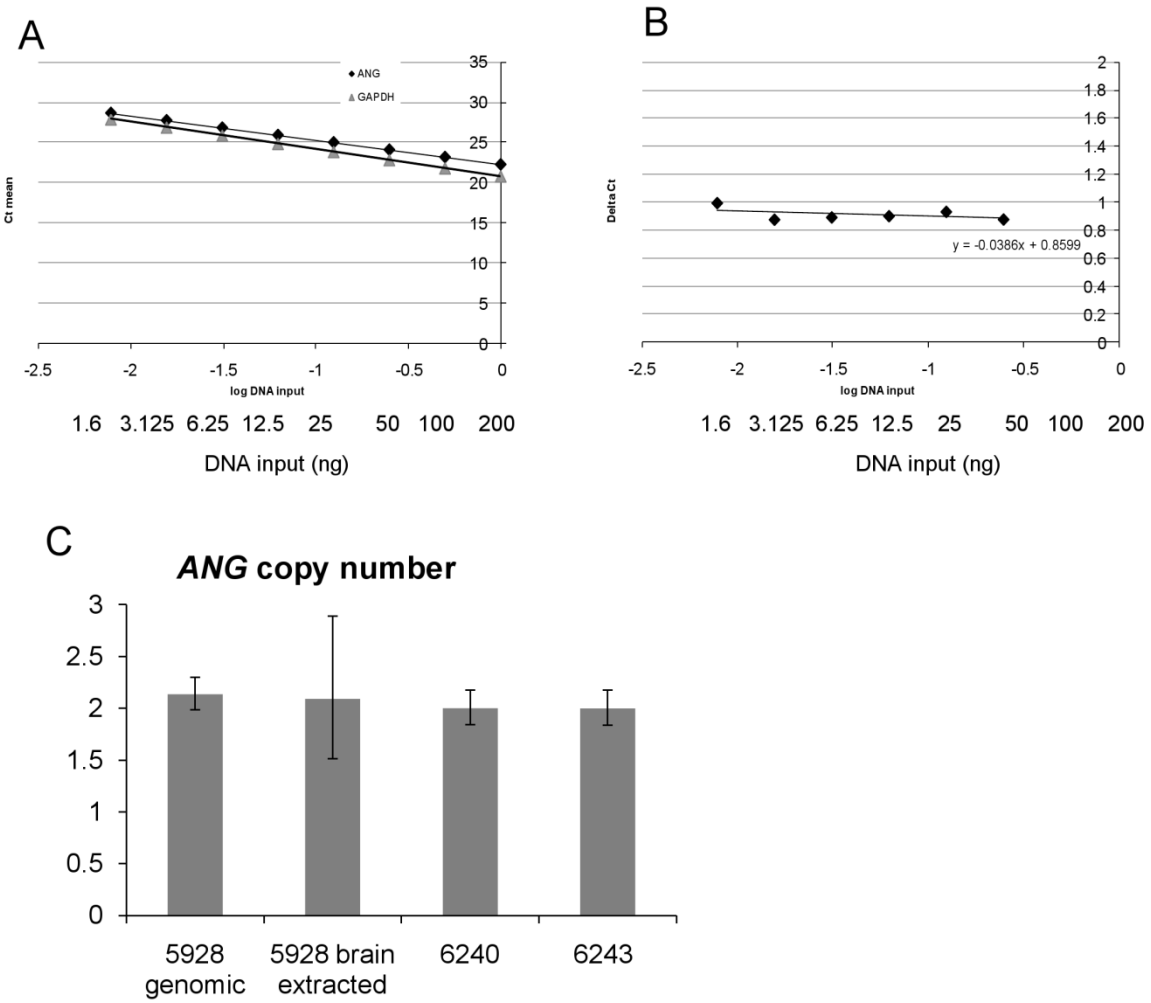

Figure 3.2 ANG copy number assay (A) Primer efficiency of *ANG* and *GAPDH* shows parallel distribution of Ct values against log DNA input (B) The slope of a semi-log regression line of Delta Ct values against log DNA input is less than 0.1, indicating suitability of this primer pair for the comparative Ct method (ΔΔCt method). (C) Sample 5928 has equal copy number to samples 6240 (calibrator) and 6243 with known heterozygosity for rs11701. Brain extracted DNA yielded similar results. Error bars represent the standard deviation of the mean for four technical replicates.

3.2.3 *FUS* mutation screen

The *FUS* mutation screen was carried out in two parts. First, all 15 *FUS* exons were sequenced in five patients with known FUS pathology on post-mortem examination. Cases included 4 patients with juvenile ALS and the neuropathological phenotype of basophilic inclusions that were immunoreactive

for FUS, as well as one case of adult onset ALS with FUS positive intranuclear inclusions. These cases are described in detail in chapter 4. Next, *FUS* exon 14 and 15, which code the very C-terminal domain of FUS and have been shown to harbour the vast majority of mutations in patients with familial and sporadic ALS, as well as the 3'UTR, were screened by direct sequencing in the entire panel of ALS patients described above.

In two patients with juvenile ALS and basophilic inclusions, sequencing showed the heterozygous C1574T (P525L) mutation (figure 3.3).The mutation-positive patients were of British Caucasian and Indian ethnic origin, respectively. None of the patients had a positive family history of ALS or any other neurological illness. At the time of writing, no DNA was available from family members.

The P525L mutation is located in an evolutionary conserved residue at the very C terminal end of the protein in close vicinity to most other reported mutations in FUS (figure 3.3). It was previously described in patients with familial ALS of both North American and Italian origin (Chio et al. 2009a; Kwiatkowski et al. 2009). Protein prediction using the SIFT algorithm showed that no amino acid substitution at this residue is likely to be tolerated, and SNAP predicted the substitution to be non-neutral, while the Polyphen algorithm predicted the variant to be benign.

A further mutation in exon 15 was identified in the third patient with juvenile ALS and basophilic inclusions. This was a novel four base pair deletion (c.1554_1557delACAG) leading to a frameshift which was predicted to change the protein sequence of the terminal 8 amino acids of FUS . Because high quality forward sequencing of the exon 15 amplicon was inhibited by the preceding long poly T stretch in intron 14, this mutation was confirmed by cloning exon 15 PCR product into a sequencing vector (pCR2.1 TOPO, Invitrogen) and analysing 10

clones by direct sequencing. In keeping with a heterozygous deletion, six of the examined clones carried the deletion, while four contained the wild –type sequence (figure 3.3).

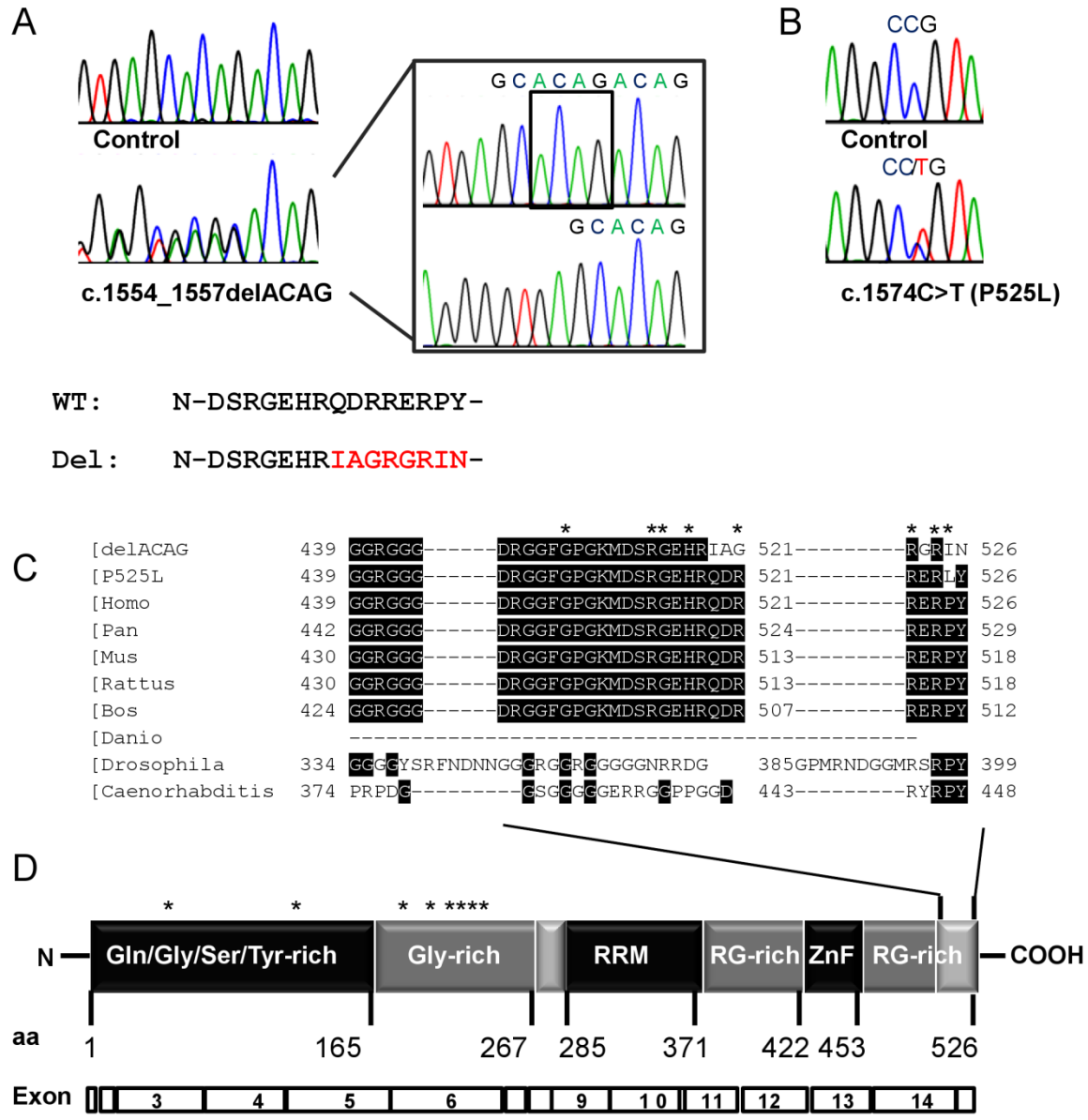

Figure 3.3 Results of *FUS* genetic screen (A) Reverse complemented reverse sequence traces of control and patient DNA showing a four base pair deletion in FUS exon 15 (c.1554_1557delACAG) confirmed by sequence analysis of cloned wild-type (insert top, bases deleted in the mutant allele are marked by the box) and mutant allele (insert bottom). The deletion is predicted to cause a frameshift with resulting alteration of the terminal eight amino acids of FUS (bottom). (B) Two patients were heterozygous for the c.1574C>T (P525L) mutation (top, control, bottom, case), altering the penultimate amino acid of FUS in an evolutionary conserved residue (C) The FUS protein and cDNA structure according to

reference sequence PRO_0000081591 (http://www.uniprot.org/uniprot/) is shown in (D). An asterisk (*) marks residues previously found to be mutated in patients with familial or sporadic ALS. (aa: amino acid). With permission from *Neurology* (Bäumer et al. 2010).

The DNA obtained from paraffin blocks of the fourth case of juvenile ALS with basophilic inclusions was highly fragmented and could not be recovered by a trial of whole genome amplification. Most PCR reactions yielded only smeared products with correspondingly noisy sequencing data. Exon 15 was amplified using two additional primers to reduce amplicon size and sequencing traces were of sufficient quality to rule out a mutation in this exon.

No coding changes were identified in the patient with FUS-positive intranuclear inclusions. However, a T to C conversion was identified in intron 5 (IVS5 -21T>C) in proximity to the poly T tract. This variant could plausibly disrupt splicing of exon 6 by interfering with the polypyrimidine tract or branch point, but has been described as a common polymorphism in the population (rs74015090). No coding changes in exons 14 or 15 were identified in the panel of 160 patients with sporadic and familial ALS. The previously described SNP GA031398 (NM_004960 c.*41G>A) was identified in the 3'UTR of two patients with sporadic ALS.

3.2.4 *TARDBP*

3.2.4.1 TARDBP mutation screen

The patient cohort described above was included in the *TARDBP* mutation screen.

All *TARDBP* coding exons (exons 2-6) as well as flanking introns and 128 base pairs of the 3'UTR were PCR amplified and directly sequenced.

Overall, sequence variation was rare with 3 observed SNPs (figure 3.4). The 198T>C (A66A) variant was found in a patient with SALS. It was previously

described in patients with SALS, but has also been reported in healthy controls (table 3.3).

The 945G>A (A315A) variant was also found in a patient with SALS. This change has been reported in several patients with SALS, but only one healthy control (Guerreiro et al. 2008).

The 962 G>C (A321G) variant was identified in a Caucasian patient with sporadic ALS who had died before completion of this study. The diagnosis of ALS was made 6 months after onset of progressive asymmetrical arm and truncal weakness and wasting in the presence of preserved deep tendon reflexes. The disease progressed rapidly and the patient died at the age of 54 of respiratory failure, 20 months after symptom onset. The 962 G>C (A321G) variant is a novel mutation in exon 6, predicted to change alanine for glycine in an evolutionarily highly conserved region in the C terminal domain of TDP-43 (figure 3.4). It has not been described in over 2500 healthy control subjects in whom *TARDBP* was fully sequenced (table 3.3).

Bioinformatic analyses of the A321G variant using SIFT, Polyphen and SNAP algorithms classed this variant as “tolerated”, “benign”, and “neutral” respectively, although the reliability of the prediction was only moderate (4 on a scale of 0 to 9 in the case of SNAP).

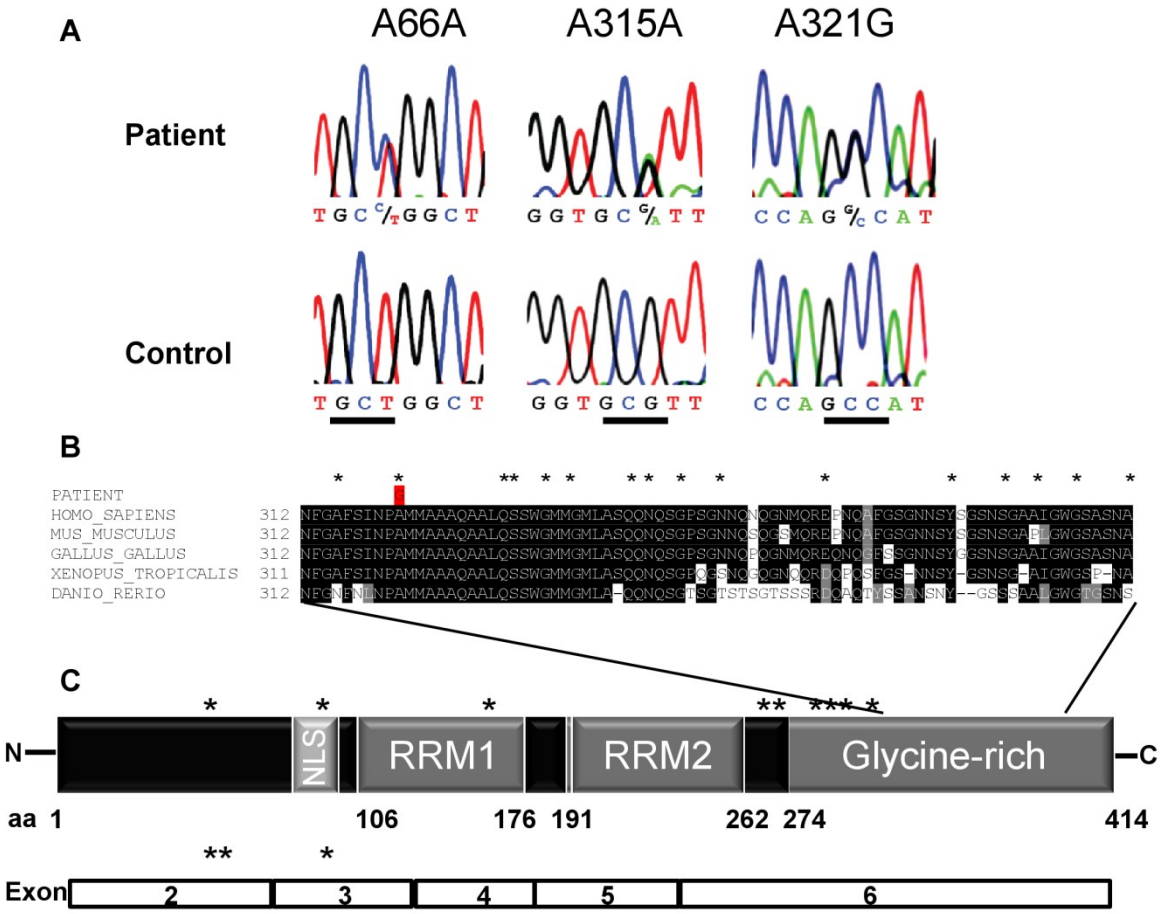

Figure 3.4 Results of the *TARDBP* mutation screen (A) Sequencing chromatograms of variants identified in patients (above) and control sequences (bottom). (B) Protein sequence alignment showing the A321G mutation in a highly conserved amino acid residue. (C) TDP-43 protein structure and TARDBP cDNA. Residues previously found to be mutated in patients with ALS are marked by an asterisk.

3.2.4.2 TARDBP copy number assay

To assess *TARDBP* copy number, a qPCR based assay with primers spanning *TARDBP* exon 3 and intron 4 was designed and validated. An initial screen in a 96-well format revealed several samples showing higher than average copy number with high standard deviation. These samples were individually re-amplified and shown to have no copy number variation (figure 3.5).

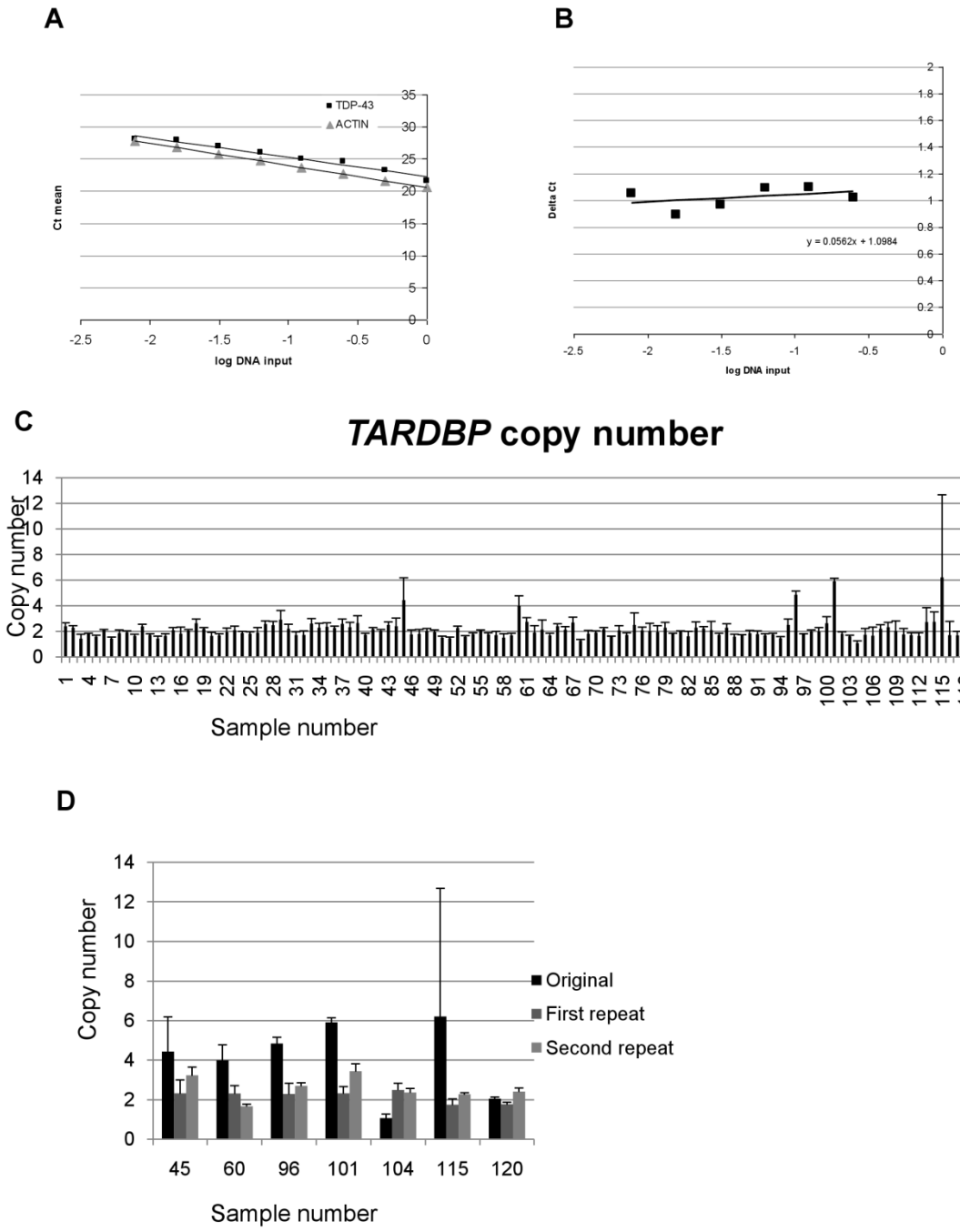

Figure 3.5 *TARDBP* copy number assay Primer efficiency for *TDP-43* and *Actin* shows parallel distribution of Ct values against log DNA input (B) The slope of a semi-log regression line of Delta Ct values against log DNA input is less than 0.1, indicating suitability of this primer pair for the comparative Ct method (ΔΔCt method). (C) Several samples in a panel of 128 patient DNAs show TDP-43 copy number other than two. (D) On repeat amplification, copy number was two in all cases. Error bars represent standard deviation of the mean of 3 technical replicates.

3.3 Discussion

3.3.1 *FVT1* screen

No obvious deleterious variants were identified in the *FVT1* screen in patients with ALS or a variety of other motor neuron disorders that could be summarised under the umbrella term of spinal muscular atrophies. Several limitations apply to this screen. First, the sample size was relatively small, and although it is probably safe to say that *FVT1* mutations are not a common cause of motor neuron disorders, the working hypothesis of this was that individually rare variants can contribute to disease in a population. Given the low frequency of mutations in some clearly causative ALS genes (e.g. 0.6% in *ANG),* it is possible that a screen of 215 heterogeneous cases would miss patients with mutations in *FVT1*. The small sample size, and heterogeneity of the studied population, also caution against an overinterpretation of the significance of the statistically significant association between ALS disease status and the presence of the C/T genotype in SNP rs2003149. This is best seen as a preliminary finding that needs to be replicated in a much larger sample size. Secondly, the screening strategy was not designed to detect non-coding intronic, 5' UTR, 3'UTR or promoter variants. Furthermore, while DHPLC has been consistently reported to achieve sensitivities in mutation screens of above 96% (O'Donovan et al. 1998; Xiao and Oefner 2001), and appears to be superior to direct sequencing in detecting low frequency mutations as occur in mosaicism or heteroplasmy (Jones et al. 2001), detection of homozygous changes may be more difficult. Homozygous base pair changes do not form heteroduplexes, and DHPLC detection relies on the differential elution profile of fragments containing A/T versus C/G base pairs at the site of interest, and comparison with a sample of known genotype. While high detection rates for

homozygosity have been reported (O'Donovan et al. 1998), experience from this screen shows that homozygous changes may be underreported. The polymorphic SNP rs2003149 was detected in heterozygosity by DHPLC, but eventually genotyped by PCR-RFLP, because the G/G genotype could not reliably distinguished from the A/A genotype by DHPLC.

Leaving aside these limitations, other interpretations of the negative result are that either mutations in *FVT1* are always lethal in humans (and are therefore not detected in an adult population) or FVT1 function in humans is redundant or not as relevant to motor neurons as it is in cattle. This raises the more general question of whether phenotypically similar diseases in different species necessarily have similar pathophysiology. Autosomal recessive SMA has also been reported, for example, in the domestic cat (He et al. 2005). The causative gene has been identified as *LIX1* (Fyfe et al. 2006), a gene that has high expression in spinal cord, is highly conserved from cat to humans and is likely to a function in RNA metabolism based on secondary structure prediction. Previous work from our laboratory screened *LIX1* and found no mutations (Parkinson et al. 2008). On the other hand, positional cloning efforts mapped the disease locus of canine degenerative myelopathy, a neurodegenerative disease occurring in various breeds of dog that resembles ALS, to *Sod1* (Awano et al. 2009) and identified the E40K mutation in an amino acid residue also mutated in human ALS. Unlike most cases of human SOD1-related ALS, canine degenerative myelopathy is an autosomal recessive trait. Despite the negative results in *FVT1* and *LIX1*, the finding of SOD1-related motor neuron disease in dogs shows that genetic diseases in animals can be useful in identifying candidate genes for broadly similar phenotypes in humans.

3.3.2 *ANG, FUS and TARDBP* screen

3.3.2.1 General remarks

ANG, *FUS* and *TARDBP* were screened in patients with ALS only. No mutations were identified in *ANG,* which is in keeping with the overall very low reported mutation frequency. The results of the *FUS* and *TARDBP* mutation screen contribute to the existing information of the mutation spectrum in these genes in several ways. First, the finding of mutations in *FUS* or *TARDBP* in four out of a total of 165 patients is in keeping with the view that individually rare mutations in several genes can together explain a significant proportion of cases. ALS is an example of locus heterogeneity, which is common in syndromes resulting from failure of a common pathway (Strachan 2004). Since *FUS*, *TARDBP*, *ANG* and possibly *SOD1* function in RNA metabolism in general, it is conceivable that most cases of ALS can eventually be explained by mutations in genes involved in related pathways. Second, with the exception of the SOD1 I113T mutation, all mutations identified here occurred in seemingly sporadic cases of ALS. In the absence of parental DNA one can only speculate about the relevance of this finding. Non-paternity is always a possibility in clinical practice, but is unlikely to explain all four cases. *De novo* single base pair missense mutations are not uncommon and have been described in several neurological disorders, for example Neurofibromatosis (Huson et al. 1989; Jadayel et al. 1990). They frequently arise from the paternal chromosome (Glaser et al. 2006). No data are available on the new mutation rate in *TARDBP* or *FUS*. Variable expression is a possibility, and the absence of a family history does not rule out subtle clinical abnormalities in mutation carrying relatives, who were not systematically examined for this study. Age-related penetrance is a possibility in the patient with

the *TARDBP* mutation, but the *FUS* mutations occurred in very young onset cases.

3.3.2.2 FUS mutations

The FUS P525L mutation has been described twice in cases of familial ALS. Both families were unusual in that the age of onset was extremely young. One case with an autosomal dominant family history exhibited disease onset with at 22 years with a disease duration of 6 months (Kwiatkowski et al. 2009), while in a three-generation Italian family index cases had ages of onset of 29, 33, 17 and 22, with an average disease duration of less than 12 months (Chio et al. 2009a), indicating the aggressive nature of this mutation.

Most other reported mutations cluster in the very C-terminal domain of FUS. Modelling of the C-terminal H517Q and R521G (Kwiatkowski et al. 2009), as well as the R521H and R521C (Vance et al. 2009) mutations in CV-1,SKNAS and N2A, as well as rat cortical neurons, revealed a difference in cellular distribution of mutant versus wild-type protein, with increased cytoplasmic protein in case of FUS mutants. This finding implies that alterations of the C-terminal domain of this nuclear-cytosolic shuffling protein alter its sub-cellular localisation. In fact, the C-terminal domain contains an atypical nuclear localisation signal that constitutes a binding site for karyopherin beta2 (transportin) (Lee et al. 2006). In addition, protein-protein interactions that are mediated via the FUS C-terminal domain, such as with the SR protein FUSIP1 (Yang et al. 1998a) might be disrupted, leading to dysfunction of aspects of RNA metabolism such as pre-mRNA splicing even before frank protein aggregation occurs. Furthermore, the C-terminal domain of FUS is responsible for recognition of the FUS RNA target sequence GGUG (Wang et al. 2008b).

The novel c.1554_1557delACAG mutation is predicted to substantially alter the C-terminal domain at protein level by substituting six of the last eight amino acids, suggesting a mechanism of pathogenesis similar, but possibly more severe, to that of point mutations. On the other hand, the alteration at nucleotide level alone could potentially alter terminal exon recognition by disrupting SR protein binding sites, as suggested by the ESE finder analysis, as well as alter mRNA expression by changing the sequence of the 3'UTR in keeping with the frameshift and novel STOP codon. No RNA was obtainable for this case to check that the predicted mRNA is actually expressed in the tissue.

The neuropathological consequences of the FUS mutations will be described in chapter 5.

3.3.2.3 TARDBP mutations

Three variants were identified in the *TARDBP* screen. Two synonymous changes (A66A, A315A) have been previously reported in ALS cases as well as in healthy control probands, although the A315A variant appears to be overrepresented in patients. The A321G mutation is located in the C-terminal domain of TDP-43, in close vicinity of most other reported mutations. The clustering of mutations in this region of the protein is even more pronounced than in FUS, and stresses the likely importance of this domain for ALS pathogenesis.

A functional analysis of the identified *TARDBP* variants is the aim of the next chapter, while aspects of TDP-43 neuropathology are discussed in chapter 5.

4 Functional Analysis of TDP-43 mutations

4.1 Introduction

4.1.1 TDP-43 structure and function

TDP-43 is a highly conserved 43 kDa nuclear protein with structural similarities to proteins described as heterogeneous ribonucleoproteins (hnRNPs) (Krecic and Swanson 1999), which are predominantly nuclear proteins with various functions in RNA processing including transcription, splicing as well as mRNA transport and stability (see chapter 1).

TDP-43 contains a bipartite N-terminal nuclear localization signal (NLS1 and NLS2) (Winton et al. 2008a), two RNA recognition motifs (RRMs) (Buratti and Baralle 2001) and a C-terminal domain that is rich in glycine residues. The first RRM is relevant for RNA and DNA binding, while the C-terminal domain does not directly bind nucleic acids, but mediates functions such as splicing (Buratti et al. 2005) and transcription regulation (Abhyankar et al. 2007) via interaction with other proteins, for example hnRNPA2 (D'Ambrogio et al. 2009). In addition to protein-protein interactions, the C-terminal domain might be directly relevant for cellular distribution of TDP-43, given that a characteristic neuropathological feature of ALS caused by C-terminal TDP-43 mutations is the cytosolic re-distribution of the protein. In fact, several hnRNPs contain more than one functional nuclear localisation signal (Michael et al. 1995; Michael et al. 1997) and shuttle continuously between nucleus and cytoplasm (Pinol-Roma and Dreyfuss 1992).

One of the best characterised functions of TDP-43 is the regulation of pre-mRNA splicing, in particular of CFTR exon 9 (Buratti and Baralle 2001; Buratti et al. 2001;

Buratti et al. 2004; Ayala et al. 2006), but other targets have also been described, including the Apo AII exon 3 (Mercado et al. 2005) and SMN (Bose et al. 2008). RNA cross-linking experiments have demonstrated that TDP-43 specifically binds to (UG)m repeat sequences (Buratti et al. 2001). The CFTR intron 8 contains a polymorphic (TG)nTm stretch close to the exon 9 3' splice site, the length of which correlates with the degree of exon skipping. Exon skipping is thought to be mediated by TDP-43 and other proteins that TDP-43 binds via its C-terminal domain (Buratti et al. 2005). The best characterised of these is hnRNP A2 (D'Ambrogio et al. 2009).

Finally, another proposed function of TDP-43 is that of a nuclear matrix scaffolding protein, based upon the observation in one publication that TDP-43 co-localises with the nuclear structures Cajal bodies, gems and SC-35 speckles, and co-immunoprecipitates with SMN (Wang et al. 2002). However, this report was based primarily on data obtained from overexpressing a short mouse TDP-43 isoform in Hek293 cells, which resulted in a staining pattern distinct from that of endogenous TDP-43.

4.1.2 Aims of chapter 4

Three variants in *TARDBP* were identified in the genetic screen described in chapter 3. The aim of this chapter is to analyse the effect of these variants in TDP-43 function.

Two of these variants (A66A and A315A) are not protein changing, but might alter splicing of the TDP-43 mRNA. The potential effect on splicing will be examined using a *cis*-splicing reporter minigene system. The third variant (A321G) is located in exon 6, which encodes for the C-terminal glycine rich domain of TDP-43, in

close vicinity to most other previously reported mutations. The genetic evidence that C-terminal TDP-43 mutations overall are pathogenic is compelling, given the absence of any variation in large numbers of control probands (see chapter 3, table 3.3), the segregation with disease in familial cases and the absence of linkage to other loci in families with *TARDBP* mutations (Sreedharan et al. 2008), while direct proof of pathogenicity for individual, private mutations occurring in seemingly sporadic cases is more difficult. The A321G mutation identified here has not been described before, although the same amino acid residue is mutated in another case (Kirby et al. 2009). The alanine (R=CH3) to glycine (R=H) substitution is a conservative amino acid change; all protein prediction algorithms used have defined this change as neutral. The A321G variant will be examined with respect to its effect on cell viability, cellular distribution, *trans*-splicing effect on other transcripts and its response to cellular stressors.

4.2 Results

4.2.1 *Cis*-splicing effects of the A66A variant

The 198T>C (A66A) variant was identified in a patient with sporadic ALS. It is located in exon 2, the first protein coding exon. No splice variants involving this exon are present in Ensembl. However, bioinformatic analysis using ESEfinder 3.0 identified the presence of several exonic splice enhancer elements and the presence of the 198T>C variant is predicted to abolish an SC-53 binding site (figure 4.1A). To assess whether this predicted change has an effect on TDP-43 splicing in *cis*, a splicing reporter minigene was cloned containing TDP-43 exon 2 and 200 base pairs of adjacent intron (figure 4.1B). The minigene containing wild-type and mutant sequence was transfected into the human neuronal cell line SH-

SY5Y, and the splicing pattern was analysed by RT-PCR using flanking primers located in the adjacent minigene exons. The 5' splice site was mutated in two residues as a positive control for the assay. RT-PCR analysis showed almost complete exon 2 inclusion in this assay for both wild-type and mutant (198T>C) sequence. A mutation introduced at position 3 of the 5' splice site produced no noticeable change in exon inclusion, and only the mutation at position 2 of the 5' splice site led to a significantly different splicing pattern consistent with the recognition of a novel 5' splice site in intron 2, while the majority of transcript still contained the correctly spliced transcript (figure 4.1C).

These results indicated that exon 2 recognition is extremely strong, in keeping with the absence of known splice isoforms involving this exon, and the predicted SC-35 site altered by the 198T>C variant is redundant for exon recognition. At the time of this experiment, 13 out of 1145 patients with ALS were found to carry the 198T>C variant, as opposed to 12 out of 1770 controls. Taken together, the genetic and experimental data suggest that the 198T>C variant is a benign polymorphism.

4.2.2 *Cis*-splicing effects of the A315A variant

The 945G>A (A315A) variant is located in the 3' terminal exon 6 of TDP-43. Bioinformatic analysis with ESEfinder 3.0 identified a SC-35 site that is altered by the variant (figure 4.2). Splicing patterns of 3' terminal exons are much more difficult to model *in vitro* than internal exons, for which a flanking primer approach can be used. This became obvious when TDP-43 exon 6 with adjacent intron 5 and part of the 3'UTR was cloned into the splicing reporter minigene backbone utilised for the A66A variant, and analysed like an internal exon. RT-PCR analysis showed that the main band obtained both for wild-type and mutant sequence did not correspond to the size expected for complete inclusion of exon 6. Instead,

direct sequencing revealed the utilisation of a cryptic splice site 117 base pairs into exon 6 proximal to the A315A variant.

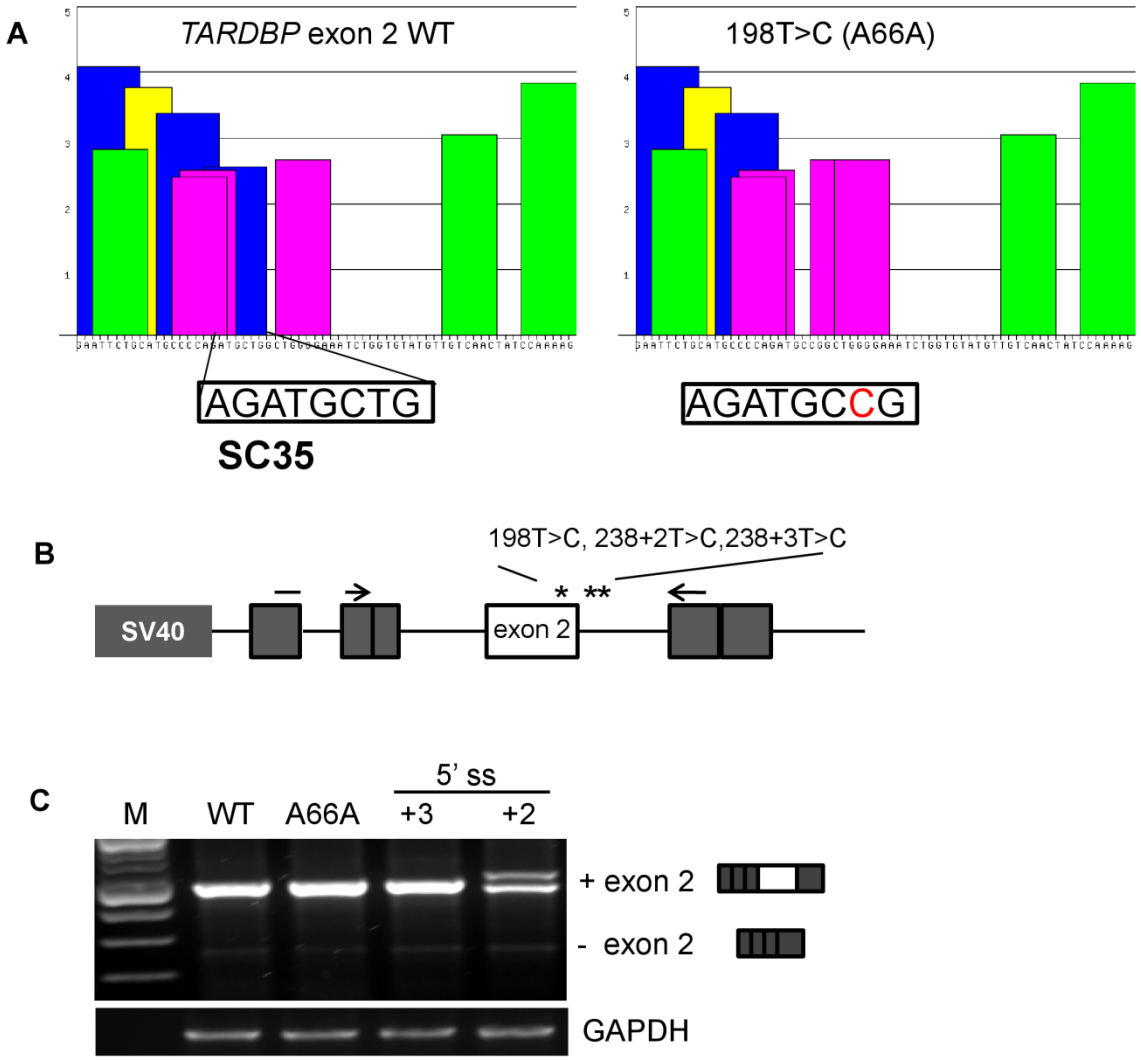

Figure 4.1 A66A *cis*-splicing minigene (A) Graphical output of ESEfinder 3.0 results for wild-type (left) and A66A (right) sequence. The latter leads to the abolition of a SC35 binding site. (B) Schematic of the A66A *cis*-splicing minigene containing TDP-43 exon 2 plus adjacent intronic sequence as an internal exon between two hybrid minigene exons under the control of the SV40 promoter. (C) 1.5% agarose gel of RT-PCR resulting from transfection of SH-SY5Y cells showing almost complete exon 2 inclusion for wild-type and A66A, while a splice site mutation leads to a novel intron 2 splice site.

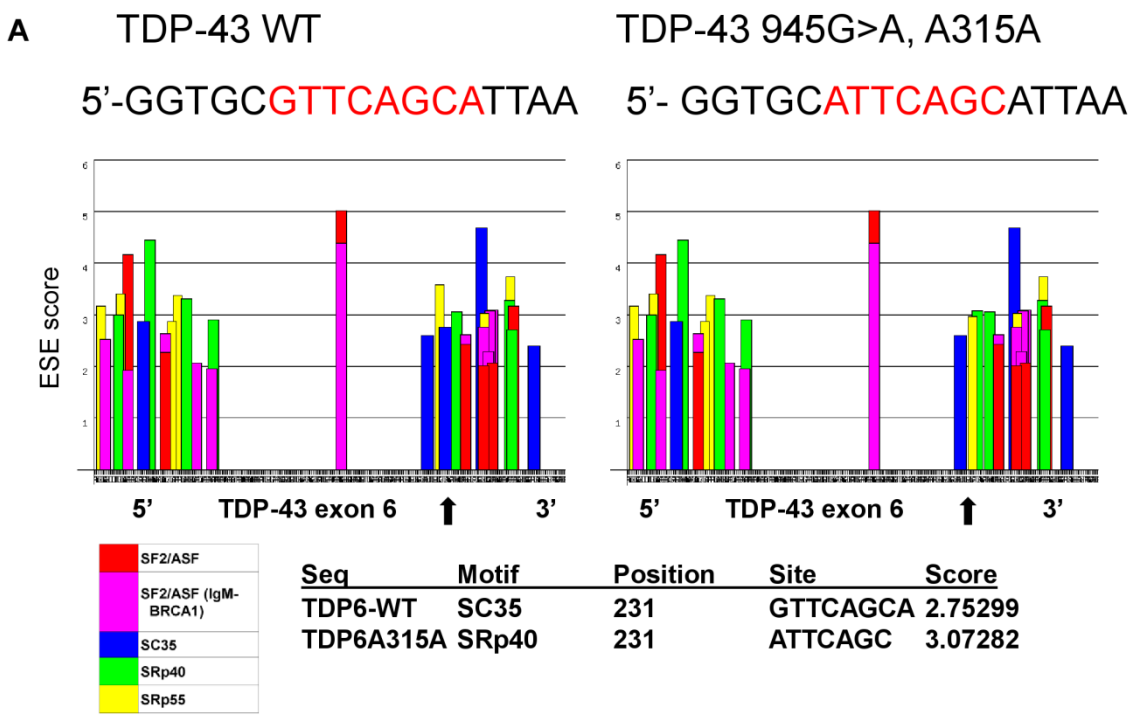

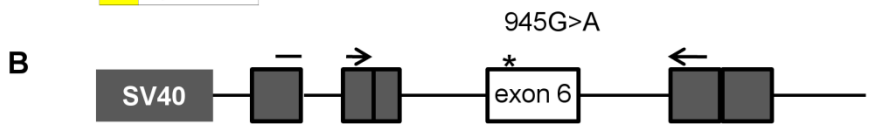

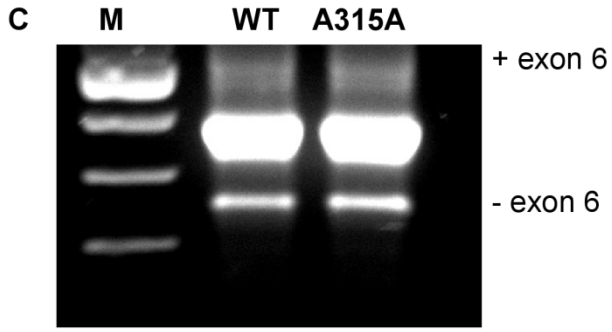

D

TAATAAAACTAAAAGCTGTATTGGGGGTTTAAATGAAATGAGTGTTCATTGCTTATT
TTTCCTCTGGCTTTAGATAAATTAATGCTTGTAATCTAAGTTTTGTTGCTACTTTAA
ATATATGAATCAGTGGTTTAATCTTCTTTGTTTACATCCCTTATTTCTTATAGATTG
CGCAGTCTCTTTGTGGAGAGGACTTGATCATTAAAGGAATCAGCGTTCATATATCCA
ATGCCGAACCTAAGCACAATAGCAATAGACAGTTAGAAAGAAGTGGAAGATTTGGTG
GTAATCCAGGTGGCTTTGGGAATCAGGGTGGATTTGGTAATAGCAGAGGGGGTGGAG
CTGGTTTGGGAAACAATCAAGGTAGTAATATGGGTGGTGGGATGAACTTTGGTGCGT
TCAGCATTAATCCAGCCATGATGGCTGCCGCCCAGGCAGCACTACAGAGCAGTTGGG
GTATGATGGGCATGTTAGCCAGCCAGCAGAACCAGTCAGGCCCATCGGGTAATAACC
AAAACCAAGGCAACATGCAGAGGGAGCCAAACCAGGCCTTCGGTTCTGGAAATAACT
CTTATAGTGGCTCTAATTCTGGTGCAGCAATTGGTTGGGGATCAGCATCCAATGCAG
GGTCGGGCAGTGGTTTTAATGGAGGCTTTGGCTCAAGCATGGATTCTAAGTCTTCTG
GCTGGGGAATGTAGACAGTGGGGTTGTGGTTGGTTGGTATAGAATGGTGGGAATTCA
AATTTTTCTAAACTCATGGTAAGTATATTGTAAAATA

Figure 4.2 A315A *cis*-splicing minigene (A) ESEfinder output indicating alteration of a SC35 binding site by the variant sequence and creation of a

potential SRp40 site. (B) Schematic of the cis splicing minigene showing the 3' terminal TDP-43 exon 6 as an internal minigene exon. (C) Agarose gel of RT-PCR showing no difference between wild-type and A315A. (D) Direct sequencing of the RT-PCR top band (expected size 768 base pairs) revealed utilisation of a novel 5' splice site (underlined and red in minigene exonic sequence with red background) and loss of over 400 base pairs of exon 6.

This result demonstrated that the absence of the canonical 5' splice site prevents TDP-43 exon 6 recognition as an internal exon in this artificial context, and that the extended 3'UTR and possibly more distal end-forming *cis* elements are necessary for exon definition. The A315A minigene was therefore not a suitable instrument to assess exon 6 splicing. Next, insertional mutagenesis was employed to add the complete 3'UTR to the existing minigene (figure 4.3). The intended assay consisted of RT-PCR with a forward primer in minigene exon 1, and reverse primer in the TDP-43 3'UTR. This approach would detect utilisation of cryptic splice sites activated by modification of the ESE, but not necessarily alteration of overall TDP-43 expression levels. HEK293T cells were utilised for RNA isolation due to improved transfection efficiency and SV40 promoter-driven expression compared to SH-SY5Y cells. Both wild-type and A315A-mutant led to a 760 base pair band corresponding to full exon 6 inclusion in the minigene transcript, whereas the construct carrying a mutation in position 1 of the 3' splice site of exon 6 showed multiple bands indicating incorrect exon recognition. There was no obvious difference between wild-type and A315A mutation, but the experimental design did not allow for assessment of subtle expression level differences. To enhance the presence of any aberrant transcript, nonsense-mediated decay was inhibited by applying the translational inhibitor cycloheximide before harvesting of RNA, which brought out an additional unexpected band in the A315A-mutant, but not wild-type RT-PCR. However, the result could not be repeated when the

reverse transcription step of the RT-PCR was performed with sequence specific primers, suggesting that some of the results could have been artefactual.

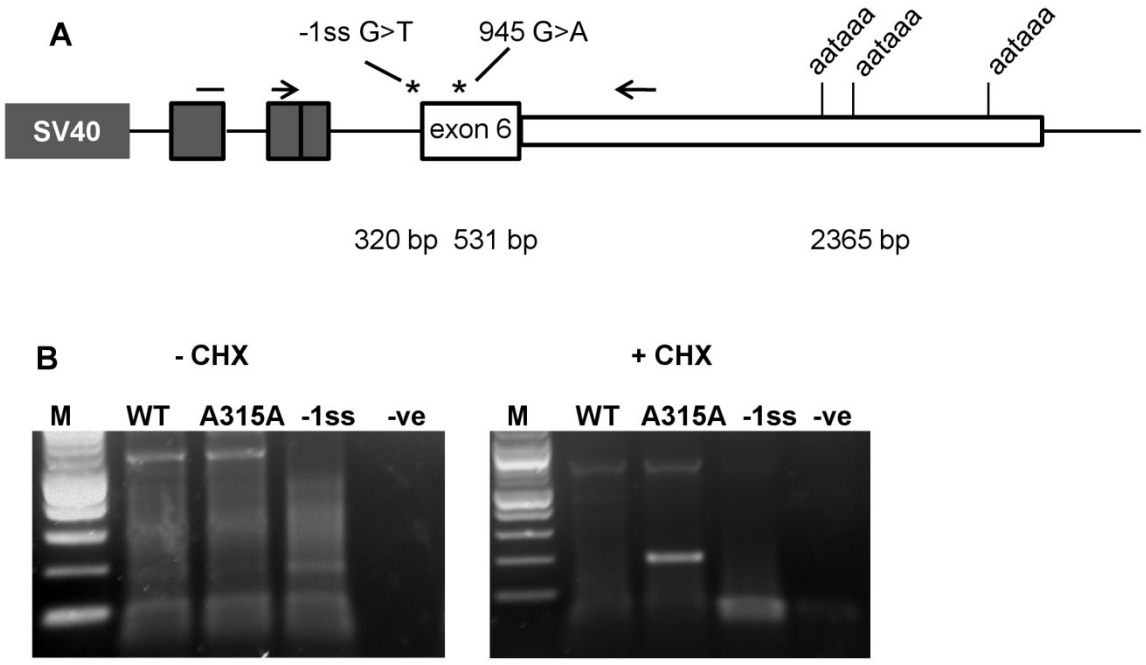

Figure 4.3 A315A 3'UTR minigene (A) Schematic of minigene containing TDP-43 exon 6 as a terminal exon including the 3'UTR with three putative poly-adenylation signals. (B) Hek293T cells transfected with the minigene express equal amounts of wild-type (WT) and A315A TDP-43 in this context, while a splice site mutation abolishes exon recognition. After treatment with cycloheximide,blocking nonsense mediated decay by inducing translational arrest, a novel isoform is apparent for the A315A variant. M, 100 base pair molecular weight marker.

The results so far had implied a possible difference in TDP-43 exon 6 splicing in the presence of the A315A variant, but the utilised assay was not robust enough due to less than optimal transfection efficiency, expression levels and PCR protocols, or a combination of all factors. Therefore, a third strategy was employed to analyse the effect of the variant on the strength of the putative ESE. A minigene specifically designed to test ESE sequences resulted in robust transfection and expression in SH-SY5Y cells with highly uniform RT-PCR results. This experiment

supported the notion that the A315A variant leads to weakening of an ESE, although the magnitude of the observed effect was small. Taken together with the available genetic data this implies that the A315A variant is potentially pathogenic or a susceptibility factor.

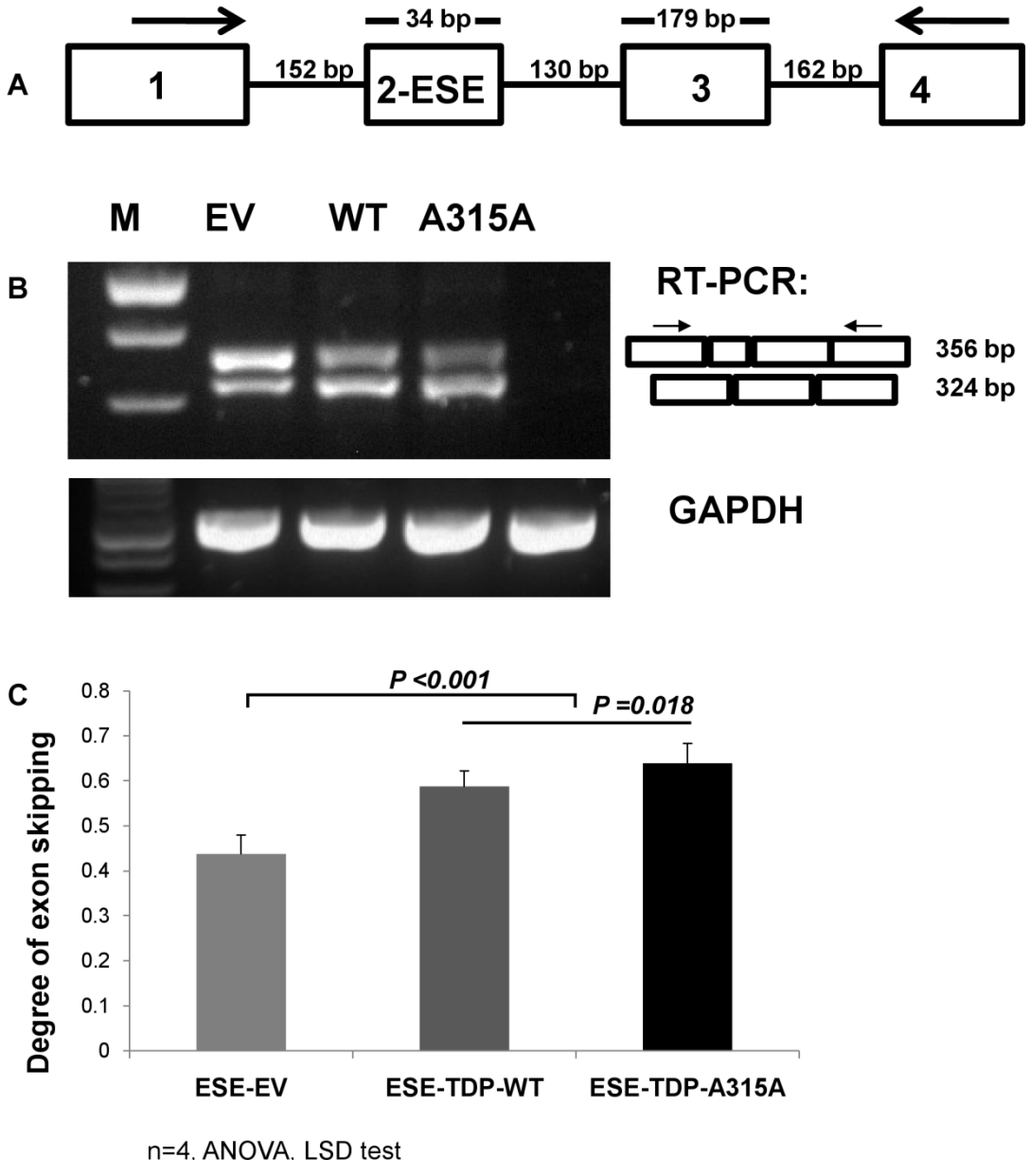

Figure 4.4 A315A-ESE minigene (A) Schematic of the 4.11.12muC minigene containing a 34 base pair exon to specifically test exonic splicing enhancer (ESE) sequences. (B) RT-PCR results visualised on 3% agarose gel show marked difference in the strength of the substituted ESE sequence (EV) and the TDP-43 exon 6 ESE, which leads to a higher degree of exon skipping, which is more

pronounced in the A315A compared to wild-type sequence. (C) Quantification of four independent transfection experiments in SH-SY5Y cells shows a small but significant difference between the wild-type and A315A sequence in the ANOVA with Least Significant Difference (LSD) post-hoc test.

4.2.3 Expression of wild-type and mutant TDP-43

FLAG-tagged TDP-43 was cloned into a mammalian expression vector with wild-type sequence, as well as the D169G, A321G, Q331K and M337V mutations. All constructs expressed equally well in Hek293T cells, with predominantly nuclear localisation and a staining pattern similar to that of endogenous TDP-43. No difference was discernible between wild type and mutant constructs. An assay to assess cell viability was performed (MTT assay), which showed no difference between wild-type and any of the mutants.

Increased exposure of Western blots did not show any increase in low molecular weight fragments, as has been reported for the Q331K and M337V mutations overexpressed in CHO cells (Sreedharan et al. 2008).

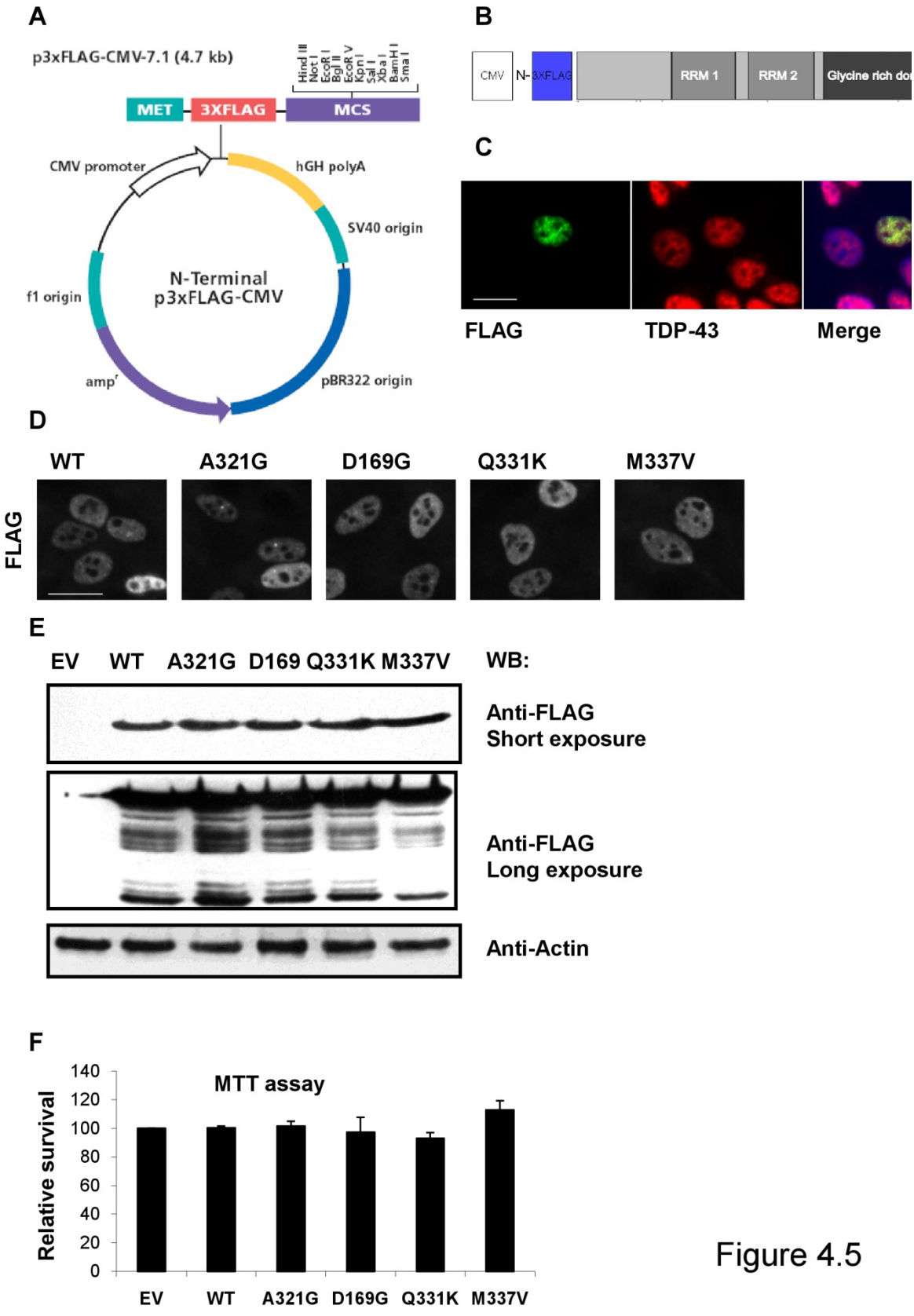

Figure 4.5

Figure 4.5 p3XFLAG-TDP-43 expression (A) Schematic of the p3XFLAG mammalian expression vector with CMV promoter (B) TDP-43 cDNA construct

with N-terminal 3XFLAG-tag. (C) Expression of 3XFLAG-TDP-43 in Hek293T cells showed predominantly nuclear localisation and a granular staining pattern similar to endogenous TDP-43. (D) Wild-type (WT) and various point mutations show and identical nuclear expression pattern. (E) All cDNA constructs expressed equally well with no difference in degradation products as assessed by Western blot for FLAG. (F) and no difference in cell viability in the MTT assay (G).

4.2.3.1 Sub-cellular distribution of wild-type and mutant TDP-43

Since one of the pathological hallmarks of TDP-43 proteinopathies is the cytoplasmic redistribution of TDP-43 (see chapter 5), the proportion of cytoplasmic TDP-43 was assessed by nuclear-cytosolic fractionation and subsequent Western blotting of cell lysates. Cells containing prominent cytosolic TDP-43 on immunocytochemistry were also quantified. In addition to the point mutations mentioned above, a truncated C-terminal deletion mutant (TDP-43ΔCT), missing amino acids 263-414, was used in this experiment to address the role of the C-terminal domain in cellular localisation. While wild-type TDP-43 localised predominantly to the nucleus, TDP-43ΔCT displayed equal nuclear and cytosolic distribution, as well as loss of the fine granular staining pattern in the nucleus. It therefore appears that the C-terminal domain is important for nuclear shuttling, but that loss of this region does not completely abrogate nuclear import. The fact that C-terminal point mutations did not alter cellular localisation suggests that small changes in the C-terminal domain are tolerated.

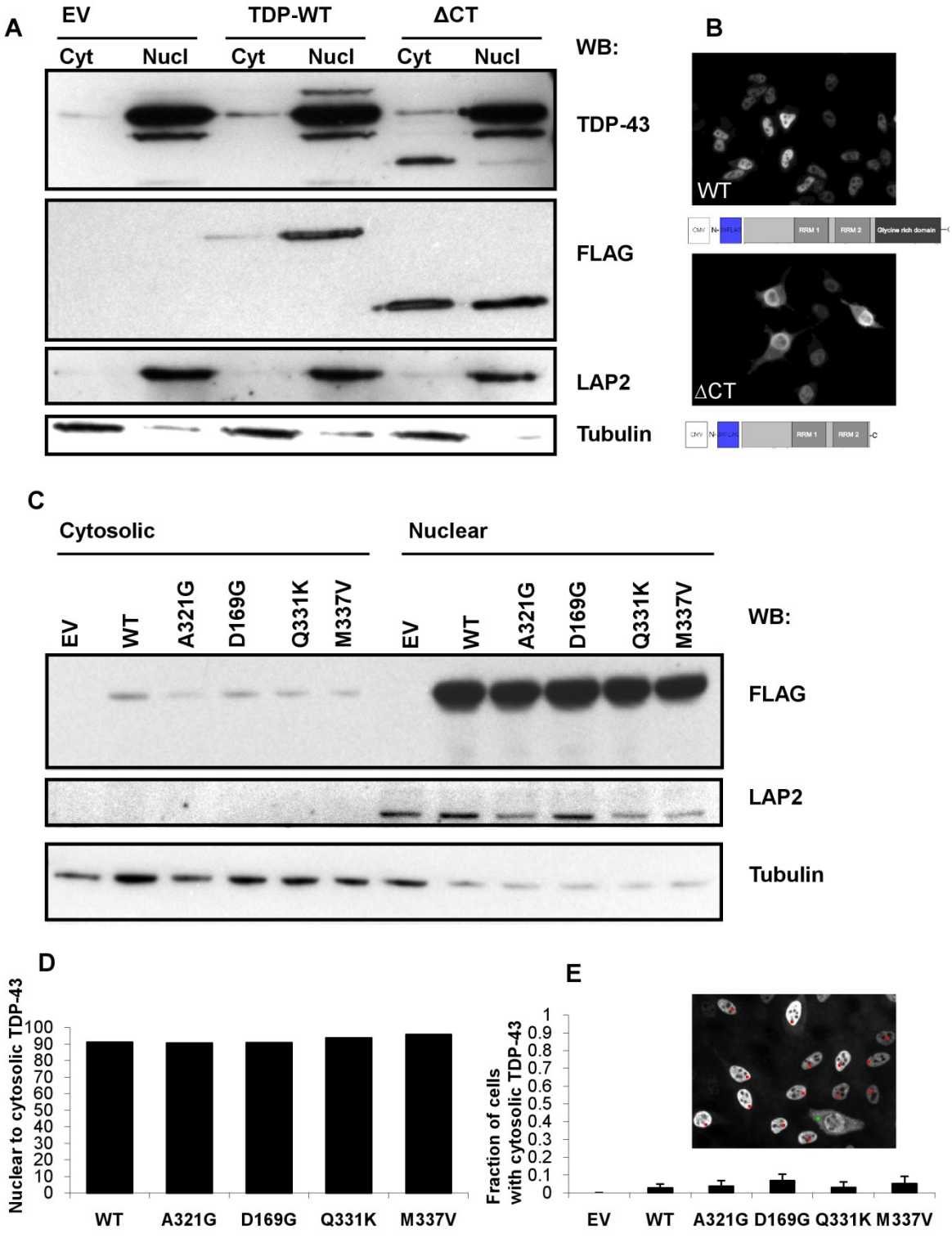

Figure 4.6 Cellular distribution of TDP-43 (A) Western blot of fractionated Hek293T cell lysates after transfection with wild-type (WT) or C-terminally deleted TDP-43 (ΔCT) shows predominantly nuclear (nucl) expression of endogenous TDP-43 and TDP-WT, whereas TDP-43-ΔCT shows prominent cytosolic (cyt) localisation. Nuclear/cytosolic fractionation was monitored by Western blot against the nuclear antigen LAP2 and the cytosolic tubulin. (B) Immunocytochemistry is in

keeping with Western blot results with marked cytosolic TDP-43-ΔCT. (C) Western blot of fractionated cell lysates after transfection with wild-type or point mutant TDP-43 and (D) quantification of nuclear to cytosolic ratio shows no difference between genotypes. (E) Every population of transfected cells contains a number of cells with prominent cytosolic TDP-43 expression, reflecting high expression levels, stage of transfection or both. No difference of the fraction of cytosolic TDP-43 containing cells was apparent between genotypes. Error bars represent the standard deviation of the mean counts of three independent transfection experiments.

4.2.3.2 Effect of proteasome inhibition

Cleaved TDP-43 resulting in distinct lower molecular weight species is a feature of ALS (see chapter 5). Several groups reported the presence of additional 28 kDa (Kabashi et al. 2008a) or 25 and 35 kDa (Rutherford et al. 2008) bands in the insoluble fraction of patient lymphoblastoid cell line lysates treated with the proteasome inhibitor MG132. The functional significance of this is unclear. It could mean that TDP-43 cleavage products are cleared through the proteasome, inhibition of which would lead to enhanced visibility of the fragments. Alternatively, proteasome inhibition could be causal in producing the fragments, for instance via secondary caspase activation and proteolytic, caspase mediated cleavage.

To test the hypothesis that mutant TDP-43, but not wild-type, would form distinct cleavage products either induced by or enhanced through proteasome inhibition, Hek293T cells were transfected with TDP-43 constructs and treated with MG132. Proteasome inhibition was monitored by Western blotting for HSP70, a heat shock protein known to be up-regulated under this condition. Western blotting for FLAG and TDP-43 showed increased cleaved TDP-43 species, but no qualitative difference between mutant and wild-type TDP-43, suggesting that mutations in TDP-43 do not in themselves lead to novel cleavage products (figure 4.7). Immunostaining of cells treated with MG132 showed cytosolic granules in a

proportion of cells, with no significant difference between wild-type and mutant TDP-43.

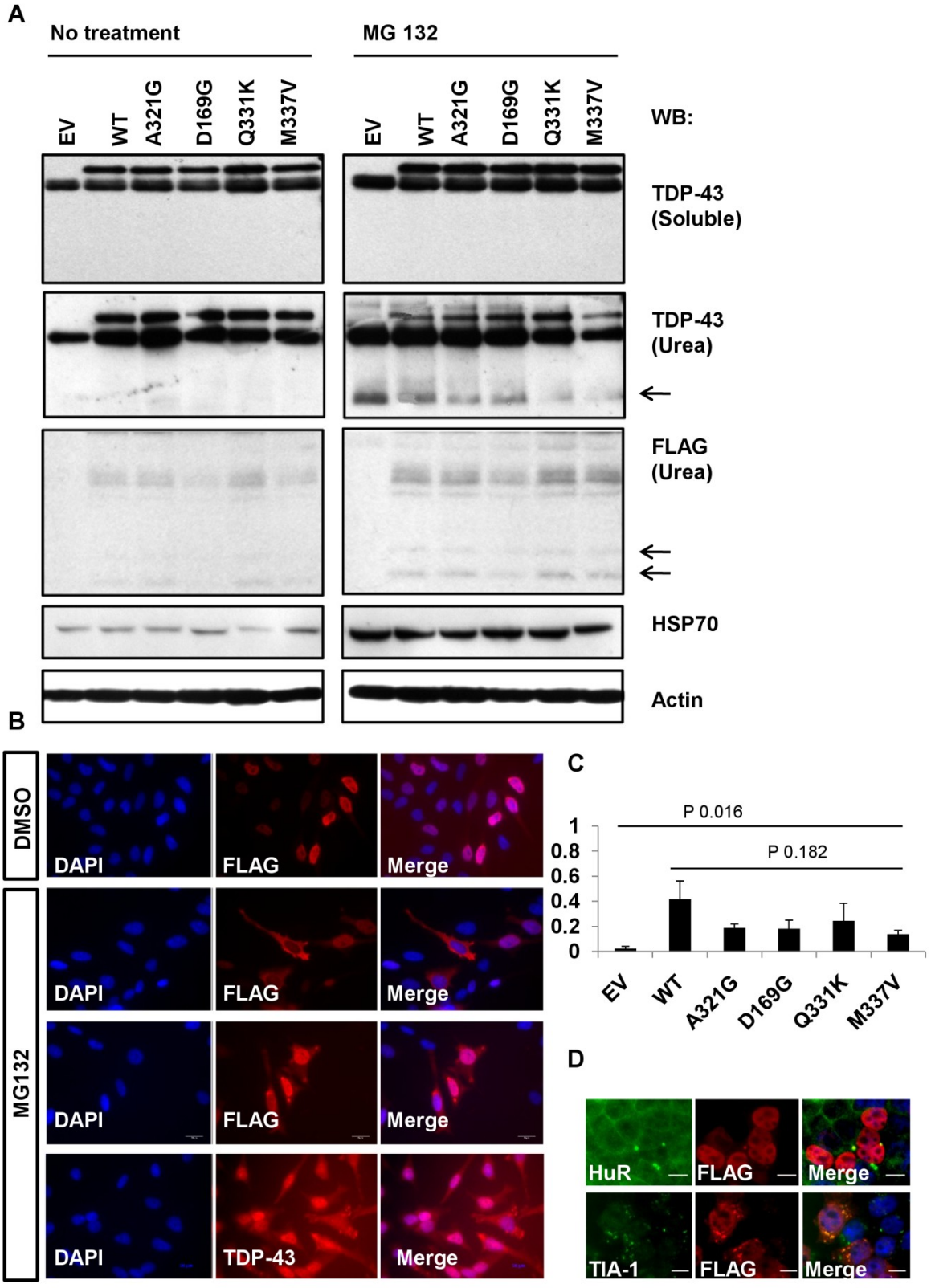

Figure 4.7 Effect of proteasome inhibition (A) Hek293T cells transfected with wild-type (WT) or mutant TDP-43, or empty vector only (EV), treated with the proteasome inhibitor MG132 show low molecular weight TDP-43 species (arrow) visible on Western blot of the urea (insoluble) fraction for TDP-43 and FLAG independent of genotype. (B) Immunocytochemistry of MG132 treated cells shows variable degrees of cytosolic redistribution and dense cytosolic aggregates for both endogenous and transfected (FLAG) TDP-43. (C) Quantification of fraction of cells with TDP-43 (for EV) or FLAG-positive cytosolic granules shows more granules in transfected compared to untransfected cells, but no significant difference between genotypes in transfected cells. Kruskal-Wallis test. (D) The FLAG-positive cytosolic granules co-localise with the stress granule markers TIA-1 and HuR.

4.2.4 Effect of cell stress on TDP-43 positive cytosolic granules

Double-labelling of cells transfected with FLAG-TDP-43 with and without MG132 treatment showed that the observed FLAG positive cytosolic granules in MG132 treated cells also stained positive for the stress granule markers HuR and TIA-1, suggesting that TDP-43 is involved in a physiological stress response, which has also been observed by others (Colombrita et al. 2009a). To further investigate this, SH-SY5Y cells were treated with the robust stress granule inducer sodium arsenite, which reliably induced HuR/TIA-1 positive cytosolic granules in a proportion of cells that were indistinguishable to those observed under MG132 treatment. Cytosolic granules did not stain positive for another nuclear splicing factor, SC-35, suggesting that this is not just a non-specific response leading to re-distribution of nuclear antigens to the cytoplasm through for instance damage to the nuclear membrane. Both wild-type and mutant FLAG-tagged TDP-43 co-localised in stress granules, and there was no qualitative or statistically significant quantitative difference in stress granule formation between wild-type and mutant. The number of stress-granule containing cells was higher in transfected compared to untransfected cells (figure 4.7 C), in keeping with the observation that many

stress granule components can nucleate stress granules when overexpressed (Kedersha and Anderson 2007).

Finally, stress granules were induced in cells transfected with TDP-43 constructs containing both an N-terminal FLAG-tag as well as a C-terminal HA-tag. Both anti-FLAG and anti-HA antibodies equally recognised wild-type, A321G and M337V TDP-43 in nuclei and cytosolic granules, indicating that the cytosolic granules contain full length TDP-43 and are not preferentially made up of a cleaved species.

4.2.5 *Trans*-acting effects of TDP-43 on splicing

The TDP-43 C-terminal domain is critical for its role in splicing regulation of other transcripts. To assess whether point mutations alter the splicing inhibitory function, a well established *trans*- splicing assay based on alternative splicing of the CFTR exon 9 was utilised. This showed that wild-type TDP-43, when co-transfected with the CFTR minigene, has a strong negative effect on splicing of CFTR exon 9 and leads to exon skipping. The C-terminally deleted TDP-43, in contrast, lacked this property and did not cause CFTR exon 9 skipping. When the same experiment was repeated comparing wild-type and point mutants, no difference between genotypes was apparent, again suggesting that C-terminal point mutations do not abolish the C-terminal function, at least within the sensitivity of this assay (figure 4.9).

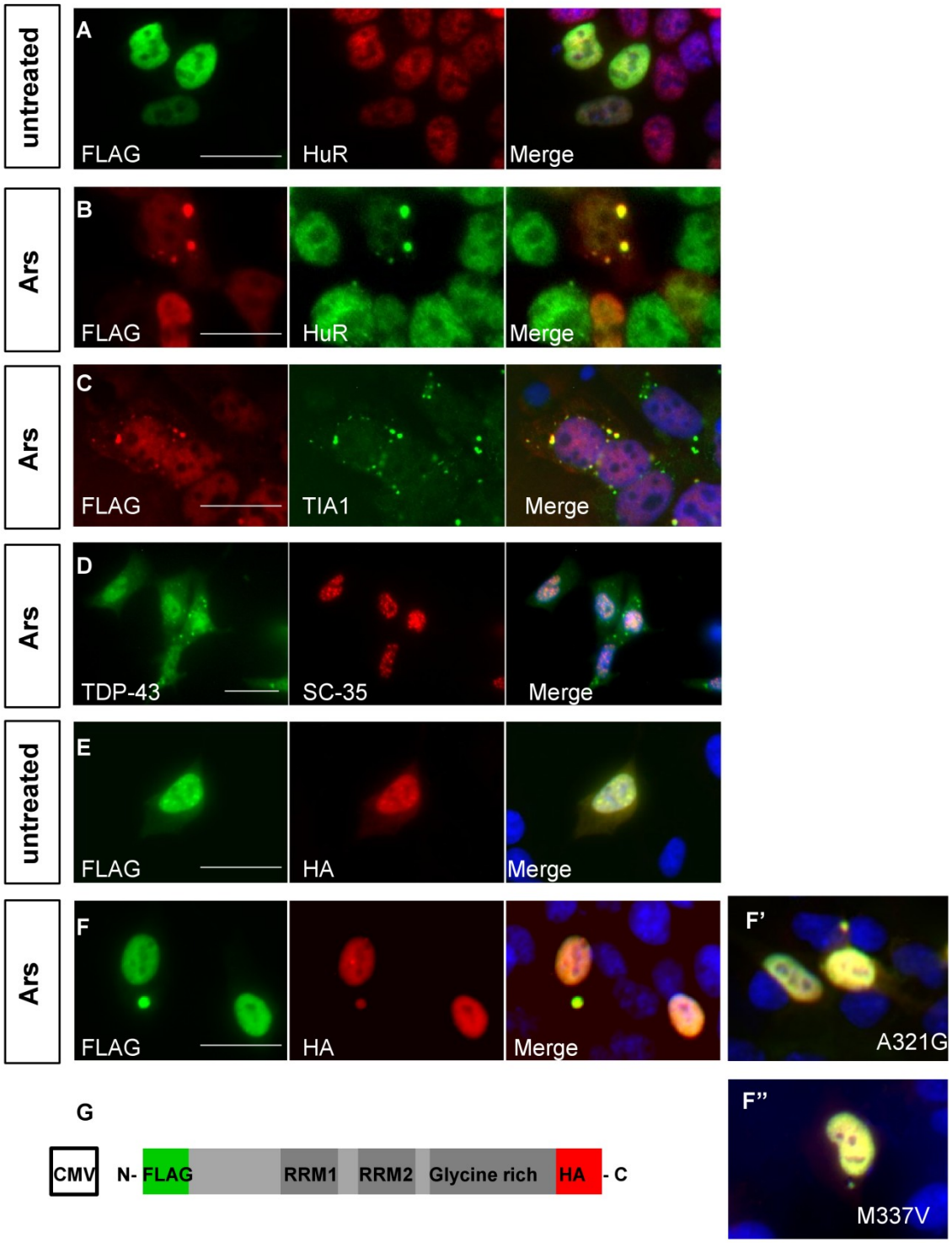

Figure 4.8 TDP-43 forms stress granules in cell culture SH-SY5Y cells transfected with wild-type or mutant TDP-43, with and without treatment with 1mM sodium meta-arsenite for one hour (A) FLAG-TDP-43 in untreated cells shows nuclear localisation similar to the stress granule marker HuR and colocalises with it (B) and TIA-1 (C) in cytosolic granules after arsenite treatment. (D) Endogenous

TDP-43 also forms cytosolic granules, but the nuclear splicing factor SC35 does not. (E) N- and C-terminally tagged TDP-43 is recognised equally by anti-FLAG and anti-HA antibodies. (F) Both N- and C-terminal domains are present in stress granules in wild-type (F), A321G (F') and M337V (F'') TDP-43. (G) Cartoon depicting the structure of the double-tagged TDP-43 construct with N-terminal 3XFLAG-tag and C-terminal HA-tag under the control of the CMV promoter. Scale bars 20 µm. Ars, arsenite.

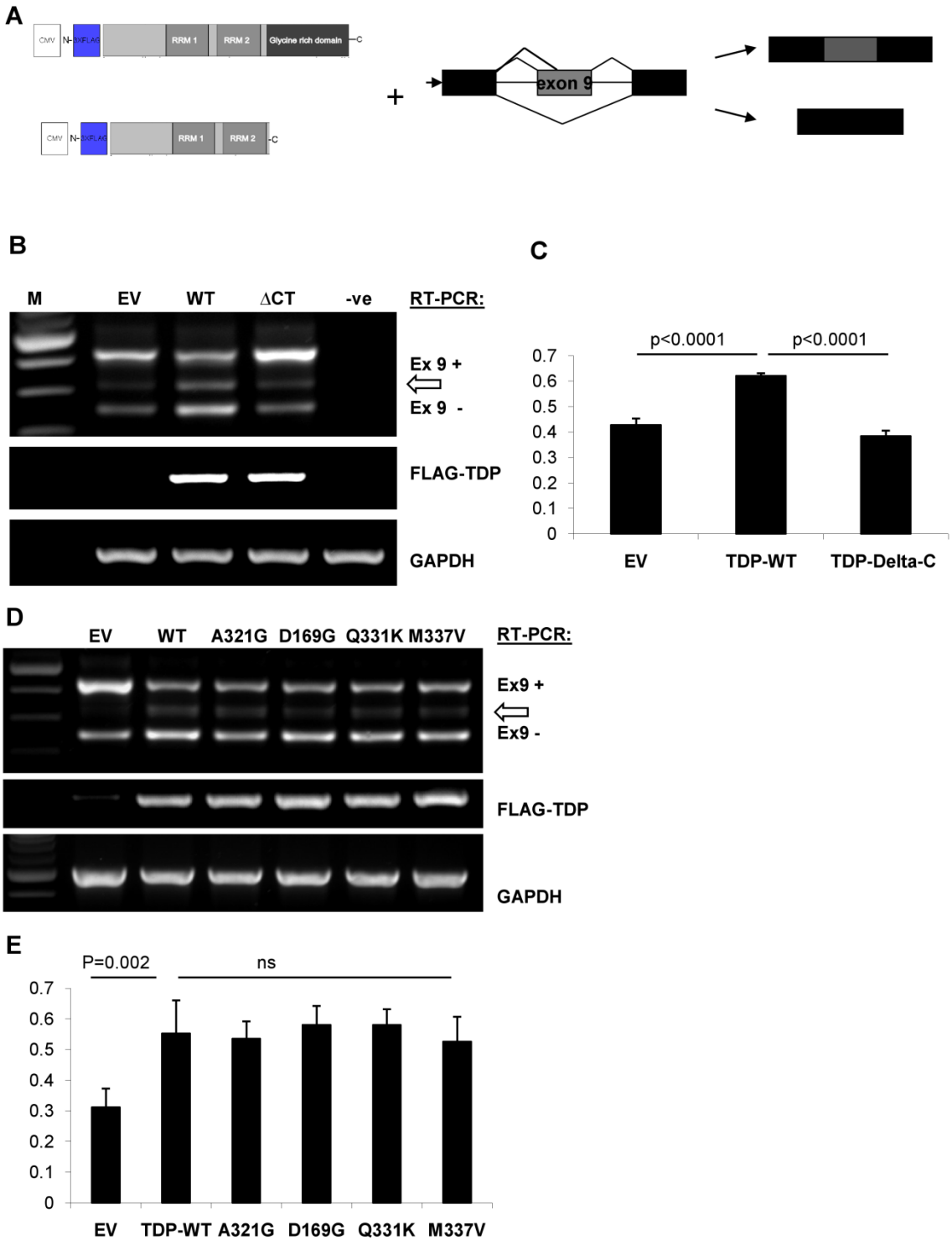

Figure 4.9 Effect of wild-type and mutant TDP-43 on CFTR splicing (A) schematic of HeLa cell transfection with full-length (wild-type or mutant) and/or C-terminally deleted 3xFLAG-TDP-43 and the CFTR splicing minigene with resulting isoforms +/- exon 9 on RT-PCR. A minor product results from activation of a cryptic splice site in exon 9. (B) RT-PCR results for empty vector (EV), TDP-43 wild-type (WT) and C-terminally deleted TDP-43 (ΔCT) show exon skipping induced by wild-type, but not C-terminally deleted TDP-43. The open arrow in (B) and (D) indicates a previously described minor splice variant resulting from activation of a cryptic splice site in exon 9. (C) Densitometric quantification of (B) expressed as the degree of exon skipping (-ex 9 /total CFTR), One-way ANOVA, LSD test. (D) Identical experiment performed with co-transfection of wild-type and point-mutant TDP-43 shows exon skipping induced by wild-type, but also by mutant TDP-43 with no difference in the degree of exon skipping induced between genotypes (E). Error bars represent standard deviation of the mean of three independent transfection experiments. Transfection efficiency was monitored by RT-PCR for FLAG-TDP-43, and reverse transcription by RT-PCR for GAPDH.

While CFTR is the best characterised TDP-43 target, a report that TDP-43 might modulate splicing of the SMN2 gene by increasing levels of full length SMN compared to transcripts lacking exon 7 (Bose et al. 2008) is potentially more relevant to motor neuron disease pathophysiology, as reduced SMN levels might be a risk factor for ALS. When TDP-43 was over-expressed in HeLa cells, no effect on endogenous *SMN2* exon 7 splicing was apparent, independent of the amount of TDP-43 present. The primers used in this assay did not distinguish, however, between transcript derived from *SMN1* or *SMN2*, leading to reduced sensitivity of the RT-PCR for subtle degrees of differential splicing because the abundance of *SMN1* derived full length SMN was so high compared to SMN-Δ7. In addition, there was no difference between overexpression of wild-type or mutant TDP-43, although the absence of an effect of wild-type TDP-43 on endogenous SMN splicing questions the suitability of this assay to test the differential effect of mutations.

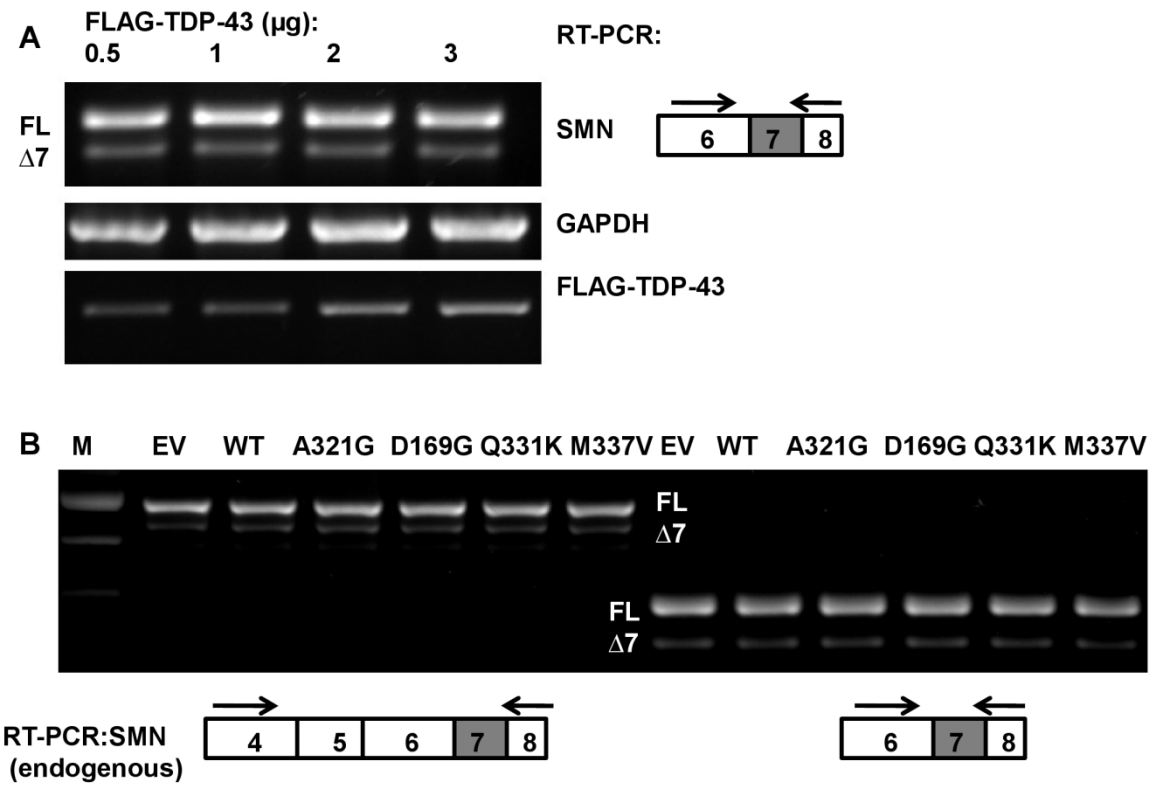

Figure 4.10 Effect of TDP-43 on SMN splicing (A) HeLa cells transfected with increasing amounts of TDP-43 show no difference in the degree of SMN exon 7 inclusion. (B) The majority of SMN transcript contains exon 7, as assessed by two different RT-PCR protocols. There is no obvious effect of either wild-type (WT) or point mutant TDP-43 overexpression on SMN exon 7 skipping. FL, full length; Δ7, SMN lacking exon 7; EV, empty vector.

4.2.6 Interaction of TDP-43 with SMN

Independent of the potential effect of TDP-43 on splicing of the SMN transcript, TDP-43 has been described as a SMN protein binding partner (see above and (Wang et al. 2002)). To assess whether SMN binding could be used as a robust read-out for mutation analysis, Hek293T cells were transiently transfected with both wild-type and mutant (A321G) FLAG-TDP-43, which was then immunoprecipitated using an anti-FLAG antibody. To see whether TDP-43 would co-immunoprecipitate SMN, membranes were probed with an SMN antibody, which revealed distinct but faint bands for both wild-type and mutant, suggesting

a weak interaction between SMN and TDP-43 that is not significantly altered by the presence of mutations, which is further supported by the observation that the co-immunoprecipitation is independent of the presence of the C-terminal domain. Overall, the interaction appeared weak and extremely sensitive to small alterations in the IP buffer. There was only occasional, partial colocalisation of endogenous TDP-43 with SMN in Hek239T cells, and no clear colocalisation of overexpressed FLAG-TDP-43 with HA-SMN. Together with the results presented in chapter five which show that colocalisation of SMN and TDP-43 is only infrequent, these findings argue against a critical constitutive interaction between SMN and TDP-43, and suggest that the TDP-43-SMN co-IP is not a useful tool to assess differences between TDP-43 genotypes. In addition, overexpression of tagged proteins is very artificial and can lead to false positive results.

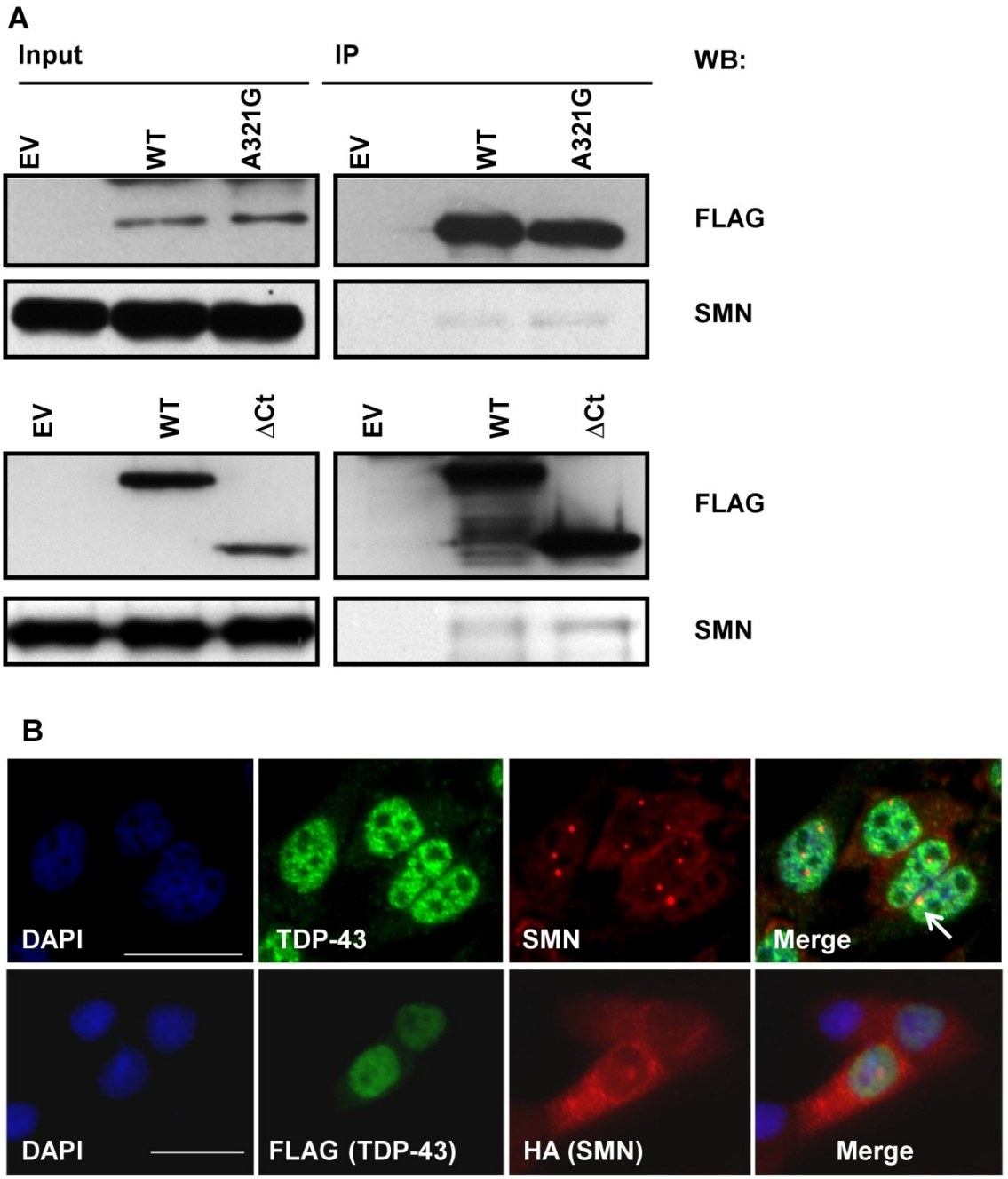

Figure 4.11 Interaction of TDP-43 with SMN (A) Lysates of Hek293T cells transfected with empty vector (EV), wild-type, A321G or C-terminally deleted (ΔCt) TDP-43 were immunoprecipitated with an anti-FLAG antibody followed by Western blotting for SMN, showing weakly positive bands indicating a degree of co-immunoprecipitation of SMN with TDP-43 for wild-type, A321G and also the C-terminally deleted TDP-43. (B) Immunocytochemistry for TDP-43 (endogenous, top, FLAG-tagged, bottom) and SMN (endogenous, top, HA-tagged, bottom) in Hek293T cells shows only infrequent partial colocalisation (arrow) in gems.

4.3 Discussion

This chapter attempted to address the question of pathogenicity of both synonymous and protein changing TDP-43 variants. To examine synonymous variants, a *cis*-splicing minigene system was employed which showed that the A66A variant is likely to be a benign variant with no effect on TDP-43 splicing, in agreement with the available genetic data. The preliminary data relating to the A315A variant suggest that further analysis is warranted. A weakened ESE could potentially lead to a truncated protein by activation of a cryptic splice site proximal to the STOP codon, and a truncation mutation (Y374X) has been reported to be pathogenic (Daoud et al. 2009). On the other hand, the A315A variant was detected in a patient with ALS harbouring the protein changing G287S mutation on the other TDP-43 allele (Corrado et al. 2009b), as well as in a patient with MND-FTD, whose affected relative did not harbour the variant (Benajiba et al. 2009), suggesting that it was not the primary disease causing mutation in these cases. The difficulty in modelling 3' terminal exon variants in minigene systems could be overcome by more sophisticated models such as dual luciferase constructs allowing for simultaneous quantification of transfection efficiency and expression levels of the target sequence. The optimal approach to study splice variants in the native context however is to look at expression *in vivo*. Given the relatively high frequency of the A315A variant, it should be possible to obtain RNA from spinal cord and brain from patients with this change to definitively assess the splicing pattern associated with it.

The most striking feature overall of the functional analysis of the protein changing variants is the similarity of wild-type and mutant in all assays employed. The staining pattern, sub-cellular distribution and splicing inhibitory function is identical

for wild-type and all tested mutants, while the C-terminal deletion construct showed altered localisation and splicing function, in keeping with other reports stressing the importance of the TDP-43 C-terminal domain for cellular localisation (Ayala et al. 2008b) and splicing inhibition (D'Ambrogio et al. 2009).The latter is thought to be dependent on the interaction of TDP-43 with hnRNPA2, which has been mapped to TDP-43 residues 321-366, the region containing many TDP-43 mutations. However, the TDP-43 mutations Q331K, M337V (which were also analysed here) and G348C were found not to alter the TDP-43/hnRNP A2 interaction, possibly due to the extensive number of polar and hydrophobic interactions that likely contribute to the protein-protein interaction, and did also not modify the splicing inhibitory function in a CFTR minigene assay (D'Ambrogio et al. 2009), confirming the results presented in this work. TDP-43 mutations found in patients are thus unlikely to be simple loss of function mutations. The fact that no obvious cellular phenotype emerged in cell culture after transient transfection is perhaps not surprising given the fact that TDP-43 mutations in humans are tolerated for many decades before the phenotype emerges. In addition, TDP-43 mutations are present only in the minority of cases of TDP-43 proteinopathies, which shows that wild-type TDP-43 can be part of the same pathogenetic events as mutant TDP-43, which might mechanistically act as a susceptibility factor for TDP-43 disease rather than a primary, necessary cause. In this work, there was a trend for wild-type TDP-43 to form more stress granules compared to mutant TDP-43. Stress granule formation is a feature of translationally active, healthy cells and is suppressed in cells in which translation is stalled due to various causes (Kedersha and Anderson 2007). The reduced number of stress granule forming mutant TDP-43 expressing cells could thus be a subtle sign of toxicity not visible in

other assays. TDP-43 toxicity for mutant but not wild-type has been described in a chick embryo model (Sreedharan et al. 2008), which revealed increased cell death and developmental abnormalities. Surprisingly, these deficits were absent for the SOD1 G93A mutation tested as a control implying a mutant TDP-43 specific effect. The significance of this developmental model for late onset neurodegenerative disease remains to be defined.

Overexpressing mutant (A315T, G348C, A382T) and wild-type TDP-43 in Neuro2A cells did not show a phenotypic difference, whereas primary motor neurons microinjected with these constructs displayed signs of aggregation and toxicity that was more pronounced for two of the mutants than for wild-type or A382T-TDP-43. Zebrafish overexpressing TDP-43 developed a motor phenotype that was again more pronounced for the mutant than for the wild-type form (Kabashi et al. 2009). This is in keeping with the notion that any difference between TDP-43 mutations and wild-type is gradual rather than categorical. Of note, the first published TDP-43 transgenic mouse developed pathological features reminiscent of ALS by over-expressing wild-type TDP-43 (Wegorzewska et al. 2009).

Independent of the TDP-43 mutation status, cleavage of TDP-43, which can be mediated through caspases (Zhang et al. 2007b; Dormann et al. 2009) and the accumulation of C-terminal insoluble fragments are features of TDP-43 neuropathology (see chapter 5) that have been re-capitulated to various degrees in cell culture systems. For example, overexpression of 25-kDa C-terminal fragments has been shown to lead to cell toxicity, as well as aggregation followed by phosphorylation and ubiquitination (Zhang et al. 2009), and loss of splicing inhibitory function (Igaz et al. 2009). C-terminal fragments that aggregate could

further sequester endogenous TDP-43, but the data are conflicting at present (Nonaka et al. 2009). Taken together with previous reports, the findings presented here suggest that TDP-43 disease can be facilitated by TDP-43 mutations, while the differences to wild-type TDP-43 are subtle. The down-stream effects of TDP-43 proteinopathies could include toxic gain of function of cleaved TDP-43 species or loss of nuclear or cytosolic function secondary to aggregation of TDP-43 in cytosolic inclusions.

The next chapter will address whether some of the aspects of TDP-43 diseases can be studied in a commonly used mouse model of ALS, the SOD1 G93A mouse. In addition, it will expand on the potential interaction of SMN and TDP-43 by examining TDP-43 expression in an SMA mouse model, and SMN expression in human TDP-43 positive ALS. Finally, the specificity of TDP-43 pathology will be examined in cases of ALS with basophilic inclusions.

5 Neuropathology of TDP-43 and FUS

5.1 Introduction

5.1.1 Neuropathology of ALS

5.1.1.1 TDP-43 pathology

Since the discovery of TDP-43 as the core constituent of ubiquitinated inclusions in ALS and FTLD (Arai et al. 2006; Neumann et al. 2006), several publications have demonstrated the sensitivity of TDP-43 immunohistochemistry in labelling ubiquitinated inclusions in ALS (Mackenzie et al. 2007; Tan et al. 2007) and FTLD (Cairns et al. 2007; Davidson et al. 2007; Higashi et al. 2007a; Seelaar et al. 2007), including neuronal cytoplasmic inclusions, dystrophic neurites, neuronal intranuclear inclusions and glial cytoplasmic inclusions. In addition to labelling pathological inclusions, TDP-43 staining of affected cells is characterised by a dramatic reduction of the physiological nuclear immunoreactivity suggesting abnormal redistribution of TDP-43 in disease states.

Biochemical analysis of TDP-43 on lysates of diseased brain and spinal cord tissue has consistently shown a unique profile of bands in the urea fraction in a serial fractionation protocol intended to enrich for insoluble protein species. Characteristically, TDP-43 immunoblotting shows a high molecular weight smear corresponding to polyubiquitinated species, a 45 kDa band as well as 25 kDa band in addition to the expected 43 kDa band (Neumann et al. 2006), suggesting C-terminal cleavage of TDP-43 as well as hyperphosphorylation. The latter was confirmed by demonstrating mobility shift of the 45 kDa band after phosphatase treatment. While many RNA binding proteins are physiologically phosphorylated, the notion that TDP-43 is pathologically phosphorylated in disease gained support

from studies generating phosphospecific antibodies against TDP-43 that specifically label pathological inclusions, while not staining physiological nuclear TDP-43 (Hasegawa et al. 2008; Inukai et al. 2008; Kametani et al. 2009). TDP-43 is predicted to contain 64 potential phosphorylation sites, many of which are located in the C-terminal domain. Phosphospecific antibodies against several different synthetic peptides with phospho-sites stain pathological inclusions, while antibodies against phosphoserines 409 and 410 (pS409/410) appear to produce the most specific results for staining pathological TDP-43 (Inukai et al. 2008).

Abnormal TDP-43 has been identified in all cases of sporadic ALS, as well as forms of familial ALS not due to mutations in SOD1, but not in cases of SOD1 linked familial ALS (Mackenzie et al. 2007; Tan et al. 2007), suggesting that SOD1 mutations mediate disease through a distinct mechanism.

In cases of FTLD, TDP-43 pathology has been identified in the majority of cases with ubiquitin pathology, including those due to mutations in progranulin (*GRN)* and valosin-containing protein *(VCP),* but not in cases with mutations in charged multivesicular body protein 2b *(CHMP2b*) (Cairns et al. 2007).

The uniform features of TDP-43 neuropathology in most cases of ALS and FTLD-U, together with the conspicuous absence of TDP-43 pathology in otherwise phenotypically very similar cases suggests that TDP-43 occupies a specific role upstream in the pathophysiology of the genetically heterogeneous disorders ALS and FTLD, rather than being a downstream effect secondary to neuronal damage.

On the other hand, the role of TDP-43 in other neurodegenerative disorders is far from clear at present. The Perry syndrome, caused by mutations in dynactin (Farrer et al. 2009; Vilarino-Guell et al. 2009), appears to be a primary TDP-43

proteinopathy but has no phenotypic similarity to ALS (Wider et al. 2009). In addition, neurodegenerative disorders with predominant tau or alpha-synuclein pathology have been found to display variable degrees of TDP-43 pathology. For example, Arai et al described TDP-43 staining of Pick bodies in Pick's disease, neurofibrillary tangles in Alzheimer's disease and coiled-structures in corticobasal degeneration (Arai et al. 2006), and later found a high incidence of TDP-43 pathology in Alzheimer's disease and diffuse Lewy body disease using phospho-specific TDP-43 antibodies and a highly sensitive technique with free floating sections and automatic immuno-stainers (Arai et al. 2009). Others have found TDP-43 pathology in the parkinsonism-dementia complex and ALS of Guam (Geser et al. 2008), Lewy body disease, Parkinson's disease with and without dementia (Nakashima-Yasuda et al. 2007), Alzheimer's disease and hippocampal sclerosis (Amador-Ortiz et al. 2007; Higashi et al. 2007b; Hu et al. 2008; Uryu et al. 2008) and argyrophilic grain disease (Fujishiro et al. 2009), but not in progressive supranuclear palsy or basophilic inclusion disease (see below).

Importantly, all non-ALS/FTLD neurodegenerative disorders examined for TDP-43 pathology (with the exception of the Perry syndrome) have other major pathological features such as tau or alpha synuclein positive inclusions that dominate the histological picture, while the TDP-43 pathology is present in a variable proportion of cases only, and TDP-43 is only abnormal in restricted anatomical areas in these cases. TDP-43 pathology is concomitant and not primary in these disorders, suggesting that TDP-43 is either altered in response to the primary pathology, or these disorders share a common aetiological factor.

No studies have systematically analysed TDP-43 pathology of human non-ALS motor neuron disorders.

5.1.1.2 Basophilic inclusion disease

Sporadic juvenile ALS with onset below 25 years of age is exceedingly rare (Alonso et al. 2009) and has been proposed to constitute a distinct clinical entity (Nelson and Prensky 1972; Gouveia and de Carvalho 2007). This is supported by distinct histological findings in all reported autopsy cases (Nelson and Prensky 1972; Oda et al. 1978; Matsumoto et al. 1992; Matsumoto et al. 1993; Aizawa et al. 2000). All cases showed the presence of basophilic intraneuronal inclusions on standard H&E and Nissl stains, which is an uncommon finding in late onset ALS (Murayama et al. 1990).

Nelson and Prensky observed a close spatial relationship of basophilic inclusions with the Nissl substance, and could demonstrate that staining intensity of the inclusions markedly diminished after treating sections with ribonuclease, suggesting that RNA was a key component of these inclusions (Nelson and Prensky 1972). In keeping with this finding, Oda et al showed in an ultrastructural study using electron microscopy that basophilic inclusions in a 17 year old girl contained free ribosomes and endoplasmatic reticulum in addition to more poorly defined tubular structures (Oda et al. 1978). Immunohistochemical studies showed that labelling with anti-ubiquitin antibodies, which stain inclusions in typical adult onset ALS, was not a reliable marker of basophilic inclusions (Matsumoto et al. 1992; Aizawa et al. 2000).

While most reports of basophilic inclusions stem from cases of very early onset, juvenile ALS, there are some reports of indistinguishable pathology in adult onset ALS cases (Kusaka et al. 1990; Sasaki et al. 2001), which shows that neither purely clinical, nor neuropathological criteria alone are fully satisfactory in classifying these diseases.

Apart from motor neuron disease, basophilic inclusions are also prominent features in a subtype of frontotemporal lobar degeneration (FTLD) (Josephs et al. 2003). FTLD is generally classified according to the dominant abnormal protein that can be detected by immunohistochemistry. The main groups are FTLD-tau, with tau positive neuronal inclusions, as well as FTLD-U, in which inclusions can be visualised by antibodies against components of the ubiquitin-proteasome system, such as ubiquitin or p62 (Mackenzie et al. 2009). The majority of cases of FTLD-U are TDP-43 proteinopathies, whereas a minority are TDP-43 negative. Some neuropathologically distinct types of FTLD fall outside this classification system, including neuronal intermediate filament inclusion disease (NIFID) and FTLD with basophilic inclusions (FTLD-BID).

Like TDP-43 proteinopathies, which can underlie ALS, FTLD or FTLD-MND, there are some cases of FTLD of the basophilic inclusion type with associated motor neuron disease (Holton et al. 2002; Ishihara et al. 2006), implying that basophilic inclusion disease is an entity that can find variable clinical expression, making neuropathological findings in cases of adult onset ALS or FTLD with basophilic inclusions relevant to this study of young onset ALS. A recent study of adult onset ALS with basophilic inclusions (Fujita et al. 2008) re-analysed two previously reported cases (Kusaka et al. 1990; Kusaka et al. 1993) with the intention of identifying whether the inclusions, rather than being non-specific aggregates of RNA and associated proteins, would contain specific groups of RNA binding proteins. Indeed, their study identified TIA1, PABP1 and rpS6 (a marker of the small ribosomal subunit) in inclusions, while rpL28 (marker of the large ribosomal subunit) and the decapping enzyme Dcp1 and TDP-43 were absent. The specific

constellation of RNA binding proteins could be interpreted as showing that basophilic inclusions arise from stress granules (see chapter 1).

5.1.2 Aims of chapter 5

The aims of work in this chapter were to further define the spectrum of TDP-43 pathology in subtypes of motor neuron disease, both in mouse models and available human tissue. First, TDP-43 pathology was examined in the most commonly used mouse model of ALS, the SOD1 G93A transgenic mouse (Turner and Talbot 2008). While TDP-43 pathology is present in almost all cases of ALS, it appears to be absent in familial ALS due to SOD1 mutations (Mackenzie et al. 2007). Sporadic and non-SOD1 related familial ALS, together with certain types of FTLD, can therefore be seen as TDP-43 spectrum proteinopathies, whereas SOD1 familial ALS may be a phenocopy of sporadic ALS with a different aetiopathogenesis (Kwong et al. 2008). This also means that the SOD1 G93A mouse might not accurately reflect the pathology found in the vast majority of human cases. Indeed, there is evidence that there is no TDP-43 redistribution in three mouse models of SOD1 ALS (Robertson et al. 2007). However, mouse models do not always reflect every aspect of human disease (Hafezparast et al. 2002), and the absence of TDP-43 redistribution does not rule out the presence of abnormal biochemical TDP-43 species. In particular, while ALS in humans is clearly an age dependent disease, all aspects of ALS neuropathology might not emerge within the short lifespan of the mouse. In the first part of this chapter, the cellular distribution of TDP-43 is examined in the SOD1G93A model of ALS, together with its expression level and biochemical state. To examine a potential role of TDP-43 in SMA, evidence of TDP-43 redistribution, altered expression or biochemistry is assessed in a common model of severe SMA, the 'SMNΔ7 mouse'

(Le et al. 2005). Further details on this mouse model are given in chapter 6. TDP-43 pathology in this non-ALS motor neuron disease model would point towards a non-specific role of TDP-43 in motor neuron injury, as suggested, for example, by the observation of transient TDP-43 redistribution after axotomy (Moisse et al. 2009b) (see chapter 1), or an interaction of TDP-43 with SMN.

In the second part of this chapter, the clinicopathological subtype of young onset ALS with basophilic inclusions is examined for TDP-43 pathology. With emerging information about the role of *FUS* in ALS (see chapter 3), cases included in this work are also examined for FUS pathology.

5.2 Results

5.2.1 TDP-43 expression in mouse models of ALS and SMA

5.2.2 Histopathology

First, spinal cords of end stage SOD1 G93A (four months) and Smn-/-; SMN2; SMNΔ7 mice (P13), together with their unaffected wild-type or Smn+/+; SMN2; SMNΔ7 littermates, were examined for ubiquitin or TDP-43 histopathology. A minimum of 2 non-adjacent lumbar spinal cord sections for each of 3 mice per genotype were analysed for histological features and the nuclear body counts detailed below. Motor neurons in terminal SOD1G93A mice, but not WT animals, showed extensive cytoplasmic staining with ubiquitin antibodies (figure 5.1). However, TDP-43 immunoreactivity was confined to nuclei only (figure 5.1). Thus, in contrast to sporadic and most familial cases of human ALS, TDP-43 did not aggregate into distinct inclusions and was not mislocalised from the nucleus to the cytoplasm in anterior horn cells of SOD1G93A mice. Interestingly, it appeared that some of the nuclei of presumed reactive astroglia in endstage SOD1G93A mice

showed a weaker TDP-43 signal than glia in WT litter mates (figures 5.1). Neither cytoplasmic TDP-43 redistribution, nor cytoplasmic ubiquitin staining was present in spinal cords of end stage SMA animals (figure 5.1h and i).

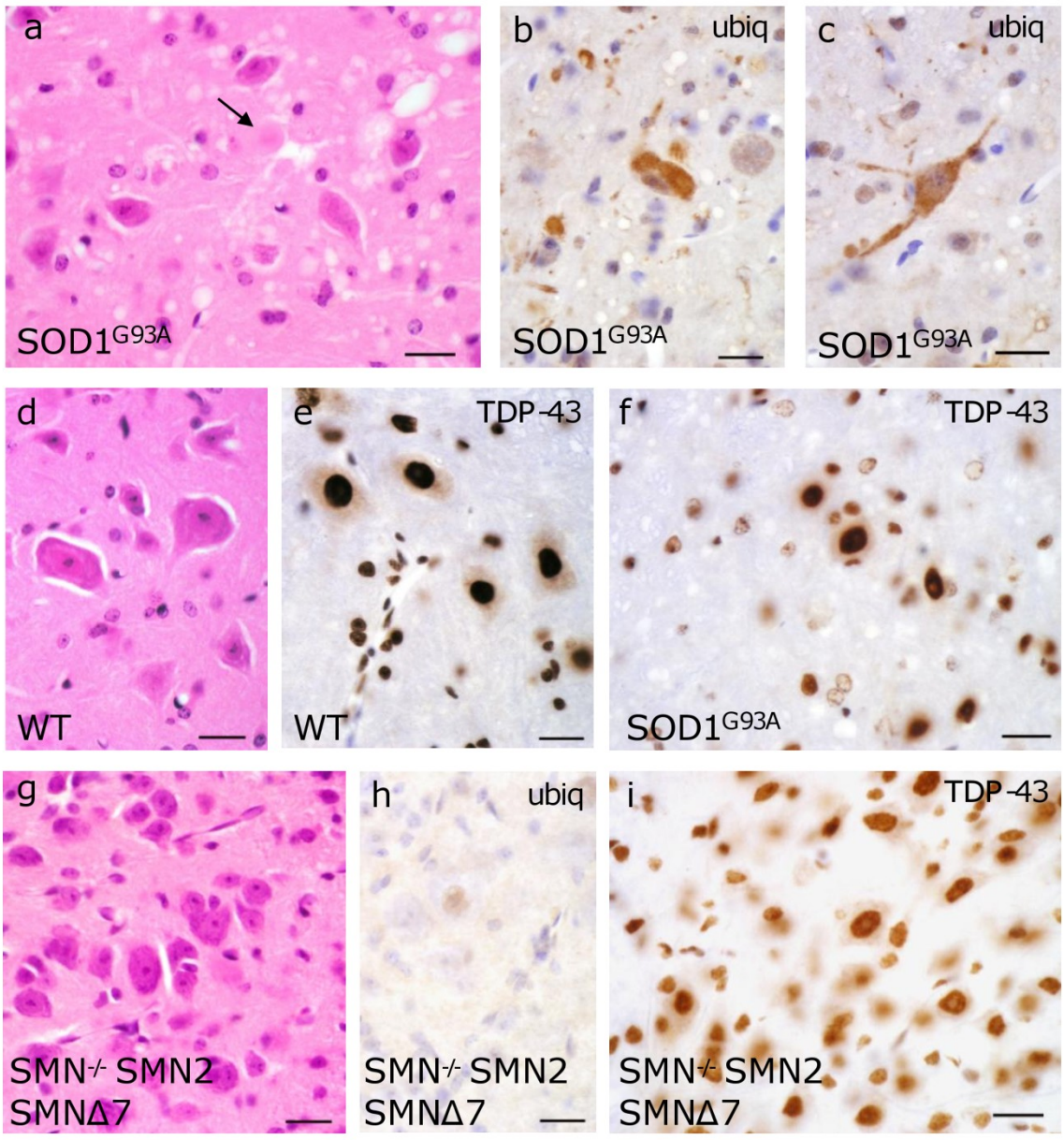

Figure 5.1 Histology of end-stage SOD1 G93A and SMNΔ7 spinal cord Lumbar spinal cord sections of transgenic SOD1^{G93A} mice (a-c, f) show anterior horn cell degeneration, hyaline aggregates (arrow) and vacuolation (a) not present in corresponding wild-type (d). Amorphous cytoplasmic aggregates are ubiquitinated and occasionally extend into proximal processes (b, c). TDP-43 remains located in the nucleus of anterior horn cells and shows no distinct aggregates (f). The appearances are essentially indistinguishable from wild-type (e) apart from possible slightly weaker TDP-43 signal in presumed reactive glia (f).

Samples from transgenic $SMN^{+/+}$ SMN2 SMNΔ7 spinal cord (g-i) show residual motor neurons (g) without ubiquitin positivity (h) and preserved nuclear TDP-43 signal (i). Scale bar in all images = 20 μm. Figure compiled by Dr Olaf Ansorge.

5.2.3 Nuclear architecture

Another aspect of TDP-43 pathology in human ALS is loss of nuclear TDP-43, and nuclear TDP-43 inclusions are a feature of some types of FTLD (Sampathu et al. 2006). Despite the absence of any obvious cytoplasmic TDP-43 pathology, its nuclear architecture was therefore examined next. TDP-43 immunoreactivity visualised by immunofluorescence within the nucleus was unaltered both in SOD1G93A and SMA animals when compared to their WT controls (figure 5.2). TDP-43 staining was granular, with sparing of the nucleolus, but showed discrete areas of high signal intensity suggesting the presence of distinct nuclear speckles. To quantify the number of TDP-43 speckles per section, an auto-thresholding algorithm was used to separate areas of high signal from background granular staining. Comparison of TDP-43 nuclear body counts between WT and motor neuron disease animals revealed no significant difference (figure 5.3). Several limitations apply to this approach, however. First, the analysis was limited to motor neurons that were easily identifiable on the basis of their shape, possibly missing diseased cells with altered morphology. Likewise, cells that harboured ubiquitinated inclusions and those that did not were not distinguished. Thirdly, while quantification of TDP-43 speckles is useful as an addition to qualitative assessment, the definition of what constitutes a TDP speckle is arbitrary and dependent on the intensity of the stain and the threshold setting during image acquisition.

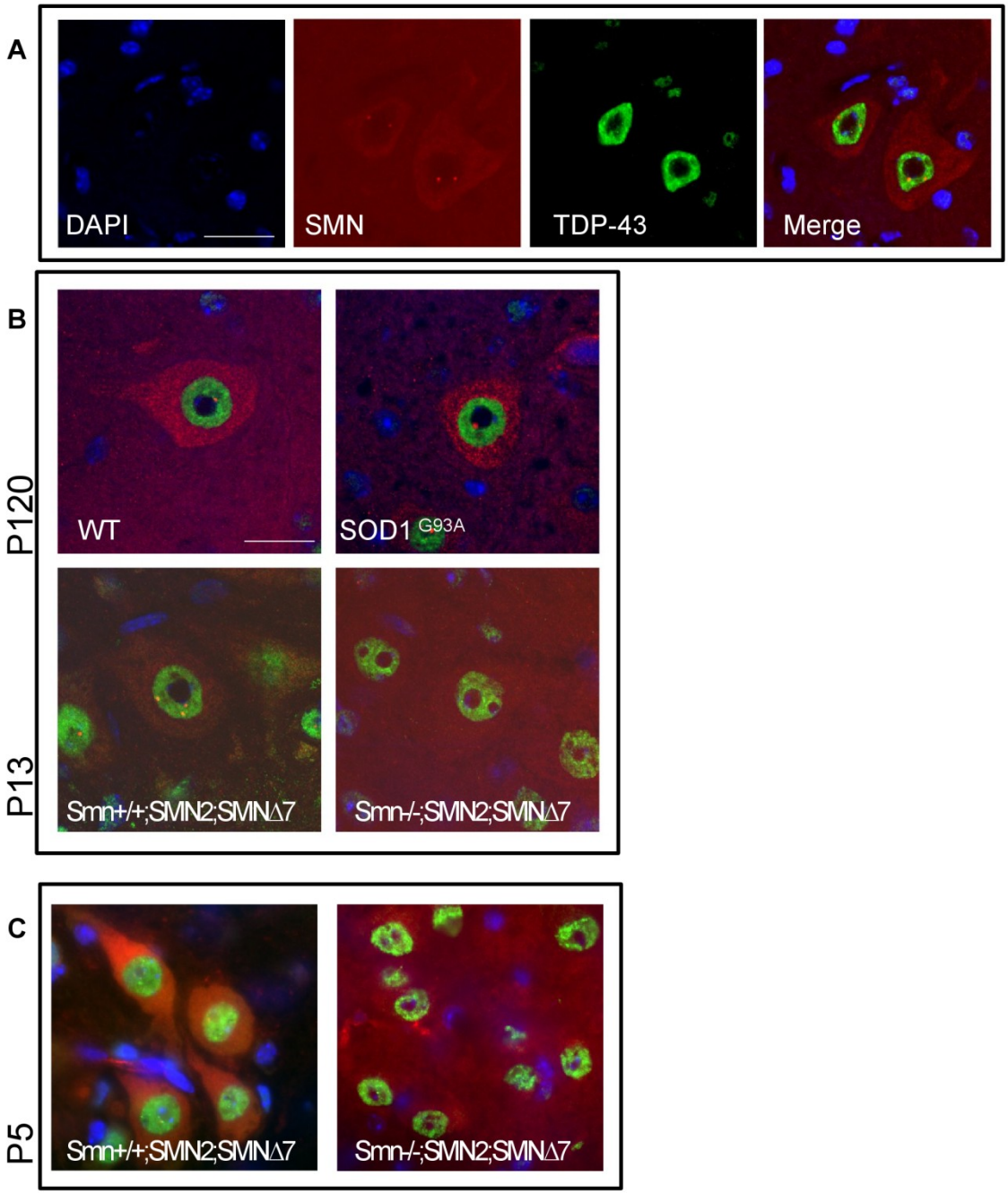

Figure 5.2 TDP-43 and SMN double labelling in spinal cord of SOD1 G93A and SMA mice (A) Confocal micrographs of wild-type motor neuron showing cytoplasmic and dot-like nuclear SMN stain in gems and nuclear TDP-43 stain sparing the nucleolus (B) Merged double labelling confocal images of representative motor neurons of SOD1 G93A and SMA (Smn-/-;SMN2;SMNΔ7) mice and unaffected (WT, Smn+/+;SMN2;SMNΔ7) littermates showing no difference in TDP-43 staining pattern but reduced SMN stain and loss of gems in the SMA mice. (C) TDP-43 staining is also identical between genotypes in pre-symptomatic (P5) SMA mice (images taken with a standard epifluorescence microscope).

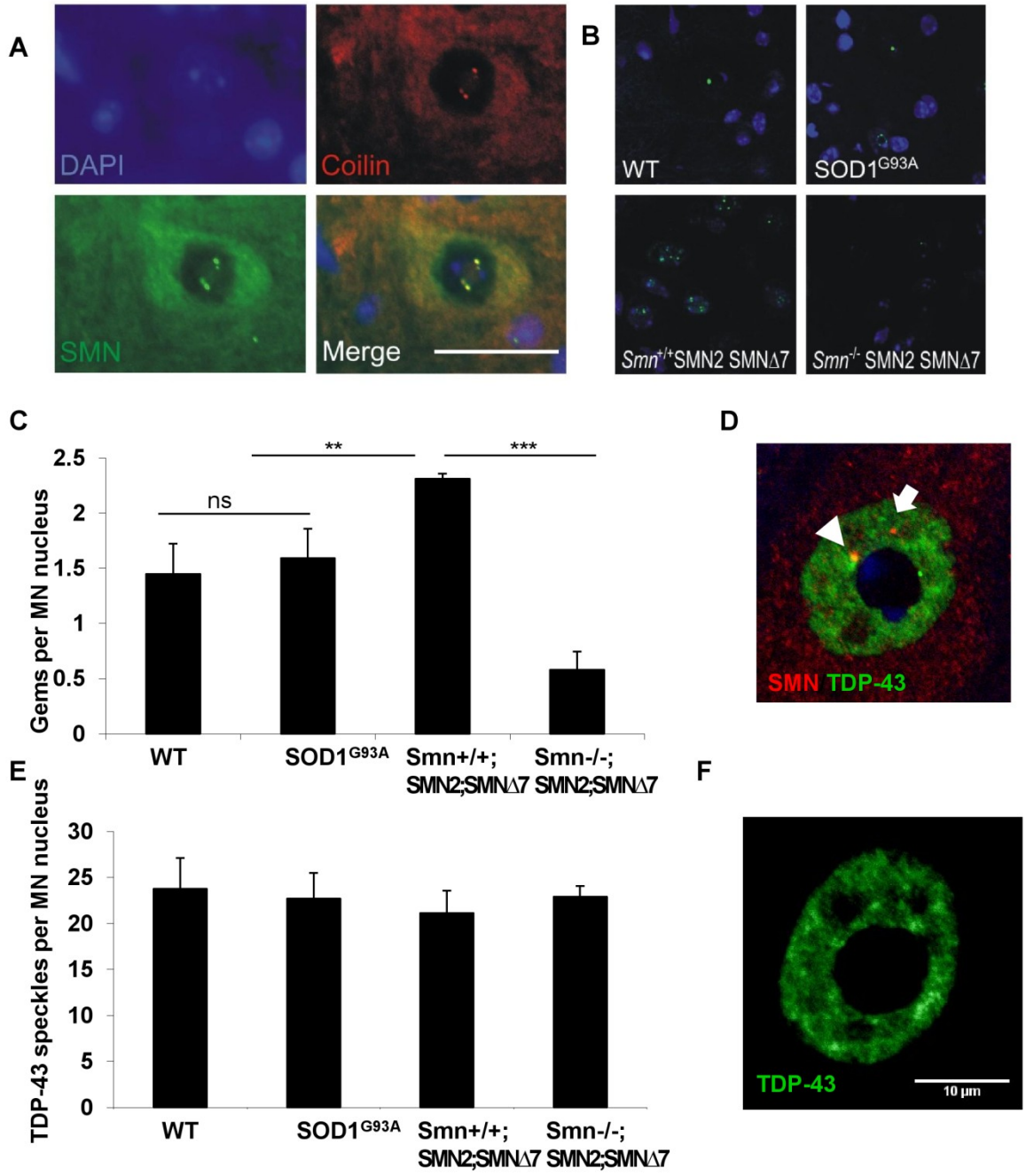

Figure 5.3 Nuclear body architecture in SOD1 G93A and SMA mice (A) Wild-type mouse spinal cord sections stained for coilin and SMN. Coilin colocalises with SMN in the motor neuron nucleus. Scale bar 20 µm. (B) Coilin immunohistochemistry confirms reduction of Cajal bodies in the SMA mouse, but equal distribution between SOD1^{G93A} and WT animals. (C) Quantification of Cajal bodies per motor neuron nucleus for each genotype. Unpaired two-tailed t-test, p=0.0004 (***) and p=0.002 (**). Error bars represent standard deviation. (D) Gems as visualised by SMN stain (arrow) only occasionally and partially overlap with TDP-43 (arrowhead) (E) Quantification of neuronal TDP-43 nuclear speckles in spinal cord sections shows no significant difference between genotypes (One

way ANOVA not significant). (F) Representative 0.9μm thick confocal section through motor neuron nucleus used for quantification.

5.2.4 Biochemistry

In spite of evidence against TDP-43 redistribution or alteration of nuclear architecture, TDP-43 expression at transcript or protein levels might have been altered, which was examined next. mRNA levels of TDP-43 were therefore quantified from three brain sub-regions and spinal cord using real-time PCR (figure 5.4). TDP-43 transcript levels were similar across frontal cortex, brainstem, cerebellum and spinal cord in disease versus control mice in both SOD1 G93A and SMNΔ7. For assessment of protein expression and potential post-translational modifications, brain and spinal cords were sequentially extracted in buffers of increasing ionic and detergent strength then analysed with immunoblotting. Full-length TDP-43 and a lower migrating species were detected in most fractions of transgenic mice, particularly abundant in low salt extracts (figure 5.4). However, the appearance and migration of TDP-43 was not altered in diseased animals compared to wild-type controls. Endogenous and transgenic SOD1 was distributed across all fractions in ALS tissue with increased solubility of dimeric mutant SOD1 in urea (figure 5a). To test for the presence of hyperphosphorylated TDP-43 in mice, urea extracts from CNS were dialysed and phosphatase treated (figure 5.4), as no phospho-specific antibody was available when these experiments were performed. The persistence of an upper band suggested no phospho-TDP-43 species.

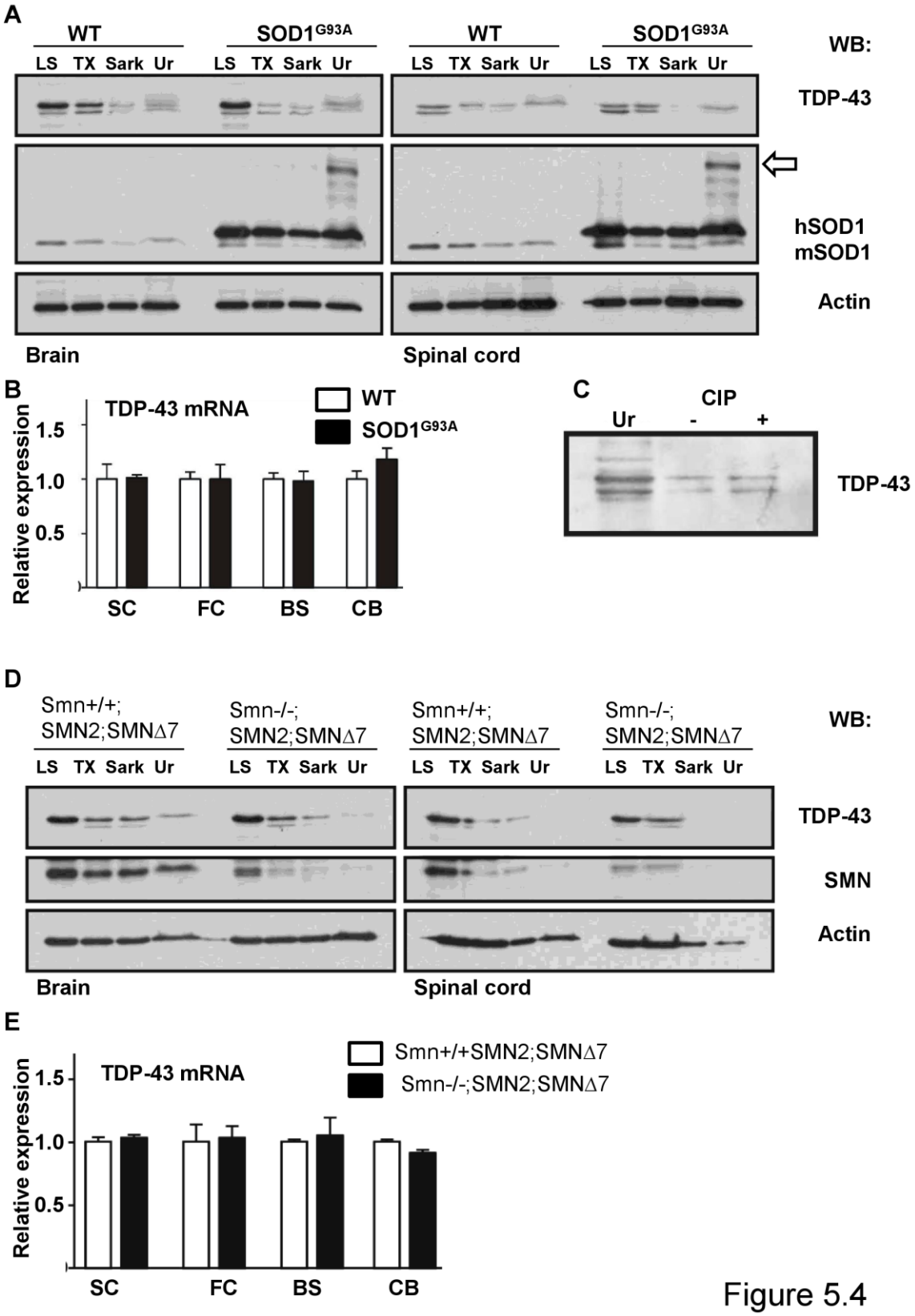

Figure 5.4 TDP-43 mRNA and protein expression in G93A and SMA mice (A) Western blot analysis of brain and spinal cord extracts from wild-type (WT) and SOD1 G93A mice after serial fractionation in buffers of increasing strength at 4

months of age shows no evidence of altered TDP-43 expression or solubility in disease mice. Open arrow, putative dimeric hSOD1 species. (B) Quantitative RT-PCR analysis of TDP-43 expression in brain regions and spinal cords from SOD1G93A and WT mice. (C) Phosphatase treatment of brain urea extracts shows no band shift. (D) Western blot analysis of brain and spinal cord extracts from SMA mice (Smn-/-;SMN2;SMNΔ7) and unaffected littermates (Smn+/+;SMN2;SMNΔ7) after serial fractionation in buffers of increasing strength at end stage (P13) shows reduced SMN expression, but no evidence of altered TDP-43 expression or solubility in disease mice. (E) Quantitative RT-PCR analysis of TDP-43 expression in brain regions and spinal cords from SMA and control mice. LS, low salt; TX, Triton-X; Sark, Sarkosyl; Ur, urea; SC, spinal cord; FC, frontal cortex; BS, brain stem; CB, cerebellum; CIP calf intestinal phosphatase. Error bars represent standard deviation of the mean for mRNA expression.

5.2.5 SMN expression in mouse models of ALS and SMA

Given the reported interaction of TDP-43 with SMN in the nucleus (Wang et al. 2002), and the indirect evidence from genetic studies of a role of SMN levels as a modifier or risk factor for ALS (reviewed in chapter 1), SMN expression was examined next.

In healthy motor neurons of WT mice, SMN localised to the cytoplasm and distinct nuclear bodies called gems, or gemini of Cajal bodies (figures 5.2, 5.3). Gems are nuclear structures closely related to Cajal bodies (previously termed coiled bodies) (Liu and Dreyfuss 1996). Gems and Cajal bodies colocalise in many, but not all tissues and cell types (Young et al. 2001), and depletion of SMN levels has been reported to reduce the number of typical Cajal bodies as assessed by the marker p80-coilin (Girard et al. 2006). Spinal cord sections were double labelled with anti-SMN and anti-p80 Coilin antibodies, which showed colocalisation of gems with Cajal bodies in all examined motor neurons, in keeping with the results reported by Young et al (Young et al. 2001) and suggesting that, in spinal cord, gems and Cajal bodies are in fact one nuclear structure.

In SMA animals, there was a marked reduction of cytoplasmic SMN staining as well as significant loss of gems/Cajal bodies (figures 5.3) on SMN and coilin staining.

There was no difference in SMN staining pattern or number of gems between the SOD1G93A and WT animals (figures 5.2, 5.3). Of note, the gem count was significantly higher in the Smn+/+; SMN2; SMNΔ7 animals than in the SOD1G93A animals. This difference might be due to the presence of increased levels of SMNΔ7 expressed from the SMNΔ7 and SMN2 transgenes in the SMA animals, because exon seven is necessary for cytoplasmic localisation and lack of this could lead to nuclear accumulation of SMN, but the different developmental state (13 days versus 4 months) or the different background strain could also play a role.

SMN levels were markedly reduced in the Smn-/-; SMN2; SMNΔ7 mice on Western blot (figure 5.4), but no change in SMN protein levels or SMN distribution between soluble and insoluble fractions was obvious in brain or spinal cord of the SOD1 G93A mice (figure 5.5)

The spatial relationship between gems and TDP-43 was inconsistent. Approximately 30% of gems showed partial overlap with TDP-43, while the majority of gems were clearly distinct from TDP-43 speckles. TDP-43 is thus not a constitutive component of gems or Cajal bodies, and the observed partial co-localisation in a fraction of motor neuron nuclei might just reflect the abundance of TDP-43 in the nucleus, although it could also be caused by transient, dynamic interaction. Of note, this study focussed on nuclear TDP-43 and SMN, while a

potential interaction in the cytoplasm of soma, the dendritic or axonal compartment was not specifically examined.

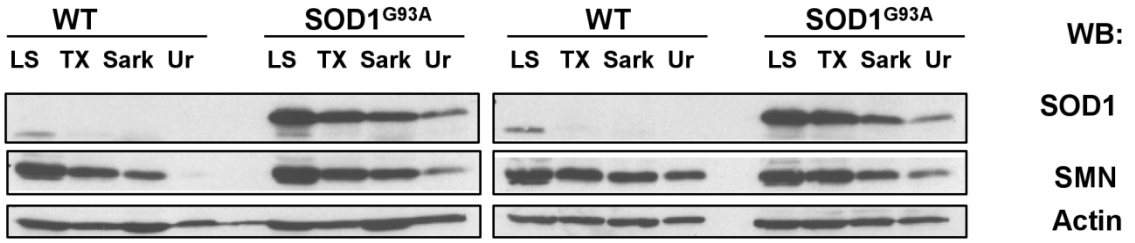

Figure 5.5 SMN protein expression in SOD1 G93A mice Western blot analysis of brain and spinal cord extracts from wild-type (WT) and SOD1 G93A mice after serial fractionation in buffers of increasing strength at 4 months of age shows no evidence of altered SMN expression or solubility in disease mice. LS, low salt; TX, Triton-X; Sark, Sarkosyl; Ur, urea.

5.2.5.1 SMN expression in human TDP-43 positive ALS

The results of the TDP-43 and SMN double labelling studies described above argued against a role for TDP-43 as a nuclear body scaffolding protein as has been suggested (Wang et al. 2002). However, given that normal nuclear TDP-43 architecture was observed in both the SOD1 G93A and SMNΔ7 mice, no assessment of SMN immunostaining in cells with nuclear TDP-43 depletion was possible. This was addressed in a preliminary experiment on three cases of sporadic ALS that were TDP-43 positive. Spinal cord sections were double labelled with anti-SMN or anti-coilin and anti-TDP-43 antibodies. All sections included motor neurons with normal nuclear TDP-43, as well as partial or complete TDP-43 nuclear loss. Gems and Cajal bodies were present in motor neuron nuclei with normal TDP-43 staining pattern, and also in cells with varying degrees of nuclear TDP-43 depletion. These results showed that nuclear TDP-43 is not necessary to maintain gem or Cajal body structure (figure 5.6). SMN was

also absent from dense cytoplasmic TDP-43 inclusions, in keeping with a previous report (Neumann et al. 2007), which further argued against a direct TDP-43/SMN interaction.

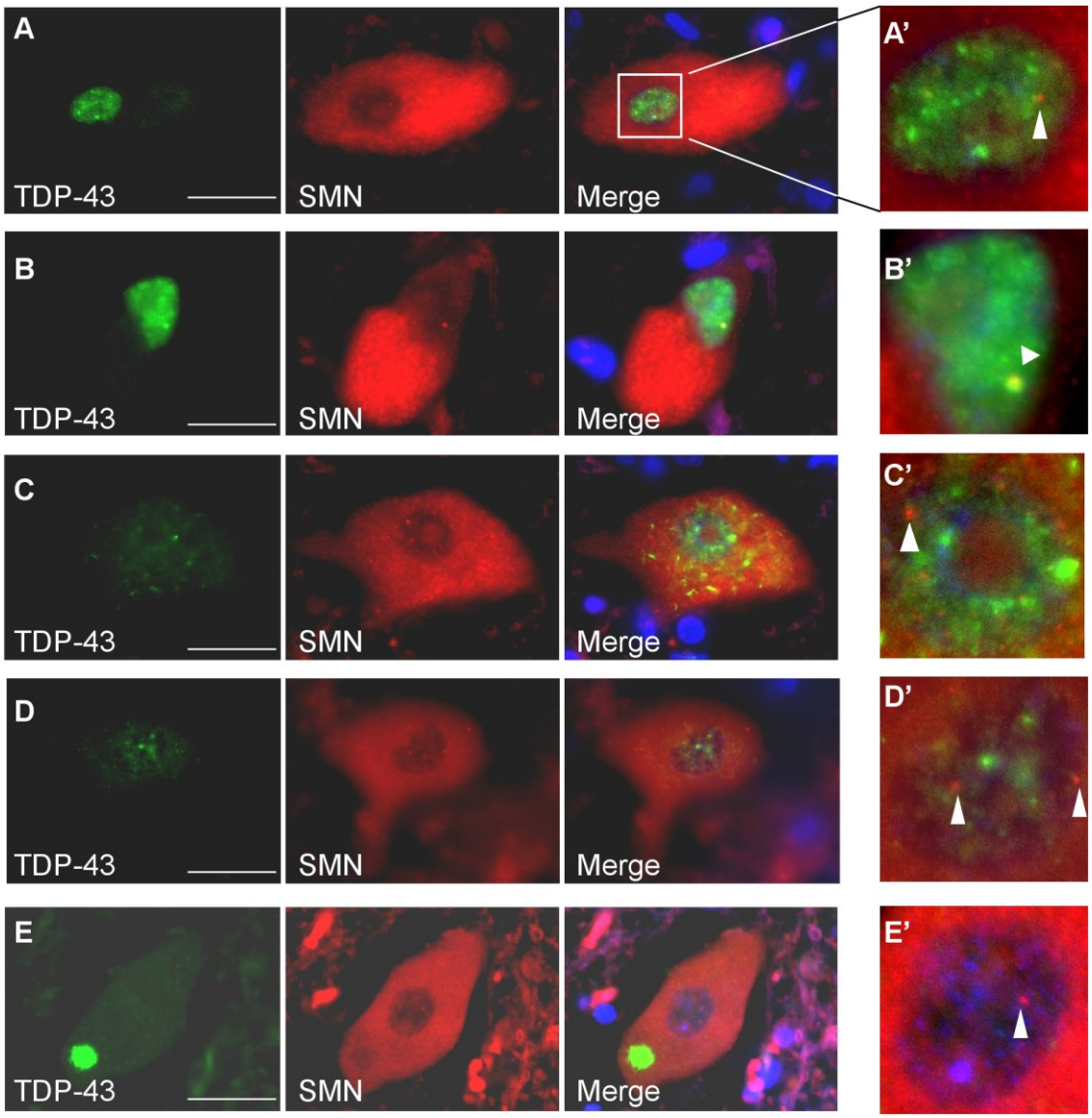

Figure 5.6 SMN expression in human TDP-43 positive ALS TDP-43 and SMN double labelling immunofluorescent micrographs of spinal motor neurons with varying degrees of TDP-43 pathology. (A,B) Motor neurons with normal nuclear TDP-43 staining pattern contain gems (arrowheads in enlarged figures A' and B') that only occasionally colocalise with TDP-43 speckles (B'), similar to the findings in figure 5.3. (C, D) Motor neurons with reduction in nuclear TDP-43 immunoreactivity and diffuse cytoplasmic TDP-43 show preserved gems (arrowheads in C', D'). (E) Motor neuron with complete nuclear TDP-43 depletion

and dense cytoplasmic inclusion, which is negative for SMN, shows preserved gem (E'). Scale bars 40 μm.

5.2.6 Basophilic inclusion disease in young onset ALS

The results so far have shown that although TDP-43 can react to various external stimuli by aggregating in stress granules and might be expected to be part of pathology in numerous diseases, TDP-43 pathology is absent in SMA and SOD1-related motor neuron diseases. In order to further characterise the specificity of TDP-43 pathology in ALS, a clinically and pathologically distinct subset of patients with young onset motor neuron disease with basophilic inclusions was examined.

5.2.6.1 Description of cases

Patient 1 was a 22 year old Caucasian female with a six month history of widespread, progressive muscle weakness of asymmetrical onset initially affecting left hip flexion. She had no bulbar, sensory, cognitive or sphincter symptoms. Frank upper motor neuron signs were absent. EMG showed widespread acute denervation. She died from respiratory failure approximately 10 months after onset of symptoms. She had an older, unaffected sister and there was no history of neurological disease in her family.

Patient 2 was an 18 year old female of Indian origin who developed painful left upper arm weakness, which progressed to more distal left arm weakness within six weeks, before spreading to the right arm and both legs. She had no sensory, sphincter, cognitive or bulbar symptoms, but showed evidence of tongue wasting and a brisk jaw jerk on examination. She died 11 months after symptom onset. She had an unaffected older brother and no family history.

Patient 3 was a 25 year old Caucasian female who developed a pure motor syndrome affecting the arms following a Caesarian section performed for pre-eclampsia. Weakness progressed to affect the legs over several months, with neurophysiological signs of lower motor neuron damage. Ten months after symptom onset she developed bulbar dysfunction and respiratory failure requiring mechanical ventilation, which was performed for 27 months before her death. She had no sensory, sphincter or cognitive involvement. There was no known family history.

Patient 4 was an 18-year-old Caucasian male with mild learning difficulties and congenital deformities of both feet and ankles that were interpreted as a *forme-fruste* of arthrogryposis. No other joints were affected. Presenting symptoms included bilateral arm weakness rapidly spreading to involve neck muscles, followed by swallowing difficulties. On examination tongue, shoulder girdle and hand muscles were wasted and fasciculating. Muscle tone was initially normal but reflexes were brisk and plantars were extensor. Blood tests and MRI scans of brain and spinal cord were normal. Bulbar disease was rapidly progressive and the patient died 6 months after onset of symptoms. There were two healthy siblings and no family history

5.2.6.2 Neuropathology and immunohistochemistry

None of the cases exhibited cerebral atrophy (figure 5.7A). However, anterior roots of the spinal cord were shrunken at all levels. Corticospinal tract degeneration varied from mild to severe; dorsal columns were always spared (figure 5.7B, C). Cytoplasmic basophilic neuronal inclusions were present in all cases. In cases 1, 2 and 4, these were most prominent in the motor cortex and lower motor neurons of the hypoglossal nerve and spinal cord. Rare basophilic

inclusions were present in the substantia nigra, nuclei raphe, inferior olives and dentate nucleus of the cerebellum. Remarkably, in cases 1, 2 and 4, samples including the central sulcus showed an abrupt transition of inclusions between primary motor and sensory cortex. In case 3 inclusions were present in multiple neocortical regions in addition to the motor system; this case also showed severe involvement of the substantia nigra. Inclusions in granule cells of the hippocampus were not seen in any case.

Basophilic aggregates appeared in a range of morphologies with tinctorial features similar to Nissl substance (endoplasmic reticulum studded with ribosomes, or rough endoplasmic reticulum (RER)), as has been described previously (Nelson and Prensky 1972). Indeed, some neurons showed only minimal coarsening of Nissl substance or redistribution to star-shaped foci or perinuclear zones, whilst others showed the large confluent or multilobular inclusions that have been most commonly described as the defining feature of this form of ALS (figure 5.7). Ultrastructurally, these aggregates consist of haphazardly arranged short filaments often studded with electron dense granules, in keeping with origin from RER or related organelles (figure 5.7G).

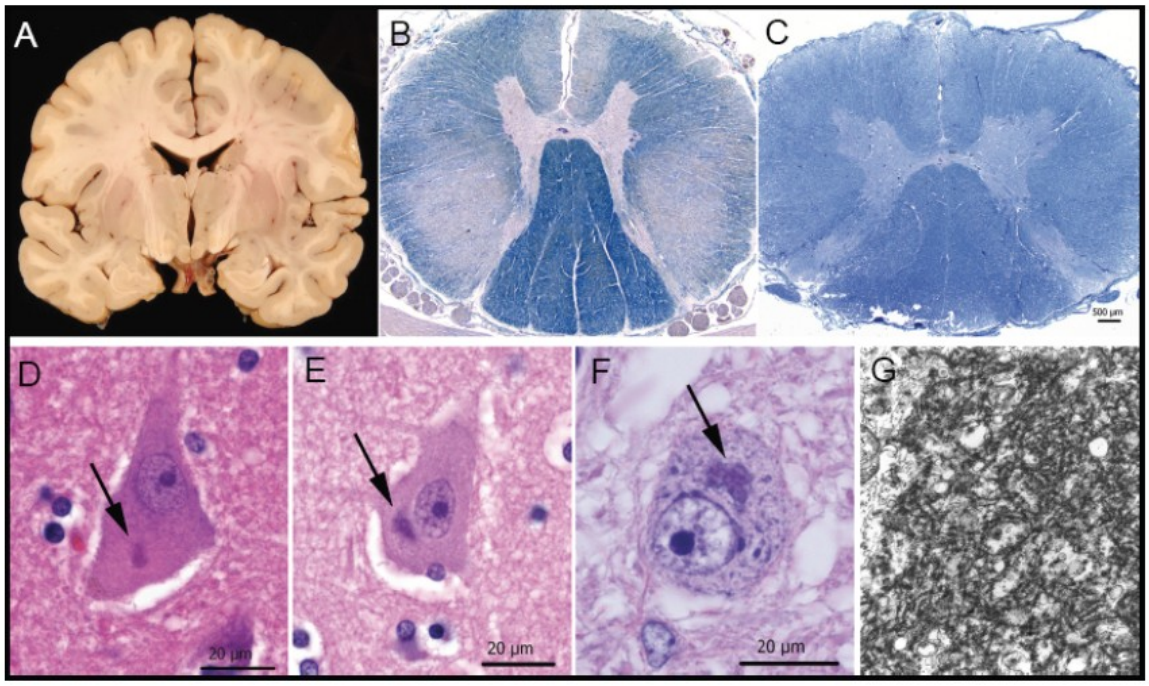

Figure 5.7 Neuropathology of ALS with basophilic inclusions and *FUS* mutations (A) No evidence of frontotemporal atrophy (Case 1, P525L mutation). Severe (B, case 1) and mild (C, case 2) degeneration of the corticospinal tract in the P525L *FUS* mutation. (D-F) Compact basophilic neuronal cytoplasmic inclusions (arrows) were present in upper and lower motor neurons of all cases with *FUS* mutations. (D) case 2, Betz cell, (E) case 4, Betz cell, (F) case 1, Nucleus hypoglossus. (G) Fragments of straight filaments studded with electron dense granules characterize a spinal cord neuronal cytoplasmic inclusion in case 1 with the *FUS* P525L mutation (x15000 magnification). Luxol fast blue cresyl violet (B, C), heamatoxylin-eosin (D-F). Figure compiled by Dr Olaf Ansorge. With permission from *Neurology* (Bäumer et al. 2010).

Staining with antibodies against ubiquitin and sequestosome-1 (p62) revealed variable, often dot-like staining with ubiquitin, but clear and homogenous labelling with p62. In particular, p62 also showed a range of morphologies corresponding to the observations made on haematoxylin and eosin stain, including labelling of coarsened Nissl substance, a feature that is not seen in normal neurons (figure 5.8). Probing of sections with antibody to TDP-43 did not show staining of aggregates, and nuclear TDP-43 was normal in all cells. Sections were next stained with an anti-PABP antibody, based on the observation made by Fujita et al

(Fujita et al. 2008). This showed that the inclusions could be recognised by PABP staining alone. To test whether the inclusions in the young onset cases contain stress granule components as described in the adult onset cases, sections were stained with TIA-1, TIA-R, HuR and FMRP antibodies, all known stress granule markers. TIA-1 and the related protein TIA-R are translational repressors that facilitate stress granule formation by prion-like aggregation (Gilks et al. 2004), while HuR is an mRNA stabilising protein (Anderson and Kedersha 2008). FMRP (Fragile X Mental Retardation Protein) is an RNA binding protein absence of which causes mental retardation. It can act as a translational repressor (Mazroui et al. 2002) and possesses self-nucleating properties similar to TIA1/R. It can be used as a stress granule marker (Kedersha and Anderson 2007). The TIA-1 and TIA-R antibodies gave specific staining of microglia, while both neuronal nuclei and inclusions were not labelled. Of note, the TIA-1 antibody was a different one to that used by Fuji et al. The HuR antibody did not work on paraffin sections. And the FMRP staining revealed some labelling of cytoplasmic inclusions but was overall less impressive than the PABP stain. Sections were next examined by staining with antibodies against SMN, which, as discussed above, do not label TDP-43 positive inclusions. SMN was, however, found to colocalise with PABP in primary neuronal cultures (Zhang et al. 2007a). Both mouse and rabbit SMN antibodies labelled cytoplasmic inclusions in all cases.

Finally, given the recent description of FUS mutations in cases of ALS (reviewed in chapter 3), sections were stained with an anti-FUS antibody, which revealed by far the most extensive pathology of all tested antibodies. A range of morphologies was observed, similar to those described above for P62 immunohistochemistry. In addition to pathology in neuronal perikarya, we also observed granular and

compact neuronal nuclear inclusions, glial cytoplasmic inclusions, and dystrophic neurites (figure 5.8). As has been observed before (Neumann et al. 2009a; Neumann et al. 2009b) currently available FUS antibodies require case-by-case adjustment of the protocol depending on fixation time. Dilutions can be titered in such a way that staining only reveals presumed aggregated FUS or also presumed physiological FUS. In this study, FUS was present in normal cells in both nuclei and cytoplasm to a degree that varied between cell types, in agreement with previous reports.

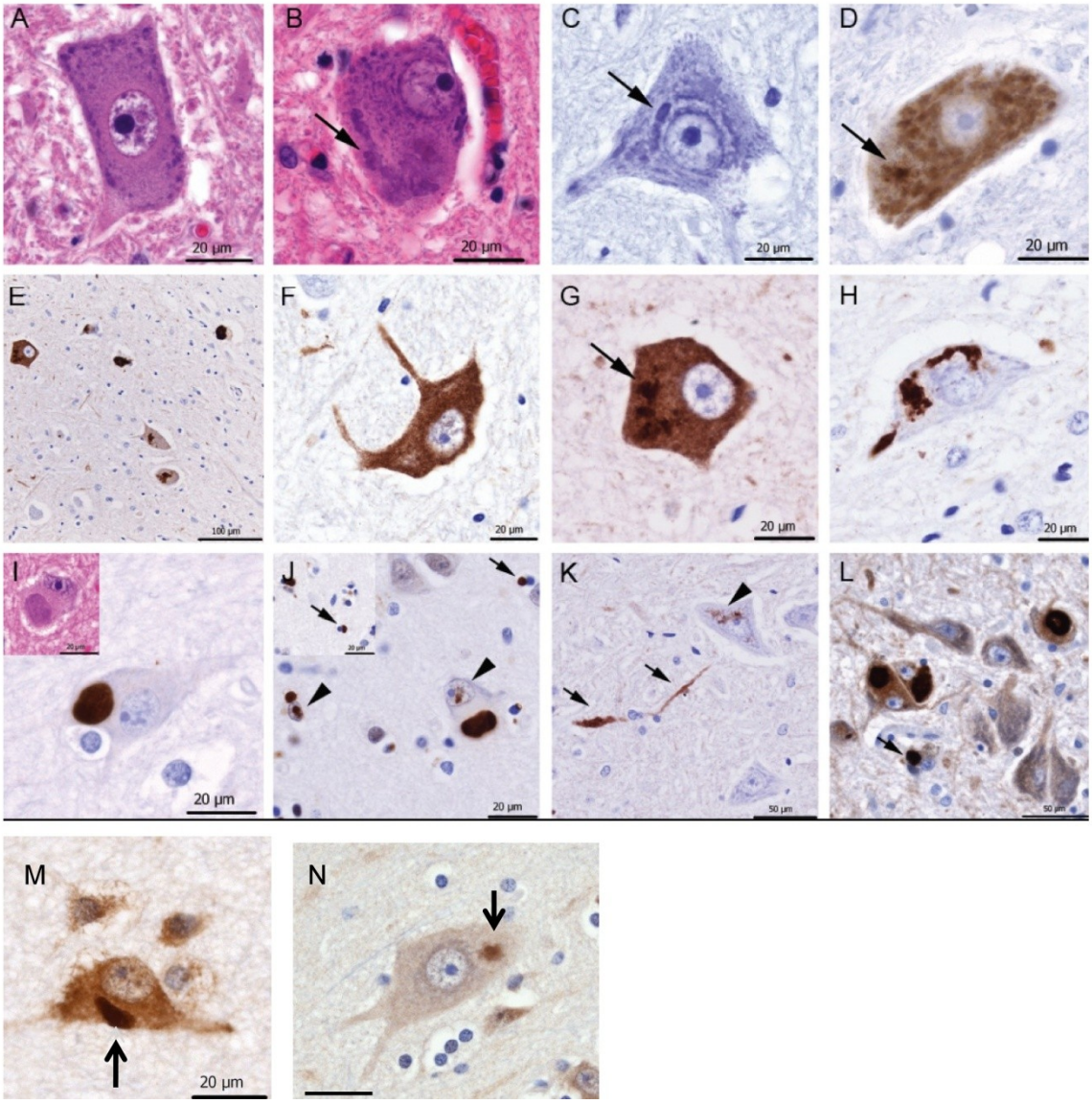

Figure 5.8 Morphological and immunohistochemical characterisation of FUS pathology (A) A normal lower motor neuron from a control case. Note the thin crisp nuclear membrane and basophilic Nissl substance at the periphery of the cytoplasm. A consistent feature of FUS mutation cases on routine haematoxylin-eosin and cresyl-violet stains was disruption, clumping and redistribution of Nissl substance in motor neurons (arrows, B-C). p62 (sequestosome-1) antibody does not normally label Nissl substance but does so in a neuron in a FUS P525L case which also shows a small aggregation focus (arrow, D). Numerous presumed pathological FUS protein deposits can be seen when antibodies are titrated in a way that does not stain normal diffuse nuclear FUS (E-L). (E) Overview of the hypoglossal nucleus in FUS P525L case 1. (F-I) Granular (F) to increasingly compact cytoplasmic FUS deposition (I). The latter correlating with the large basophilic inclusions that define this type of ALS (I, inset). Nuclear (arrowheads, J) and glial (arrows, J) as well as neuritic (arrowheads, K) FUS pathology is also present. Note granular perinuclear neuronal FUS deposit (arrow, K). (L) Only case 3 had extensive neuronal and glial (arrow) FUS pathology outside the corticospinal system and the substantia nigra shown here. Inclusions are labelled by antibodies against PABP (M) and SMN (N). With permission from *Neurology* (Bäumer et al. 2010).

5.2.6.3 Immunofluorescence

In accordance with the bright field results, double labelling with p62 and TDP-43, confirmed that no p62 positive inclusions were immunoreactive for TDP-43, and all cells containing p62 positive inclusions displayed normal nuclear TDP-43 stain. Inclusions showed variable immunoreactivity for PABP, and many of the inclusions were also positive for SMN. Inclusions were not convincingly labelled with the FMRP antibody. Bright field microscopy suggested that labeling with the anti-FUS antibody was the most sensitive marker of pathology in all four patients with basophilic inclusions, and in keeping with this immunofluorescence double labeling showed that all P62 positive inclusions were positive for FUS, but not all FUS positive inclusions stained positive for P62. Cells containing FUS positive inclusions showed variable nuclear FUS staining intensity.

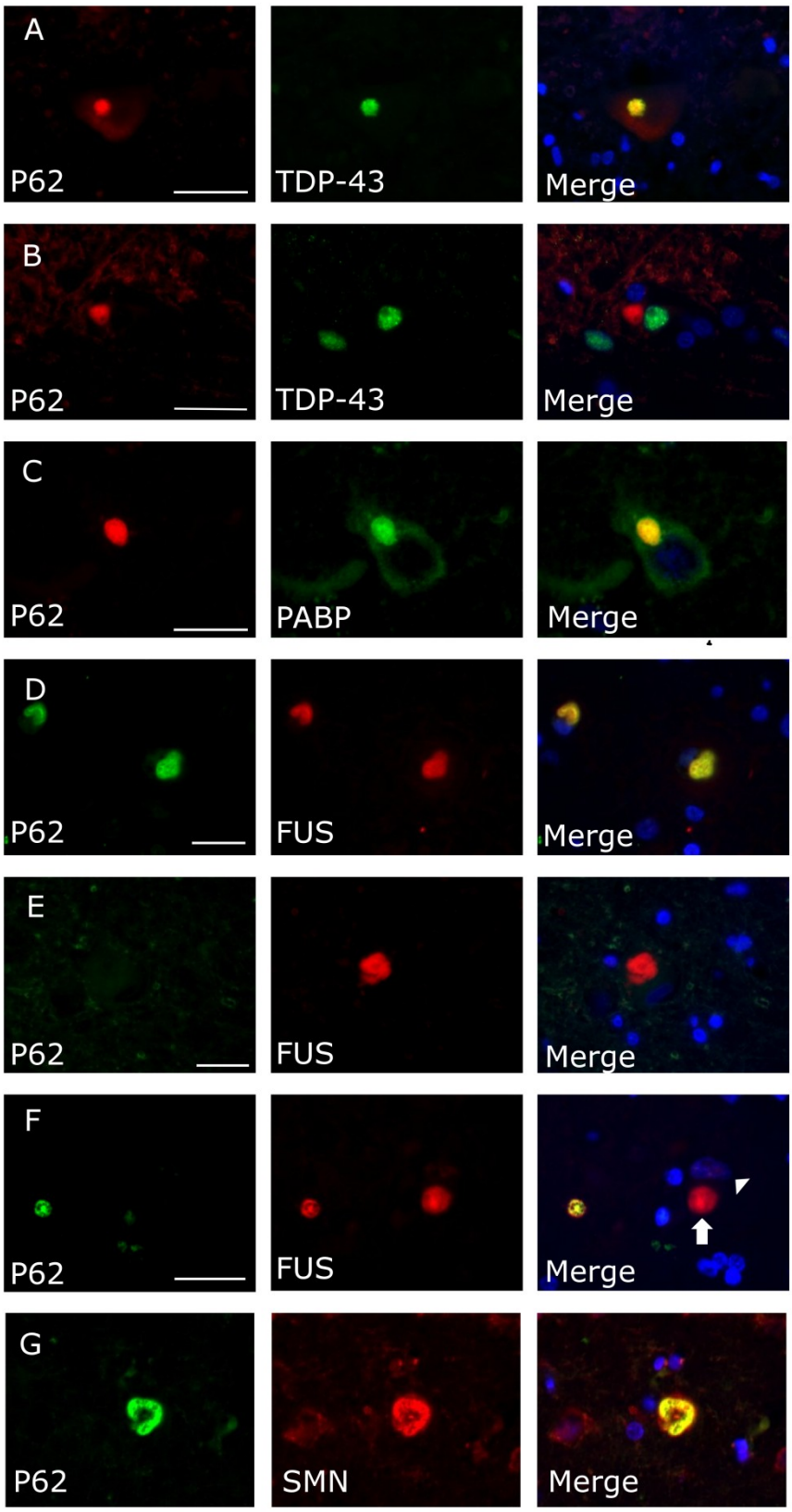

Figure 5.9 Characterisation of FUS pathology by immunofluorescence Double labelling immunofluorescent micrographs of cortical neurons. (A) Compact

cytoplasmic inclusions in classical sporadic ALS are labelled with p62 and TDP-43. (B) Compact basophilic inclusions are also labelled by p62, but are negative for TDP-43, which retains its normal nuclear distribution. (C) Most basophilic inclusions are immunostained with PABP antibody, indicating the presence of poly-adenylated RNA. (D) Basophilic inclusions that are p62 positive are also FUS positive (D), but not all FUS inclusions contain p62 (E, F arrow). FUS nuclear staining is sometimes not completely abolished in cells with cytoplasmic FUS inclusions (F, arrowhead). (G) Many p62 positive inclusions stain for SMN, as opposed to TDP-43 positive inclusions (figure 5.6). Scale bar 40 μm.

5.2.6.4 Molecular genetic analysis

Given the striking FUS pathology in all cases in the absence of TDP-43 pathology, genetic analysis was focussed on *FUS*. Genomic DNA was available for only one case, and was extracted from an existing fresh frozen muscle biopsy, fresh frozen cerebellar tissue obtained on autopsy and formalin fixed, paraffin embedded brain tissue, respectively, for the other three cases. The DNA extracted from paraffin tissue was severely degraded and performed poorly in PCRs, but FUS exons 14 and 15 could be amplified by using smaller amplicon sizes and nested PCRs. No mutation was identified in these exons. The P525L mutation was identified in two cases, and the novel c.1554_1557delACAG mutation in another (see chapter 3, figure 3.3).

5.2.6.5 Western blotting

Fresh frozen spinal cord tissue was available for one case with the P525L mutation. The sample was compared to a spinal cord sample of a patient who died of non-neurological illness (control) and a case of adult onset, sporadic ALS. Given the presence of FUS positive cytoplasmic inclusions, the hypothesis was that the basophilic inclusion case would contain increased levels of insoluble FUS. To test this hypothesis, tissue was sequentially extracted in two buffers of increasing strength. This showed that FUS was present in the soluble fraction in

all cases, and only small amounts were found in the insoluble fraction, arguing against the presence of significant amounts of insoluble FUS in basophilic inclusions. The FUS immunoblot revealed a main band of approximately 75 kDa in all cases, as well as a distinct second band of slightly lower molecular weight in the control and sporadic ALS case only. One possible explanation for this was the presence of phosphorylated FUS in the upper and non-phosphorylated FUS in the lower band, together with an increased fraction of phosphorylated FUS in the case of basophilic inclusions. To rule out this possibility, samples were re-extracted in buffer without phosphate inhibitors, and treated with protein phosphatase (PP). No band shift was evident in this experiment, arguing against a significant proportion of phosphorylated FUS in the tested lysates, although the lower band was still present in controls, but absent in the case. A duplicate gel was probed with a different FUS antibody recognising the N-terminal amino acids as opposed to the middle epitope. Surprisingly, FUS detection by this antibody was markedly reduced in the basophilic case compared to controls, while giving stronger signal for the lower band compared to the first antibody used. It is possible that BID samples contain a FUS protein whereby the N-terminal epitope is masked. The lack of epitope cannot be due to truncation as the later would result in a shift in electromobility. The answer may lie in the apparent size of FUS as observed by Western blotting. FUS has a predicted molecular weight of 53kDa yet all reports of FUS expression show a 75kDa species, independent of the epitope used to raise the antibody. Such a large shift in molecular weight is unlikely to be caused by methylation (small modification), phosphorylation (as determined by PP1 treatment, Fig. 5.10B) or glycosylation (no glycosylation sites are present in FUS). It is possible that FUS undergoes tight association with a binding partner that can

not be dissociated under standard denaturing conditions, such that FUS appears 20kDa higher than its expected size. The association of FUS with a binding partner could be affected in BID patients such that the NT region is affected, leading to problems with localisation or solubility. This is highly speculative but could form the basis for future analysis of the role of FUS in BID pathology. The Western blot findings have to be considered preliminary given the single specimen available, as well as two other complicating factors. First, the post-mortem delay was four days in the case of basophilic inclusion disease, which might have resulted in a significant degree of proteolysis, possibly affecting the immunoreactivity with the N-terminal antibody more than that of the middle epitope antibody. Secondly, the spinal cord specimen available showed no distinct grey/white matter boundaries, which might have led to sampling error by including unaffected white matter in the experiment while missing affected grey matter areas that might show increased insoluble protein.

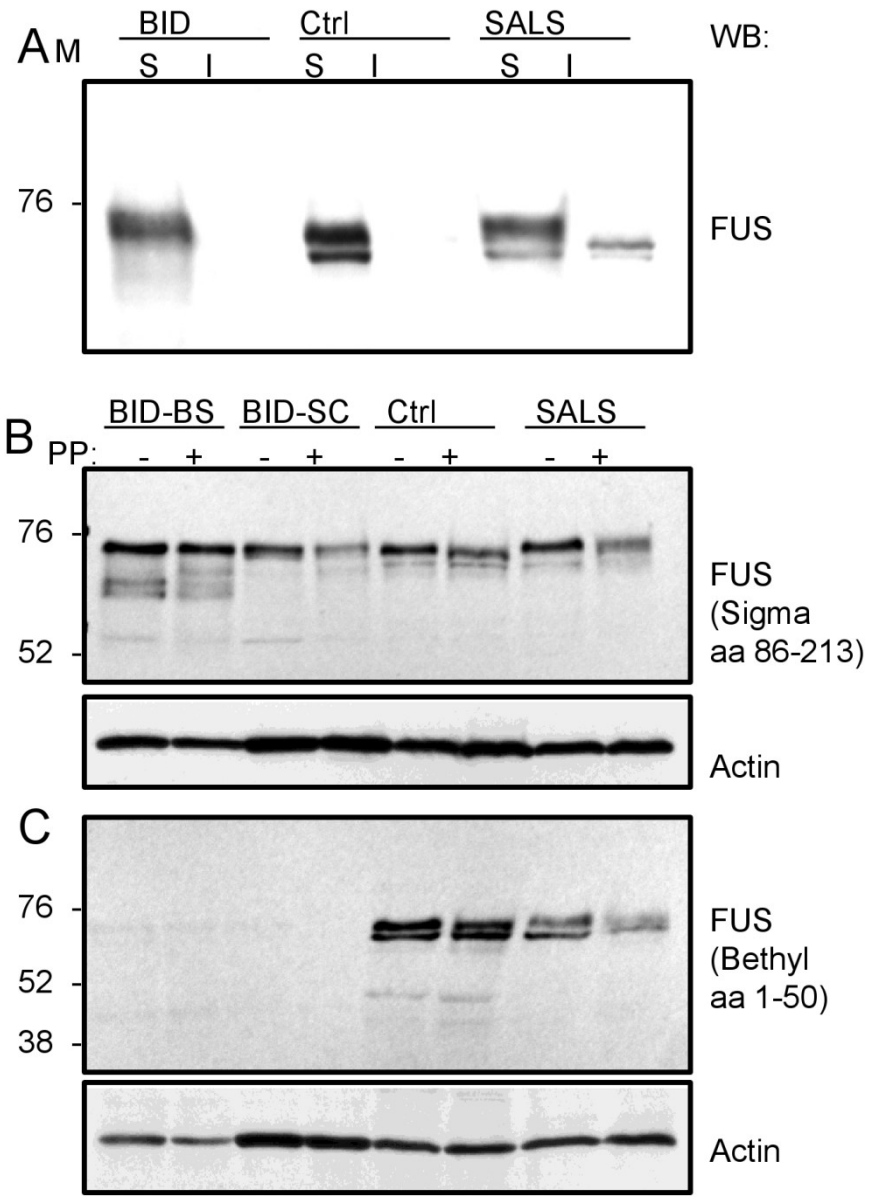

Figure 5.10 FUS protein expression in basophilic inclusion disease (A) Western blot of protein extracted from brain and spinal cord samples in RIPA soluble and insoluble fractions (7.5% SDS-Polyacrilamide gel). While there was no increase of insoluble FUS in the BID case, the sample lacked the distinct second band visible in both control and SALS spinal cord. (B) Western blot with and without phosphatase treatment. (C) Detection of FUS with Bethyl lab anti-FUS (NT) antibody. BID, basophilic inclusion disease; BS, brainstem; SC, spinal cord; Ctrl, Control; SALS sporadic amyotrophic lateral sclerosis; S, soluble; I insoluble; M, molecular weight marker (kDa); PP, phosphatase.

5.3 Discussion

5.3.1 TDP-43 and SMN expression in motor neuron disease mouse models

TDP-43 pathology characterised by cytoplasmic inclusions and nuclear depletion is the hallmark of ALS and FTLD-U pathology. This chapter demonstrated that this pathology is, however, not present in the distinct clinicopathological ALS subtype of basophilic inclusion disease, and is further absent in mouse models of SOD1-related ALS and SMA, on both biochemical and morphological grounds.

The findings in the SOD1G93A mouse provide clear evidence that this model does not share the characteristic pathological and biochemical hallmarks of TDP-43 pathology known from human sporadic ALS cases, similar to a report on the G37R and G85R SOD1 mice (Robertson et al. 2007). This has important implications for the understanding of disease pathophysiology, suggesting that SOD1 related ALS is in fact a different disease to TDP-43 –ALS, even though both finally lead to motor neuron degeneration and an identical clinical course. SOD1 mouse models are extensively used in mice in drug trials for ALS, but so far translation of the results into human clinical trials has been all but disappointing, partly due to methodological issues in mouse drug trial designs (Benatar 2007). While some drugs that showed efficacy in mouse drug trials, e.g. riluzole (Gurney et al. 1996) have marginal efficacy in humans, this probably means that they exert a non-specific effect or act downstream from the disease-initiating pathological events. Clearly, a TDP-43 mouse model of ALS is needed to assess the degree of overlap between pathways of motor neuron degeneration in SOD1 and TDP-43 mediated disease for more efficient drug development. Although the core features of human sporadic TDP-43 pathology were not identified in our experimental setting of

SOD1G93A disease, it is conceivable that SOD1 and TDP-43 pathways interact at other, more subtle or as yet unidentified levels. For example, temporary alterations in TDP-43 expression or function over the course of SOD1-related ALS, cell-type specific changes (glial versus neuronal), or variations relating to specific SOD1 genotypes remain to be identified. Recent work identifying a covalently altered SOD1 species which is common to SALS and SOD1-FALS spinal cord suggests that it would be premature to conclude that there is no overlap between TDP-43 and SOD1 pathology (Gruzman et al. 2007).

SMN levels on Western blotting, and gem counts did not differ between wild-type and SOD1 G93A mice in this study. This is in contrast to work by Turner et al (Turner et al. 2009), who found reduced SMN levels in NSC-34 cells transfected with mutant, but not wild-type SOD1, as well as in symptomatic SOD1 G93A mouse spinal cord. The SMN reduction observed in this paper was subtle, and might only have become apparent by extracting whole spinal cord in RIPA buffer rather than performing serial fractionation, as in this work, with the main aim of identifying differences in solubility.

The second aim of this study was to address the possibility that TDP-43 expression or nuclear architecture might be altered in SMA. Wang et al proposed that TDP-43 acts as a nuclear body scaffolding protein in general and a SMN interacting protein more specifically (Wang et al. 2002). A reduction in nuclear SMN might thus alter TDP-43 distribution and vice versa. While there is a distinct possibility that SMA is caused by loss of a neuron-specific, non-canonical function of SMN, e.g. in neuronal development, neurite outgrowth or axonal transport (Briese et al. 2005), there is mounting evidence that SMN deficiency leads to tissue-dependent differential defects in snRNP biogenesis and splicing (Gabanella

et al. 2007; Zhang et al. 2008). This is in keeping with the finding of a marked reduction of Cajal bodies, which are sites of ribonuclear protein (RNP) maturation and snRNA modification (Ogg and Lamond 2002; Stanek and Neugebauer 2006), in motor neuron nuclei of SMA animals. The reduction in SMN protein and Cajal bodies was not accompanied by an alteration of TDP-43 mRNA or protein levels, nor a qualitative or quantitative change in nuclear distribution of TDP-43. This implies that SMA pathogenesis is not mediated by TDP-43, although, given the asymmetrical distribution of the two proteins, the abundance of TDP-43 in the nucleus might have masked small regional changes in cytoplasm or neurites. A more rigorous examination of TDP-43 distribution in the cell including the cytoplasm as well as careful examination of axonal processes may be needed to arrive at a definitive answer.

On the other hand, the demonstration of gems in human motor neuron nuclei independent of their TDP-43 content argues strongly against a fundamental function of TDP-43 as a nuclear scaffolding protein.

5.3.2 Basophilic inclusion disease

The study of young onset ALS with basophilic inclusions provided another striking example of the conspicuous absence of TDP-43 pathology in ALS cases that appeared clinically indistinguishable from other cases of sporadic ALS – with the exception, of course, of the extremely young age of onset. Only cases with early onset ALS were included in this work, however, while basophilic inclusions have been reported in adult onset ALS as well (see chapter 5.1). The small number of cases in this work, and in the literature in general, makes extrapolation of specific clinical features in individual patients difficult. The significance of clinical features consistent with mild cognitive impairment in two of the cases here is therefore

difficult to judge, although one of the earliest descriptions of this disorder was also based on a case of a 12 year old girl with BID that was “mildly mentally retarded” (Nelson and Prensky 1972). Some cases were described to have prominent autonomic involvement (Oda et al. 1978), and one of the cases presented here had urinary urgency.

This work demonstrates that young onset ALS with basophilic inclusions, predicted to be a distinct subtype of ALS purely on morphological grounds (Nelson and Prensky 1972) is indeed molecularly and genetically distinct from the classical form of sporadic ALS, which is a TDP-43 proteinopathy that may be associated with *TARDBP* mutations. All cases of young onset ALS with basophilic inclusions showed extensive FUS pathology by immunohistochemistry, and all three cases with available DNA for complete sequencing showed *FUS* mutations. Recently, frontotemporal lobar degeneration (FTLD) with FUS pathology (FTLD-FUS) has been reported (Munoz et al. 2009; Neumann et al. 2009a). Disease onset of FTLD-FUS with basophilic inclusions occurred significantly later (average of 46 years) and progression was slower than in this series. FTLD-FUS previously described as neuronal intermediate filament inclusion disease (Neumann et al. 2009b) and atypical FTLD with ubiquitin-only inclusions (Neumann et al. 2009a) are not characterized by basophilic inclusions.

Cytoplasmic aggregation of FUS has been described in 4 cases with the R521G

R521C and R521H mutations (Kwiatkowski et al. 2009; Vance et al. 2009) and two cases of the R521H mutation (Blair et al. 2009). However, these reports do not describe any other neuropathological features. The FUS mutations were different from those observed here, and it remains therefore to be seen if the range of

cytopathological features described here is common to all cases of ALS-FUS with FUS mutations, or whether ALS with basophilic inclusions is a distinct subtype of ALS-FUS, due to specific mutations or genetic or environmental modifiers.

FUS clearly emerged as the main protein constituent of basophilic inclusions. Like TDP-43, FUS is a nuclear-cytosolic shuttling protein with DNA and RNA binding properties (Zinszner et al. 1997) and various functions in RNA metabolism from transcription regulation (Uranishi et al. 2001) and mRNA splicing (Yang et al. 1998a) (Meissner et al. 2003; Sato et al. 2005) (Meissner et al. 2003) to regulation of mRNA transport and local translation regulation in neurites (Kanai et al. 2004; Fujii and Takumi 2005; Yoshimura et al. 2006), stress granule formation (Andersson et al. 2008) as well as microRNA processing (Gregory et al. 2004). At present, one can only speculate that altered distribution of FUS is caused by mutations and could as consequence sequester RNA and other RNA binding proteins with subsequent disturbance of RNA metabolism. In fact, the presence of large, basophilic inclusions that are mostly positive for the poly-A binding protein is striking evidence of altered RNA homeostasis in affected cells. It was not possible to resolve whether the presence of PABP in basophilic inclusions is indicative of an origin of basophilic inclusions specifically from stress granules, as has been suggested (Fujita et al. 2008). Staining for key stress granule components other than PABP was negative in this study, possibly due to use of different antibodies. The presence of PABP immunoreactivity might be related to the presence of polyadenylated mRNA, rather than specific stress granule structures. However, the close association of basophilic inclusions with Nissl substance visible on H&E and Nissl stains, as well as ribosomes visible in the EM study is a strong indicator that the origin of the inclusions is related to protein translation. In addition, the

finding of SMN in basophilic inclusions, but not TDP-43 positive inclusions in ALS-TDP-43 suggests that SMN might be specifically involved in basophilic inclusion disease pathogenesis. Interestingly, a FUS containing fusion protein (TLS-CHOP) has been shown to localise to the Cajal body (Goransson et al. 2002), and although there are no reports of a direct interaction between FUS with SMN, both proteins bind NFAR proteins (nuclear factors associated with dsRNA) (Saunders et al. 2001), which would suggest that FUS is involved in pathways linked to SMN function.

6 Alternative splicing events in mouse models of SMA

6.1 Introduction

The previous chapters have demonstrated that mutations in genes involved in RNA metabolism can cause motor neuron disease, while many of the proteins involved have functions at many levels from splicing to mRNA translation. It is mostly unclear which of these functions is predominantly affected by disease. Spinal muscular atrophy is often seen as a "splicing" disease (Cooper et al. 2009), and further understanding of its pathophysiology might have wider implications for motor neuron diseases in general, particularly given the possible role of SMN expression levels as a risk factor for ALS and the involvement of both SMN and FUS in ALS with basophilic inclusions as described above. This final chapter will therefore focus on alternative splicing in SMA using a mouse model and exon specific microarrays. The splicing controversy in the SMA field will be reviewed after an overview of SMA mouse models.

6.1.1 Mouse models of SMA

The SMN protein is highly conserved between human and mouse, with an amino acid homology of 83% and similar spatial expression pattern. However, the genetic structure in mice differs significantly. In contrast to humans, mice only have one *Smn* gene. This has important implications for modelling the human disease. Early attempts to recapitulate SMA in mice by ablating *Smn* resulted in embryonic lethality (Schrank et al. 1997) while mice heterozygous for the knock-out allele (Smn+/-) have a normal life span, although they show motor neuron loss and loss of large fibre axons at 6 months of age (Jablonka et al. 2000). The introduction of transgenes containing the human *SMN2* gene as a bacterial

artificial chromosome (BAC) leads to rescue of the embryonic lethality (Hsieh-Li et al. 2000; Monani et al. 2000). Although the human SMN2 gene predominantly produces mRNA lacking exon 7, the rescue effect is based on the production of at least some full length SMN mRNA and functional SMN protein. This effect was observed in two slightly different transgenic mice. Monani et al used the *Smn* knock-out created by targeted insertion of the E.coli Lac Z cassette into *Smn* exon 2 and added a 35.5kb human genomic BAC encompassing the entire *SMN2* locus and endogenous promoter region, which inserted with either 1 or 8 copies (leading to “low copy” and “high copy” number lines). Hsieh-Li et al targeted *Smn* exon 7 by inserting a hypoxanthine phosphoribosyl-transferase (HPRT) cassette, and then added a transgene containing a 115-kb genomic DNA fragment encompassing not only the human *SMN2 gene,* but also part of centromeric *NAIP* and the intact centromeric *SERF1* genes. In both mice, length of survival correlated with *SMN2* copy number and thus SMN dosage. In the former model, low *SMN2* copy number mice (*Smn-/-;SMN2* low) have a lifespan of approximately 6 days (Monani et al. 2000), while the high copy number mice show complete rescue and have a normal life span.

The *Smn-/-;SMN2* low mouse model formed the genetic basis for a bewildering array of more complicated double transgenic mice testing the function of specific SMN isoforms or mutations. Among them, the *Smn-/-; SMN2; SMN∆7* mouse is of particular importance. This mouse was first generated to rule out that SMN∆7, the predominant isoform produced by the *SMN2* gene, is detrimental to cells in high quantities, as might be expected to occur during treatment with substances activating the *SMN* promoter (Kerr et al. 2000; Vyas et al. 2002; Le et al. 2005). The presence of a human *SMN∆7* cDNA transgene on the severe *SMN2* low

background led to an increase in survival of these mice from about 6 to 13 days, proving that SMNΔ7 is not only not toxic, but in fact can lead to a partial rescue, thought to be due the formation of functional heterotypic complexes between full length SMN and SMNΔ7 (Le et al. 2005). The SMNΔ7 mouse has become the most widely used mouse model of severe SMA in both studies on SMA pathophysiology as well as drug trials.

Both *Smn-/-;SMN2* low and *Smn-/-;SMN2;SMNΔ7* mice are phenotypically normal at birth, and then develop motor deficits at about P2 and P7, heralding a rapid decline in motor function ultimately resulting in severe wasting, stunted growth and death from neuromuscular respiratory failure at P6 and P13, respectively. Both models have normal numbers of motor neurons at birth, but loss of motor neurons in the symptomatic stage, estimated to be 35% of wild type numbers at P5 in the *SMN2* low mouse and about 20% at P9 in the SMNΔ7 mouse (Monani et al. 2000; Le et al. 2005). Motor neuron loss is preceded in both models by abnormalities at the neuromuscular junction including loss of motor nerve terminals and denervation, neurofilament accumulation, shrinkage of the post-synaptic endplate (Le et al. 2005; Murray et al. 2008) as well as NMJ immaturity characterized by failure to form the typical pretzel like structure along with the continuous expression of fetal acetylcholine receptor (AChR) isoforms (Kariya et al. 2008). NMJ abnormalities occur in both proximal and distal muscles and seem to be independent of the spinal level of innervating motor neurons. However, certain subtypes of motor neurons have been suggested to be more susceptible than others. For instance, a striking difference in NMJ defects has been shown between motor neurons innervating two different parts of the same muscle (Murray et al. 2008), which was attributed to Fast Synapsing characteristics. Other

motor neuron characteristics, e.g. fast fatigable or fast fatigue resistant status, and muscle fibre type might also contribute to selective vulnerability, as they do, for example, in models of ALS (Frey et al. 2000; Schaefer et al. 2005; Saxena et al. 2009).

6.1.2 The splicing controversy in SMA

How SMN deficiency leads to motor neuron loss in SMA is poorly understood. SMN is a highly evolutionarily conserved, ubiquitously expressed protein, and complete loss of SMN is incompatible with life. The highly selective cell loss is difficult to reconcile with the ubiquitous expression unless a unique, motor neuron specific function is inferred. However, SMN is currently best characterised for its "housekeeping" function: As part of a multi-protein complex, SMN is responsible for core steps in the biogenesis of small nuclear ribonuclear proteins (snRNPs), components of the spliceosome, the cellular machinery that controls splicing of pre-mRNAs (Meister et al. 2001; Pellizzoni et al. 2002). In particular, SMN acts in the cytoplasmic assembly of Sm core proteins on snRNAs, followed by further maturation steps and import of snRNPs into the nucleus (Pellizzoni 2007) (see chapter 1.3.1). Given equal levels of SMN, the activity of snRNP assembly is dependent on developmental stage and tissue type. In mouse spinal cord, snRNP assembly is highest during embryogenesis and early postnatal development and then falls to a baseline level when myelination occurs (Gabanella et al. 2005). When SMN levels are reduced in mouse models of SMA, snRNP assembly activity measured by *in vitro* assays drops dramatically, while steady state snRNP levels measured in tissues are only mildly reduced (Gabanella et al. 2007). Interestingly, a sub-set of snRNPs belonging to the minor spliceosome seems to be differentially affected (Gabanella et al. 2007; Zhang et al. 2008). Several strands of evidence

support the notion that reduced snRNP assembly is causative of SMA. The subtle motor neuron loss that can be found late in mice heterozygous for *Smn* can be accelerated by crossing them with mice heterozygous for gemin2, another core component of the SMN complex. This is associated with a reduction in U snRNP assembly (Jablonka et al. 2002). In zebrafish, motor neuron degeneration can be induced by silencing not only SMN, but also gemin2. The observed defects can be rescued by direct injection of U snRNPs (Winkler et al. 2005). Reducing SMN levels in HeLa cells by RNAi leads to an increased error rate in splice site pairing, which has also been observed in SMA patient derived fibroblasts (Fox-Walsh and Hertel 2009). Finally, a recent study in SMA mice found that at end-stage, widespread splicing abnormalities can be found in several tissues including the spinal cord. Importantly, different transcripts were found to be altered in a tissue specific manner (Zhang et al. 2008).

While both snRNP assembly dysfunction and splicing abnormalities have been documented in models of SMA, several questions remain. It is still unclear whether splicing abnormalities are causative of SMA, or whether they are a late occurrence in disease, either as a consequence of spliceosome dysfunction or as an epiphenomenon in a state of severe physiological alterations secondary to respiratory distress, hypoxia and malnutrition. If spliceosome dysfunction is critical, the mechanism of splicing alterations needs to be further delineated. Are absolute levels of snRNPs important, or is there evidence for incorrect pairing of RNA species with Sm proteins? The role of SMN in spliceosome assembly is only one of many functions that are potentially altered in SMA, including roles in transcription regulation (Strasswimmer et al. 1999; Williams et al. 2000; Pellizzoni

et al. 2001), axonal transport of mRNA and RNPs (Rossoll et al. 2002; Rossoll et al. 2003) as well as local translation regulation (Jablonka et al. 2004).

6.1.3 Aims of this chapter

The main aim of the work presented in this chapter was to investigate whether abnormalities in splicing described previously are the cause or a consequence of disease. This question is of prime importance to the field of SMA research and currently intensely debated. As summarized above, there is now considerable theoretical and experimental evidence of the role of SMN in spliceosome assembly, but direct proof of a link between splicing abnormalities and SMN deficiency in *in vivo* models is only present in symptomatic stages. It is difficult to prove experimentally that the splicing abnormalities seen in SMA cause disease, since inducing splicing abnormalities by lowering SMN levels will also diminish other functions of the protein that might then equally contribute to the observed phenotype. It seems, however, reasonable to assume that if splicing abnormalities are indeed causative of disease, they should be detectable before symptom onset. To test the question of causality, it was therefore hypothesized that abnormal splicing precedes disease onset in SMA. To test this hypothesis, serial exon specific microarrays were performed on cDNA derived from spinal cord taken from the SMNΔ7 mouse. This model was discussed above and was chosen because it develops severe SMA but has a clear pre-symptomatic phase, it is widely used in studies of SMA and abnormal splicing has been described to occur in it (Zhang et al. 2008).

6.2 Results

6.2.1 Phenotype of the SMN∆7 Mouse

6.2.1.1 Survival and weight development

SMA mice (*Smn-/-;SMN2;SMN∆7*) lived no longer than 14 days. Only subtle differences in weight were apparent before P7, but did not reliably predict genotype in individual mice. At P7, a failure of the righting reflex became apparent, and most SMA mice appeared slightly smaller than their control (*Smn+/+;SMN2;SMN∆7*) littermates. At P13, mice appeared emaciated, were unable to right themselves, and showed signs of respiratory distress. Heterozygous (*Smn+/-;SMN2;SMN∆7*) littermates were indistinguishable from mice homozygous for *Smn* (figure 6.1).

6.2.1.2 SMN expression and motor neuron counts

SMN expression in SMA spinal cord as measured by Western blot was reduced to about 15% of control levels at all time points, and SMN immunohistochemistry showed markedly reduced staining. On Hematoxylin and Eosin (H&E) staining, a paucity of large motor neurons in the ventral horn was apparent at end stage (P13) (figure 6.2).

A

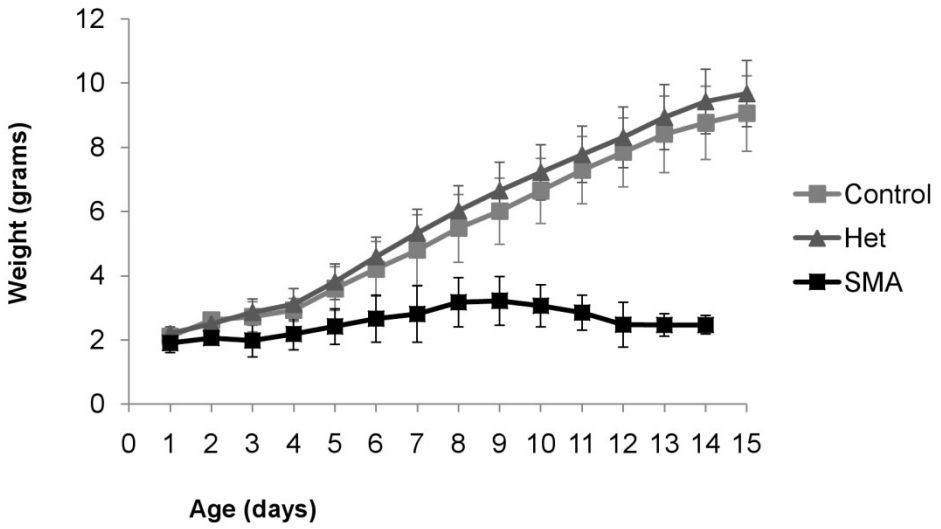

B

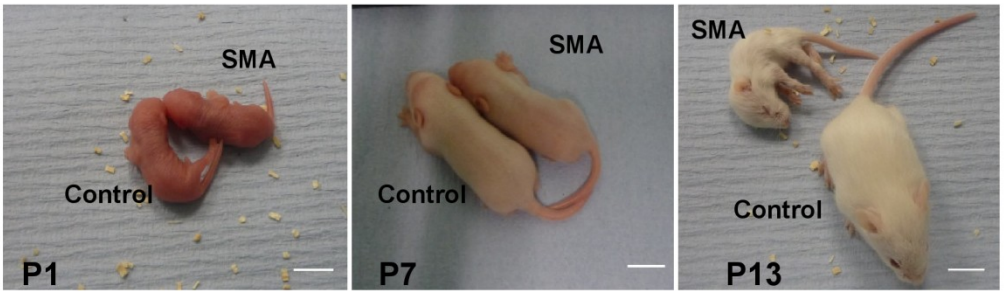

Figure 6.1 Weight development of SMA mice (A) SMA mice showed weight development comparable to control mice and mice heterozygous for Smn until post-natal day 7, when weight gain slowed. At P10, weight loss became apparent. (B) Representative photographs of SMA and control mice at P1, P7 and P13. Scale bar 1 cm. Error bars represent the standard deviation of the mean. n=6 for each genotype and time point.

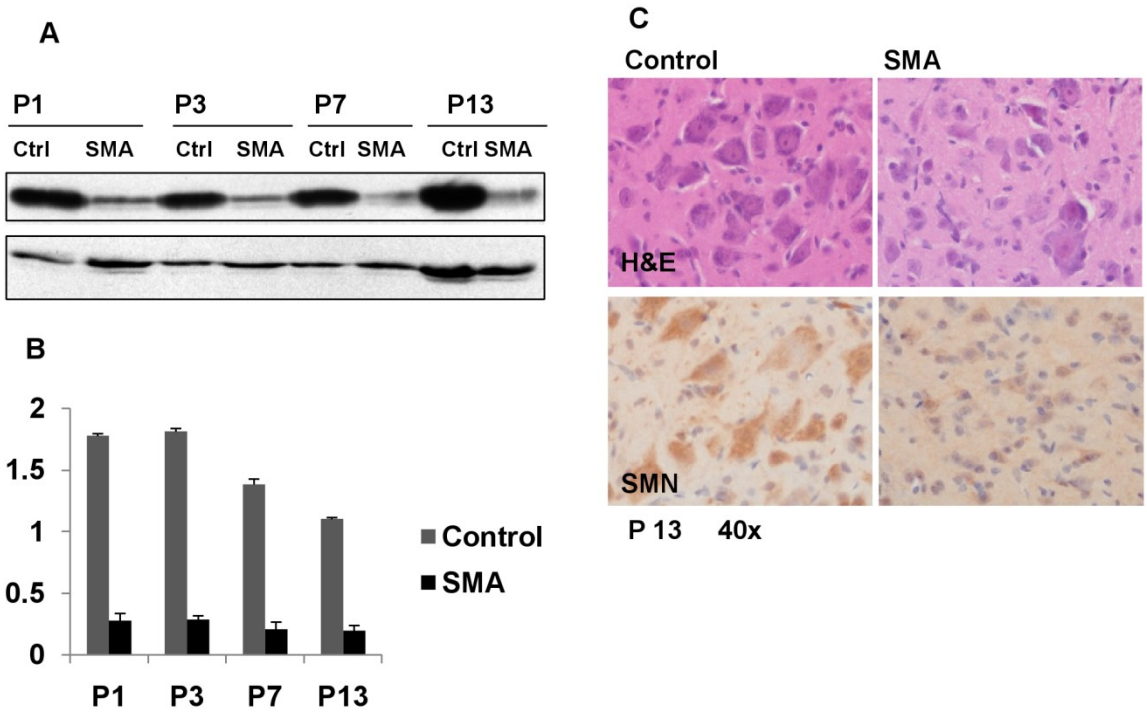

Figure 6.2 SMN expression in SMNΔ7 spinal cord (A) Western blot of spinal cord lysates shows markedly reduced SMN levels at P1, P3, P7 and P13. (B) Densitometric quantification of three independent blots shows SMN reduction to approximately 15% of control (error bars: standard deviation of the mean). (C) Representative H&E stain of the ventral horn at P13 showing paucity of motor neurons and SMN immunostaining showing reduced SMN immunoreactivity in SMA animals.

To quantify motor neuron loss over time, serial motor neuron counts were performed blind to genotype, after establishing excellent intra-rater reliability for the technique as shown by the very high intra-class correlation coefficient of 0.997 (figure 6.3).

At end stage disease (P13) there was no difference between motor neuron counts in control and heterozygous animals, while both differed significantly from numbers in SMA animals, which were reduced by approximately 30% (figure 6.4 A).

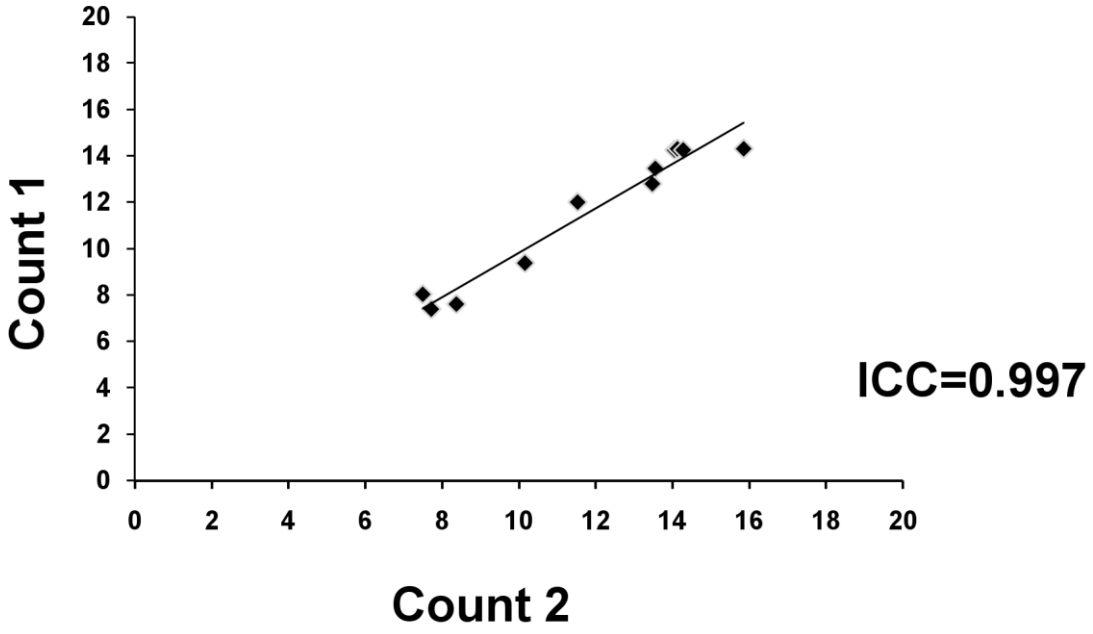

Figure 6.3 Intraclass correlation coefficient for motor neuron counts Results of repeated motor neuron counts correlate well and yield a high intraclass correlation coeffiecient of 0.997.

When sections obtained from cervical, thoracic and lumbar regions were examined separately, more motor neurons were found in the cervical and lumbar regions compared with the thoracic spinal cord, in keeping with the presence of motor neuron pools innervating the forelimbs and hind limbs of the mouse in the former (figure 6.4 B). Lumbar spinal cord sections were then used to establish a time course of motor neuron loss. The first significant difference between control and SMA mice was discernible at P7, which coincided with the onset of motor difficulties and divergence of weight development.

Weight development, motor phenotype and motor neuron count were used to define time points for a serial mRNA expression analysis experiment as pre-symptomatic (P1), early symptomatic (P7) and late symptomatic (P13).

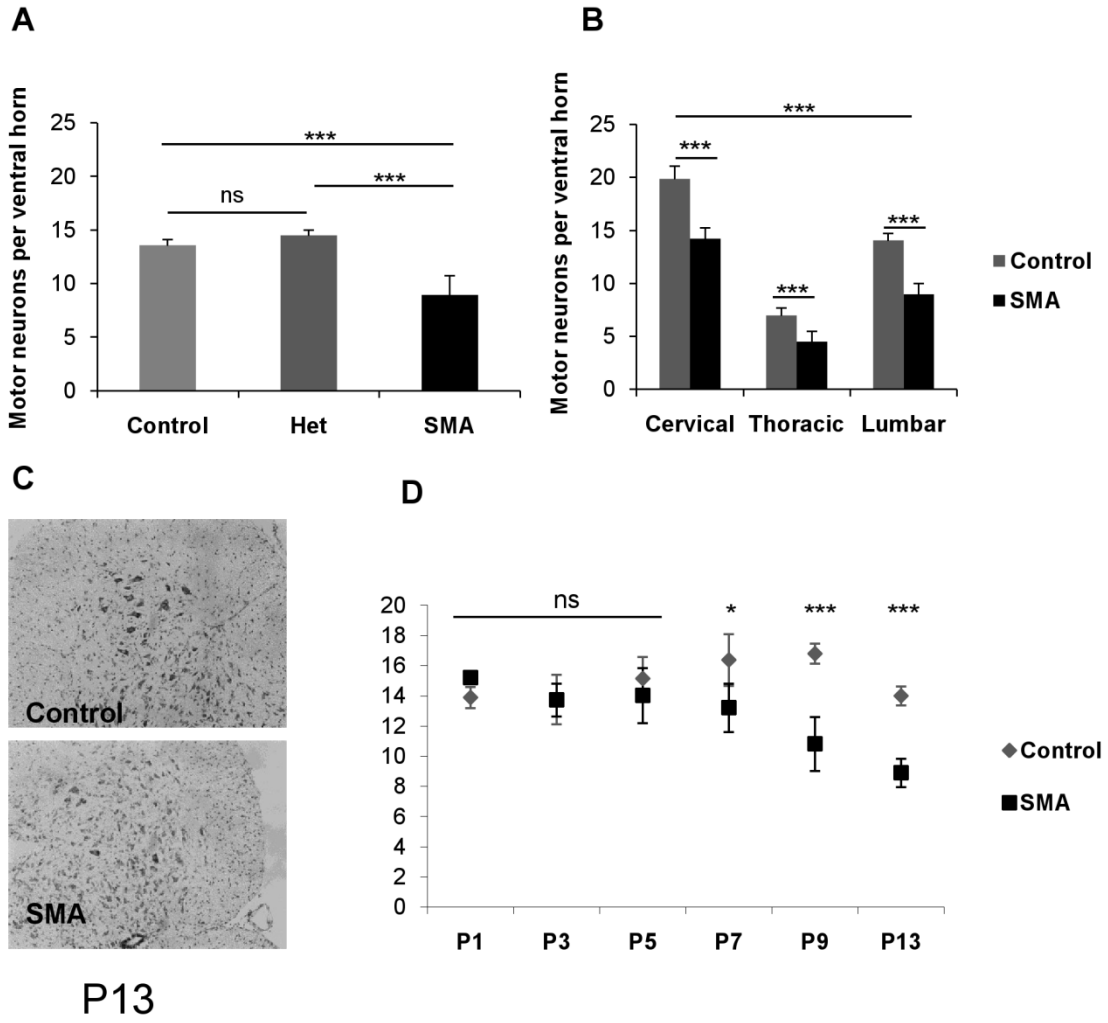

Figure 6.4 Motor neuron counts in SMNΔ7 spinal cord

(A) Comparison between control (*Smn+/+;SMN2;SMNΔ7*), heterozygous (*Smn+/-;SMN2;SMNΔ7*) and SMA (*Smn-/-;SMN2;SMNΔ7*) at P13 shows no difference between control and hetereozygous animals, but decreased motor neuron counts in SMA animals (One way ANOVA and LSD test). (B) Comparison between genotypes in cervical, thoracic and lumbar spinal cord shows significantly different motor neuron numbers in different regions, with reduction of motor neuron numbers in SMA animals in all regions (Two way ANOVA and LSD test, ***=p<0.001). (C) Representative images of cresyl violet stain of P13 ventral horns in control and SMA mice. (D) Motor neuron time course in lumbar spinal cord shows motor neuron loss over time and significant differences between genotypes

from P7 (One way ANOVA for SMA animals F =9.481, p<0.001; two-tailed t-test between genotypes P7: p=0.016, P9, P13: p<0.001).

6.2.2 Microarray quality parameters

RNA was extracted from whole spinal cord. RNA integrity as assessed on the BioAnalyser was excellent, with RNA integrity numbers between 8.6 and 10, where 10 indicates indicates the most intact, and 1 the most degraded RNA (Mueller et al. 2004). All Affymetrix recommended QC metrics were analysed using the Affymetrix Expression Console Software and showed consistent sample quality for all time points and genotypes as well as satisfactory hybridisation and labelling quality of the array.

6.2.3 Expression analysis at gene level

To assess expression changes at the gene level, two independent, complementary analyses were performed, using slightly different transcript definitions and statistical analyses. First, altered gene expression was analysed that included the core probe sets on the Affymetrix GeneChip Mouse Exon 1.0 ST Array, which includes 17,800 conservatively defined transcripts and full length mRNAs according to RefSeq (http://www.ncbi.nlm.nih.gov/RefSeq/).

When using a p value of 0.05 and a fold-change of 1.5 as cut-off for biological significance, 142 genes were up-or down regulated in spinal cord of SMA mice compared with their control littermates at end stage (P13), with a maximal fold-change of 3.9. Importantly, the degree of change between SMA and control mice was much smaller at the early-symptomatic (P7) and pre-symptomatic (P1) stage, with only 23 and 12 genes changed, respectively (figure 6.5 A, appendix 1). This finding strongly argues against a critical function of SMN in transcription

regulation, but also shows that if widespread splicing changes occur in SMA, they do not lead to a pre-symptomatic systemic change in whole transcript level mRNA expression, which could be a theoretical outcome of mis-splicing events through nonsense-mediated decay.

Next, changes between time-points were examined for each genotype. Overall, the number of genes differentially expressed between time-points in control mice was higher by a factor of ten when compared to changes between genotypes (figure 6.5 B), suggesting that the immediate post-natal period is associated with major changes in gene expression in the spinal cord in normally maturing mice.

An additional data analysis was performed in which probes were grouped into sets, each corresponding to a gene in the Ensembl (version 49) annotation database (Dai et al. 2005), yielding larger number of genes than the RefSeq core probe sets. Time point-specific differential expression between cases and controls was quantified by fitting a linear model on a gene-by-gene basis (Smyth et al. 2005; Team 2008). Of 21,911 genes examined, 693 genes exhibited case/control differences at P13, as opposed to 92 at P7, and 83 at P1 (figure 6.5 C). In addition to the bigger number of genes included in this analysis, it differed from the initial approach by performing the statistical analysis across all time points, while the first analysis was performed for each time point separately. Notwithstanding these differences, both approaches were in accord regarding the principal finding of increasing expression changes over time and very little difference between genotypes at pre-symptomatic stages.

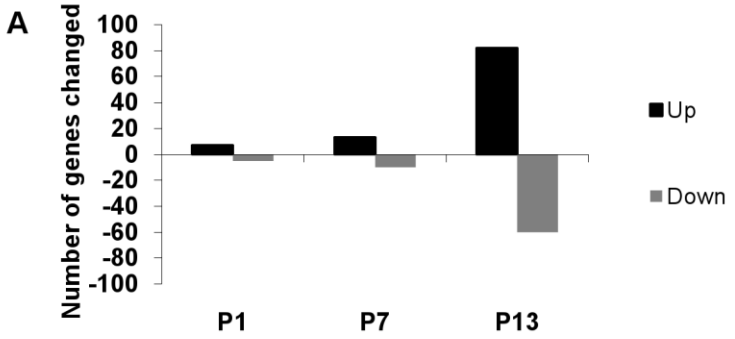
A
Number of genes changed
100
80
60
40
20
0
-20
-40
-60
-80
-100
P1
P7
P13
Up
Down

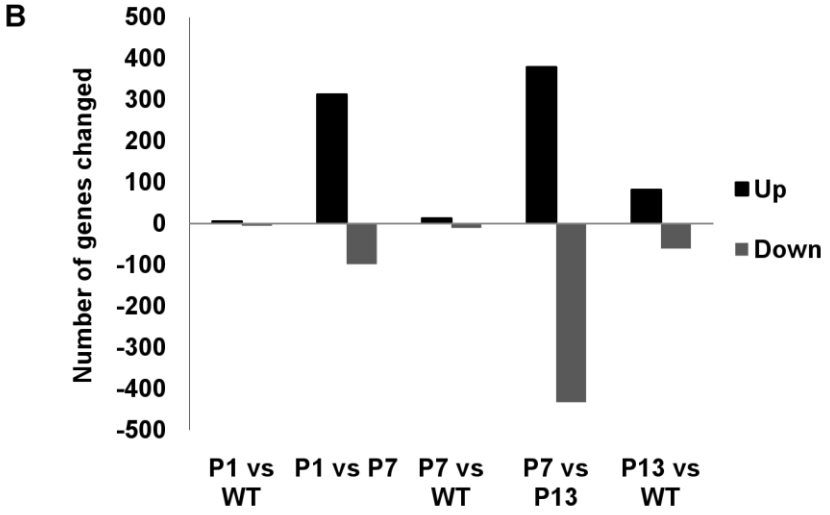
B
Number of genes changed
500
400
300
200
100
0
-100
-200
-300
-400
-500
P1 vs WT
P1 vs P7
P7 vs WT
P7 vs P13
P13 vs WT
Up
Down

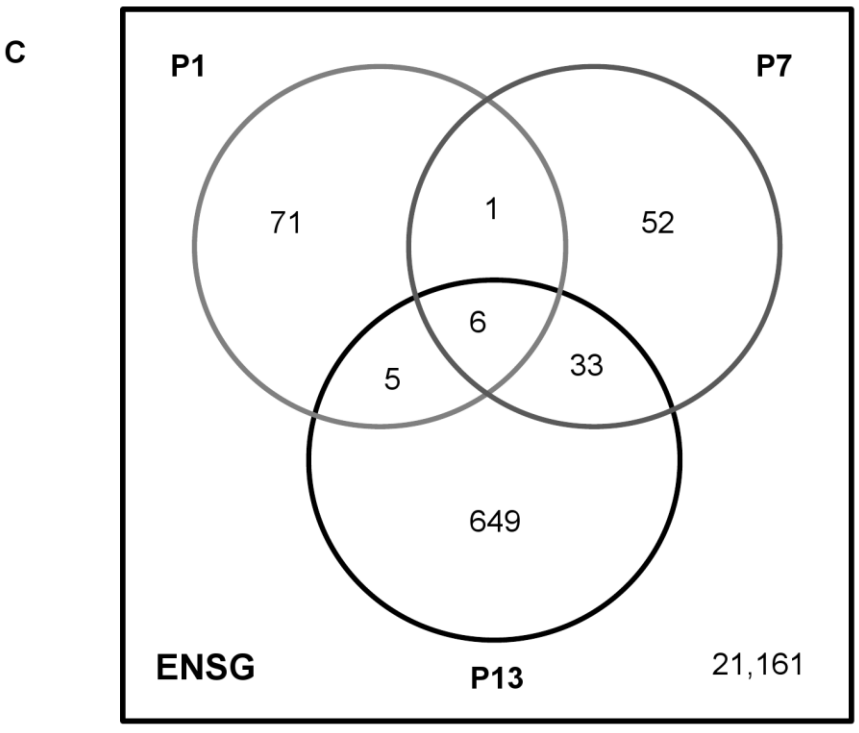
C
P1
P7
71
1
52
6
5
33
649
ENSG
P13
21,161

Figure 6.5 Global transcriptome changes increase over time (A) Number of genes up-or down regulated more than 1.5 fold in SMA mice compared to control using a p-value cut-off of <0.05. There is an exponential increase in gene expression changes at end stage compared to pre-symptomatic and early symptomatic stages. (B) Gene expression changes between time points are of much larger scale than changes between genotypes. For clarity, between- time point changes are for control animals only. (C) Venn diagram showing the number of differentially expressed genes in the Ensembl gene based analysis at different time points. Only few genes are differentially expressed at all time points.

6.2.4 Expression analysis at exon level

A key aim of this study was to assess the amount of splicing variation in the spinal cord of an SMA mouse model compared to control mouse spinal cord at several time points during disease progression. Because exon specific microarrays are relatively novel, and analysis methods have not been fully developed and validated, two complementary statistical approaches were used to investigate the number of differentially expressed exons. First, the splicing index was derived (Srinivasan et al. 2005), which is a logarithmic value based on the ratio of array probe-set intensities (corresponding to expression levels of individual exons) to overall gene level expression, where an SI value of 0 indicates equal expression of a particular exon in relation to the gene as a whole between cases and controls. Using a Splicing Index of |SI| >0.5 as an arbitrary cut-off, 252 potential alternative splicing events were identified at the late-symptomatic stage (P13), but only 5 at the early symptomatic (P7) and 16 at the pre-symptomatic (P1) stage (figure 6.6). This initial analysis suggested that alternative splicing events are a consequence of disease progression in SMA, rather than the primary cause.

Since the splicing index method is known to lead to inaccuracies if complex splicing patterns are present, such as splicing of multiple exons in one gene, and might thus underestimate the level of differential exon use present, an additional

analysis was performed comparing expression levels of individual exons between genotypes at each time point, with the assumption that every alternative splicing event would lead to at least one differentially expressed exon. In this analysis, probes were grouped into sets, each corresponding to an Ensembl exon (Dai et al. 2005). Time point-specific differential expression between cases and controls was quantified by fitting a linear model on an exon-by-exon basis (Smyth et al. 2005; Team 2008). The p-value cut-off for significant differences between genotypes at the exon level was chosen to balance sensitivity with a reasonable false discovery rate (FDR), as estimated by a permutation-based analysis (methods and table A5). At a p-value threshold of 10^{-4}, there were 812 significantly differentially expressed exons at P13, compared to 66 at P7, and 72 at P1 (figure 6.6 B); a total of 211,567 exons were examined. This provided additional evidence that the vast majority of alternative splicing events occur at late stage disease in the SMNΔ7 mouse model of SMA.

A

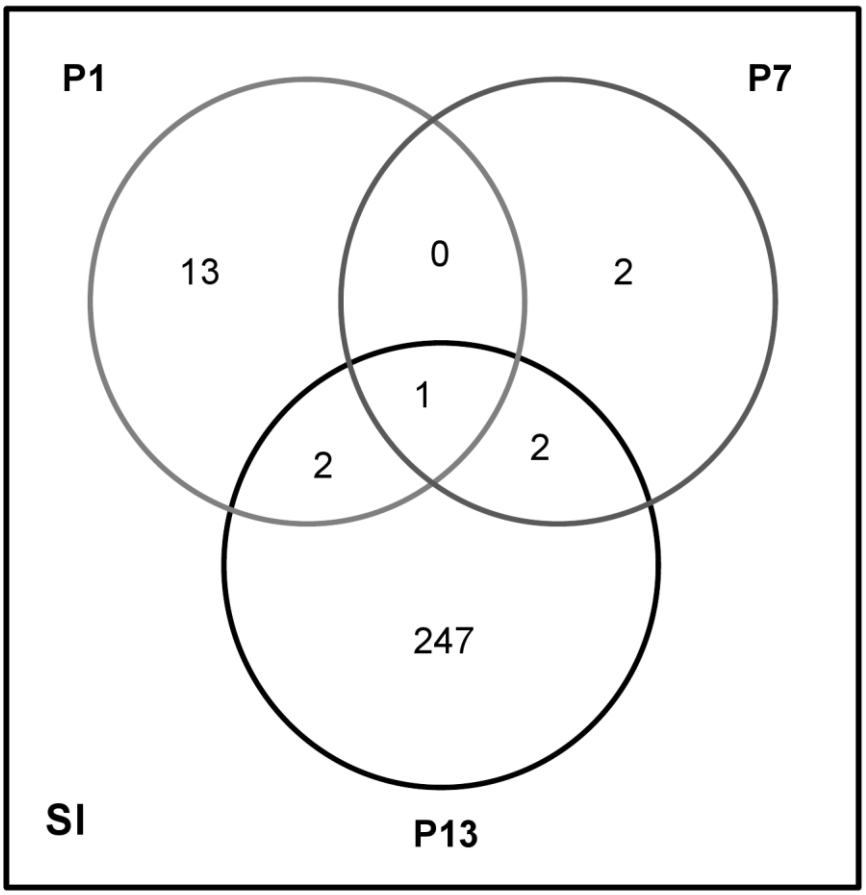

B

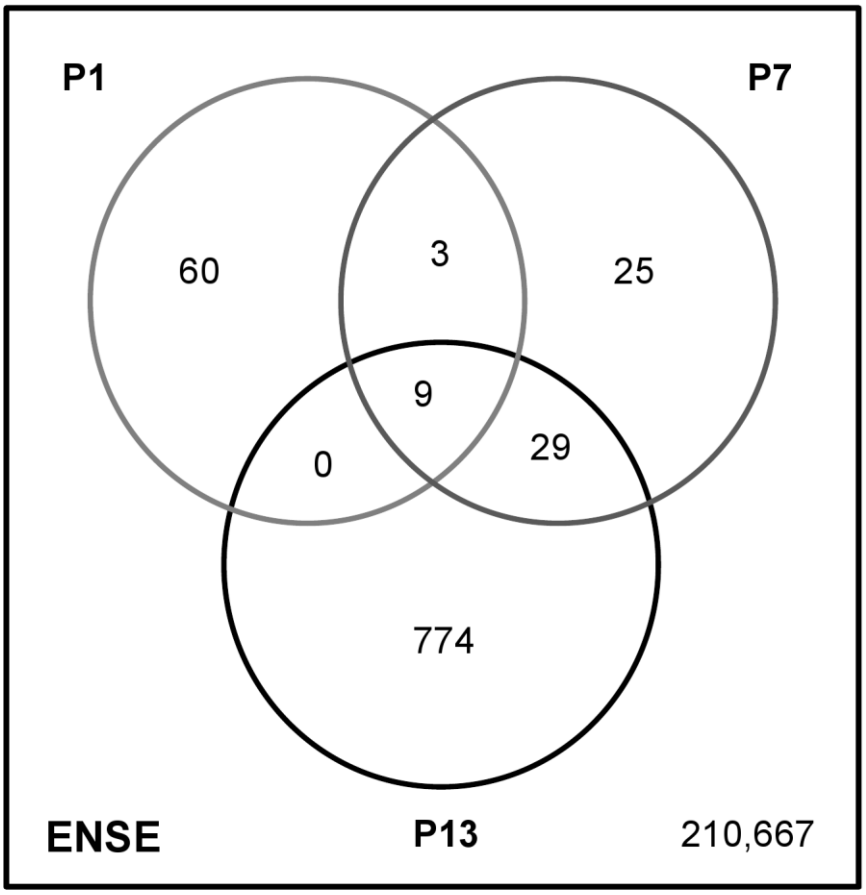

Figure 6.6 Exon-level changes are a late occurrence in SMA mice (A) Venn diagram depicting potential splicing events as evidenced by a Splicing Index |SI| >0.5. 252 alternative splicing events are present at late-symptomatic SMA mice compared to controls, but only 5 at P7 and 16 at P1. (B) Venn diagram depicting exon-level changes of Ensembl exons between genotypes at each time point investigated. At P1, P7 and P13, each of 211567 exons was tested for differential expression between SMA and control. 812 exons were associated with disease status at P13, compared to 72 exons at P1 and 66 exons at P7. Very little overlap exists between time points. Not every exon-level change is necessarily due to an alternative splicing event, but every alternative splicing event will produce an exon-level change.

6.2.5 Pathway based analysis

In the SMN Δ7 mouse model, the early postnatal days appeared particularly relevant to disease development. Our earlier finding of massive gene expression changes between time points in post-natal wild-type mice (figure 7.5B) indicates that events relevant to disease in the SMNΔ7 mouse model coincide with transcriptome changes associated with normal post-natal development or maturation. To analyse which pathways were physiologically activated during this time, gene expression in control mice (Smn+/+;SMN2;SMNΔ7) was first compared between P1 and P7, and subsequently between P7 and P13. Using GO-Elite software, pathways enriched with genes involved in spinal cord cell proliferation, axon development, oligodendrocyte development and myelination were identified as significantly altered, reflecting physiological events during the rapid growth of the spinal cord. When the same analysis was performed for the SMA mice, a strikingly different pattern emerged. With the exception of two GO IDs pertaining to nervous system development, all physiologically activated pathways were absent in both the P1 v P7 and P7 v P13 analyses (table A4). At P13, genes relating to cellular responses to DNA damages became prominent in the SMA mice (appendix 1). This analysis suggested that in the SMN Δ7 mouse

model there is an inhibition or a failure of activation of the normal physiological pathways of post-natal spinal cord maturation.

6.2.6 Validation of individual expression changes

Differential expression of a selection of targets was validated by semi-quantitative and quantitative RT-PCR. In addition to the target displaying the highest fold change at P13 (Cdkn1a), validation focussed on targets exhibiting at least one differentially expressed exon at all time points in the ENSE analysis. For each target, the graphical output of the ENSE analysis was scrutinised for possible splicing changes as indicated by differential expression of one or more exons compared to overall gene level expression, and semi-quantitative RT-PCR was performed with primers spanning these exons. qRT-PCR using primers located in constitutive exons was used to determine overall gene level expression changes (see methods and figure 2.3 for details of the validation procedure).

6.2.6.1 Cdkn1a

The gene with the highest-fold change between genotypes at P13 was Cdkn1a (cyclin-dependent kinase inhibitor 1 (p21) ENSMUSG00000023067), a cyclin-dependent kinase inhibitor that is known to be activated by p53 in response to DNA damage (Shibue et al. 2003) and has important functions in the regulation of cell cycle progression and cellular differentiation (Sitko et al. 2008; Tusell et al. 2009) (figure 2.3, figure 6.7A). Differential expression was evident at P7, co-inciding with the onset of morphological changes and motor deficit. The pattern of change in the expression of Cdkn1a after onset of disease symptoms was suggestive of a response to spinal cord injury from the primary disease process. There was no evidence of splice isoforms of Cdkn1a.

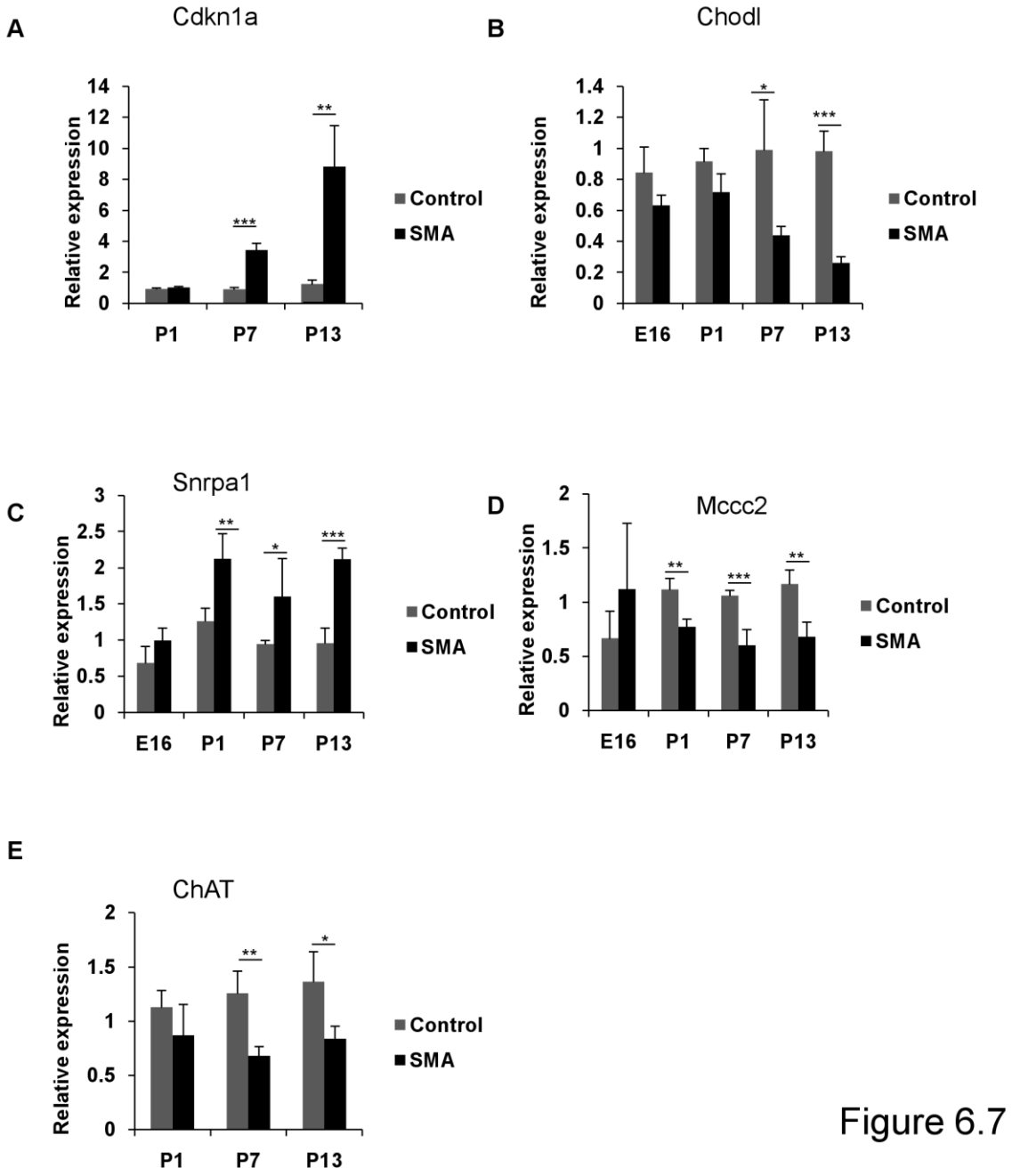

Figure 6.7

Figure 6.7: Array validation by qRT-PC Quantitative RT-PCR was carried out for all time points on the gene displaying the highest fold-change in late-symptomatic mice, but no change at the pre-symptomatic stage (A: Cdkn1a) as well as several targets found to be differentially expressed at several time points in the exon array ENSE analysis (B-E: Chodl, Snrp1a, Mccc2, Chat). Genes showing differential expression at P1 were also examined at embryonic stage E16. Expression is shown relative to control animals. GAPDH was used as the endogenous control. All qRT-PCR results are in agreement with the expression change predicted by the array. Error bars show the standard deviation of the mean for both 4 control and 4 SMA animals per time point. See section 2.14.7.3

and figure 2.4 for details of the qRT-PCR. An unpaired t-test was performed between genotypes to test for significance (* =p<0.05, **=p<0.01,***=p<0.001).

6.2.6.2 Chodl

Chodl (Chondrolectin Precursor (Transmembrane protein MT75), ENSMUSG00000022860) is the mouse orthologue of the human chondrolectin gene *CHODL*. The predicted protein is a type I transmembrane protein with a C-type lectin carbohydrate domain (Weng et al. 2003). Its *in vivo* function is currently unknown, but it has been shown to interact with Rab geranylgeranyl transferase (Claessens et al. 2008). Expression in adult mice was shown to be mainly in skeletal muscle, testes and brain (Weng et al. 2003), but EST libraries contain the highest number of entries in sympathetic ganglion and spinal cord (http://www.ncbi.nlm.nih.gov/UniGene/ESTProfileViewer.cgi?uglist=Mm.77895). Its expression pattern in the spinal cord in *in situ* studies is highly suggestive of predominant expression in motor neurons (http://mousespinal.brain-map.org/imageseries/show.html?id=100020444) (figure 6.8 A).

Immunohistochemistry for Chodl using a commercially available antibody for human CHODL confirmed this expression pattern in human adult spinal cord (figure 6.12 B). Staining of mouse spinal cord also showed preferential staining of anterior horn cells, although somewhat less specifically so (figure 6.12 A, A-D). The difference between mouse and human staining could be explained by the specificity of the antibody, the different developmental stage examined, or both. There was reduced Chodl immunoreactivity in SMA mice, but remaining anterior horn cells retained substantial Chodl staining, which indicated that the reduced Chodl expression is at least partially due to loss of motor neurons. On the other

hand, when controlled for Chat, Chodl mRNA expression was still significantly reduced at P13, suggesting that reduced Chodl mRNA loss is independent of, or goes beyond, motor neuron loss (figure 6.8 B).

Western blotting for Chodl using the antibody employed for immunohistochemistry revealed only non-specific bands, and FLAG-tagged overexpressed Chodl was not recognised by the Chodl antibody.

There are three known Chodl splice variants, with variation resulting from alternative terminal exons. While Chodl expression was uniformly reduced across the 5' part of the transcript, the ENSE analysis suggested differential expression at the 3' end. There was no difference in signal derived from the alternative terminal exon of Chodl isoform 2, whereas terminal exons of transcripts 1 and 3 showed a progressive reduction. This finding was confirmed using qRT-PCR with primers spanning both constitutive exons at the 5'end of the gene, as well as two alternative 3' terminal exons. Taking into account the known transcript structure of Chodl, the findings were in keeping with a preferential loss of Chodl isoforms 1 and 3, with relative sparing of isoform 2 (figure 6.9).

When Chodl expression was analysed in different tissues at P13, overall Chodl was found to be reduced in SMA mice compared to control only in spinal cord, but not in kidney or skeletal muscle. However, a trend towards a relative increase in Chodl isoform 2 in SMA mice was also visible in these tissues (figure 6.9).

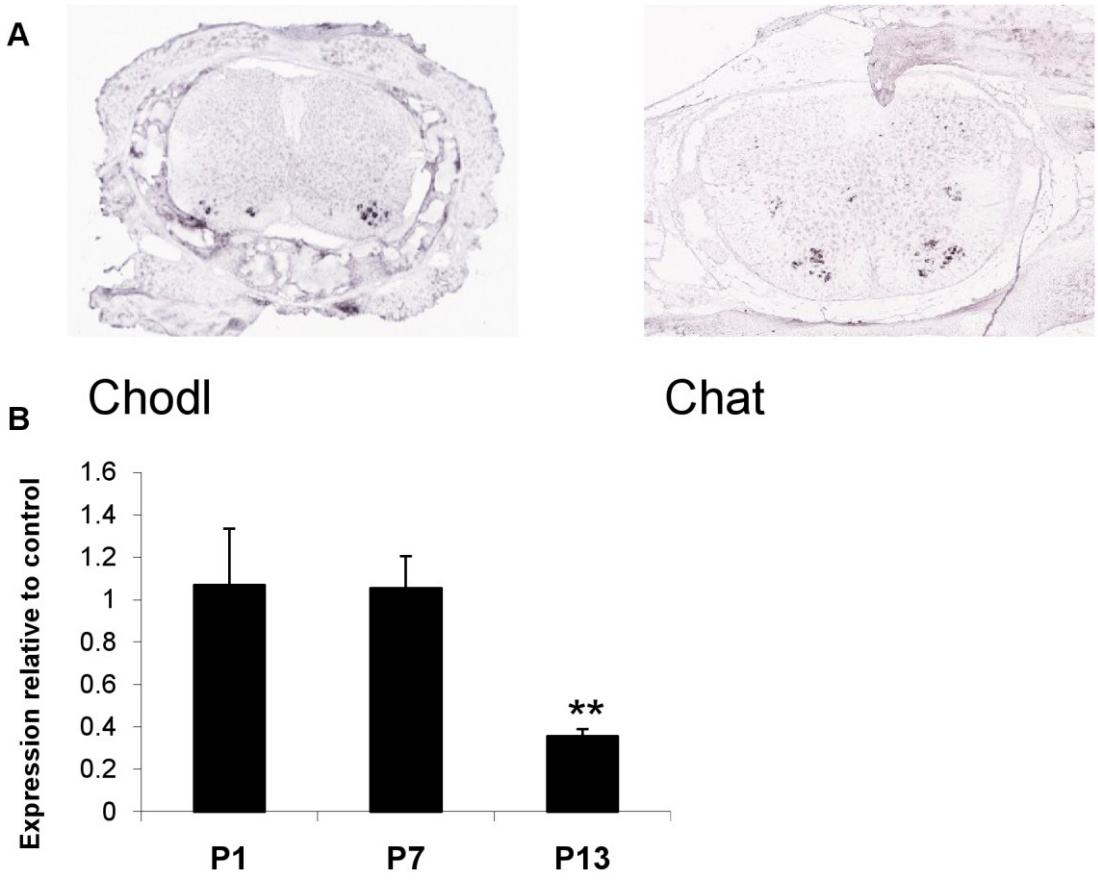

Figure 6.8 Chodl expression normalised for Chat expression (A) In situ hybridisation of Chodl (left) and Chat (right) (Allen Brain Atlas) shows predominant expression of both mRNAs in anterior horn cells. (B) qRT-PCR for Chodl using Chat, rather than Gapdh, as the endogenous control. Results are displayed as expression in SMA mice relative to average expression in control mice (* = $p<0.01$).

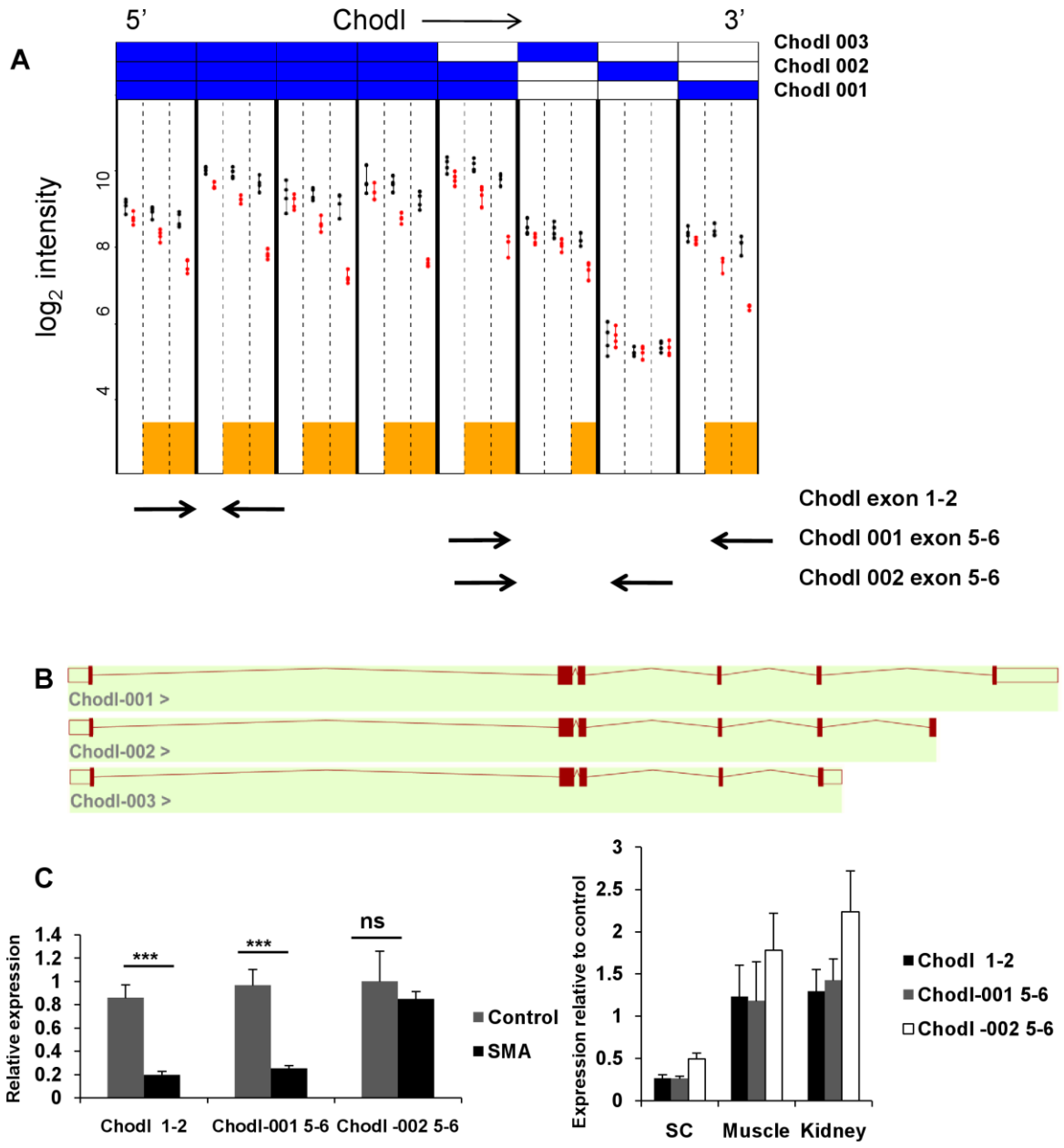

Figure 6.9 Differential expression of Chodl (A) Graphical output of the exon-level analysis for Chodl. Each column, delineated by bold black lines, corresponds to the pre-processed data from a single Ensembl exon. The vertical axis displays $\log_2$ expression for control (black) and SMA (red) animals, with each point corresponding to an individual animal. Each column is subdivided by vertical dashed lines into time points P1, P7, and P13 (left to right). Orange boxes mark those (exon, time point) combinations that exhibit significant differential expression between cases and controls. Expression of Chodl constitutive exons is reduced progressively from P1 to P13, but there is no difference between SMA and control for the alternative terminal exon ENSMUSE00000556896 indicating an isoform shift towards Chodl-002 (ENSMUST69148) in the SMA mice. Arrows indicate location of qRT-PCR primers for validation. (B) Chodl gene structure (adapted from Ensembl). The three known transcripts vary in their terminal 3' exon use. (C) qRT-PCR results at P13 showing marked reduction in Chodl when measured

using primers located in the constitutive exons 1-2 and the terminal exon of Chodl-001, while no significant difference of alternative exon ENSMUSE00000556896 exists between control and SMA (***=p<0.001). (D) qRT-PCR at P13 on spinal cord (SC), muscle and kidney samples displayed as expression in SMA relative to control for a constitutive exon and two alternative terminal exons. Overall Chodl expression is not reduced in muscle or kidney, but there is a trend towards more utilization of ENSMUSE0000055689, in keeping with proportionally more Chodl-002 transcript.

6.2.6.3 Mccc2

Mccc2 is the gene encoding the methylcrotonoyl-CoA carboxylase beta chain (ENSMUSG00000021646), an enzyme important in valine, leucine and isoleucine metabolism. Mccc2 has three known isoforms. The ENSE analysis indicated an overall reduction in Mccc2 expression in SMA mice compared to controls. This was confirmed by qRT-PCR (figure 6.7). The difference was apparent at P1, but was not found at E16.5.

ENSMUSE00000680088, the terminal exon of transcript Mccc2-203, appeared to be spared from the overall reduction, and RT-PCR for this transcript suggested that Mccc2-203 was in fact upregulated in SMA compared to controls. This was not immediately evident from the array output, as most exons are shared between transcripts and the exon signal in the ENSE analysis will be a composite of exon use of several transcripts (figure 6.10).

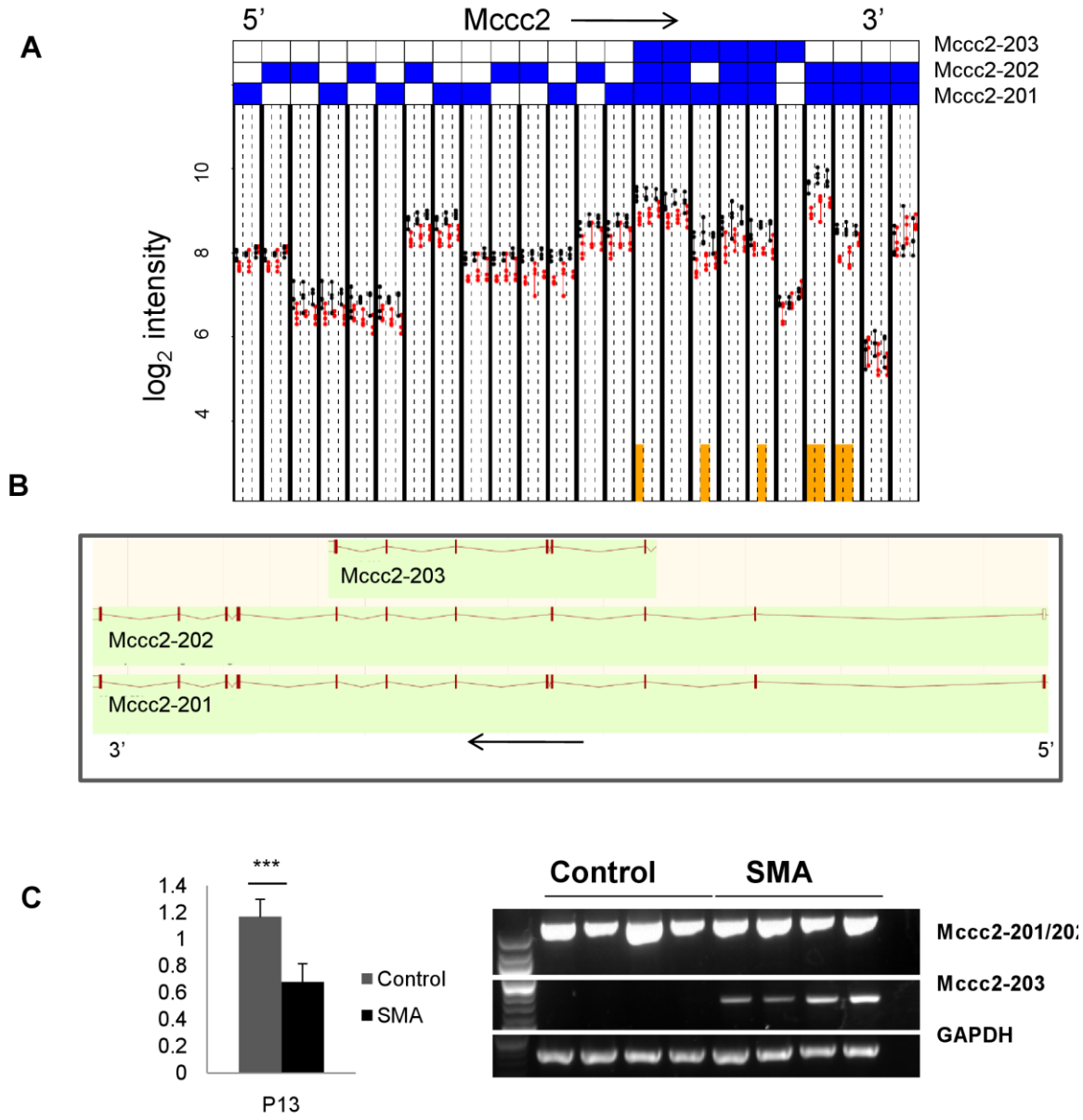

Figure 6.10 Mccc2 expression (A) Graphical output of exon array for Mccc2 (B) Mccc2 gene structure adapted from Ensembl (C) At P13, qRT-PCR across exons present in isoforms Mccc2-201 (ENSMUST00000091326) and Mccc2-202 (ENSMUST00000022148) shows reduced expression in SMA compared to control (*** $p<0.001$, unpaired t-test). (D) As opposed to Mccc2-201 and Mccc2-202, the Mccc2-203 isoform (ENSMUST00000109383 shows) increased expression in SMA at P13

6.2.6.4 Snrpa1

Snrpa1 (ENSMUSG00000030512) is the gene encoding the U2 small nuclear ribonucleoprotein A', a component of the spliceosomal A complex (Behzadnia et al. 2007). Snrpa1 expression was increased in SMA mice compared to controls at all array time points approximately two fold. However, there was no difference at E16.5 (figure 6.7 C). There is only one known isoform, and there was no evidence of altered splicing of Snrpa1 in either ENSE analysis or exon spanning RT-PCR. The increased expression was also present at the protein level. Western blotting showed an approximately 1.4 fold increase in Snrpa1 expression at P13 (figure 6.12 C). While no other spliceosomal components were differentially expressed, the Snrpa1 change might reflect a compensatory response of the cell to Smn deficiency.

6.2.6.5 Uspl1

Uspl1 (ENSMUSG00000041264) is the gene encoding the ubiquitin-specific peptidase-like protein 1, which is involved in ubiquitin dependent protein catabolic processes. There are six known transcripts in Ensembl. Uspl1 was up-regulated in SMA compared to control mice at all time points. In addition, Uspl1 showed a consistent change in both the splicing index and the ENSE analysis. Uspl1 exon 2 ENSMUSE00000351955) is a cassette exon absent in transcripts Uspl1-006 (ENSMUST00000121416) and -007 (ENSMUST00000117878). The increased use of Uspl1 exon 2 in the SMA mice was confirmed by RT-PCR and qRT-PCR, and was consistent with an isoform shift with relatively higher levels of exon 2 containing transcripts Uspl1 -001-005 in SMA (figure 6.11). This isoform shift was more pronounced at end stage and early symptomatic stages than at earlier time points P1 and E16.5. To test whether the isoform shift was spinal cord specific, the

RT-PCR was performed on RNA extracted from skeletal muscle and kidney samples of P13 mice. While an increase in exon 2 inclusion in SMA mice was evident in both, it was much more pronounced in skeletal muscle than in spinal cord or kidney (figure 6.11). Western blotting for Uspl1 showed multiple bands consistent with the known protein isoforms. The major isoform detected was approximately 70 kDa. No obvious difference was noticeable at the protein level between control and SMA mice, in keeping with the minimal overall increase at mRNA level. Immunohistochemistry for Uspl1 showed widespread, cytoplasmic expression in spinal cord cells with a preference for the grey matter (figure 6.12.B, I-J).

6.2.6.6 Chat

Chat (ENSMUSG00000021919), the gene encoding choline acetyltransferase, the key enzyme in motor neuronal synthesis of acetylcholine, showed reduced expression at gene level at P7 and P13 (figure 6.7 E). There is only one known isoform, and no splice variants were detectable by RT-PCR.

In the spinal cord, Chat is expressed predominantly in motor neurons, although small numbers of Chat expressing cells are also present in the central gray matter, the intermediate gray matter and in preganglionic autonomic nuclei (Barber et al. 1984). Loss of Chat was confirmed by Western blotting and immunohistochemistry. The latter confirmed strong expression of Chat in anterior horn cells. In SMA, remaining anterior horn cells retained strong Chat immunoreactivity, indicating that reduced Chat expression is at least partially due to loss of motor neurons (figure 6.12).

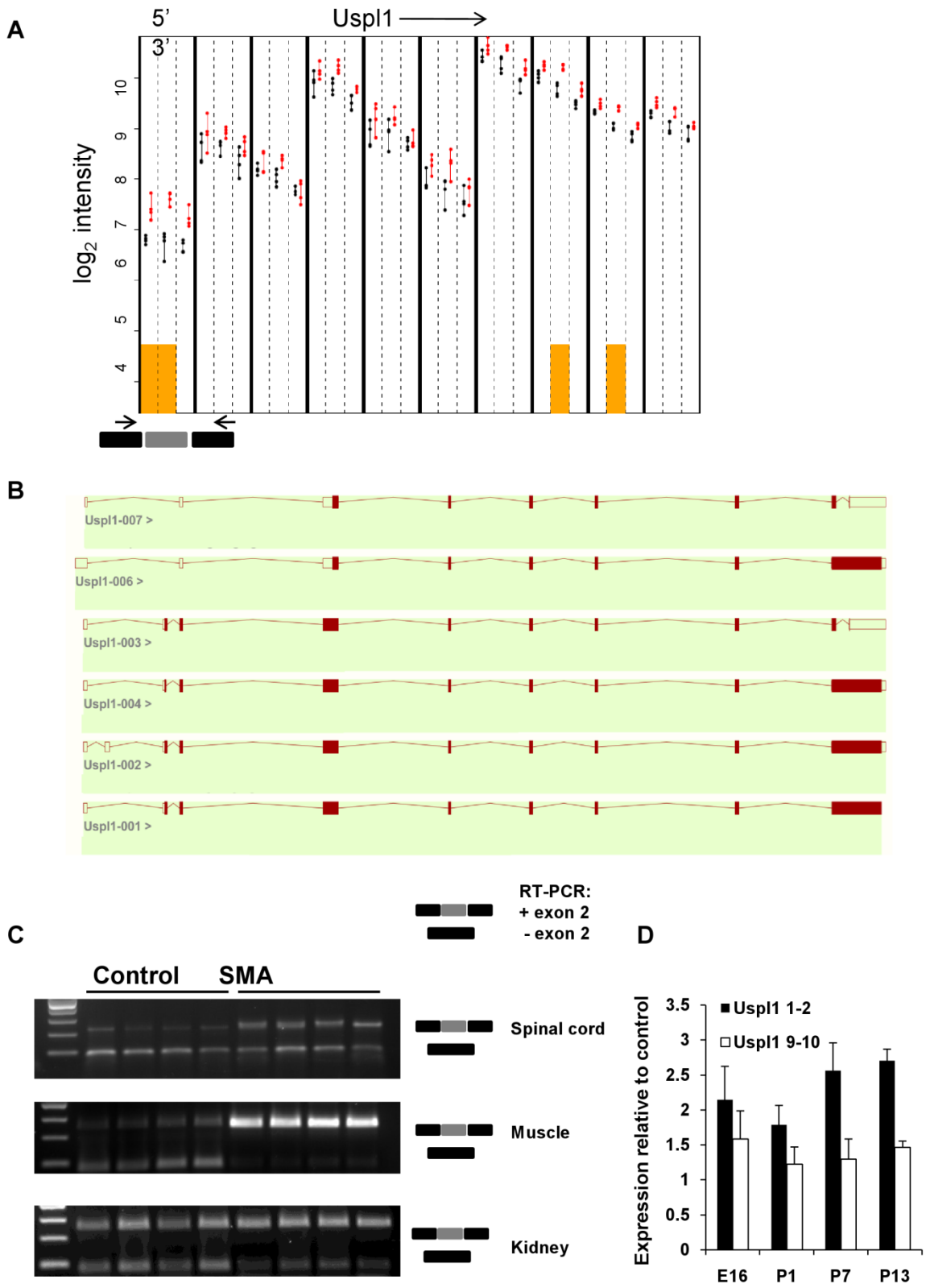
A
5'
3'
Uspl1
log2 intensity
4
5
6
7
8
9
10
B
Uspl1-007 >
Uspl1-006 >
Uspl1-003 >
Uspl1-004 >
Uspl1-002 >
Uspl1-001 >
C
RT-PCR:
+ exon 2
- exon 2
Control
SMA
Spinal cord
Muscle
Kidney
D
Uspl1 1-2
Uspl1 9-10
Expression relative to control
3.5
3
2.5
2
1.5
1
0.5
0
E16
P1
P7
P13

Figure 6.11

Figure 6.11 Alternative splicing of Uspl1 (A) Graphical output of exon-level analysis for Uspl1. Each column, delineated by bold black lines, corresponds to the preprocessed data from a single Ensembl exon. The vertical axis displays $\log_2$ expression for control (black) and SMA (red) animals, with each point corresponding to an individual animal. Each column is subdivided by vertical dashed lines into time points P1, P7, and P13 (left to right). Orange boxes mark those (exon, time point) combinations that exhibit significant differential expression between cases and controls. Expression of Uspl1 is higher in SMA mice for all exons, but this difference is more pronounced for the first exon detected by the array, which corresponds to Uspl1 exon 2 (ENSMUSE00000351955), reflecting a potential alternative splicing event. (B) Uspl1 gene structure adapted from Ensembl. (C) Validation of the alternative splicing event by RT-PCR. Cartoon depicting primer position in Uspl1 exon 1 and 3. RT-PCR was performed on four biological replicates at P13 showing exon 2 skipping in control mice, and increased exon 2 usage in SMA mice. The difference of the exon 2+/exon 2- ratio between genotypes is tissue specific and most pronounced in muscle and less obvious in kidney. (D) qRT-PCR results for exon 2 and exon 9 showing a relatively higher increase in Uspl1 exon 2 expression over Uspl1 exon 9 expression in the SMA mice compared to control. The differential expression is more pronounced at symptomatic compared to pre-symptomatic stages.

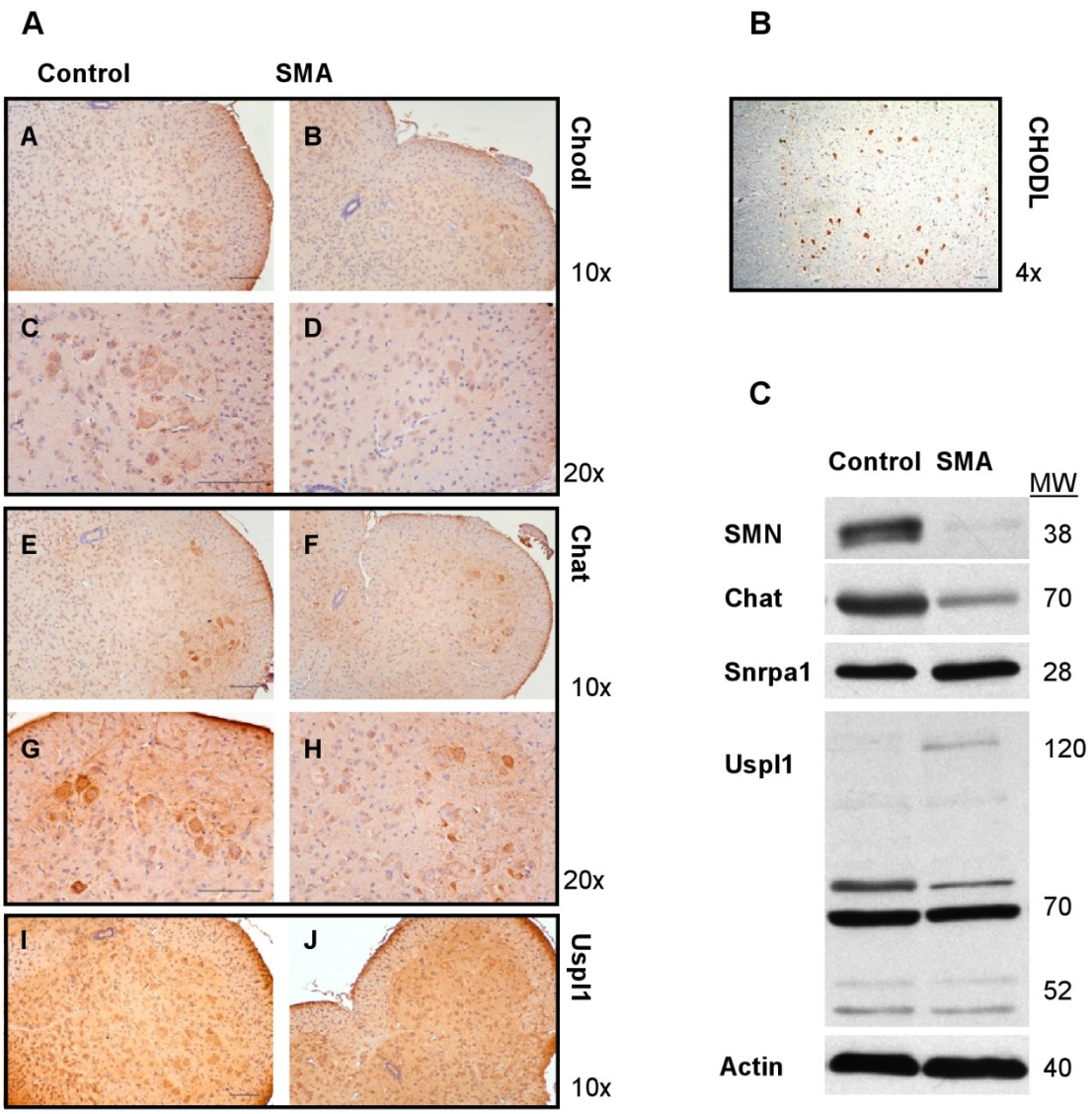

Figure 6.12 Validation of array findings at protein level (A) Immunohistochemistry for Chodl on spinal cord sections of P13 control (A,C) and SMA (B,D) mice shows reduced Chodl immunoreactivity in the ventral horn of SMA mice, but no complete loss of Chodl from remaining anterior horn cells. Similar results are obtained for Chat in control (E,G) and SMA (F,H) mice. Both Chodl and Chat preferentially stain large anterior horn cells. Staining for Uspl1 (I,J) shows ubiquitous cytoplasmic Uspl1 expression with preference of the grey matter. (B) Chodl immunohistochemistry on adult human spinal cord shows very specific labelling of motor neurons in the ventral horn, supporting the importance of Chodl for motor neurons. (C) Western blotting of P13 spinal cord lysates shows reduced Smn and Chat protein levels, minimal increase of Snrpa1 and no overall difference in Uspl1. The Uspl1 1 antibody detected multiple bands in keeping with several known Uspl1 isoforms. MW, molecular weight in kDa. Scale bars 100 µm.

6.2.7 Correlation of splicing events with intron type

To assess whether alternative splicing events detected in the array were associated with a particular intron type, all genes associated with at least one exon change in the ENSE analysis were screened for the presence of U12 type introns using the publically available U12 Intron Database (Alioto 2007), in which all known introns of 20 species, including human and mouse, are semi automatically annotated according to the presence or absence of the U12 consensus sequences for the 5'splice site and branch point, i.e. sequences recognised by the U12 snRNA containing minor spliceosome, but not the U2 snRNA containing major spliceosome. Two genes changed at P1 had U12 introns, as well as 0 at P7 and 10 at P13. However, only in the case of Vash1 (ENSG000000712460, Vasohibin-1) was the U12 –type intron 4-5 associated with a significant change at exon level of the following exon (ENSMUSE00000294318). In all other cases, the U12 type intron was not adjacent to differentially expressed exons.

6.3 Validation of pathway analysis

The gene ontology analysis between time points and genotypes implied activation of genes related to DNA damage in SMA mice late in the disease. Similar changes could theoretically be brought about by gliosis. To rule out gliosis in SMA mice, immunohistochemistry for GFAP was performed, which showed some variability between animals, but no convincing difference between genotypes (figure 7.13A).

In addition, the pathway analysis implied a failure of activation of the normal physiological pathways of post-natal spinal cord maturation in SMA mice. To identify a correlate for this observation, the proliferation marker PCNA was

examined in Western blots and immunohistochemistry of spinal cord sections. Overall PCNA levels were reduced in SMA mice at P13 (figure 7.13). Immunohistochemistry showed PCNA positive cells in all regions of the spinal cord, although no anterior horn cell was positive. Notably, several PCNA positive cells were present in the ependymal zone of the central canal on every section taken from control mice, but never seen on SMA mouse sections. The central canal ependymal zone shares similarities with the subventricular zone in the brain, and harbours cells with stem cell potential even in adulthood (Hamilton et al. 2009). The findings are in keeping with reduced cell proliferation in SMA mice compared with controls.

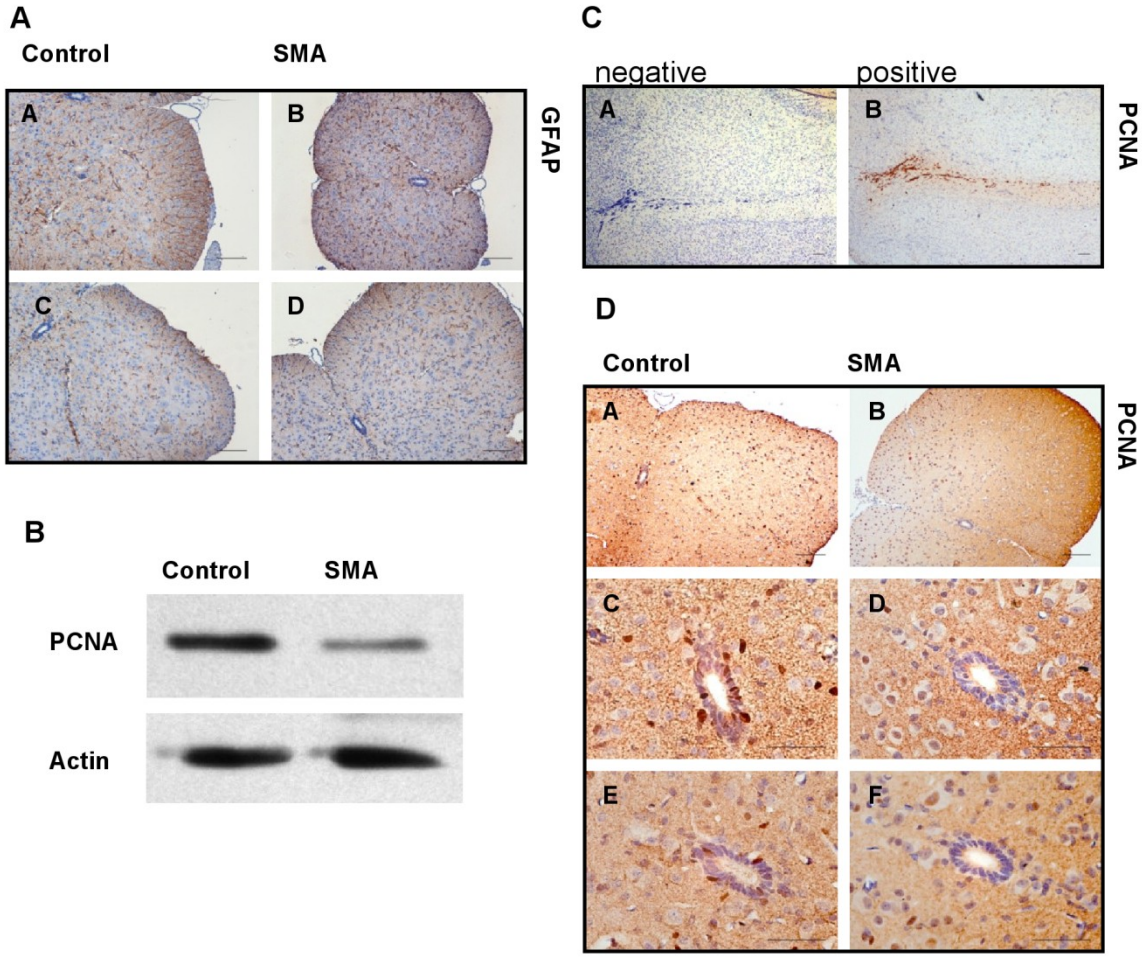

Figure 6.13 Markers of spinal cord proliferation and gliosis (A) GFAP immunohistochemistry of control (A,C) and SMA (B,D) mice shows no significant difference in spinal cord gliosis at P13. (B) Western blotting for the cell proliferation marker PCNA (Proliferating Cell Nuclear Antigen antibody) shows a decrease in SMA. (C) The specificity of the antibody is shown by staining of rostral migratory stream cells ((A) no primary antibody, (B) rabbit anti-PCNA 1:2500) in mouse brain. (D) The central canal ependymal zone contains several PCNA positive cells in control (A,C,E), but not in SMA mice (B,D,F). GFAP, glial fibrillary acidic protein

6.4 Discussion

This chapter describes a detailed assessment of transcriptional changes over time in the spinal cord of a commonly used severe mouse model of SMA, using time points correlated with key phenotypic and pathological changes. Alterations in a subset of genes involved in post-natal neurodevelopmental pathways in SMA were identified, and splicing alterations were shown to be only a late occurrence in disease.

Survival, weight development and motor phenotype of our SMNΔ7 mouse colonies were similar to that described by others (Le et al. 2005; Butchbach et al. 2007), with a change in outward appearance and development of motor deficits apparent at P7. Recent studies have identified morphological changes at the neuromuscular junction as early events in SMA (Kariya et al. 2008; Murray et al. 2008) with neurofilament accumulation occurring as early as P5 in the SMNΔ7 model. This structural change at the distal end of the motor neuron is closely followed in our study by a significant loss of large motor neurons at P7, indicating that although synaptic changes are the earliest identified feature of SMA it ultimately is a disease of the entire lower motor neuron. Of note, motor neuron loss was present

to a similar degree across the entire spinal cord, in contrast to the previous finding of a rostral-caudal gradient with relative sparing of the lumbar region (Kariya et al. 2008). Motor neuron loss at P7 was reflected in the reduction at transcript level of choline acetyl transferase (Chat), the key enzyme in motor neuronal synthesis of acetylcholine (figure 6.7 E). This finding, as well as that of reduced levels of Chodl, which seems to be highly expressed in anterior horn cells (figure 6.8, 6.12), shows that even though whole spinal cord was used for the array, important cell-type specific changes were detectable.

The key finding of this study is that differential splicing events are a late occurrence in SMA, and are therefore unlikely to contribute to early disease pathogenesis. Zhang et al (Zhang et al. 2008) described widespread splicing abnormalities in several tissues including the spinal cord at end-stage disease in the same mouse model employed in this study and attributed this finding to dysfunction of the spliceosome secondary to SMN deficiency. However, it remained unclear from their study whether splicing abnormalities had preceded the onset of symptoms, as would be predicted from the crucial role of SMN in spliceosome assembly, particularly in embryonic and early post-natal development (Gabanella et al. 2005). In addition, the presence of widespread splicing defects in organs other than the spinal cord is difficult to interpret in the light of apparent tissue specificity of the disease if splicing abnormalities are indeed thought to be relevant to the mechanism of motor neuron degeneration. To determine the degree of variation in splicing between SMA and control mice, two complementary methods of analysis were employed, the splicing index, as well as an exon based analysis (ENSE). The latter analysis can be seen as a measure of the upper bounds of alternative splicing events present at a given p value, because no

alternative splicing event could occur without expression change in at least one exon. The number of changes found in late symptomatic mice was not large given the large number of exons examined (>200,000). When the same analysis was performed, comparing between genotypes at pre-symptomatic and early symptomatic time points, only very few exon-level changes were present.

Importantly, a similar pattern of exon expression changes was found in the more severe Smn-/-;SMN2 mouse model, corroborating the main finding in the SMNΔ7 mice (Baumer et al. 2009). Overall, the data indicate that the majority of splicing changes are not a direct consequence of SMN deficiency, but rather a consequence of disease progression, probably representing physiological isoform-shifts in response to cell stress. There is evidence that oxidative stress can induce shifts in alternative splicing, and that neurons may be more vulnerable to this process than other cells (Maracchioni et al. 2007). Even though it is difficult to compare levels of SMN reduction in 2 very different situations, it could be argued that SMN deficiency to the degree observed in either the SMNΔ7 or *Smn-/-;SMN2* mouse, although associated with severe reduction in snRNP assembly capacity *in vitro* (Gabanella et al. 2007), does not lead to a systematic breakdown of splicing fidelity *in vivo* until the disease is well established.

While these results do not support the hypothesis that widespread, systematic splicing abnormalities cause SMA, another possibility is that splicing of one or several transcripts is critically affected by SMN deficiency, and that the few splicing changes observed early in the SMNΔ7 mice contribute to SMA pathogenesis, followed by a cascade of loss of splicing fidelity or secondary effects. In fact, at least one of the genes identified by the array (Uspl1) is differentially spliced between SMA and control mice even at the embryonic phase,

albeit to a lesser degree than at the symptomatic stages. Of note, the isoform shift observed in this particular gene is more pronounced in muscle than in spinal cord, and less marked in kidney, an organ not affected by SMA pathology.

The data presented here could be seen as contradicting the findings of Zhang et al (Zhang et al. 2008), who show differential splicing patterns between genotypes at end stage disease in SMNΔ7 mice. In this paper, alternative exon usage is interpreted as 'widespread' and 'aberrant', which is partially supported by sequencing results of a few transcripts that show exon skipping and generation of premature stop codons. When both datasets (i.e. the data presented here and the spinal cord array data deposited by Zhang et al) are analysed in parallel, however, there is clearly a high degree of concordance between differentially expressed probe sets. In particular, the directionality of differential expression is extremely consistent across both studies (Baumer et al. 2009). This means that although the raw data of both studies are very similar, different conclusions are reached. The work presented here includes data from two additional time points as points of reference for the number of differentially expressed exons at end stage disease, which allows making a more meaningful statement about the extent of differential splicing events than a vague qualitative remark such as 'widespread' (i.e. that there are more differential splicing events at P13 than at P1 or P7). In addition, it shows that differentially expressed exons do not necessarily imply 'aberrant' splicing, but can represent shifts in expression between physiologically occurring isoforms.

Independent of whether or not splicing changes are ultimately responsible for SMA disease initiation, this study identified several pathways that might shed light on SMA pathogenesis and disease progression. Analysis of transcriptional

changes between genotypes in this study took place on a background of large scale physiological changes between time points, reflecting rapid neuronal development in the early post-natal days. Analysis of the changes between time points identified several pathways related to normal neuronal development. Surprisingly, in the SMA mice the majority of physiological transcriptional changes seen in control mice were absent even between the early time points P1 and P7. This finding not only indicates that abnormal post-natal neuronal development might underlie early events in SMA but might explain general delayed growth and failure to thrive in the SMA mice. Importantly, this finding is supported by the reduction in PCNA positive cells in SMA.

In this study, gene expression was examined in the entire spinal cord. It was not possible to distinguish which cell types contribute most to expression changes, even though changes that plausibly originate from motor neurons, such as Chat and Chodl, are clearly present. The neurodevelopmental pathways identified as altered in this study can be associated with other cell types, including oligodendrocytes and cells in the posterior spinal cord. While this is a preliminary finding, it clearly warrants further studies examining the role of non-motor neuronal cells in SMA. Human autopsy cases indicate involvement of sensory neurons in the dorsal root ganglia, Clarke's column and the thalamus in SMA (Towfighi et al. 1985), (Shishikura et al. 1983), (Hayashi et al. 1998; Kuru et al. 2009), although the majority of studies were undertaken before the molecular diagnosis of SMA was available. More recent clinical studies showed that severe SMN-related SMA is associated with widespread neuronal degeneration, including sensory pathways (Rudnik-Schoneborn et al. 2003). Subtle sensory neuron abnormalities have also been detected in a severe mouse model of SMA (Jablonka et al. 2006). However,

there is no study systematically investigating the role of non-motoneuronal cells in SMA spinal cord.

In conclusion, these data show that alternative splicing events predominantly occur late in SMA, while alterations of post-natal neurodevelopmental pathways precede overt symptom onset. Further studies should continue to focus on the role of SMN in the post-natal maturation and development of the neuromuscular system including spinal cord motor neurons.

7 Conclusions and future directions

7.1 Summary

Amyotrophic lateral sclerosis is an invariably fatal, devastating neurodegenerative disease with a life time risk of about 1:250 - 1:400 (Johnston et al. 2006). Autosomal recessive spinal muscular atrophy has a carrier frequency of 1:35 (Cusin et al. 2003), making it one of the most frequent recessive disorders in humans. While neither ALS nor SMA can thus be considered rare, the overall disease burden caused by motor neuron disorders in general, including the heterogeneous group of individually less common distal spinal muscular atrophies, is highly significant. No effective therapies are currently available for any of these disorders. Much research emphasis has been put on the role of SOD1 in the aetiology of ALS, based on the finding of *SOD1* mutations in a sub-group of patients with ALS (Rosen et al. 1993), but recent years have seen a paradigm shift in the field (Lagier-Tourenne and Cleveland 2009), triggered by the discovery of the nucleic acid binding protein TDP-43 as the core constituent of ubiquitinated inclusions in ALS, as well as the finding of mutations in the *TARDBP* and *FUS* genes, both encoding proteins with similar functions in various aspects of RNA metabolism. The shift towards an interest in RNA metabolism was just beginning to crystallise while this work was undertaken, but now appears to be at the centre stage of motor neuron disease research interest.

This thesis took a combined genetic, molecular and neuropathological approach to study aspects of motor neuron disease related to RNA metabolism. The genetic work presented in chapter 3 identified novel variants in *TARDBP* and *FUS* in patients with sporadic ALS, adding to the growing body of evidence that both

familial and sporadic ALS have in fact a genetic basis. The functional characterisation of some of the identified variants was undertaken in chapter 4. The results highlighted that differences between wild-type and mutant protein are likely to be very subtle in the case of late onset, low penetrance mutations, and various approaches including more complex model systems will be needed to fully understand how they lead to disease. The similarity between wild-type and mutant TDP-43 is also underlined by two recent publications of TDP-43 transgenic mouse models achieving motor neuron disease in mice by the over-expression of wild-type TDP-43 alone (Wegorzewska et al. 2009; Wils et al. 2010). In addition to the analysis of coding variants, the use of *cis*-splicing minigene systems illustrated some of the approaches that can be utilised in vitro to further characterise genetic variants of uncertain significance. The neuropathological approaches presented in chapter 5 proved to be invaluable in testing hypotheses generated by *in vitro* studies, for example the interaction between SMN and TDP-43, but also in discovering new aspects of disease that lead to downstream molecular analysis, such as the presence of both FUS and SMN in basophilic inclusions. Neuropathology has also highlighted that mouse models, such as the SOD1 G93A mouse, need to be used with awareness of their limitations in fully reflecting human disease. Chapter 6 then presented the results of an experiment that could only be carried out using mouse models, the temporal analysis of transcriptome changes and alternative splicing events spinal cord of an SMA mouse model.

7.2 A model of shared vulnerability

The apparent dichotomy between the phenotypic similarity of motor neuron disorders and the marked genetic heterogeneity could be reconciled by a model of shared vulnerability of motor neurons to disturbance of a common pathway. TDP-

43 pathology characterises the majority of cases of ALS, but the TDP-43 negative cases are frequently positive for neuronal cytoplasmic inclusions involving a related protein, FUS. SMA neuropathology is not characterised by protein aggregation, but is functionally linked to TDP-43 and FUS proteinopathies by the role of SMN in RNA metabolism. SOD1 positive ALS might be the exception to this, but recent work also demonstrates a role for SOD1 in RNA handling (Strong 2009; Volkening et al. 2009).

TDP-43, FUS, SMN and many other proteins implicated in motor neuron disorders have physiological functions in various RNA processing steps from transcription to translation (see chapter 1 and table 7.1) and loss of this function can occur by genetic deletion or pathological sequestration of protein. However, specific disease-causing RNA handling deficits have yet to be identified for the majority of motor neuron disorders.

Disorder	**Gene**	**Trans-cription**	**Splicing**	**mRNA transport and stability**	**Trans-lation**	**Stress response**
SMA	*SMN*	(Strasswimmer et al. 1999; Pellizzoni et al. 2001)	(Winkler et al. 2005; Gabanella et al. 2007; Zhang et al. 2008)	(Rossoll et al. 2002; Rossoll et al. 2003)		(Hua and Zhou 2004b)
	IGHMBP2				(Guenther et al. 2009)	
	GARS (distal HMN)				(Antonellis et al. 2006; Chihara et al.	

					2007)	
	DCTN1 (distal HMN)			(Puls et al. 2003)		
	GLE1 (LCCS1)			(Nousiainen et al. 2008)	(Bolger et al. 2008)	
ALS	*SOD1* (ALS1)			(Lu et al. 2007; Li et al. 2009; Volkening et al. 2009)		
	SETX (ALS4)	(Surawee ra et al. 2009)	(Surawee ra et al. 2009)		putative	
	TARDBP (ALS10)	(Ou et al. 1995; Abhyankar et al. 2007)	(Buratti et al. 2001; Mercado et al. 2005; Bose et al. 2008)	(Strong et al. 2007)	(Wang et al. 2008a)	(Colombrita et al. 2009b; Moisse et al. 2009a; Moisse et al. 2009b)
	FUS (ALS6)	(Wang et al. 2008b)	(Yang et al. 1998a; Meissner et al. 2003)	(Zinszner et al. 1997; Kanai et al. 2004; Fujii and Takumi 2005)		(Andersson et al. 2008)
	ANG (ALS9)	(Xu et al. 2002; Xu et al. 2003; Tsuji et al. 2005)			(Saxena et al. 1992)	(Yamasaki et al. 2009)

Table 7.1 Overview of major genes implicated in forms of spinal muscular atrophy and amyotrophic lateral sclerosis. Most genes produce proteins with physiological functions in various aspects of RNA metabolism. RNA transport, stability and translation control are intricately linked and the distinction can be arbitrary.

With growing understanding of gene expression in neurons, several of the diverse mechanisms previously implicated in the motor neuron disease pathogenesis can be integrated into a concept of shared vulnerability. For instance, axonal transport deficits are likely to impair transport of RNA granules; glutamate toxicity could lead to altered local translation of mRNAs in dendrites by altering the phosphorylation status of RNA binding proteins; oxidative stress can lead to oxidised RNA species and faulty translation; the unfolded protein response can trigger a stress response involving RNA binding proteins. Some of these mechanisms are likely to be of particular importance in motor neurons given their specific anatomical features detailed in chapter 1, including their extremely long axons and extensive dendritic branching. On the other hand, some findings might well be relevant to the field of neurodegeneration in general. In fact, as detailed in chapter 5, TDP-43 pathology is found in variety of neurodegenerative disorders. In addition, a shared genetic vulnerability to neurodegeneration is suggested by the clustering of ALS, Parkinson's disease and dementia in many ALS kindreds (Fallis and Hardiman 2009).

While this growing understanding of motor neuron disease pathophysiology does not immediately translate into new therapies, it seems unlikely that a cure for these devastating disorders can be developed without a thorough understanding of the basic disease mechanisms.

7.3 Future directions

The vast majority of ALS cases still have no known genetic cause, although it is likely that a large amount of variance can be explained by multiple rare variants, possibly in genes active in related pathways. The emergence of new technologies

such as next generation sequencing (Mardis 2008) will make it possible to sequence a large number of candidate genes and discover new variants, but will need to be combined with powerful bioinformatic tools because of the vast amount of data. Many variants discovered are likely to be of uncertain significance, as exemplified by the synonymous changes identified in *TARDBP*, and will need functional studies to clarify their significance. Functional assays for putative *cis*-splicing mutations can be extremely complex, as shown by the A315A variant, for which no definite answer could be reached, and are ideally founded upon splicing patterns observed in patient tissue. This, in turn, requires systematic collection of tissue samples suitable not only for histology, but also for RNA and protein extraction.

The results presented in the last chapter go some way to answer the question of whether splicing fidelity is globally impaired at the onset of SMA, which appears to be not the case. Further studies would be needed, however, to rule out motor neuron specific differential splicing events. This could be achieved by laser-capture micro-dissection of motor neuron and subsequent microarray or RNA sequencing. Finally, an attempt should then be made to assess whether the observed differences can be functionally linked to SMN deficiency. This would require a dual approach of trying to recapitulate the splicing event of interest, for example exon skipping of Uspl1 exon 2, by inducing SMN deficiency by RNA interference, as well as identifying the immediate *trans*-acting protein factors modulating exon 2 recognition and their link to SMN.

Overall, the combination of multiple techniques and approaches will be crucial in trying to unravel the complexities of motor neuron diseases.

8 References

Abelson, J.F., Kwan, K.Y., O'Roak, B.J., Baek, D.Y., Stillman, A.A., Morgan, T.M., Mathews, C.A., Pauls, D.L., Rasin, M.R., Gunel, M. et al. 2005. Sequence variants in SLITRK1 are associated with Tourette's syndrome. *Science* **310**(5746): 317-320.

Abhyankar, M.M., Urekar, C., and Reddi, P.P. 2007. A novel CpG-free vertebrate insulator silences the testis-specific SP-10 gene in somatic tissues: role for TDP-43 in insulator function. *J Biol Chem* **282**(50): 36143-36154.

AceView. Homo sapiens complex locus FVT1, encoding follicular lymphoma variant translocation 1. In.

Acharya, K.K., Govind, C.K., Shore, A.N., Stoler, M.H., and Reddi, P.P. 2006. cis-requirement for the maintenance of round spermatid-specific transcription. *Dev Biol* **295**(2): 781-790.

Affymetrix. 2005. Alternative Transcript Analysis Methods for Exon Arrays. In, Affymetrix White Papers.

-. 2009. Identifying and Validating Alternative Splicing Events - An introduction to managing data provided by GeneChip® Exon Arrays. In, Affymetrix Technical Notes.

Aizawa, H., Kimura, T., Hashimoto, K., Yahara, O., Okamoto, K., and Kikuchi, K. 2000. Basophilic cytoplasmic inclusions in a case of sporadic juvenile amyotrophic lateral sclerosis. *J Neurol Sci* **176**(2): 109-113.

Alioto, T.S. 2007. U12DB: a database of orthologous U12-type spliceosomal introns. *Nucleic Acids Res* **35**(Database issue): D110-115.

Alonso, A., Logroscino, G., Jick, S.S., and Hernan, M.A. 2009. Incidence and lifetime risk of motor neuron disease in the United Kingdom: a population-based study. *Eur J Neurol* **16**(6): 745-751.

Amador-Ortiz, C., Lin, W.L., Ahmed, Z., Personett, D., Davies, P., Duara, R., Graff-Radford, N.R., Hutton, M.L., and Dickson, D.W. 2007. TDP-43 immunoreactivity in hippocampal sclerosis and Alzheimer's disease. *Ann Neurol* **61**(5): 435-445.

Aman, P., Panagopoulos, I., Lassen, C., Fioretos, T., Mencinger, M., Toresson, H., Hoglund, M., Forster, A., Rabbitts, T.H., Ron, D. et al. 1996. Expression patterns of the human sarcoma-associated genes FUS and EWS and the genomic structure of FUS. *Genomics* **37**(1): 1-8.

Anderson, P. and Kedersha, N. 2006. RNA granules. *J Cell Biol* **172**(6): 803-808.

-. 2008. Stress granules: the Tao of RNA triage. *Trends Biochem Sci* **33**(3): 141-150.

-. 2009. RNA granules: post-transcriptional and epigenetic modulators of gene expression. *Nat Rev Mol Cell Biol* **10**(6): 430-436.

Andersson, M.K., Stahlberg, A., Arvidsson, Y., Olofsson, A., Semb, H., Stenman, G., Nilsson, O., and Aman, P. 2008. The multifunctional FUS, EWS and TAF15 proto-oncoproteins show cell type-specific expression patterns and involvement in cell spreading and stress response. *BMC Cell Biol* **9**: 37.

Antonellis, A., Ellsworth, R.E., Sambuughin, N., Puls, I., Abel, A., Lee-Lin, S.Q., Jordanova, A., Kremensky, I., Christodoulou, K., Middleton, L.T. et al. 2003. Glycyl tRNA synthetase mutations in Charcot-Marie-Tooth disease type 2D and distal spinal muscular atrophy type V. *Am J Hum Genet* **72**(5): 1293-1299.

Antonellis, A. and Green, E.D. 2008. The role of aminoacyl-tRNA synthetases in genetic diseases. *Annu Rev Genomics Hum Genet* **9**: 87-107.

Antonellis, A., Lee-Lin, S.Q., Wasterlain, A., Leo, P., Quezado, M., Goldfarb, L.G., Myung, K., Burgess, S., Fischbeck, K.H., and Green, E.D. 2006. Functional analyses of glycyl-tRNA synthetase mutations suggest a key role for tRNA-charging enzymes in peripheral axons. *J Neurosci* **26**(41): 10397-10406.

Arai, T., Hasegawa, M., Akiyama, H., Ikeda, K., Nonaka, T., Mori, H., Mann, D., Tsuchiya, K., Yoshida, M., Hashizume, Y. et al. 2006. TDP-43 is a component of ubiquitin-positive tau-negative inclusions in frontotemporal lobar degeneration and amyotrophic lateral sclerosis. *Biochem Biophys Res Commun* **351**(3): 602-611.

Arai, T., Mackenzie, I.R., Hasegawa, M., Nonoka, T., Niizato, K., Tsuchiya, K., Iritani, S., Onaya, M., and Akiyama, H. 2009. Phosphorylated TDP-43 in Alzheimer's disease and dementia with Lewy bodies. *Acta Neuropathol* **117**(2): 125-136.

Awano, T., Johnson, G.S., Wade, C.M., Katz, M.L., Johnson, G.C., Taylor, J.F., Perloski, M., Biagi, T., Baranowska, I., Long, S. et al. 2009. Genome-wide association analysis reveals a SOD1 mutation in canine degenerative myelopathy that resembles amyotrophic lateral sclerosis. *Proc Natl Acad Sci U S A* **106**(8): 2794-2799.

Ayala, Y.M., Misteli, T., and Baralle, F.E. 2008a. TDP-43 regulates retinoblastoma protein phosphorylation through the repression of cyclin-dependent kinase 6 expression. *Proc Natl Acad Sci U S A*.

Ayala, Y.M., Pagani, F., and Baralle, F.E. 2006. TDP43 depletion rescues aberrant CFTR exon 9 skipping. *FEBS Lett* **580**(5): 1339-1344.

Ayala, Y.M., Pantano, S., D'Ambrogio, A., Buratti, E., Brindisi, A., Marchetti, C., Romano, M., and Baralle, F.E. 2005. Human, Drosophila, and C.elegans TDP43: nucleic acid binding properties and splicing regulatory function. *J Mol Biol* **348**(3): 575-588.

Ayala, Y.M., Zago, P., D'Ambrogio, A., Xu, Y.F., Petrucelli, L., Buratti, E., and Baralle, F.E. 2008b. Structural determinants of the cellular localization and shuttling of TDP-43. *J Cell Sci* **121**(Pt 22): 3778-3785.

Barber, R.P., Phelps, P.E., Houser, C.R., Crawford, G.D., Salvaterra, P.M., and Vaughn, J.E. 1984. The morphology and distribution of neurons containing choline acetyltransferase in the adult rat spinal cord: an immunocytochemical study. *J Comp Neurol* **229**(3): 329-346.

Bass, B.L. 2002. RNA editing by adenosine deaminases that act on RNA. *Annu Rev Biochem* **71**: 817-846.

Baumer, D., Lee, S., Nicholson, G., Davies, J.L., Parkinson, N.J., Murray, L.M., Gillingwater, T.H., Ansorge, O., Davies, K.E., and Talbot, K. 2009. Alternative splicing events are a late feature of pathology in a mouse model of spinal muscular atrophy. *PLoS Genet* **5**(12): e1000773.

Bäumer, D., Hilton, D., Paine, S.M., Turner, M.R., Lowe, J., Talbot, K., and Ansorge, O. 2010. Juvenile ALS with basophilic inclusions is a FUS proteinopathy with FUS mutations. *Neurology* **75**:611-618

Bechade, C., Rostaing, P., Cisterni, C., Kalisch, R., La Bella, V., Pettmann, B., and Triller, A. 1999. Subcellular distribution of survival motor neuron (SMN) protein: possible involvement in nucleocytoplasmic and dendritic transport. *Eur J Neurosci* **11**(1): 293-304.

Beghi, E., Logroscino, G., Chio, A., Hardiman, O., Mitchell, D., Swingler, R., Traynor, B.J., and Consortium, E. 2006. The epidemiology of ALS and the role of population-based registries. *Biochim Biophys Acta* **1762**(11-12): 1150-1157.

Behzadnia, N., Golas, M.M., Hartmuth, K., Sander, B., Kastner, B., Deckert, J., Dube, P., Will, C.L., Urlaub, H., Stark, H. et al. 2007. Composition and three-dimensional EM structure of double affinity-purified, human prespliceosomal A complexes. *EMBO J* **26**(6): 1737-1748.

Beleza-Meireles, A. and Al-Chalabi, A. 2009. Genetic studies of amyotrophic lateral sclerosis: controversies and perspectives. *Amyotroph Lateral Scler* **10**(1): 1-14.

Belzil, V.V., Valdmanis, P.N., Dion, P.A., Daoud, H., Kabashi, E., Noreau, A., Gauthier, J., for the, S.D.t., Hince, P., Desjarlais, A. et al. 2009. Mutations in FUS cause FALS and SALS in French and French Canadian populations. *Neurology*.

Benajiba, L., Le Ber, I., Camuzat, A., Lacoste, M., Thomas-Anterion, C., Couratier, P., Legallic, S., Salachas, F., Hannequin, D., Decousus, M. et al. 2009. TARDBP mutations in motoneuron disease with frontotemporal lobar degeneration. *Ann Neurol* **65**(4): 470-473.

Benatar, M. 2007. Lost in translation: treatment trials in the SOD1 mouse and in human ALS. *Neurobiol Dis* **26**(1): 1-13.

Benjamini, Y. and Hochberg, Y. 1995. Controlling the false discovery rate: A practical and powerful approach to multiple testing. *J R Statist Soc B* **57**: 289-300.

Bertolotti, A., Lutz, Y., Heard, D.J., Chambon, P., and Tora, L. 1996. hTAF(II)68, a novel RNA/ssDNA-binding protein with homology to the pro-oncoproteins TLS/FUS and EWS is associated with both TFIID and RNA polymerase II. *EMBO J* **15**(18): 5022-5031.

Besse, F. and Ephrussi, A. 2008. Translational control of localized mRNAs: restricting protein synthesis in space and time. *Nat Rev Mol Cell Biol* **9**(12): 971-980.

Bicker, S. and Schratt, G. 2008. microRNAs: tiny regulators of synapse function in development and disease. *J Cell Mol Med* **12**(5A): 1466-1476.

Bilen, J., Liu, N., and Bonini, N.M. 2006a. A new role for microRNA pathways: modulation of degeneration induced by pathogenic human disease proteins. *Cell Cycle* **5**(24): 2835-2838.

Bilen, J., Liu, N., Burnett, B.G., Pittman, R.N., and Bonini, N.M. 2006b. MicroRNA pathways modulate polyglutamine-induced neurodegeneration. *Mol Cell* **24**(1): 157-163.

Blair, I.P., Williams, K.L., Warraich, S.T., Durnall, J.C., Thoeng, A.D., Manavis, J., Blumbergs, P.C., Vucic, S., Kiernan, M.C., and Nicholson, G.A. 2010. FUS mutations in amyotrophic lateral sclerosis: clinical, pathological, neurophysiological and genetic analysis. *J Neurol Neurosurg Psychiatry*; **81**(6):639-45

Blauw, H.M., Veldink, J.H., van Es, M.A., van Vught, P.W., Saris, C.G., van der Zwaag, B., Franke, L., Burbach, J.P., Wokke, J.H., Ophoff, R.A. et al. 2008. Copy-number variation in sporadic amyotrophic lateral sclerosis: a genome-wide screen. *Lancet Neurol* **7**(4): 319-326.

Bodmer, W. and Bonilla, C. 2008. Common and rare variants in multifactorial susceptibility to common diseases. *Nat Genet* **40**(6): 695-701.

Bolger, T.A., Folkmann, A.W., Tran, E.J., and Wente, S.R. 2008. The mRNA export factor Gle1 and inositol hexakisphosphate regulate distinct stages of translation. *Cell* **134**(4): 624-633.

Borroni, B., Bonvicini, C., Alberici, A., Buratti, E., Agosti, C., Archetti, S., Papetti, A., Stuani, C., Di Luca, M., Gennarelli, M. et al. 2009. Mutation within TARDBP leads to Frontotemporal Dementia without motor neuron disease. *Hum Mutat*.

Bose, J.K., Wang, I.F., Hung, L., Tarn, W.Y., and Shen, C.K. 2008. TDP-43 overexpression enhances exon 7 inclusion during the survival of motor neuron pre-mRNA splicing. *J Biol Chem* **283**(43): 28852-28859.

Boucard, A.A., Chubykin, A.A., Comoletti, D., Taylor, P., and Sudhof, T.C. 2005. A splice code for trans-synaptic cell adhesion mediated by binding of neuroligin 1 to alpha- and beta-neurexins. *Neuron* **48**(2): 229-236.

Brengues, M., Teixeira, D., and Parker, R. 2005. Movement of eukaryotic mRNAs between polysomes and cytoplasmic processing bodies. *Science* **310**(5747): 486-489.

Briese, M., Richter, D.U., Sattelle, D.B., and Ulfig, N. 2006. SMN, the product of the spinal muscular atrophy-determining gene, is expressed widely but selectively in the developing human forebrain. *J Comp Neurol* **497**(5): 808-816.

Bromberg, Y., Yachdav, G., and Rost, B. 2008. SNAP predicts effect of mutations on protein function. *Bioinformatics* **24**(20): 2397-2398.

Brooks, B.R., Miller, R.G., Swash, M., and Munsat, T.L. 2000. El Escorial revisited: revised criteria for the diagnosis of amyotrophic lateral sclerosis. *Amyotroph Lateral Scler Other Motor Neuron Disord* **1**(5): 293-299.

Buratti, E. and Baralle, F.E. 2001. Characterization and functional implications of the RNA binding properties of nuclear factor TDP-43, a novel splicing regulator of CFTR exon 9. *J Biol Chem* **276**(39): 36337-36343.

Buratti, E., Brindisi, A., Giombi, M., Tisminetzky, S., Ayala, Y.M., and Baralle, F.E. 2005. TDP-43 binds heterogeneous nuclear ribonucleoprotein A/B through its C-terminal tail: an important region for the inhibition of cystic fibrosis transmembrane conductance regulator exon 9 splicing. *J Biol Chem* **280**(45): 37572-37584.

Buratti, E., Brindisi, A., Pagani, F., and Baralle, F.E. 2004. Nuclear factor TDP-43 binds to the polymorphic TG repeats in CFTR intron 8 and causes skipping of exon 9: a functional link with disease penetrance. *Am J Hum Genet* **74**(6): 1322-1325.

Buratti, E., Dork, T., Zuccato, E., Pagani, F., Romano, M., and Baralle, F.E. 2001. Nuclear factor TDP-43 and SR proteins promote in vitro and in vivo CFTR exon 9 skipping. *Embo J* **20**(7): 1774-1784.

Burnashev, N., Monyer, H., Seeburg, P.H., and Sakmann, B. 1992. Divalent ion permeability of AMPA receptor channels is dominated by the edited form of a single subunit. *Neuron* **8**(1): 189-198.

Butchbach, M.E., Edwards, J.D., and Burghes, A.H. 2007. Abnormal motor phenotype in the SMNDelta7 mouse model of spinal muscular atrophy. *Neurobiol Dis* **27**(2): 207-219.

Cairns, N.J., Neumann, M., Bigio, E.H., Holm, I.E., Troost, D., Hatanpaa, K.J., Foong, C., White, C.L., 3rd, Schneider, J.A., Kretzschmar, H.A. et al. 2007. TDP-43 in familial and sporadic frontotemporal lobar degeneration with ubiquitin inclusions. *Am J Pathol* **171**(1): 227-240.

Campbell, L., Potter, A., Ignatius, J., Dubowitz, V., and Davies, K. 1997. Genomic variation and gene conversion in spinal muscular atrophy: implications for disease process and clinical phenotype. *Am J Hum Genet* **61**(1): 40-50.

Cartegni, L., Chew, S.L., and Krainer, A.R. 2002. Listening to silence and understanding nonsense: exonic mutations that affect splicing. *Nat Rev Genet* **3**(4): 285-298.

Cartegni, L., Wang, J., Zhu, Z., Zhang, M.Q., and Krainer, A.R. 2003. ESEfinder: A web resource to identify exonic splicing enhancers. *Nucleic Acids Res* **31**(13): 3568-3571.

Carthew, R.W. and Sontheimer, E.J. 2009. Origins and Mechanisms of miRNAs and siRNAs. *Cell* **136**(4): 642-655.

Chang, Y., Kong, Q., Shan, X., Tian, G., Ilieva, H., Cleveland, D.W., Rothstein, J.D., Borchelt, D.R., Wong, P.C., and Lin, C.L. 2008. Messenger RNA oxidation occurs early in disease pathogenesis and promotes motor neuron degeneration in ALS. *PLoS One* **3**(8): e2849.

Chen, Y.Z., Bennett, C.L., Huynh, H.M., Blair, I.P., Puls, I., Irobi, J., Dierick, I., Abel, A., Kennerson, M.L., Rabin, B.A. et al. 2004. DNA/RNA helicase gene mutations in a form of juvenile amyotrophic lateral sclerosis (ALS4). *Am J Hum Genet* **74**(6): 1128-1135.

Chen, Y.Z., Hashemi, S.H., Anderson, S.K., Huang, Y., Moreira, M.C., Lynch, D.R., Glass, I.A., Chance, P.F., and Bennett, C.L. 2006. Senataxin, the yeast Sen1p orthologue: characterization of a unique protein in which recessive mutations cause ataxia and dominant mutations cause motor neuron disease. *Neurobiol Dis* **23**(1): 97-108.

Chih, B., Engelman, H., and Scheiffele, P. 2005. Control of excitatory and inhibitory synapse formation by neuroligins. *Science* **307**(5713): 1324-1328.

Chih, B., Gollan, L., and Scheiffele, P. 2006. Alternative splicing controls selective trans-synaptic interactions of the neuroligin-neurexin complex. *Neuron* **51**(2): 171-178.

Chihara, T., Luginbuhl, D., and Luo, L. 2007. Cytoplasmic and mitochondrial protein translation in axonal and dendritic terminal arborization. *Nat Neurosci* **10**(7): 828-837.

Chio, A., Restagno, G., Brunetti, M., Ossola, I., Calvo, A., Mora, G., Sabatelli, M., Monsurro, M.R., Battistini, S., Mandrioli, J. et al. 2009a. Two Italian kindreds with familial amyotrophic lateral sclerosis due to FUS mutation. *Neurobiol Aging* **30**(8): 1272-1275.

Chio, A., Schymick, J.C., Restagno, G., Scholz, S.W., Lombardo, F., Lai, S.L., Mora, G., Fung, H.C., Britton, A., Arepalli, S. et al. 2009b. A two-stage genome-wide association study of sporadic amyotrophic lateral sclerosis. *Hum Mol Genet* **18**(8): 1524-1532.

Claessens, A., Weyn, C., and Merregaert, J. 2008. The cytoplasmic domain of chondrolectin interacts with the beta-subunit of Rab geranylgeranyl transferase. *Cell Mol Biol Lett* **13**(2): 250-259.

Colombrita, C., Zennaro, E., Fallini, C., Weber, M., Sommacal, A., Buratti, E., Silani, V., and Ratti, A. 2009a. TDP-43 is recruited to stress granules in conditions of oxidative insult.. *J Neurochem* **111**(4): 1051-1061.

-. 2009b. TDP-43 is recruited to stress granules in conditions of oxidative insult. *J Neurochem* **111**(4): 1051-1061.

Condeelis, J. and Singer, R.H. 2005. How and why does beta-actin mRNA target? *Biol Cell* **97**(1): 97-110.

Conforti, F.L., Sprovieri, T., Mazzei, R., Ungaro, C., La Bella, V., Tessitore, A., Patitucci, A., Magariello, A., Gabriele, A.L., Tedeschi, G. et al. 2008. A novel Angiogenin gene mutation in a sporadic patient with amyotrophic lateral sclerosis from southern Italy. *Neuromuscul Disord* **18**(1): 68-70.

Cooper, T.A., Wan, L., and Dreyfuss, G. 2009. RNA and disease. *Cell* **136**(4): 777-793.

Corrado, L., Battistini, S., Penco, S., Bergamaschi, L., Testa, L., Ricci, C., Giannini, F., Greco, G., Patrosso, M.C., Pileggi, S. et al. 2007. Variations in the coding and regulatory sequences of the angiogenin (ANG) gene are not associated to ALS (amyotrophic lateral sclerosis) in the Italian population. *J Neurol Sci* **258**(1-2): 123-127.

Corrado, L., Del Bo, R., Castellotti, B., Ratti, A., Cereda, C., Penco, S., Soraru, G., Carlomagno, Y., Ghezzi, S., Pensato, V. et al. 2009a. Mutations of FUS Gene in Sporadic Amyotrophic Lateral Sclerosis. 2010. *J Med Genet*; **47**(3):190-4.

Corrado, L., Ratti, A., Gellera, C., Buratti, E., Castellotti, B., Carlomagno, Y., Ticozzi, N., Mazzini, L., Testa, L., Taroni, F. et al. 2009b. High frequency of TARDBP gene mutations in Italian patients with amyotrophic lateral sclerosis. *Hum Mutat* **30**(4): 688-694.

Cougot, N., Babajko, S., and Seraphin, B. 2004. Cytoplasmic foci are sites of mRNA decay in human cells. *J Cell Biol* **165**(1): 31-40.

Cougot, N., Bhattacharyya, S.N., Tapia-Arancibia, L., Bordonne, R., Filipowicz, W., Bertrand, E., and Rage, F. 2008. Dendrites of mammalian neurons contain specialized P-body-like structures that respond to neuronal activation. *J Neurosci* **28**(51): 13793-13804.

Crabtree, B., Thiyagarajan, N., Prior, S.H., Wilson, P., Iyer, S., Ferns, T., Shapiro, R., Brew, K., Subramanian, V., and Acharya, K.R. 2007. Characterization of human angiogenin variants implicated in amyotrophic lateral sclerosis. *Biochemistry* **46**(42): 11810-11818.

Cronin, S., Blauw, H.M., Veldink, J.H., van Es, M.A., Ophoff, R.A., Bradley, D.G., van den Berg, L.H., and Hardiman, O. 2008. Analysis of genome-wide copy number variation in Irish and Dutch ALS populations. *Hum Mol Genet* **17**(21): 3392-3398.

Cronin, S., Greenway, M.J., Ennis, S., Kieran, D., Green, A., Prehn, J.H., and Hardiman, O. 2006. Elevated serum angiogenin levels in ALS. *Neurology* **67**(10): 1833-1836.

Cronin, S., Tomik, B., Bradley, D.G., Slowik, A., and Hardiman, O. 2009. Screening for replication of genome-wide SNP associations in sporadic ALS. *Eur J Hum Genet* **17**(2): 213-218.

Crozat, A., Aman, P., Mandahl, N., and Ron, D. 1993. Fusion of CHOP to a novel RNA-binding protein in human myxoid liposarcoma. *Nature* **363**(6430): 640-644.

Cusin, V., Clermont, O., Gerard, B., Chantereau, D., and Elion, J. 2003. Prevalence of SMN1 deletion and duplication in carrier and normal populations: implication for genetic counselling. *J Med Genet* **40**(4): e39.

D'Ambrogio, A., Buratti, E., Stuani, C., Guarnaccia, C., Romano, M., Ayala, Y.M., and Baralle, F.E. 2009. Functional mapping of the interaction between TDP-43 and hnRNP A2 in vivo. *Nucleic Acids Res* **37**(12): 4116-4126.

Dai, M., Wang, P., Boyd, A., Kostov, G., Athey, B., Jones, E., Bunney, W., Myers, R., Speed, T., Akil, H. et al. 2005. Evolving gene/transcript definitions

significantly alter the interpretation of GeneChip data. *Nucleic Acids Research* **33**(20): e175-e175.

Damiani, D., Alexander, J.J., O'Rourke, J.R., McManus, M., Jadhav, A.P., Cepko, C.L., Hauswirth, W.W., Harfe, B.D., and Strettoi, E. 2008. Dicer inactivation leads to progressive functional and structural degeneration of the mouse retina. *J Neurosci* **28**(19): 4878-4887.

Damme, P.V., Goris, A., Race, V., Hersmus, N., Dubois, B., Bosch, L.V., Matthijs, G., and Robberecht, W. 2009. The occurrence of mutations in FUS in a Belgian cohort of patients with familial ALS. 2010. *Eur J Neurol* May;**17**(5):754-6.

Daoud, H., Valdmanis, P.N., Kabashi, E., Dion, P., Dupre, N., Camu, W., Meininger, V., and Rouleau, G.A. Contribution of TARDBP mutations to sporadic amyotrophic lateral sclerosis. 2009. *J Med Genet* **46**(2):112-4.

Davidson, Y., Kelley, T., Mackenzie, I.R., Pickering-Brown, S., Du Plessis, D., Neary, D., Snowden, J.S., and Mann, D.M. 2007. Ubiquitinated pathological lesions in frontotemporal lobar degeneration contain the TAR DNA-binding protein, TDP-43. *Acta Neuropathol* **113**(5): 521-533.

DeGracia, D.J., Rudolph, J., Roberts, G.G., Rafols, J.A., and Wang, J. 2007. Convergence of stress granules and protein aggregates in hippocampal cornu ammonis 1 at later reperfusion following global brain ischemia. *Neuroscience* **146**(2): 562-572.

Del Bo, R., Ghezzi, S., Corti, S., Pandolfo, M., Ranieri, M., Santoro, D., Ghione, I., Prelle, A., Orsetti, V., Mancuso, M. et al. 2009. TARDBP (TDP-43) sequence analysis in patients with familial and sporadic ALS: identification of two novel mutations. *Eur J Neurol* **16**(6): 727-732.

Del Bo, R., Scarlato, M., Ghezzi, S., Martinelli-Boneschi, F., Corti, S., Locatelli, F., Santoro, D., Prelle, A., Briani, C., Nardini, M. et al. 2008. Absence of angiogenic genes modification in Italian ALS patients. *Neurobiol Aging* **29**(2): 314-316.

di Penta, A., Mercaldo, V., Florenzano, F., Munck, S., Ciotti, M.T., Zalfa, F., Mercanti, D., Molinari, M., Bagni, C., and Achsel, T. 2009. Dendritic LSm1/CBP80-mRNPs mark the early steps of transport commitment and translational control. *J Cell Biol* **184**(3): 423-435.

Dion, P.A., Daoud, H., and Rouleau, G.A. 2009. Genetics of motor neuron disorders: new insights into pathogenic mechanisms. *Nat Rev Genet* **10**(11): 769-782.

Dormann, D., Capell, A., Carlson, A.M., Shankaran, S.S., Rodde, R., Neumann, M., Kremmer, E., Matsuwaki, T., Yamanouchi, K., Nishihara, M. et al. 2009. Proteolytic processing of TAR DNA binding protein-43 by caspases produces C-terminal fragments with disease defining properties independent of progranulin. *J Neurochem* **110**(3): 1082-1094.

Eisen, A. 2009. Amyotrophic lateral sclerosis-Evolutionary and other perspectives. *Muscle Nerve* **40**(2): 297-304.

el-Hamidi, M., Leipold, H.W., Vestweber, J.G., and Saperstein, G. 1989. Spinal muscular atrophy in Brown Swiss calves. *Zentralbl Veterinarmed A* **36**(10): 731-738.

Elvira, G., Wasiak, S., Blandford, V., Tong, X.K., Serrano, A., Fan, X., del Rayo Sanchez-Carbente, M., Servant, F., Bell, A.W., Boismenu, D. et al. 2006. Characterization of an RNA granule from developing brain. *Mol Cell Proteomics* **5**(4): 635-651.

EntrezGene. Entrez Gene: FVT1 follicular lymphoma variant translocation 1. In.
Fallis, B.A. and Hardiman, O. 2009. Aggregation of neurodegenerative disease in ALS kindreds. *Amyotroph Lateral Scler* **10**(2): 95-98.
Fan, L. and Simard, L.R. 2002. Survival motor neuron (SMN) protein: role in neurite outgrowth and neuromuscular maturation during neuronal differentiation and development. *Hum Mol Genet* **11**(14): 1605-1614.
Farrer, M.J., Hulihan, M.M., Kachergus, J.M., Dachsel, J.C., Stoessl, A.J., Grantier, L.L., Calne, S., Calne, D.B., Lechevalier, B., Chapon, F. et al. 2009. DCTN1 mutations in Perry syndrome. *Nat Genet* **41**(2): 163-165.
Feiguin, F., Godena, V.K., Romano, G., D'Ambrogio, A., Klima, R., and Baralle, F.E. 2009. Depletion of TDP-43 affects Drosophila motoneurons terminal synapsis and locomotive behavior. *FEBS Lett* **583**(10): 1586-1592.
Fox-Walsh, K.L. and Hertel, K.J. 2009. Splice-site pairing is an intrinsically high fidelity process. *Proc Natl Acad Sci U S A* **106**(6): 1766-1771.
Frey, D., Schneider, C., Xu, L., Borg, J., Spooren, W., and Caroni, P. 2000. Early and selective loss of neuromuscular synapse subtypes with low sprouting competence in motoneuron diseases. *J Neurosci* **20**(7): 2534-2542.
Fujii, R., Okabe, S., Urushido, T., Inoue, K., Yoshimura, A., Tachibana, T., Nishikawa, T., Hicks, G.G., and Takumi, T. 2005. The RNA binding protein TLS is translocated to dendritic spines by mGluR5 activation and regulates spine morphology. *Curr Biol* **15**(6): 587-593.
Fujii, R. and Takumi, T. 2005. TLS facilitates transport of mRNA encoding an actin-stabilizing protein to dendritic spines. *J Cell Sci* **118**(Pt 24): 5755-5765.
Fujishiro, H., Uchikado, H., Arai, T., Hasegawa, M., Akiyama, H., Yokota, O., Tsuchiya, K., Togo, T., Iseki, E., and Hirayasu, Y. 2009. Accumulation of phosphorylated TDP-43 in brains of patients with argyrophilic grain disease. *Acta Neuropathol* **117**(2): 151-158.
Fujita, K., Ito, H., Nakano, S., Kinoshita, Y., Wate, R., and Kusaka, H. 2008. Immunohistochemical identification of messenger RNA-related proteins in basophilic inclusions of adult-onset atypical motor neuron disease. *Acta Neuropathol* **116**(4): 439-445.
Fyfe, J.C., Menotti-Raymond, M., David, V.A., Brichta, L., Schaffer, A.A., Agarwala, R., Murphy, W.J., Wedemeyer, W.J., Gregory, B.L., Buzzell, B.G. et al. 2006. An approximately 140-kb deletion associated with feline spinal muscular atrophy implies an essential LIX1 function for motor neuron survival. *Genome Res* **16**(9): 1084-1090.
Gabanella, F., Butchbach, M.E., Saieva, L., Carissimi, C., Burghes, A.H., and Pellizzoni, L. 2007. Ribonucleoprotein assembly defects correlate with spinal muscular atrophy severity and preferentially affect a subset of spliceosomal snRNPs. *PLoS ONE* **2**(9): e921.
Gabanella, F., Carissimi, C., Usiello, A., and Pellizzoni, L. 2005. The activity of the spinal muscular atrophy protein is regulated during development and cellular differentiation. *Hum Mol Genet* **14**(23): 3629-3642.
Gallagher, S.R. and Desjardins, P.R. 2008. Quantitation of DNA and RNA with absorption and fluorescence spectroscopy. *Curr Protoc Protein Sci* **Appendix 3**: Appendix 4K.
Gallouzi, I.E., Brennan, C.M., Stenberg, M.G., Swanson, M.S., Eversole, A., Maizels, N., and Steitz, J.A. 2000. HuR binding to cytoplasmic mRNA is perturbed by heat shock. *Proc Natl Acad Sci U S A* **97**(7): 3073-3078.

Gass, J., Cannon, A., Mackenzie, I.R., Boeve, B., Baker, M., Adamson, J., Crook, R., Melquist, S., Kuntz, K., Petersen, R. et al. 2006. Mutations in progranulin are a major cause of ubiquitin-positive frontotemporal lobar degeneration. *Hum Mol Genet* **15**(20): 2988-3001.

Ge, W.W., Wen, W., Strong, W., Leystra-Lantz, C., and Strong, M.J. 2005. Mutant copper-zinc superoxide dismutase binds to and destabilizes human low molecular weight neurofilament mRNA. *J Biol Chem* **280**(1): 118-124.

Gellera, C., Colombrita, C., Ticozzi, N., Castellotti, B., Bragato, C., Ratti, A., Taroni, F., and Silani, V. 2008. Identification of new ANG gene mutations in a large cohort of Italian patients with amyotrophic lateral sclerosis. *Neurogenetics* **9**(1): 33-40.

Geser, F., Winton, M.J., Kwong, L.K., Xu, Y., Xie, S.X., Igaz, L.M., Garruto, R.M., Perl, D.P., Galasko, D., Lee, V.M. et al. 2008. Pathological TDP-43 in parkinsonism-dementia complex and amyotrophic lateral sclerosis of Guam. *Acta Neuropathol* **115**(1): 133-145.

Giavazzi, A., Setola, V., Simonati, A., and Battaglia, G. 2006. Neuronal-specific roles of the survival motor neuron protein: evidence from survival motor neuron expression patterns in the developing human central nervous system. *J Neuropathol Exp Neurol* **65**(3): 267-277.

Gijselinck, I., Sleegers, K., Engelborghs, S., Robberecht, W., Martin, J.J., Vandenberghe, R., Sciot, R., Dermaut, B., Goossens, D., van der Zee, J. et al. 2007. Neuronal inclusion protein TDP-43 has no primary genetic role in FTD and ALS. *Neurobiol Aging*.

Gilks, N., Kedersha, N., Ayodele, M., Shen, L., Stoecklin, G., Dember, L.M., and Anderson, P. 2004. Stress granule assembly is mediated by prion-like aggregation of TIA-1. *Mol Biol Cell* **15**(12): 5383-5398.

Giorgi, C. and Moore, M.J. 2007. The nuclear nurture and cytoplasmic nature of localized mRNPs. *Semin Cell Dev Biol* **18**(2): 186-193.

Girard, C., Neel, H., Bertrand, E., and Bordonne, R. 2006. Depletion of SMN by RNA interference in HeLa cells induces defects in Cajal body formation. *Nucleic Acids Res* **34**(10): 2925-2932.

Gitcho, M.A., Baloh, R.H., Chakraverty, S., Mayo, K., Norton, J.B., Levitch, D., Hatanpaa, K.J., White, C.L., 3rd, Bigio, E.H., Caselli, R. et al. 2008. TDP-43 A315T mutation in familial motor neuron disease. *Ann Neurol*. **63**(4):535-8.

Gitcho, M.A., Bigio, E.H., Mishra, M., Johnson, N., Weintraub, S., Mesulam, M., Rademakers, R., Chakraverty, S., Cruchaga, C., Morris, J.C. et al. 2009. TARDBP 3'-UTR variant in autopsy-confirmed frontotemporal lobar degeneration with TDP-43 proteinopathy. *Acta Neuropathol*. **118**(5):633-45.

Giuditta, A., Chun, J.T., Eyman, M., Cefaliello, C., Bruno, A.P., and Crispino, M. 2008. Local gene expression in axons and nerve endings: the glia-neuron unit. *Physiol Rev* **88**(2): 515-555.

Glaser, R.L., Ramsay, J.P., and Morison, I.M. 2006. The imprinted gene and parent-of-origin effect database now includes parental origin of de novo mutations. *Nucleic Acids Res* **34**(Database issue): D29-31.

Goransson, M., Elias, E., Stahlberg, A., Olofsson, A., Andersson, C., and Aman, P. 2005. Myxoid liposarcoma FUS-DDIT3 fusion oncogene induces C/EBP beta-mediated interleukin 6 expression. *Int J Cancer* **115**(4): 556-560.

Goransson, M., Wedin, M., and Aman, P. 2002. Temperature-dependent localization of TLS-CHOP to splicing factor compartments. *Exp Cell Res* **278**(2): 125-132.

Gouveia, L.O. and de Carvalho, M. 2007. Young-onset sporadic amyotrophic lateral sclerosis: a distinct nosological entity? *Amyotroph Lateral Scler* **8**(6): 323-327.

Graham, A.J., Macdonald, A.M., and Hawkes, C.H. 1997. British motor neuron disease twin study. *J Neurol Neurosurg Psychiatry* **62**(6): 562-569.

Greenway, M.J., Alexander, M.D., Ennis, S., Traynor, B.J., Corr, B., Frost, E., Green, A., and Hardiman, O. 2004. A novel candidate region for ALS on chromosome 14q11.2. *Neurology* **63**(10): 1936-1938.

Greenway, M.J., Andersen, P.M., Russ, C., Ennis, S., Cashman, S., Donaghy, C., Patterson, V., Swingler, R., Kieran, D., Prehn, J. et al. 2006. ANG mutations segregate with familial and 'sporadic' amyotrophic lateral sclerosis. *Nat Genet* **38**(4): 411-413.

Greger, I.H., Khatri, L., Kong, X., and Ziff, E.B. 2003. AMPA receptor tetramerization is mediated by Q/R editing. *Neuron* **40**(4): 763-774.

Gregory, R.I., Yan, K.P., Amuthan, G., Chendrimada, T., Doratotaj, B., Cooch, N., and Shiekhattar, R. 2004. The Microprocessor complex mediates the genesis of microRNAs. *Nature* **432**(7014): 235-240.

Grohmann, K., Rossoll, W., Kobsar, I., Holtmann, B., Jablonka, S., Wessig, C., Stoltenburg-Didinger, G., Fischer, U., Hubner, C., Martini, R. et al. 2004. Characterization of Ighmbp2 in motor neurons and implications for the pathomechanism in a mouse model of human spinal muscular atrophy with respiratory distress type 1 (SMARD1). *Hum Mol Genet* **13**(18): 2031-2042.

Grohmann, K., Schuelke, M., Diers, A., Hoffmann, K., Lucke, B., Adams, C., Bertini, E., Leonhardt-Horti, H., Muntoni, F., Ouvrier, R. et al. 2001. Mutations in the gene encoding immunoglobulin mu-binding protein 2 cause spinal muscular atrophy with respiratory distress type 1. *Nat Genet* **29**(1): 75-77.

Gu, W., Pan, F., Zhang, H., Bassell, G.J., and Singer, R.H. 2002. A predominantly nuclear protein affecting cytoplasmic localization of beta-actin mRNA in fibroblasts and neurons. *J Cell Biol* **156**(1): 41-51.

Guenther, U.P., Handoko, L., Laggerbauer, B., Jablonka, S., Chari, A., Alzheimer, M., Ohmer, J., Plottner, O., Gehring, N., Sickmann, A. et al. 2009. IGHMBP2 is a ribosome-associated helicase inactive in the neuromuscular disorder distal SMA type 1 (DSMA1). *Hum Mol Genet* **18**(7): 1288-1300.

Guerreiro, R.J., Schymick, J.C., Crews, C., Singleton, A., Hardy, J., and Traynor, B.J. 2008. TDP-43 is not a common cause of sporadic amyotrophic lateral sclerosis. *PLoS ONE* **3**(6): e2450.

Hamilton, L.K., Truong, M.K., Bednarczyk, M.R., Aumont, A., and Fernandes, K.J. 2009. Cellular organization of the central canal ependymal zone, a niche of latent neural stem cells in the adult mammalian spinal cord. *Neuroscience*.

Hanz, S., Perlson, E., Willis, D., Zheng, J.Q., Massarwa, R., Huerta, J.J., Koltzenburg, M., Kohler, M., van-Minnen, J., Twiss, J.L. et al. 2003. Axoplasmic importins enable retrograde injury signaling in lesioned nerve. *Neuron* **40**(6): 1095-1104.

Harding, H.P., Calfon, M., Urano, F., Novoa, I., and Ron, D. 2002. Transcriptional and translational control in the Mammalian unfolded protein response. *Annu Rev Cell Dev Biol* **18**: 575-599.

Harding, H.P., Zhang, Y., Zeng, H., Novoa, I., Lu, P.D., Calfon, M., Sadri, N., Yun, C., Popko, B., Paules, R. et al. 2003. An integrated stress response

regulates amino acid metabolism and resistance to oxidative stress. *Mol Cell* **11**(3): 619-633.
Hasegawa, M., Arai, T., Nonaka, T., Kametani, F., Yoshida, M., Hashizume, Y., Beach, T.G., Buratti, E., Baralle, F., Morita, M. et al. 2008. Phosphorylated TDP-43 in frontotemporal lobar degeneration and amyotrophic lateral sclerosis. *Ann Neurol* **64**(1): 60-70.
Hayashi, M., Arai, N., Murakami, T., Yoshio, M., Oda, M., and Matsuyama, H. 1998. A study of cell death in Werdnig Hoffmann disease brain. *Neurosci Lett* **243**(1-3): 117-120.
Hayward, C., Colville, S., Swingler, R.J., and Brock, D.J. 1999. Molecular genetic analysis of the APEX nuclease gene in amyotrophic lateral sclerosis. *Neurology* **52**(9): 1899-1901.
He, Q., Lowrie, C., Shelton, G.D., Castellani, R.J., Menotti-Raymond, M., Murphy, W., O'Brien, S.J., Swanson, W.F., and Fyfe, J.C. 2005. Inherited motor neuron disease in domestic cats: a model of spinal muscular atrophy. *Pediatr Res* **57**(3): 324-330.
Hicks, G.G., Singh, N., Nashabi, A., Mai, S., Bozek, G., Klewes, L., Arapovic, D., White, E.K., Koury, M.J., Oltz, E.M. et al. 2000. Fus deficiency in mice results in defective B-lymphocyte development and activation, high levels of chromosomal instability and perinatal death. *Nat Genet* **24**(2): 175-179.
Higashi, S., Iseki, E., Yamamoto, R., Minegishi, M., Hino, H., Fujisawa, K., Togo, T., Katsuse, O., Uchikado, H., Furukawa, Y. et al. 2007a. Appearance pattern of TDP-43 in Japanese frontotemporal lobar degeneration with ubiquitin-positive inclusions. *Neurosci Lett* **419**(3): 213-218.
-. 2007b. Concurrence of TDP-43, tau and alpha-synuclein pathology in brains of Alzheimer's disease and dementia with Lewy bodies. *Brain Res* **1184**: 284-294.
Holton, J.L., Revesz, T., Crooks, R., and Scaravilli, F. 2002. Evidence for pathological involvement of the spinal cord in motor neuron disease-inclusion dementia. *Acta Neuropathol* **103**(3): 221-227.
Hsieh-Li, H.M., Chang, J.G., Jong, Y.J., Wu, M.H., Wang, N.M., Tsai, C.H., and Li, H. 2000. A mouse model for spinal muscular atrophy. *Nat Genet* **24**(1): 66-70.
Hu, G.F., Strydom, D.J., Fett, J.W., Riordan, J.F., and Vallee, B.L. 1993. Actin is a binding protein for angiogenin. *Proc Natl Acad Sci U S A* **90**(4): 1217-1221.
Hu, W.T., Josephs, K.A., Knopman, D.S., Boeve, B.F., Dickson, D.W., Petersen, R.C., and Parisi, J.E. 2008. Temporal lobar predominance of TDP-43 neuronal cytoplasmic inclusions in Alzheimer disease. *Acta Neuropathol* **116**(2): 215-220.
Hua, Y. and Zhou, J. 2004a. Rpp20 interacts with SMN and is re-distributed into SMN granules in response to stress. *Biochem Biophys Res Commun* **314**(1): 268-276.
-. 2004b. Survival motor neuron protein facilitates assembly of stress granules. *FEBS Lett* **572**(1-3): 69-74.
Huang, Y.S., Jung, M.Y., Sarkissian, M., and Richter, J.D. 2002. N-methyl-D-aspartate receptor signaling results in Aurora kinase-catalyzed CPEB phosphorylation and alpha CaMKII mRNA polyadenylation at synapses. *EMBO J* **21**(9): 2139-2148.

Husi, H., Ward, M.A., Choudhary, J.S., Blackstock, W.P., and Grant, S.G. 2000. Proteomic analysis of NMDA receptor-adhesion protein signaling complexes. *Nat Neurosci* **3**(7): 661-669.

Huson, S.M., Compston, D.A., Clark, P., and Harper, P.S. 1989. A genetic study of von Recklinghausen neurofibromatosis in south east Wales. I. Prevalence, fitness, mutation rate, and effect of parental transmission on severity. *J Med Genet* **26**(11): 704-711.

Huttelmaier, S., Zenklusen, D., Lederer, M., Dictenberg, J., Lorenz, M., Meng, X., Bassell, G.J., Condeelis, J., and Singer, R.H. 2005. Spatial regulation of beta-actin translation by Src-dependent phosphorylation of ZBP1. *Nature* **438**(7067): 512-515.

Ichikawa, H., Shimizu, K., Hayashi, Y., and Ohki, M. 1994. An RNA-binding protein gene, TLS/FUS, is fused to ERG in human myeloid leukemia with t(16;21) chromosomal translocation. *Cancer Res* **54**(11): 2865-2868.

Igaz, L.M., Kwong, L.K., Chen-Plotkin, A., Winton, M.J., Unger, T.L., Xu, Y., Neumann, M., Trojanowski, J.Q., and Lee, V.M. 2009. Expression of TDP-43 C-terminal Fragments in Vitro Recapitulates Pathological Features of TDP-43 Proteinopathies. *J Biol Chem* **284**(13): 8516-8524.

Iko, Y., Kodama, T.S., Kasai, N., Oyama, T., Morita, E.H., Muto, T., Okumura, M., Fujii, R., Takumi, T., Tate, S. et al. 2004. Domain architectures and characterization of an RNA-binding protein, TLS. *J Biol Chem* **279**(43): 44834-44840.

International HapMap, C. 2003. The International HapMap Project. *Nature* **426**(6968): 789-796.

Inukai, Y., Nonaka, T., Arai, T., Yoshida, M., Hashizume, Y., Beach, T.G., Buratti, E., Baralle, F.E., Akiyama, H., Hisanaga, S. et al. 2008. Abnormal phosphorylation of Ser409/410 of TDP-43 in FTLD-U and ALS. *FEBS Lett* **582**(19): 2899-2904.

Irizarry, R.A., Bolstad, B.M., Collin, F., Cope, L.M., Hobbs, B., and Speed, T.P. 2003. Summaries of Affymetrix GeneChip probe level data. *Nucleic Acids Res* **31**(4): e15.

Ishihara, K., Araki, S., Ihori, N., Shiota, J., Kawamura, M., and Nakano, I. 2006. An autopsy case of frontotemporal dementia with severe dysarthria and motor neuron disease showing numerous basophilic inclusions. *Neuropathology* **26**(5): 447-454.

Iwahashi, H., Eguchi, Y., Yasuhara, N., Hanafusa, T., Matsuzawa, Y., and Tsujimoto, Y. 1997. Synergistic anti-apoptotic activity between Bcl-2 and SMN implicated in spinal muscular atrophy. *Nature* **390**(6658): 413-417.

Jablonka, S., Bandilla, M., Wiese, S., Buhler, D., Wirth, B., Sendtner, M., and Fischer, U. 2001. Co-regulation of survival of motor neuron (SMN) protein and its interactor SIP1 during development and in spinal muscular atrophy. *Hum Mol Genet* **10**(5): 497-505.

Jablonka, S., Holtmann, B., Meister, G., Bandilla, M., Rossoll, W., Fischer, U., and Sendtner, M. 2002. Gene targeting of Gemin2 in mice reveals a correlation between defects in the biogenesis of U snRNPs and motoneuron cell death. *Proc Natl Acad Sci U S A* **99**(15): 10126-10131.

Jablonka, S., Karle, K., Sandner, B., Andreassi, C., von Au, K., and Sendtner, M. 2006. Distinct and overlapping alterations in motor and sensory neurons in a mouse model of spinal muscular atrophy. *Hum Mol Genet* **15**(3): 511-518.

Jablonka, S., Schrank, B., Kralewski, M., Rossoll, W., and Sendtner, M. 2000. Reduced survival motor neuron (Smn) gene dose in mice leads to motor neuron degeneration: an animal model for spinal muscular atrophy type III. *Hum Mol Genet* **9**(3): 341-346.

Jablonka, S., Wiese, S., and Sendtner, M. 2004. Axonal defects in mouse models of motoneuron disease. *J Neurobiol* **58**(2): 272-286.

Jadayel, D., Fain, P., Upadhyaya, M., Ponder, M.A., Huson, S.M., Carey, J., Fryer, A., Mathew, C.G., Barker, D.F., and Ponder, B.A. 1990. Paternal origin of new mutations in von Recklinghausen neurofibromatosis. *Nature* **343**(6258): 558-559.

James, P.A. and Talbot, K. 2006. The molecular genetics of non-ALS motor neuron diseases. *Biochim Biophys Acta* **1762**(11-12): 986-1000.

Jensen, K.B., Dredge, B.K., Stefani, G., Zhong, R., Buckanovich, R.J., Okano, H.J., Yang, Y.Y., and Darnell, R.B. 2000. Nova-1 regulates neuron-specific alternative splicing and is essential for neuronal viability. *Neuron* **25**(2): 359-371.

Jimenez-Diaz, L., Geranton, S.M., Passmore, G.M., Leith, J.L., Fisher, A.S., Berliocchi, L., Sivasubramaniam, A.K., Sheasby, A., Lumb, B.M., and Hunt, S.P. 2008. Local translation in primary afferent fibers regulates nociception. *PLoS One* **3**(4): e1961.

Johnston, C.A., Stanton, B.R., Turner, M.R., Gray, R., Blunt, A.H., Butt, D., Ampong, M.A., Shaw, C.E., Leigh, P.N., and Al-Chalabi, A. 2006. Amyotrophic lateral sclerosis in an urban setting: a population based study of inner city London. *J Neurol* **253**(12): 1642-1643.

Jones, A.C., Sampson, J.R., and Cheadle, J.P. 2001. Low level mosaicism detectable by DHPLC but not by direct sequencing. *Hum Mutat* **17**(3): 233-234.

Jordanova, A., Irobi, J., Thomas, F.P., Van Dijck, P., Meerschaert, K., Dewil, M., Dierick, I., Jacobs, A., De Vriendt, E., Guergueltcheva, V. et al. 2006. Disrupted function and axonal distribution of mutant tyrosyl-tRNA synthetase in dominant intermediate Charcot-Marie-Tooth neuropathy. *Nat Genet* **38**(2): 197-202.

Josephs, K.A., Holton, J.L., Rossor, M.N., Braendgaard, H., Ozawa, T., Fox, N.C., Petersen, R.C., Pearl, G.S., Ganguly, M., Rosa, P. et al. 2003. Neurofilament inclusion body disease: a new proteinopathy? *Brain* **126**(Pt 10): 2291-2303.

Kabashi, E., Lin, L., Tradewell, M.L., Dion, P.A., Bercier, V., Bourgouin, P., Rochefort, D., Bel Hadj, S., Durham, H.D., Vande Velde, C. et al. 2009. Gain and loss of function of ALS-related mutations of TARDBP (TDP-43) cause motor deficits in vivo. *Hum Mol Genet*. 19(4):671-83.

Kabashi, E., Valdmanis, P.N., Dion, P., Spiegelman, D., McConkey, B.J., Vande Velde, C., Bouchard, J.P., Lacomblez, L., Pochigaeva, K., Salachas, F. et al. 2008a. TARDBP mutations in individuals with sporadic and familial amyotrophic lateral sclerosis. *Nat Genet* **40**(5): 572-574.

Kabashi, E., Valdmanis, P.N., Dion, P., Spiegelman, D., McConkey, B.J., Velde, C.V., Bouchard, J.P., Lacomblez, L., Pochigaeva, K., Salachas, F. et al. 2008b. TARDBP mutations in individuals with sporadic and familial amyotrophic lateral sclerosis. *Nat Genet*. **40**(5): 572-574.

Kametani, F., Nonaka, T., Suzuki, T., Arai, T., Dohmae, N., Akiyama, H., and Hasegawa, M. 2009. Identification of casein kinase-1 phosphorylation sites on TDP-43. *Biochem Biophys Res Commun* **382**(2): 405-409.

Kanai, Y., Dohmae, N., and Hirokawa, N. 2004. Kinesin transports RNA: isolation and characterization of an RNA-transporting granule. *Neuron* **43**(4): 513-525.

Kandel, E.R., Schwartz, J.H., and Jessell, T.H. 2000. *Principles of Neural Science*. McGraw-Hill.

Kariya, S., Park, G.H., Maeno-Hikichi, Y., Leykekhman, O., Lutz, C., Arkovitz, M.S., Landmesser, L.T., and Monani, U.R. 2008. Reduced SMN protein impairs maturation of the neuromuscular junctions in mouse models of spinal muscular atrophy. *Hum Mol Genet* **17**(16): 2552-2569.

Kashima, T. and Manley, J.L. 2003. A negative element in SMN2 exon 7 inhibits splicing in spinal muscular atrophy. *Nat Genet* **34**(4): 460-463.

Kawahara, Y., Ito, K., Sun, H., Aizawa, H., Kanazawa, I., and Kwak, S. 2004. Glutamate receptors: RNA editing and death of motor neurons. *Nature* **427**(6977): 801.

Kawai, T., Fan, J., Mazan-Mamczarz, K., and Gorospe, M. 2004. Global mRNA stabilization preferentially linked to translational repression during the endoplasmic reticulum stress response. *Mol Cell Biol* **24**(15): 6773-6787.

Kedersha, N. and Anderson, P. 2007. Mammalian stress granules and processing bodies. *Methods Enzymol* **431**: 61-81.

Kedersha, N., Chen, S., Gilks, N., Li, W., Miller, I.J., Stahl, J., and Anderson, P. 2002. Evidence that ternary complex (eIF2-GTP-tRNA(i)(Met))-deficient preinitiation complexes are core constituents of mammalian stress granules. *Mol Biol Cell* **13**(1): 195-210.

Kedersha, N., Cho, M.R., Li, W., Yacono, P.W., Chen, S., Gilks, N., Golan, D.E., and Anderson, P. 2000. Dynamic shuttling of TIA-1 accompanies the recruitment of mRNA to mammalian stress granules. *J Cell Biol* **151**(6): 1257-1268.

Kerr, D.A., Nery, J.P., Traystman, R.J., Chau, B.N., and Hardwick, J.M. 2000. Survival motor neuron protein modulates neuron-specific apoptosis. *Proc Natl Acad Sci U S A* **97**(24): 13312-13317.

Kiebler, M.A. and Bassell, G.J. 2006. Neuronal RNA granules: movers and makers. *Neuron* **51**(6): 685-690.

Kiebler, M.A., Hemraj, I., Verkade, P., Kohrmann, M., Fortes, P., Marion, R.M., Ortin, J., and Dotti, C.G. 1999. The mammalian staufen protein localizes to the somatodendritic domain of cultured hippocampal neurons: implications for its involvement in mRNA transport. *J Neurosci* **19**(1): 288-297.

Kieran, D., Sebastia, J., Greenway, M.J., King, M.A., Connaughton, D., Concannon, C.G., Fenner, B., Hardiman, O., and Prehn, J.H. 2008. Control of motoneuron survival by angiogenin. *J Neurosci* **28**(52): 14056-14061.

Kihara, A. and Igarashi, Y. 2004. FVT-1 is a mammalian 3-ketodihydrosphingosine reductase with an active site that faces the cytosolic side of the endoplasmic reticulum membrane. *J Biol Chem* **279**(47): 49243-49250.

Kim, J., Inoue, K., Ishii, J., Vanti, W.B., Voronov, S.V., Murchison, E., Hannon, G., and Abeliovich, A. 2007. A MicroRNA feedback circuit in midbrain dopamine neurons. *Science* **317**(5842): 1220-1224.

Kirby, J., Goodall, E.F., Smith, W., Highley, J.R., Masanzu, R., Hartley, J.A., Hibberd, R., Hollinger, H.C., Wharton, S.B., Morrison, K.E. et al. 2009.

Broad clinical phenotypes associated with TAR-DNA binding protein (TARDBP) mutations in amyotrophic lateral sclerosis. *Neurogenetics*.

Knowles, R.B., Sabry, J.H., Martone, M.E., Deerinck, T.J., Ellisman, M.H., Bassell, G.J., and Kosik, K.S. 1996. Translocation of RNA granules in living neurons. *J Neurosci* **16**(24): 7812-7820.

Koenig, E. and Martin, R. 1996. Cortical plaque-like structures identify ribosome-containing domains in the Mauthner cell axon. *J Neurosci* **16**(4): 1400-1411.

Koenig, E., Martin, R., Titmus, M., and Sotelo-Silveira, J.R. 2000. Cryptic peripheral ribosomal domains distributed intermittently along mammalian myelinated axons. *J Neurosci* **20**(22): 8390-8400.

Kosik, K.S. 2006. The neuronal microRNA system. *Nat Rev Neurosci* **7**(12): 911-920.

Kovacs, G.G., Murrell, J.R., Horvath, S., Haraszti, L., Majtenyi, K., Molnar, M.J., Budka, H., Ghetti, B., and Spina, S. 2009. TARDBP variation associated with frontotemporal dementia, supranuclear gaze palsy, and chorea. *Mov Disord*.

Krebs, S., Medugorac, I., Rother, S., Strasser, K., and Forster, M. 2007. A missense mutation in the 3-ketodihydrosphingosine reductase FVT1 as candidate causal mutation for bovine spinal muscular atrophy. *Proc Natl Acad Sci U S A* **104**(16): 6746-6751.

Krebs, S., Medugorac, I., Russ, I., Ossent, P., Bleul, U., Schmahl, W., and Forster, M. 2006. Fine-mapping and candidate gene analysis of bovine spinal muscular atrophy. *Mamm Genome* **17**(1): 67-76.

Krecic, A.M. and Swanson, M.S. 1999. hnRNP complexes: composition, structure, and function. *Curr Opin Cell Biol* **11**(3): 363-371.

Krichevsky, A.M. and Kosik, K.S. 2001. Neuronal RNA granules: a link between RNA localization and stimulation-dependent translation. *Neuron* **32**(4): 683-696.

Kuhnlein, P., Sperfeld, A.D., Vanmassenhove, B., Van Deerlin, V., Lee, V.M., Trojanowski, J.Q., Kretzschmar, H.A., Ludolph, A.C., and Neumann, M. 2008. Two German kindreds with familial amyotrophic lateral sclerosis due to TARDBP mutations. *Arch Neurol* **65**(9): 1185-1189.

Kuru, S., Sakai, M., Konagaya, M., Yoshida, M., Hashizume, Y., and Saito, K. 2009. An autopsy case of spinal muscular atrophy type III (Kugelberg-Welander disease). *Neuropathology* **29**(1): 63-67.

Kusaka, H., Matsumoto, S., and Imai, T. 1990. An adult-onset case of sporadic motor neuron disease with basophilic inclusions. *Acta Neuropathol* **80**(6): 660-665.

-. 1993. Adult-onset motor neuron disease with basophilic intraneuronal inclusion bodies. *Clin Neuropathol* **12**(4): 215-218.

Kwak, S. and Kawahara, Y. 2005. Deficient RNA editing of GluR2 and neuronal death in amyotropic lateral sclerosis. *J Mol Med* **83**(2): 110-120.

Kwiatkowski, T.J., Jr., Bosco, D.A., Leclerc, A.L., Tamrazian, E., Vanderburg, C.R., Russ, C., Davis, A., Gilchrist, J., Kasarskis, E.J., Munsat, T. et al. 2009. Mutations in the FUS/TLS gene on chromosome 16 cause familial amyotrophic lateral sclerosis. *Science* **323**(5918): 1205-1208.

Lagier-Tourenne, C. and Cleveland, D.W. 2009. Rethinking ALS: the FUS about TDP-43. *Cell* **136**(6): 1001-1004.

Lambrechts, D., Storkebaum, E., Morimoto, M., Del-Favero, J., Desmet, F., Marklund, S.L., Wyns, S., Thijs, V., Andersson, J., van Marion, I. et al. 2003. VEGF is a modifier of amyotrophic lateral sclerosis in mice and humans and protects motoneurons against ischemic death. *Nat Genet* **34**(4): 383-394.

Landers, J.E., Melki, J., Meininger, V., Glass, J.D., van den Berg, L.H., van Es, M.A., Sapp, P.C., van Vught, P.W., McKenna-Yasek, D.M., Blauw, H.M. et al. 2009. Reduced expression of the Kinesin-Associated Protein 3 (KIFAP3) gene increases survival in sporadic amyotrophic lateral sclerosis. *Proc Natl Acad Sci U S A* **106**(22): 9004-9009.

Le, T.T., Pham, L.T., Butchbach, M.E., Zhang, H.L., Monani, U.R., Coovert, D.D., Gavrilina, T.O., Xing, L., Bassell, G.J., and Burghes, A.H. 2005. SMNDelta7, the major product of the centromeric survival motor neuron (SMN2) gene, extends survival in mice with spinal muscular atrophy and associates with full-length SMN. *Hum Mol Genet* **14**(6): 845-857.

Lee, B.J., Cansizoglu, A.E., Suel, K.E., Louis, T.H., Zhang, Z., and Chook, Y.M. 2006. Rules for nuclear localization sequence recognition by karyopherin beta 2. *Cell* **126**(3): 543-558.

Lee, C.J. and Irizarry, K. 2003. Alternative splicing in the nervous system: an emerging source of diversity and regulation. *Biol Psychiatry* **54**(8): 771-776.

Lefebvre, S., Burglen, L., Reboullet, S., Clermont, O., Burlet, P., Viollet, L., Benichou, B., Cruaud, C., Millasseau, P., Zeviani, M. et al. 1995. Identification and characterization of a spinal muscular atrophy-determining gene. *Cell* **80**(1): 155-165.

Lefebvre, S., Burlet, P., Liu, Q., Bertrandy, S., Clermont, O., Munnich, A., Dreyfuss, G., and Melki, J. 1997. Correlation between severity and SMN protein level in spinal muscular atrophy. *Nat Genet* **16**(3): 265-269.

Lemmens, R., Race, V., Hersmus, N., Matthijs, G., Van Den Bosch, L., Van Damme, P., Dubois, B., Boonen, S., Goris, A., and Robberecht, W. 2009. TDP-43 M311V mutation in familial amyotrophic lateral sclerosis. *J Neurol Neurosurg Psychiatry* **80**(3): 354-355.

Lemon, R.N. 2008. Descending pathways in motor control. *Annu Rev Neurosci* **31**: 195-218.

Lerga, A., Hallier, M., Delva, L., Orvain, C., Gallais, I., Marie, J., and Moreau-Gachelin, F. 2001. Identification of an RNA binding specificity for the potential splicing factor TLS. *J Biol Chem* **276**(9): 6807-6816.

Leung, K.M., van Horck, F.P., Lin, A.C., Allison, R., Standart, N., and Holt, C.E. 2006. Asymmetrical beta-actin mRNA translation in growth cones mediates attractive turning to netrin-1. *Nat Neurosci* **9**(10): 1247-1256.

Li, Q., Lee, J.A., and Black, D.L. 2007. Neuronal regulation of alternative pre-mRNA splicing. *Nat Rev Neurosci* **8**(11): 819-831.

Li, X. and Jin, P. 2009. Macro role(s) of microRNAs in fragile X syndrome? *Neuromolecular Med* **11**(3): 200-207.

Li, X., Lu, L., Bush, D.J., Zhang, X., Zheng, L., Suswam, E.A., and King, P.H. 2009. Mutant copper-zinc superoxide dismutase associated with amyotrophic lateral sclerosis binds to adenine/uridine-rich stability elements in the vascular endothelial growth factor 3'-untranslated region. *J Neurochem* **108**(4): 1032-1044.

Lin, A.C. and Holt, C.E. 2007. Local translation and directional steering in axons. *EMBO J* **26**(16): 3729-3736.

-. 2008. Function and regulation of local axonal translation. *Curr Opin Neurobiol* **18**(1): 60-68.
Liu, Q. and Dreyfuss, G. 1996. A novel nuclear structure containing the survival of motor neurons protein. *EMBO J* **15**(14): 3555-3565.
Logroscino, G., Beghi, E., Zoccolella, S., Palagano, R., Fraddosio, A., Simone, I.L., Lamberti, P., Lepore, V., and Serlenga, L. 2005. Incidence of amyotrophic lateral sclerosis in southern Italy: a population based study. *J Neurol Neurosurg Psychiatry* **76**(8): 1094-1098.
Lorson, C.L., Hahnen, E., Androphy, E.J., and Wirth, B. 1999. A single nucleotide in the SMN gene regulates splicing and is responsible for spinal muscular atrophy. *Proc Natl Acad Sci U S A* **96**(11): 6307-6311.
Lu, L., Zheng, L., Viera, L., Suswam, E., Li, Y., Li, X., Estevez, A.G., and King, P.H. 2007. Mutant Cu/Zn-superoxide dismutase associated with amyotrophic lateral sclerosis destabilizes vascular endothelial growth factor mRNA and downregulates its expression. *J Neurosci* **27**(30): 7929-7938.
Lukiw, W.J. 2007. Micro-RNA speciation in fetal, adult and Alzheimer's disease hippocampus. *Neuroreport* **18**(3): 297-300.
Luo, L. 2002. Actin cytoskeleton regulation in neuronal morphogenesis and structural plasticity. *Annu Rev Cell Dev Biol* **18**: 601-635.
Luquin, N., Yu, B., Saunderson, R.B., Trent, R.J., and Pamphlett, R. 2009. Genetic variants in the promoter of TARDBP in sporadic amyotrophic lateral sclerosis. *Neuromuscul Disord*.
Mackenzie, I.R., Bigio, E.H., Ince, P.G., Geser, F., Neumann, M., Cairns, N.J., Kwong, L.K., Forman, M.S., Ravits, J., Stewart, H. et al. 2007. Pathological TDP-43 distinguishes sporadic amyotrophic lateral sclerosis from amyotrophic lateral sclerosis with SOD1 mutations. *Ann Neurol* **61**(5): 427-434.
Mackenzie, I.R. and Feldman, H.H. 2005. Ubiquitin immunohistochemistry suggests classic motor neuron disease, motor neuron disease with dementia, and frontotemporal dementia of the motor neuron disease type represent a clinicopathologic spectrum. *J Neuropathol Exp Neurol* **64**(8): 730-739.
Mackenzie, I.R., Neumann, M., Bigio, E.H., Cairns, N.J., Alafuzoff, I., Kril, J., Kovacs, G.G., Ghetti, B., Halliday, G., Holm, I.E. et al. 2009. Nomenclature and nosology for neuropathologic subtypes of frontotemporal lobar degeneration: an update. *Acta Neuropathol*.
Maracchioni, A., Totaro, A., Angelini, D.F., Di Penta, A., Bernardi, G., Carri, M.T., and Achsel, T. 2007. Mitochondrial damage modulates alternative splicing in neuronal cells: implications for neurodegeneration. *J Neurochem* **100**(1): 142-153.
Mardis, E.R. 2008. Next-generation DNA sequencing methods. *Annu Rev Genomics Hum Genet* **9**: 387-402.
Martin, K.C. and Ephrussi, A. 2009. mRNA localization: gene expression in the spatial dimension. *Cell* **136**(4): 719-730.
Martin, K.C. and Zukin, R.S. 2006. RNA trafficking and local protein synthesis in dendrites: an overview. *J Neurosci* **26**(27): 7131-7134.
Matsumoto, S., Goto, S., Kusaka, H., Imai, T., Murakami, N., Hashizume, Y., Okazaki, H., and Hirano, A. 1993. Ubiquitin-positive inclusion in anterior horn cells in subgroups of motor neuron diseases: a comparative study of

adult-onset amyotrophic lateral sclerosis, juvenile amyotrophic lateral sclerosis and Werdnig-Hoffmann disease. *J Neurol Sci* **115**(2): 208-213.

Matsumoto, S., Kusaka, H., Murakami, N., Hashizume, Y., Okazaki, H., and Hirano, A. 1992. Basophilic inclusions in sporadic juvenile amyotrophic lateral sclerosis: an immunocytochemical and ultrastructural study. *Acta Neuropathol* **83**(6): 579-583.

Matthews, B.J., Kim, M.E., Flanagan, J.J., Hattori, D., Clemens, J.C., Zipursky, S.L., and Grueber, W.B. 2007. Dendrite self-avoidance is controlled by Dscam. *Cell* **129**(3): 593-604.

Mazroui, R., Huot, M.E., Tremblay, S., Filion, C., Labelle, Y., and Khandjian, E.W. 2002. Trapping of messenger RNA by Fragile X Mental Retardation protein into cytoplasmic granules induces translation repression. *Hum Mol Genet* **11**(24): 3007-3017.

Mazroui, R., Sukarieh, R., Bordeleau, M.E., Kaufman, R.J., Northcote, P., Tanaka, J., Gallouzi, I., and Pelletier, J. 2006. Inhibition of ribosome recruitment induces stress granule formation independently of eukaryotic initiation factor 2alpha phosphorylation. *Mol Biol Cell* **17**(10): 4212-4219.

McEwen, E., Kedersha, N., Song, B., Scheuner, D., Gilks, N., Han, A., Chen, J.J., Anderson, P., and Kaufman, R.J. 2005. Heme-regulated inhibitor kinase-mediated phosphorylation of eukaryotic translation initiation factor 2 inhibits translation, induces stress granule formation, and mediates survival upon arsenite exposure. *J Biol Chem* **280**(17): 16925-16933.

McWhorter, M.L., Monani, U.R., Burghes, A.H., and Beattie, C.E. 2003. Knockdown of the survival motor neuron (Smn) protein in zebrafish causes defects in motor axon outgrowth and pathfinding. *J Cell Biol* **162**(5): 919-931.

Medugorac, I., Kemter, J., Russ, I., Pietrowski, D., Nuske, S., Reichenbach, H.D., Schmahl, W., and Forster, M. 2003. Mapping of the bovine spinal muscular atrophy locus to Chromosome 24. *Mamm Genome* **14**(6): 383-391.

Meissner, M., Lopato, S., Gotzmann, J., Sauermann, G., and Barta, A. 2003. Proto-oncoprotein TLS/FUS is associated to the nuclear matrix and complexed with splicing factors PTB, SRm160, and SR proteins. *Exp Cell Res* **283**(2): 184-195.

Meister, G., Buhler, D., Pillai, R., Lottspeich, F., and Fischer, U. 2001. A multiprotein complex mediates the ATP-dependent assembly of spliceosomal U snRNPs. *Nat Cell Biol* **3**(11): 945-949.

Meister, G., Eggert, C., and Fischer, U. 2002. SMN-mediated assembly of RNPs: a complex story. *Trends Cell Biol* **12**(10): 472-478.

Mercado, P.A., Ayala, Y.M., Romano, M., Buratti, E., and Baralle, F.E. 2005. Depletion of TDP 43 overrides the need for exonic and intronic splicing enhancers in the human apoA-II gene. *Nucleic Acids Res* **33**(18): 6000-6010.

Merianda, T.T., Lin, A.C., Lam, J.S., Vuppalanchi, D., Willis, D.E., Karin, N., Holt, C.E., and Twiss, J.L. 2009. A functional equivalent of endoplasmic reticulum and Golgi in axons for secretion of locally synthesized proteins. *Mol Cell Neurosci* **40**(2): 128-142.

Michael, W.M., Choi, M., and Dreyfuss, G. 1995. A nuclear export signal in hnRNP A1: a signal-mediated, temperature-dependent nuclear protein export pathway. *Cell* **83**(3): 415-422.

Michael, W.M., Eder, P.S., and Dreyfuss, G. 1997. The K nuclear shuttling domain: a novel signal for nuclear import and nuclear export in the hnRNP K protein. *EMBO J* **16**(12): 3587-3598.

Michaelidis, T.M., Sendtner, M., Cooper, J.D., Airaksinen, M.S., Holtmann, B., Meyer, M., and Thoenen, H. 1996. Inactivation of bcl-2 results in progressive degeneration of motoneurons, sympathetic and sensory neurons during early postnatal development. *Neuron* **17**(1): 75-89.

Moisse, K., Mepham, J., Volkening, K., Welch, I., Hill, T., and Strong, M.J. 2009a. Cytosolic TDP-43 expression following axotomy is associated with caspase 3 activation in NFL(-/-) mice: Support for a role for TDP-43 in the physiological response to neuronal injury. *Brain Res*. **1296:**176-86.

Moisse, K., Volkening, K., Leystra-Lantz, C., Welch, I., Hill, T., and Strong, M.J. 2009b. Divergent patterns of cytosolic TDP-43 and neuronal progranulin expression following axotomy: implications for TDP-43 in the physiological response to neuronal injury. *Brain Res* **1249**: 202-211.

Monani, U.R., Lorson, C.L., Parsons, D.W., Prior, T.W., Androphy, E.J., Burghes, A.H., and McPherson, J.D. 1999. A single nucleotide difference that alters splicing patterns distinguishes the SMA gene SMN1 from the copy gene SMN2. *Hum Mol Genet* **8**(7): 1177-1183.

Monani, U.R., Sendtner, M., Coovert, D.D., Parsons, D.W., Andreassi, C., Le, T.T., Jablonka, S., Schrank, B., Rossoll, W., Prior, T.W. et al. 2000. The human centromeric survival motor neuron gene (SMN2) rescues embryonic lethality in Smn(-/-) mice and results in a mouse with spinal muscular atrophy. *Hum Mol Genet* **9**(3): 333-339.

Motley, W., Talbot, K., and Fischbeck, K. 2010. GARS axonopathy - not every neuron's cup of tRNA *Trends in Neuroscience*(in press).

Mueller, O., Lightfoot, S., and Schroeder, A. 2004. RNA Integrity number (RIN) - Standardization of RNA quality control. *Agilent Application Note*(Publication Number 5989-1165EN).

Munch, C., Rosenbohm, A., Sperfeld, A.D., Uttner, I., Reske, S., Krause, B.J., Sedlmeier, R., Meyer, T., Hanemann, C.O., Stumm, G. et al. 2005. Heterozygous R1101K mutation of the DCTN1 gene in a family with ALS and FTD. *Ann Neurol* **58**(5): 777-780.

Munch, C., Sedlmeier, R., Meyer, T., Homberg, V., Sperfeld, A.D., Kurt, A., Prudlo, J., Peraus, G., Hanemann, C.O., Stumm, G. et al. 2004. Point mutations of the p150 subunit of dynactin (DCTN1) gene in ALS. *Neurology* **63**(4): 724-726.

Munoz, D.G., Neumann, M., Kusaka, H., Yokota, O., Ishihara, K., Terada, S., Kuroda, S., and Mackenzie, I.R. 2009. FUS pathology in basophilic inclusion body disease. *Acta Neuropathol*. **118**(5):617-27.

Munsat, T.L. and Davies, K.E. 1992. International SMA consortium meeting. (26-28 June 1992, Bonn, Germany). *Neuromuscul Disord* **2**(5-6): 423-428.

Murayama, S., Mori, H., Ihara, Y., Bouldin, T.W., Suzuki, K., and Tomonaga, M. 1990. Immunocytochemical and ultrastructural studies of lower motor neurons in amyotrophic lateral sclerosis. *Ann Neurol* **27**(2): 137-148.

Murray, L.M., Comley, L.H., Thomson, D., Parkinson, N., Talbot, K., and Gillingwater, T.H. 2008. Selective vulnerability of motor neurons and dissociation of pre- and post-synaptic pathology at the neuromuscular junction in mouse models of spinal muscular atrophy. *Hum Mol Genet* **17**(7): 949-962.

Nakashima-Yasuda, H., Uryu, K., Robinson, J., Xie, S.X., Hurtig, H., Duda, J.E., Arnold, S.E., Siderowf, A., Grossman, M., Leverenz, J.B. et al. 2007. Co-morbidity of TDP-43 proteinopathy in Lewy body related diseases. *Acta Neuropathol* **114**(3): 221-229.

Napoli, I., Mercaldo, V., Boyl, P.P., Eleuteri, B., Zalfa, F., De Rubeis, S., Di Marino, D., Mohr, E., Massimi, M., Falconi, M. et al. 2008. The fragile X syndrome protein represses activity-dependent translation through CYFIP1, a new 4E-BP. *Cell* **134**(6): 1042-1054.

Neary, D., Snowden, J.S., and Mann, D.M. 2000. Cognitive change in motor neurone disease/amyotrophic lateral sclerosis (MND/ALS). *J Neurol Sci* **180**(1-2): 15-20.

Nelson, J.S. and Prensky, A.L. 1972. Sporadic juvenile amyotrophic lateral sclerosis. A clinicopathological study of a case with neuronal cytoplasmic inclusions containing RNA. *Arch Neurol* **27**(4): 300-306.

Neumann, M., Igaz, L.M., Kwong, L.K., Nakashima-Yasuda, H., Kolb, S.J., Dreyfuss, G., Kretzschmar, H.A., Trojanowski, J.Q., and Lee, V.M. 2007. Absence of heterogeneous nuclear ribonucleoproteins and survival motor neuron protein in TDP-43 positive inclusions in frontotemporal lobar degeneration. *Acta Neuropathol* **113**(5): 543-548.

Neumann, M., Rademakers, R., Roeber, S., Baker, M., Kretzschmar, H.A., and Mackenzie, I.R. 2009a. Frontotemporal lobar degeneration with FUS pathology. *Brain*. **132**(Pt 11):2922-31

Neumann, M., Roeber, S., Kretzschmar, H.A., Rademakers, R., Baker, M., and Mackenzie, I.R. 2009b. Abundant FUS-immunoreactive pathology in neuronal intermediate filament inclusion disease. *Acta Neuropathol*. **118**(5):605-16.

Neumann, M., Sampathu, D.M., Kwong, L.K., Truax, A.C., Micsenyi, M.C., Chou, T.T., Bruce, J., Schuck, T., Grossman, M., Clark, C.M. et al. 2006. Ubiquitinated TDP-43 in frontotemporal lobar degeneration and amyotrophic lateral sclerosis. *Science* **314**(5796): 130-133.

Ng, P.C. and Henikoff, S. 2001. Predicting deleterious amino acid substitutions. *Genome Res* **11**(5): 863-874.

-. 2003. SIFT: Predicting amino acid changes that affect protein function. *Nucleic Acids Res* **31**(13): 3812-3814.

-. 2006. Predicting the effects of amino acid substitutions on protein function. *Annu Rev Genomics Hum Genet* **7**: 61-80.

Nielsen, J.S., Andresen, E., Basse, A., Christensen, L.G., Lykke, T., and Nielsen, U.S. 1990. Inheritance of bovine spinal muscular atrophy. *Acta Vet Scand* **31**(2): 253-255.

Nonaka, T., Kametani, F., Arai, T., Akiyama, H., and Hasegawa, M. 2009. Truncation and pathogenic mutations facilitate the formation of intracellular aggregates of TDP-43. *Hum Mol Genet* **18**(18): 3353-3364.

Nousiainen, H.O., Kestila, M., Pakkasjarvi, N., Honkala, H., Kuure, S., Tallila, J., Vuopala, K., Ignatius, J., Herva, R., and Peltonen, L. 2008. Mutations in mRNA export mediator GLE1 result in a fetal motoneuron disease. *Nat Genet* **40**(2): 155-157.

Nunomura, A., Hofer, T., Moreira, P.I., Castellani, R.J., Smith, M.A., and Perry, G. 2009. RNA oxidation in Alzheimer disease and related neurodegenerative disorders. *Acta Neuropathol* **118**(1): 151-166.

O'Donovan, M.C., Oefner, P.J., Roberts, S.C., Austin, J., Hoogendoorn, B., Guy, C., Speight, G., Upadhyaya, M., Sommer, S.S., and McGuffin, P. 1998. Blind analysis of denaturing high-performance liquid chromatography as a tool for mutation detection. *Genomics* **52**(1): 44-49.

O'Toole, O., Traynor, B.J., Brennan, P., Sheehan, C., Frost, E., Corr, B., and Hardiman, O. 2008. Epidemiology and clinical features of amyotrophic lateral sclerosis in Ireland between 1995 and 2004. *J Neurol Neurosurg Psychiatry* **79**(1): 30-32.

Oda, M., Akagawa, N., Tabuchi, Y., and Tanabe, H. 1978. A sporadic juvenile case of the amyotrophic lateral sclerosis with neuronal intracytoplasmic inclusions. *Acta Neuropathol* **44**(3): 211-216.

Oleynikov, Y. and Singer, R.H. 2003. Real-time visualization of ZBP1 association with beta-actin mRNA during transcription and localization. *Curr Biol* **13**(3): 199-207.

Oosthuyse, B., Moons, L., Storkebaum, E., Beck, H., Nuyens, D., Brusselmans, K., Van Dorpe, J., Hellings, P., Gorselink, M., Heymans, S. et al. 2001. Deletion of the hypoxia-response element in the vascular endothelial growth factor promoter causes motor neuron degeneration. *Nat Genet* **28**(2): 131-138.

Oprea, G.E., Krober, S., McWhorter, M.L., Rossoll, W., Muller, S., Krawczak, M., Bassell, G.J., Beattie, C.E., and Wirth, B. 2008. Plastin 3 is a protective modifier of autosomal recessive spinal muscular atrophy. *Science* **320**(5875): 524-527.

Origone, P., Caponnetto, C., Bandettini di Poggio, M., Ghiglione, E., Bellone, E., Ferrandes, G., Mancardi, G.L., and Mandich, P. 2009. Enlarging clinical spectrum of FALS with TARDBP gene mutations: S393L variant in an Italian family showing phenotypic variability and relevance for genetic counselling. *Amyotroph Lateral Scler*: 1-5.

Ou, S.H., Wu, F., Harrich, D., Garcia-Martinez, L.F., and Gaynor, R.B. 1995. Cloning and characterization of a novel cellular protein, TDP-43, that binds to human immunodeficiency virus type 1 TAR DNA sequence motifs. *J Virol* **69**(6): 3584-3596.

Pagani, F., Buratti, E., Stuani, C., Romano, M., Zuccato, E., Niksic, M., Giglio, L., Faraguna, D., and Baralle, F.E. 2000. Splicing factors induce cystic fibrosis transmembrane regulator exon 9 skipping through a nonevolutionary conserved intronic element. *J Biol Chem* **275**(28): 21041-21047.

Pagliardini, S., Giavazzi, A., Setola, V., Lizier, C., Di Luca, M., DeBiasi, S., and Battaglia, G. 2000. Subcellular localization and axonal transport of the survival motor neuron (SMN) protein in the developing rat spinal cord. *Hum Mol Genet* **9**(1): 47-56.

Parker, R. and Sheth, U. 2007. P bodies and the control of mRNA translation and degradation. *Mol Cell* **25**(5): 635-646.

Parkinson, N.J., Baumer, D., Rose-Morris, A., and Talbot, K. 2008. Candidate screening of the bovine and feline spinal muscular atrophy genes reveals no evidence for involvement in human motor neuron disorders. *Neuromuscul Disord* **18**(5): 394-397.

Paubel, A., Violette, J., Amy, M., Praline, J., Meininger, V., Camu, W., Corcia, P., Andres, C.R., Vourc'h, P., and French Amyotrophic Lateral Sclerosis Study, G. 2008. Mutations of the ANG gene in French patients with sporadic amyotrophic lateral sclerosis. *Arch Neurol* **65**(10): 1333-1336.

Pearn, J. 1978. Incidence, prevalence, and gene frequency studies of chronic childhood spinal muscular atrophy. *J Med Genet* **15**(6): 409-413.

Pellizzoni, L. 2007. Chaperoning ribonucleoprotein biogenesis in health and disease. *EMBO Rep* **8**(4): 340-345.

Pellizzoni, L., Charroux, B., Rappsilber, J., Mann, M., and Dreyfuss, G. 2001. A functional interaction between the survival motor neuron complex and RNA polymerase II. *J Cell Biol* **152**(1): 75-85.

Pellizzoni, L., Yong, J., and Dreyfuss, G. 2002. Essential role for the SMN complex in the specificity of snRNP assembly. *Science* **298**(5599): 1775-1779.

Pietrowski, D., Goldammer, T., Meinert, S., Schwerin, M., and Forster, M. 1998. Description and physical localization of the bovine survival of motor neuron gene (SMN). *Cytogenet Cell Genet* **83**(1-2): 39-42.

Pietrowski, D., Kemter, J., Medugorac, I., Goldammer, T., and Foerster, M. 1999. An AluI PCR-RFLP in the bovine survival motor neuron gene (SMN). *Anim Genet* **30**(2): 168.

Pinol-Roma, S. and Dreyfuss, G. 1992. Shuttling of pre-mRNA binding proteins between nucleus and cytoplasm. *Nature* **355**(6362): 730-732.

Pritchard, J.K. 2001. Are rare variants responsible for susceptibility to complex diseases? *Am J Hum Genet* **69**(1): 124-137.

Puls, I., Jonnakuty, C., LaMonte, B.H., Holzbaur, E.L., Tokito, M., Mann, E., Floeter, M.K., Bidus, K., Drayna, D., Oh, S.J. et al. 2003. Mutant dynactin in motor neuron disease. *Nat Genet* **33**(4): 455-456.

Pumarola, M., Anor, S., Majo, N., Borras, D., and Ferrer, I. 1997. Spinal muscular atrophy in Holstein-Friesian calves. *Acta Neuropathol* **93**(2): 178-183.

Rabbitts, T.H., Forster, A., Larson, R., and Nathan, P. 1993. Fusion of the dominant negative transcription regulator CHOP with a novel gene FUS by translocation t(12;16) in malignant liposarcoma. *Nat Genet* **4**(2): 175-180.

Rabin, S., Kim, J.M., Baughn, M., Libby, R.T., Kim, Y.J., Fan, Y., La Spada, A., Stone, B., and Ravits, J. 2009. Sporadic ALS has compartment-specific aberrant exon splicing and altered cell-matrix adhesion biology. *Hum Mol Genet*. **19**(2):313-28.

Rademakers, R., Eriksen, J.L., Baker, M., Robinson, T., Ahmed, Z., Lincoln, S.J., Finch, N., Rutherford, N.J., Crook, R.J., Josephs, K.A. et al. 2008. Common variation in the miR-659 binding-site of GRN is a major risk factor for TDP43-positive frontotemporal dementia. *Hum Mol Genet* **17**(23): 3631-3642.

Raingo, J., Castiglioni, A.J., and Lipscombe, D. 2007. Alternative splicing controls G protein-dependent inhibition of N-type calcium channels in nociceptors. *Nat Neurosci* **10**(3): 285-292.

Rimokh, R., Gadoux, M., Bertheas, M.F., Berger, F., Garoscio, M., Deleage, G., Germain, D., and Magaud, J.P. 1993. FVT-1, a novel human transcription unit affected by variant translocation t(2;18)(p11;q21) of follicular lymphoma. *Blood* **81**(1): 136-142.

Ringholz, G.M., Appel, S.H., Bradshaw, M., Cooke, N.A., Mosnik, D.M., and Schulz, P.E. 2005. Prevalence and patterns of cognitive impairment in sporadic ALS. *Neurology* **65**(4): 586-590.

Robertson, J., Sanelli, T., Xiao, S., Yang, W., Horne, P., Hammond, R., Pioro, E.P., and Strong, M.J. 2007. Lack of TDP-43 abnormalities in mutant SOD1 transgenic mice shows disparity with ALS. *Neurosci Lett* **420**(2): 128-132.

Rochette, C.F., Gilbert, N., and Simard, L.R. 2001. SMN gene duplication and the emergence of the SMN2 gene occurred in distinct hominids: SMN2 is unique to Homo sapiens. *Hum Genet* **108**(3): 255-266.

Rollinson, S., Snowden, J.S., Neary, D., Morrison, K.E., Mann, D.M., and Pickering-Brown, S.M. 2007. TDP-43 gene analysis in frontotemporal lobar degeneration. *Neurosci Lett* **419**(1): 1-4.

Ropper, A.H. and Brown, R.H. 2005. *Adams and Victor's Principles of Neurology*. McGraw Hill, New York.

Rosen, D.R., Siddique, T., Patterson, D., Figlewicz, D.A., Sapp, P., Hentati, A., Donaldson, D., Goto, J., O'Regan, J.P., Deng, H.X. et al. 1993. Mutations in Cu/Zn superoxide dismutase gene are associated with familial amyotrophic lateral sclerosis. *Nature* **362**(6415): 59-62.

Ross, A.F., Oleynikov, Y., Kislauskis, E.H., Taneja, K.L., and Singer, R.H. 1997. Characterization of a beta-actin mRNA zipcode-binding protein. *Mol Cell Biol* **17**(4): 2158-2165.

Rossoll, W., Jablonka, S., Andreassi, C., Kroning, A.K., Karle, K., Monani, U.R., and Sendtner, M. 2003. Smn, the spinal muscular atrophy-determining gene product, modulates axon growth and localization of beta-actin mRNA in growth cones of motoneurons. *J Cell Biol* **163**(4): 801-812.

Rossoll, W., Kroning, A.K., Ohndorf, U.M., Steegborn, C., Jablonka, S., and Sendtner, M. 2002. Specific interaction of Smn, the spinal muscular atrophy determining gene product, with hnRNP-R and gry-rbp/hnRNP-Q: a role for Smn in RNA processing in motor axons? *Hum Mol Genet* **11**(1): 93-105.

Rost, B., Yachdav, G., and Liu, J. 2004. The PredictProtein server. *Nucleic Acids Res* **32**(Web Server issue): W321-326.

Rothstein, J.D. 2007. TDP-43 in amyotrophic lateral sclerosis: pathophysiology or patho-babel? *Ann Neurol* **61**(5): 382-384.

Ruddy, D.M., Parton, M.J., Al-Chalabi, A., Lewis, C.M., Vance, C., Smith, B.N., Leigh, P.N., Powell, J.F., Siddique, T., Meyjes, E.P. et al. 2003. Two families with familial amyotrophic lateral sclerosis are linked to a novel locus on chromosome 16q. *Am J Hum Genet* **73**(2): 390-396.

Rudnik-Schoneborn, S., Goebel, H.H., Schlote, W., Molaian, S., Omran, H., Ketelsen, U., Korinthenberg, R., Wenzel, D., Lauffer, H., Kreiss-Nachtsheim, M. et al. 2003. Classical infantile spinal muscular atrophy with SMN deficiency causes sensory neuronopathy. *Neurology* **60**(6): 983-987.

Ruggiu, M., Herbst, R., Kim, N., Jevsek, M., Fak, J.J., Mann, M.A., Fischbach, G., Burden, S.J., and Darnell, R.B. 2009. Rescuing Z+ agrin splicing in Nova null mice restores synapse formation and unmasks a physiologic defect in motor neuron firing. *Proc Natl Acad Sci U S A* **106**(9): 3513-3518.

Rutherford, N.J., Zhang, Y.J., Baker, M., Gass, J.M., Finch, N.A., Xu, Y.F., Stewart, H., Kelley, B.J., Kuntz, K., Crook, R.J. et al. 2008. Novel mutations in TARDBP (TDP-43) in patients with familial amyotrophic lateral sclerosis. *PLoS Genet* **4**(9): e1000193.

Sampathu, D.M., Neumann, M., Kwong, L.K., Chou, T.T., Micsenyi, M., Truax, A., Bruce, J., Grossman, M., Trojanowski, J.Q., and Lee, V.M. 2006. Pathological heterogeneity of frontotemporal lobar degeneration with ubiquitin-positive inclusions delineated by ubiquitin immunohistochemistry and novel monoclonal antibodies. *Am J Pathol* **169**(4): 1343-1352.

Sasaki, S., Toi, S., Shirata, A., Yamane, K., Sakuma, H., and Iwata, M. 2001. Immunohistochemical and ultrastructural study of basophilic inclusions in adult-onset motor neuron disease. *Acta Neuropathol* **102**(2): 200-206.

Sato, S., Idogawa, M., Honda, K., Fujii, G., Kawashima, H., Takekuma, K., Hoshika, A., Hirohashi, S., and Yamada, T. 2005. beta-catenin interacts with the FUS proto-oncogene product and regulates pre-mRNA splicing. *Gastroenterology* **129**(4): 1225-1236.

Saunders, L.R., Perkins, D.J., Balachandran, S., Michaels, R., Ford, R., Mayeda, A., and Barber, G.N. 2001. Characterization of two evolutionarily conserved, alternatively spliced nuclear phosphoproteins, NFAR-1 and -2, that function in mRNA processing and interact with the double-stranded RNA-dependent protein kinase, PKR. *J Biol Chem* **276**(34): 32300-32312.

Saxena, S., Cabuy, E., and Caroni, P. 2009. A role for motoneuron subtype-selective ER stress in disease manifestations of FALS mice. *Nat Neurosci* **12**(5): 627-636.

Saxena, S.K., Rybak, S.M., Davey, R.T., Jr., Youle, R.J., and Ackerman, E.J. 1992. Angiogenin is a cytotoxic, tRNA-specific ribonuclease in the RNase A superfamily. *J Biol Chem* **267**(30): 21982-21986.

Schaefer, A., O'Carroll, D., Tan, C.L., Hillman, D., Sugimori, M., Llinas, R., and Greengard, P. 2007. Cerebellar neurodegeneration in the absence of microRNAs. *J Exp Med* **204**(7): 1553-1558.

Schaefer, A.M., Sanes, J.R., and Lichtman, J.W. 2005. A compensatory subpopulation of motor neurons in a mouse model of amyotrophic lateral sclerosis. *J Comp Neurol* **490**(3): 209-219.

Schrank, B., Gotz, R., Gunnersen, J.M., Ure, J.M., Toyka, K.V., Smith, A.G., and Sendtner, M. 1997. Inactivation of the survival motor neuron gene, a candidate gene for human spinal muscular atrophy, leads to massive cell death in early mouse embryos. *Proc Natl Acad Sci U S A* **94**(18): 9920-9925.

Schumacher, A., Friedrich, P., Diehl-Schmid, J., Ibach, B., Perneczky, R., Eisele, T., Vukovich, R., Foerstl, H., and Riemenschneider, M. 2007. No association of TDP-43 with sporadic frontotemporal dementia. *Neurobiol Aging*. **30**(1):157-9.

Schymick, J.C., Scholz, S.W., Fung, H.C., Britton, A., Arepalli, S., Gibbs, J.R., Lombardo, F., Matarin, M., Kasperaviciute, D., Hernandez, D.G. et al. 2007a. Genome-wide genotyping in amyotrophic lateral sclerosis and neurologically normal controls: first stage analysis and public release of data. *Lancet Neurol* **6**(4): 322-328.

Schymick, J.C., Talbot, K., and Traynor, B.J. 2007b. Genetics of sporadic amyotrophic lateral sclerosis. *Hum Mol Genet* **16 Spec No. 2**: R233-242.

Seelaar, H., Schelhaas, H.J., Azmani, A., Kusters, B., Rosso, S., Majoor-Krakauer, D., de Rijik, M.C., Rizzu, P., ten Brummelhuis, M., van Doorn, P.A. et al. 2007. TDP-43 pathology in familial frontotemporal dementia and motor neuron disease without Progranulin mutations. *Brain* **130**(Pt 5): 1375-1385.

Seilhean, D., Cazeneuve, C., Thuries, V., Russaouen, O., Millecamps, S., Salachas, F., Meininger, V., Leguern, E., and Duyckaerts, C. 2009. Accumulation of TDP-43 and alpha-actin in an amyotrophic lateral sclerosis patient with the K17I ANG mutation. *Acta Neuropathol*. **118**(4):561-73.

Seilhean, D., Takahashi, J., El Hachimi, K.H., Fujigasaki, H., Lebre, A.S., Biancalana, V., Durr, A., Salachas, F., Hogenhuis, J., de The, H. et al. 2004. Amyotrophic lateral sclerosis with neuronal intranuclear protein inclusions. *Acta Neuropathol* **108**(1): 81-87.

Sha, Q., Zhang, Z., Schymick, J.C., Traynor, B.J., and Zhang, S. 2009. Genome-wide association reveals three SNPs associated with sporadic amyotrophic lateral sclerosis through a two-locus analysis. *BMC Med Genet* **10**: 86.

Shan, X., Chang, Y., and Lin, C.L. 2007. Messenger RNA oxidation is an early event preceding cell death and causes reduced protein expression. *FASEB J* **21**(11): 2753-2764.

Sheth, U. and Parker, R. 2006. Targeting of aberrant mRNAs to cytoplasmic processing bodies. *Cell* **125**(6): 1095-1109.

Shibue, T., Takeda, K., Oda, E., Tanaka, H., Murasawa, H., Takaoka, A., Morishita, Y., Akira, S., Taniguchi, T., and Tanaka, N. 2003. Integral role of Noxa in p53-mediated apoptotic response. *Genes Dev* **17**(18): 2233-2238.

Shishikura, K., Hara, M., Sasaki, Y., and Misugi, K. 1983. A neuropathologic study of Werdnig-Hoffmann disease with special reference to the thalamus and posterior roots. *Acta Neuropathol (Berl)* **60**(1-2): 99-106.

Shrout, P.E. and Fleiss, J.L. 1979. Intraclass correlations: uses in assessing rater reliability. *Psychol Bull* **86**(2): 420-428.

Simpson, C.L. and Al-Chalabi, A. 2006. Amyotrophic lateral sclerosis as a complex genetic disease. *Biochim Biophys Acta* **1762**(11-12): 973-985.

Sitko, J.C., Yeh, B., Kim, M., Zhou, H., Takaesu, G., Yoshimura, A., McBride, W.H., Jewett, A., Jamieson, C.A., and Cacalano, N.A. 2008. SOCS3 regulates p21 expression and cell cycle arrest in response to DNA damage. *Cell Signal* **20**(12): 2221-2230.

Smyth, G.K. 2004. Linear models and empirical Bayes methods for assessing differential expression in microarray experiments. *Statistical Applications in Genetics and Molecular Biology* **3**(1).

Smyth, G.K., Gentleman, R., Carey, V., Dudoit, S., Irizarry, R., and Huber, W. 2005. Limma: linear models for microarray data. in *Bioinformatics and Computational Biology Solutions using R and Bioconductor*, pp. 397-420. Springer.

Sreedharan, J., Blair, I.P., Tripathi, V.B., Hu, X., Vance, C., Rogelj, B., Ackerley, S., Durnall, J.C., Williams, K.L., Buratti, E. et al. 2008. TDP-43 Mutations in Familial and Sporadic Amyotrophic Lateral Sclerosis. *Science*. **319**(5870):1668-72.

Srinivasan, K., Shiue, L., Hayes, J.D., Centers, R., Fitzwater, S., Loewen, R., Edmondson, L.R., Bryant, J., Smith, M., Rommelfanger, C. et al. 2005. Detection and measurement of alternative splicing using splicing-sensitive microarrays. *Methods* **37**(4): 345-359.

Stocker, H., Ossent, P., Heckmann, R., and Oertle, C. 1992. [Spinal muscular atrophy in Braunvieh calves]. *Schweiz Arch Tierheilkd* **134**(2): 97-104.

Storlazzi, C.T., Mertens, F., Nascimento, A., Isaksson, M., Wejde, J., Brosjo, O., Mandahl, N., and Panagopoulos, I. 2003. Fusion of the FUS and BBF2H7 genes in low grade fibromyxoid sarcoma. *Hum Mol Genet* **12**(18): 2349-2358.

Strachan, T., Read, AP. 2004. *Human Molecular Genetics* Garland Sience, London.

Strasswimmer, J., Lorson, C.L., Breiding, D.E., Chen, J.J., Le, T., Burghes, A.H., and Androphy, E.J. 1999. Identification of survival motor neuron as a transcriptional activator-binding protein. *Hum Mol Genet* **8**(7): 1219-1226.

Strong, M.J. 2008. The syndromes of frontotemporal dysfunction in amyotrophic lateral sclerosis. *Amyotroph Lateral Scler* **9**(6): 323-338.

-. 2009. The evidence for altered RNA metabolism in amyotrophic lateral sclerosis (ALS). *J Neurol Sci* **288**(1-2):1-12.

Strong, M.J., Volkening, K., Hammond, R., Yang, W., Strong, W., Leystra-Lantz, C., and Shoesmith, C. 2007. TDP43 is a human low molecular weight neurofilament (hNFL) mRNA-binding protein. *Mol Cell Neurosci* **35**(2): 320-327.

Strydom, D.J. 1998. The angiogenins. *Cell Mol Life Sci* **54**(8): 811-824.

Subramanian, V., Crabtree, B., and Acharya, K.R. 2008. Human angiogenin is a neuroprotective factor and amyotrophic lateral sclerosis associated angiogenin variants affect neurite extension/pathfinding and survival of motor neurons. *Hum Mol Genet* **17**(1): 130-149.

Suraweera, A., Becherel, O.J., Chen, P., Rundle, N., Woods, R., Nakamura, J., Gatei, M., Criscuolo, C., Filla, A., Chessa, L. et al. 2007. Senataxin, defective in ataxia oculomotor apraxia type 2, is involved in the defense against oxidative DNA damage. *J Cell Biol* **177**(6): 969-979.

Suraweera, A., Lim, Y., Woods, R., Birrell, G.W., Nasim, T., Becherel, O.J., and Lavin, M.F. 2009. Functional role for senataxin, defective in ataxia oculomotor apraxia type 2, in transcriptional regulation. *Hum Mol Genet* **18**(18): 3384-3396.

Tan, C.F., Eguchi, H., Tagawa, A., Onodera, O., Iwasaki, T., Tsujino, A., Nishizawa, M., Kakita, A., and Takahashi, H. 2007. TDP-43 immunoreactivity in neuronal inclusions in familial amyotrophic lateral sclerosis with or without SOD1 gene mutation. *Acta Neuropathol* **113**(5): 535-542.

Tanaka, M., Chock, P.B., and Stadtman, E.R. 2007. Oxidized messenger RNA induces translation errors. *Proc Natl Acad Sci U S A* **104**(1): 66-71.

Taupin, J.L., Tian, Q., Kedersha, N., Robertson, M., and Anderson, P. 1995. The RNA-binding protein TIAR is translocated from the nucleus to the cytoplasm during Fas-mediated apoptotic cell death. *Proc Natl Acad Sci U S A* **92**(5): 1629-1633.

Taylor, A.M., Berchtold, N.C., Perreau, V.M., Tu, C.H., Li Jeon, N., and Cotman, C.W. 2009. Axonal mRNA in uninjured and regenerating cortical mammalian axons. *J Neurosci* **29**(15): 4697-4707.

Team, R.D.C. 2008. *R: A Language and Environment for Statistical Computing*.

Thierry-Mieg, D. and Thierry-Mieg, J. 2006. AceView: a comprehensive cDNA-supported gene and transcripts annotation. *Genome Biol* **7 Suppl 1**: S12 11-14.

Thomas, N.H. and Dubowitz, V. 1994. The natural history of type I (severe) spinal muscular atrophy. *Neuromuscul Disord* **4**(5-6): 497-502.

Ticozzi, N., Silani, V., LeClerc, A.L., Keagle, P., Gellera, C., Ratti, A., Taroni, F., Kwiatkowski, T.J., Jr., McKenna-Yasek, D.M., Sapp, P.C. et al. 2009. Analysis of FUS gene mutation in familial amyotrophic lateral sclerosis within an Italian cohort. *Neurology* **73**(15): 1180-1185.

Tiruchinapalli, D.M., Oleynikov, Y., Kelic, S., Shenoy, S.M., Hartley, A., Stanton, P.K., Singer, R.H., and Bassell, G.J. 2003. Activity-dependent trafficking

and dynamic localization of zipcode binding protein 1 and beta-actin mRNA in dendrites and spines of hippocampal neurons. *J Neurosci* **23**(8): 3251-3261.

Towfighi, J., Young, R.S., and Ward, R.M. 1985. Is Werdnig-Hoffmann disease a pure lower motor neuron disorder? *Acta Neuropathol (Berl)* **65**(3-4): 270-280.

Troyer, D., Cash, W.C., Vestweber, J., Hiraga, T., and Leipold, H.W. 1993. Review of spinal muscular atrophy (SMA) in brown Swiss cattle. *J Vet Diagn Invest* **5**(2): 303-306.

Troyer, D., Leipold, H.W., Cash, W., and Vestweber, J. 1992. Upper motor neurone and descending tract pathology in bovine spinal muscular atrophy. *J Comp Pathol* **107**(3): 305-317.

Tsai, N.P., Tsui, Y.C., and Wei, L.N. 2009. Dynein motor contributes to stress granule dynamics in primary neurons. *Neuroscience* **159**(2): 647-656.

Tsuji, T., Sun, Y., Kishimoto, K., Olson, K.A., Liu, S., Hirukawa, S., and Hu, G.F. 2005. Angiogenin is translocated to the nucleus of HeLa cells and is involved in ribosomal RNA transcription and cell proliferation. *Cancer Res* **65**(4): 1352-1360.

Turner, B.J., Parkinson, N.J., Davies, K.E., and Talbot, K. 2009. Survival motor neuron deficiency enhances progression in an amyotrophic lateral sclerosis mouse model. *Neurobiol Dis* **34**(3): 511-517.

Turner, B.J. and Talbot, K. 2008. Transgenics, toxicity and therapeutics in rodent models of mutant SOD1-mediated familial ALS. *Prog Neurobiol* **85**(1): 94-134.

Tusell, J.M., Ejarque-Ortiz, A., Mancera, P., Sola, C., Saura, J., and Serratosa, J. 2009. Upregulation of p21Cip1 in activated glial cells. *Glia* **57**(5): 524-534.

Ule, J., Stefani, G., Mele, A., Ruggiu, M., Wang, X., Taneri, B., Gaasterland, T., Blencowe, B.J., and Darnell, R.B. 2006. An RNA map predicting Nova-dependent splicing regulation. *Nature* **444**(7119): 580-586.

Ule, J., Ule, A., Spencer, J., Williams, A., Hu, J.S., Cline, M., Wang, H., Clark, T., Fraser, C., Ruggiu, M. et al. 2005. Nova regulates brain-specific splicing to shape the synapse. *Nat Genet* **37**(8): 844-852.

Ulfhake, B. and Kellerth, J.O. 1981. A quantitative light microscopic study of the dendrites of cat spinal alpha-motoneurons after intracellular staining with horseradish peroxidase. *J Comp Neurol* **202**(4): 571-583.

Uranishi, H., Tetsuka, T., Yamashita, M., Asamitsu, K., Shimizu, M., Itoh, M., and Okamoto, T. 2001. Involvement of the pro-oncoprotein TLS (translocated in liposarcoma) in nuclear factor-kappa B p65-mediated transcription as a coactivator. *J Biol Chem* **276**(16): 13395-13401.

Uryu, K., Nakashima-Yasuda, H., Forman, M.S., Kwong, L.K., Clark, C.M., Grossman, M., Miller, B.L., Kretzschmar, H.A., Lee, V.M., Trojanowski, J.Q. et al. 2008. Concomitant TAR-DNA-binding protein 43 pathology is present in Alzheimer disease and corticobasal degeneration but not in other tauopathies. *J Neuropathol Exp Neurol* **67**(6): 555-564.

Van Deerlin, V.M., Leverenz, J.B., Bekris, L.M., Bird, T.D., Yuan, W., Elman, L.B., Clay, D., Wood, E.M., Chen-Plotkin, A.S., Martinez-Lage, M. et al. 2008. TARDBP mutations in amyotrophic lateral sclerosis with TDP-43 neuropathology: a genetic and histopathological analysis. *Lancet Neurol*.

van Es, M.A., Diekstra, F.P., Veldink, J.H., Baas, F., Bourque, P.R., Schelhaas, H.J., Strengman, E., Hennekam, E.A., Lindhout, D., Ophoff, R.A. et al.

2009a. A case of ALS-FTD in a large FALS pedigree with a K17I ANG mutation. *Neurology* **72**(3): 287-288.

van Es, M.A., Van Vught, P.W., Blauw, H.M., Franke, L., Saris, C.G., Andersen, P.M., Van Den Bosch, L., de Jong, S.W., van 't Slot, R., Birve, A. et al. 2007. ITPR2 as a susceptibility gene in sporadic amyotrophic lateral sclerosis: a genome-wide association study. *Lancet Neurol* **6**(10): 869-877.

van Es, M.A., Veldink, J.H., Saris, C.G., Blauw, H.M., van Vught, P.W., Birve, A., Lemmens, R., Schelhaas, H.J., Groen, E.J., Huisman, M.H. et al. 2009b. Genome-wide association study identifies 19p13.3 (UNC13A) and 9p21.2 as susceptibility loci for sporadic amyotrophic lateral sclerosis. *Nat Genet* **41**(10): 1083-1087.

Van Langenhove, T., van der Zee, J., Sleegers, K., Engelborghs, S., Vandenberghe, R., Gijselinck, I., Van den Broeck, M., Mattheijssens, M., Peeters, K., De Deyn, P.P. et al. Genetic contribution of FUS to frontotemporal lobar degeneration. *Neurology* **74**(5): 366-371.

Vance, C., Rogelj, B., Hortobagyi, T., De Vos, K.J., Nishimura, A.L., Sreedharan, J., Hu, X., Smith, B., Ruddy, D., Wright, P. et al. 2009. Mutations in FUS, an RNA processing protein, cause familial amyotrophic lateral sclerosis type 6. *Science* **323**(5918): 1208-1211.

Vilarino-Guell, C., Wider, C., Soto-Ortolaza, A.I., Cobb, S.A., Kachergus, J.M., Keeling, B.H., Dachsel, J.C., Hulihan, M.M., Dickson, D.W., Wszolek, Z.K. et al. 2009. Characterization of DCTN1 genetic variability in neurodegeneration. *Neurology* **72**(23): 2024-2028.

Volkening, K., Leystra-Lantz, C., Yang, W., Jaffee, H., and Strong, M.J. 2009. Tar DNA binding protein of 43 kDa (TDP-43), 14-3-3 proteins and copper/zinc superoxide dismutase (SOD1) interact to modulate NFL mRNA stability. Implications for altered RNA processing in amyotrophic lateral sclerosis (ALS). *Brain Res* **1305**:168-82.

Vyas, S., Bechade, C., Riveau, B., Downward, J., and Triller, A. 2002. Involvement of survival motor neuron (SMN) protein in cell death. *Hum Mol Genet* **11**(22): 2751-2764.

Wahl, M.C., Will, C.L., and Luhrmann, R. 2009. The spliceosome: design principles of a dynamic RNP machine. *Cell* **136**(4): 701-718.

Wamer, W.G., Yin, J.J., and Wei, R.R. 1997. Oxidative damage to nucleic acids photosensitized by titanium dioxide. *Free Radic Biol Med* **23**(6): 851-858.

Wang, I.F., Reddy, N.M., and Shen, C.K. 2002. Higher order arrangement of the eukaryotic nuclear bodies. *Proc Natl Acad Sci U S A* **99**(21): 13583-13588.

Wang, I.F., Wu, L.S., Chang, H.Y., and Shen, C.K. 2008a. TDP-43, the signature protein of FTLD-U, is a neuronal activity-responsive factor. *J Neurochem* **105**(3):797-806.

Wang, X., Arai, S., Song, X., Reichart, D., Du, K., Pascual, G., Tempst, P., Rosenfeld, M.G., Glass, C.K., and Kurokawa, R. 2008b. Induced ncRNAs allosterically modify RNA-binding proteins in cis to inhibit transcription. *Nature* **454**(7200): 126-130.

Wegorzewska, I., Bell, S., Cairns, N.J., Miller, T.M., and Baloh, R.H. 2009. TDP-43 mutant transgenic mice develop features of ALS and frontotemporal lobar degeneration. *Proc Natl Acad Sci U S A* **106**(44): 18809-18814.

Weng, L., Hubner, R., Claessens, A., Smits, P., Wauters, J., Tylzanowski, P., Van Marck, E., and Merregaert, J. 2003. Isolation and characterization of

chondrolectin (Chodl), a novel C-type lectin predominantly expressed in muscle cells. *Gene* **308**: 21-29.

Wider, C., Dickson, D.W., Stoessl, A.J., Tsuboi, Y., Chapon, F., Gutmann, L., Lechevalier, B., Calne, D.B., Personett, D.A., Hulihan, M. et al. 2009. Pallidonigral TDP-43 pathology in Perry syndrome. *Parkinsonism Relat Disord* **15**(4): 281-286.

Will, C.L. and Luhrmann, R. 2005. Splicing of a rare class of introns by the U12-dependent spliceosome. *Biol Chem* **386**(8): 713-724.

Williams, B.Y., Hamilton, S.L., and Sarkar, H.K. 2000. The survival motor neuron protein interacts with the transactivator FUSE binding protein from human fetal brain. *FEBS Lett* **470**(2): 207-210.

Willis, D., Li, K.W., Zheng, J.Q., Chang, J.H., Smit, A., Kelly, T., Merianda, T.T., Sylvester, J., van Minnen, J., and Twiss, J.L. 2005. Differential transport and local translation of cytoskeletal, injury-response, and neurodegeneration protein mRNAs in axons. *J Neurosci* **25**(4): 778-791.

Wils, H., Kleinberger, G., Janssens, J., Pereson, S., Joris, G., Cuijt, I., Smits, V., Groote, C.C., Van Broeckhoven, C., and Kumar-Singh, S. 2010. TDP-43 transgenic mice develop spastic paralysis and neuronal inclusions characteristic of ALS and frontotemporal lobar degeneration. *Proc Natl Acad Sci U S A*.

Winkler, C., Eggert, C., Gradl, D., Meister, G., Giegerich, M., Wedlich, D., Laggerbauer, B., and Fischer, U. 2005. Reduced U snRNP assembly causes motor axon degeneration in an animal model for spinal muscular atrophy. *Genes Dev* **19**(19): 2320-2330.

Winton, M.J., Igaz, L.M., Wong, M.M., Kwong, L.K., Trojanowski, J.Q., and Lee, V.M. 2008a. Disturbance of nuclear and cytoplasmic TAR DNA-binding protein (TDP-43) induces disease-like redistribution, sequestration, and aggregate formation. *J Biol Chem* **283**(19): 13302-13309.

Winton, M.J., Van Deerlin, V.M., Kwong, L.K., Yuan, W., Wood, E.M., Yu, C.E., Schellenberg, G.D., Rademakers, R., Caselli, R., Karydas, A. et al. 2008b. A90V TDP-43 variant results in the aberrant localization of TDP-43 in vitro. *FEBS Lett*.

Wirth, B. 2000. An update of the mutation spectrum of the survival motor neuron gene (SMN1) in autosomal recessive spinal muscular atrophy (SMA). *Hum Mutat* **15**(3): 228-237.

Wirth, B., Brichta, L., and Hahnen, E. 2006a. Spinal muscular atrophy: from gene to therapy. *Semin Pediatr Neurol* **13**(2): 121-131.

Wirth, B., Brichta, L., Schrank, B., Lochmuller, H., Blick, S., Baasner, A., and Heller, R. 2006b. Mildly affected patients with spinal muscular atrophy are partially protected by an increased SMN2 copy number. *Hum Genet* **119**(4): 422-428.

Wirth, B., Tessarolo, D., Hahnen, E., Rudnik-Schoneborn, S., Raschke, H., Liguori, M., Giacanelli, M., and Zerres, K. 1997. Different entities of proximal spinal muscular atrophy within one family. *Hum Genet* **100**(5-6): 676-680.

Wojtowicz, W.M., Flanagan, J.J., Millard, S.S., Zipursky, S.L., and Clemens, J.C. 2004. Alternative splicing of Drosophila Dscam generates axon guidance receptors that exhibit isoform-specific homophilic binding. *Cell* **118**(5): 619-633.

Wolfensohn, S., Lloyd, Maggie. 2003. *Handbook of Laboratory Animal Management and Welfare*. Blackwell Publishing.

Wu, D., Yu, W., Kishikawa, H., Folkerth, R.D., Iafrate, A.J., Shen, Y., Xin, W., Sims, K., and Hu, G.F. 2007. Angiogenin loss-of-function mutations in amyotrophic lateral sclerosis. *Ann Neurol* **62**(6): 609-617.

Xiao, W. and Oefner, P.J. 2001. Denaturing high-performance liquid chromatography: A review. *Hum Mutat* **17**(6): 439-474.

Xu, Z.P., Tsuji, T., Riordan, J.F., and Hu, G.F. 2002. The nuclear function of angiogenin in endothelial cells is related to rRNA production. *Biochem Biophys Res Commun* **294**(2): 287-292.

-. 2003. Identification and characterization of an angiogenin-binding DNA sequence that stimulates luciferase reporter gene expression. *Biochemistry* **42**(1): 121-128.

Yamasaki, S., Ivanov, P., Hu, G.F., and Anderson, P. 2009. Angiogenin cleaves tRNA and promotes stress-induced translational repression. *J Cell Biol* **185**(1): 35-42.

Yang, L., Embree, L.J., and Hickstein, D.D. 2000. TLS-ERG leukemia fusion protein inhibits RNA splicing mediated by serine-arginine proteins. *Mol Cell Biol* **20**(10): 3345-3354.

Yang, L., Embree, L.J., Tsai, S., and Hickstein, D.D. 1998a. Oncoprotein TLS interacts with serine-arginine proteins involved in RNA splicing. *J Biol Chem* **273**(43): 27761-27764.

Yang, Y.Y., Yin, G.L., and Darnell, R.B. 1998b. The neuronal RNA-binding protein Nova-2 is implicated as the autoantigen targeted in POMA patients with dementia. *Proc Natl Acad Sci U S A* **95**(22): 13254-13259.

Yokoseki, A., Shiga, A., Tan, C.F., Tagawa, A., Kaneko, H., Koyama, A., Eguchi, H., Tsujino, A., Ikeuchi, T., Kakita, A. et al. 2008. TDP-43 mutation in familial amyotrophic lateral sclerosis. *Ann Neurol* **63**(4): 538-542.

Yoo, S., van Niekerk, E.A., Merianda, T.T., and Twiss, J.L. 2009. Dynamics of axonal mRNA transport and implications for peripheral nerve regeneration. *Exp Neurol* **223**(1):19-27

Yoshimura, A., Fujii, R., Watanabe, Y., Okabe, S., Fukui, K., and Takumi, T. 2006. Myosin-Va facilitates the accumulation of mRNA/protein complex in dendritic spines. *Curr Biol* **16**(23): 2345-2351.

Young, P.J., Le, T.T., Dunckley, M., Nguyen, T.M., Burghes, A.H., and Morris, G.E. 2001. Nuclear gems and Cajal (coiled) bodies in fetal tissues: nucleolar distribution of the spinal muscular atrophy protein, SMN. *Exp Cell Res* **265**(2): 252-261.

Yu, B., Sawyer, N.A., Chiu, C., Oefner, P.J., and Underhill, P.A. 2006. DNA mutation detection using denaturing high-performance liquid chromatography (DHPLC). *Curr Protoc Hum Genet* **Chapter 7**: Unit7 10.

Yudin, D., Hanz, S., Yoo, S., Iavnilovitch, E., Willis, D., Gradus, T., Vuppalanchi, D., Segal-Ruder, Y., Ben-Yaakov, K., Hieda, M. et al. 2008. Localized regulation of axonal RanGTPase controls retrograde injury signaling in peripheral nerve. *Neuron* **59**(2): 241-252.

Zeitelhofer, M., Karra, D., Macchi, P., Tolino, M., Thomas, S., Schwarz, M., Kiebler, M., and Dahm, R. 2008a. Dynamic interaction between P-bodies and transport ribonucleoprotein particles in dendrites of mature hippocampal neurons. *J Neurosci* **28**(30): 7555-7562.

Zeitelhofer, M., Macchi, P., and Dahm, R. 2008b. Perplexing bodies: The putative roles of P-bodies in neurons. *RNA Biol* **5**(4): 244-248.

Zerres, K., Wirth, B., and Rudnik-Schoneborn, S. 1997. Spinal muscular atrophy--clinical and genetic correlations. *Neuromuscul Disord* **7**(3): 202-207.

Zhang, H., Xing, L., Singer, R.H., and Bassell, G.J. 2007a. QNQKE targeting motif for the SMN-Gemin multiprotein complexin neurons. *J Neurosci Res* **85**(12): 2657-2667.

Zhang, H.L., Eom, T., Oleynikov, Y., Shenoy, S.M., Liebelt, D.A., Dictenberg, J.B., Singer, R.H., and Bassell, G.J. 2001. Neurotrophin-induced transport of a beta-actin mRNP complex increases beta-actin levels and stimulates growth cone motility. *Neuron* **31**(2): 261-275.

Zhang, Y.J., Xu, Y.F., Cook, C., Gendron, T.F., Roettges, P., Link, C.D., Lin, W.L., Tong, J., Castanedes-Casey, M., Ash, P. et al. 2009. Aberrant cleavage of TDP-43 enhances aggregation and cellular toxicity. *Proc Natl Acad Sci U S A* **106**(18): 7607-7612.

Zhang, Y.J., Xu, Y.F., Dickey, C.A., Buratti, E., Baralle, F., Bailey, R., Pickering-Brown, S., Dickson, D., and Petrucelli, L. 2007b. Progranulin mediates caspase-dependent cleavage of TAR DNA binding protein-43. *J Neurosci* **27**(39): 10530-10534.

Zhang, Z., Lotti, F., Dittmar, K., Younis, I., Wan, L., Kasim, M., and Dreyfuss, G. 2008. SMN deficiency causes tissue-specific perturbations in the repertoire of snRNAs and widespread defects in splicing. *Cell* **133**(4): 585-600.

Zinszner, H., Sok, J., Immanuel, D., Yin, Y., and Ron, D. 1997. TLS (FUS) binds RNA in vivo and engages in nucleo-cytoplasmic shuttling. *J Cell Sci* **110 (Pt 15)**: 1741-1750.

Appendix 1 Gene expression changes in SMNΔ7 spinal cord

Transcripts Cluster Id	Fold change	Regulation	Gene Title	Gene Symbol
6849595	3.9	up	cyclin-dependent kinase inhibitor 1A (P21)	Cdkn1a
6822477	3.5	up	cDNA sequence BC055107	BC055107
6842587	3.5	down	Chondrolectin	Chodl
6805270	3.1	down	---	---
6971280	3.1	up	sulfotransferase family 1A, phenol-preferring, member 1	Sult1a1
7014503	2.9	down	aminolevulinic acid synthase 2, erythroid	Alas2
6809524	2.9	down	survival motor neuron 1	Smn1
6969997	2.7	down	hemoglobin, beta adult minor chain /// hemoglobin, beta adult major chain	Hbb-b2 /// Hbb-b1
6854604	2.6	up	FK506 binding protein 5	Fkbp5
6784062	2.5	down	insulin-like growth factor binding protein 4	Igfbp4
6899760	2.5	up	thioredoxin interacting protein	Txnip
6874653	2.4	up	coiled-coil domain containing 3	Ccdc3
6802026	2.3	up	pleckstrin 2	Plek2
6766301	2.2	up	PERP, TP53 apoptosis effector	Perp
6785865	2.2	up	insulin-like growth factor binding protein 3	Igfbp3
6893002	2.1	down	solute carrier family 13 (sodium-dependent dicarboxylate transporter), member 3	Slc13a3
6783673	2.1	up	Chondroadherin	Chad
6837006	2.1	down	Parvalbumin	Pvalb
6973586	2.1	up	apolipoprotein C-I /// golgi coiled coil 1	Apoc1 /// Gcc1
6854401	2.1	down	hematological and neurological expressed 1-like	Hn1l
6947932	2.0	up	Kruppel-like factor 15	Klf15
6755054	2.0	down	regulator of G-protein signaling 5	Rgs5
6825445	2.0	up	PTK2 protein tyrosine kinase 2 beta	Ptk2b
6941029	2.0	up	peroxisomal membrane protein 2	Pxmp2
6986064	2.0	up	angiotensinogen (serpin peptidase inhibitor, clade A, member 8)	Agt
6965670	2.0	up	hypoxia inducible factor 3, alpha subunit	Hif3a
6766455	2.0	up	serum/glucocorticoid regulated kinase 1	Sgk1
6755055	1.9	down	regulator of G-protein signaling 5	Rgs5
6792813	1.9	up	dicarbonyl L-xylulose reductase	Dcxr
6805381	1.9	up	histone cluster 1, H1c	Hist1h1c
7009834	1.9	down	solute carrier family 38, member 5	Slc38a5
7016678	1.9	down	Apelin	Apln
6791298	1.9	down	topoisomerase (DNA) II alpha	Top2a
6901353	1.9	up	alanine-glyoxylate aminotransferase 2-like 1	Agxt2l1
6850019	1.9	up	transporter 1, ATP-binding cassette, sub-family B (MDR/TAP)	Tap1
6769197	1.9	up	cold inducible RNA binding protein	Cirbp
6805380	1.8	down	histone cluster 1, H2bb /// histone cluster 1, H2be /// histone cluster 1, H2bg /// predicted gene, OTTMUSG00000013203 /// histone cluster 1, H2bc	Hist1h2bb /// Hist1h2be /// Hist1h2bg /// RP23-38E20.1 /// Hist1h2bc
7009748	1.8	down	diacylglycerol kinase kappa	Dgkk
6750440	1.8	down	insulin-like growth factor binding protein 2	Igfbp2
6781090	1.8	up	glutathione peroxidase 3	Gpx3
6774264	1.8	up	DNA-damage-inducible transcript 4	Ddit4
6939671	1.8	down	transmembrane protease, serine 11d	Tmprss11d
6987513	1.8	up	neuropeptide S receptor 1	Npsr1
6978290	1.8	up	metallothionein 2	Mt2
6789367	1.8	up	solute carrier family 2 (facilitated glucose transporter),	Slc2a4

			member 4	
6819275	1.8	up	leukotriene B4 receptor 2	Ltb4r2
6753068	1.8	down	RIKEN cDNA 5430435G22 gene	5430435G22Rik
6891880	1.8	down	CD93 antigen	Cd93
6783997	1.7	up	protein phosphatase 1, regulatory (inhibitor) subunit 1B	Ppp1r1b
6892899	1.7	down	secretory leukocyte peptidase inhibitor	Slpi
6820325	1.7	down	lymphocyte cytosolic protein 1	Lcp1
6787918	1.7	down	proteasome (prosome, macropain) 28 subunit, beta /// protease (prosome, macropain) 28 subunit beta B, pseudogene	Psme2 /// Psme2b-ps
6990715	1.7	up	CD109 antigen	Cd109
6961201	1.7	up	small nuclear ribonucleoprotein polypeptide A'	Snrpa1
6844316	1.7	up	proline dehydrogenase	Prodh
6889357	1.7	up	proline rich Gla (G-carboxyglutamic acid) 4 (transmembrane)	Prrg4
6781984	1.7	up	period homolog 1 (Drosophila)	Per1
6863755	1.7	up	desmocollin 3	Dsc3
6978291	1.7	up	metallothionein 1	Mt1
6785114	1.7	down	RAB37, member of RAS oncogene family	Rab37
6985813	1.7	down	potassium voltage-gated channel, subfamily G, member 4	Kcng4
6767782	1.7	up	glycoprotein 49 A /// leukocyte immunoglobulin-like receptor, subfamily B, member 4	Gp49a /// Lilrb4
6972205	1.7	up	leucine-rich and death domain containing	Lrdd
6994935	1.7	down	sterol-C5-desaturase (fungal ERG3, delta-5-desaturase) homolog (S. cerevisae)	Sc5d
6885616	1.7	up	RIKEN cDNA 1700007K13 gene	1700007K13Rik
6961987	1.7	down	protein regulator of cytokinesis 1	Prc1
6770072	1.7	down	Lumican	Lum
6966610	1.7	up	pleckstrin homology domain containing, family F (with FYVE domain) member 1	Plekhf1
6949591	1.7	up	solute carrier family 6 (neurotransmitter transporter, GABA), member 13	Slc6a13
6772802	1.7	down	ectonucleotide pyrophosphatase/phosphodiesterase 1	Enpp1
6813317	1.7	up	ribosomal protein S24	Rps24
6861662	1.7	up	phorbol-12-myristate-13-acetate-induced protein 1	Pmaip1
6823666	1.6	up	protein kinase C, delta	Prkcd
6926165	1.6	up	complement component 1, q subcomponent, beta polypeptide	C1qb
6854487	1.6	up	dual specificity phosphatase 1	Dusp1
7013389	1.6	down	kelch-like 4 (Drosophila)	Klhl4
6939241	1.6	down	kinase insert domain protein receptor	Kdr
6988366	1.6	up	sodium channel, voltage-gated, type III, beta	Scn3b
6762345	1.6	up	B-cell translocation gene 2, anti-proliferative	Btg2
6810066	1.6	down	DEP domain containing 1B	Depdc1b
6803284	1.6	up	serine (or cysteine) peptidase inhibitor, clade A, member 3C	Serpina3c
6878448	1.6	down	integrin alpha 4 /// ceramide kinase-like	Itga4 /// Cerkl
6929660	1.6	down	abhydrolase domain containing 1	Abhd1
6978336	1.6	up	chemokine (C-C motif) ligand 17	Ccl17
6890120	1.6	down	G protein-coupled receptor 176	Gpr176
6882333	1.6	down	TPX2, microtubule-associated protein homolog (Xenopus laevis)	Tpx2
6789540	1.6	down	smoothelin-like 2	Smtnl2
6792887	1.6	up	zinc finger protein 750	Zfp750
6866653	1.6	up	mitogen-activated protein kinase 4	Mapk4
6788655	1.6	down	gap junction protein, gamma 2	Gjc2
6768123	1.6	down	procollagen-proline, 2-oxoglutarate 4-dioxygenase (proline 4-hydroxylase), alpha 1 polypeptide	P4ha1
6911679	1.6	up	transformation related protein 53 inducible nuclear protein 1	Trp53inp1

7012866	1.6	down	gap junction protein, beta 1	Gjb1
6876052	1.6	up	phytanoyl-CoA dioxygenase domain containing 1 /// leucine rich repeat containing 8A	Phyhd1 /// Lrrc8a
6929861	1.6	up	regulator of G-protein signaling 12	Rgs12
6936723	1.6	up	ATG9 autophagy related 9 homolog B (S. cerevisiae)	Atg9b
6943797	1.6	down	guanine nucleotide binding protein (G protein), gamma 11	Gng11
6796902	1.6	up	thyroid stimulating hormone receptor	Tshr
6864680	1.6	down	heparin-binding EGF-like growth factor	Hbegf
6762944	1.6	down	phospholipase A2, group IVA (cytosolic, calcium-dependent)	Pla2g4a
6990327	1.6	up	aldehyde dehydrogenase family 1, subfamily A2	Aldh1a2
6813246	1.6	up	nuclear factor, interleukin 3, regulated	Nfil3
6956912	1.6	up	adiponectin receptor 2	Adipor2
6837375	1.6	up	cytochrome P450, family 2, subfamily d, polypeptide 22	Cyp2d22
6963623	1.6	down	calcitonin-related polypeptide, beta	Calcb
6865221	1.6	down	tripartite motif-containing 36	Trim36
6835353	1.6	up	angiopoietin 1	Angpt1
6854304	1.6	up	spermine binding protein-like /// spermine binding protein	Sbpl /// Sbp
6881087	1.6	up	c-mer proto-oncogene tyrosine kinase	Mertk
6962930	1.6	down	procollagen-proline, 2-oxoglutarate 4-dioxygenase (proline 4-hydroxylase), alpha polypeptide III	P4ha3
6852882	1.6	up	tumor-associated calcium signal transducer 1	Tacstd1
6933591	1.6	up	D-amino acid oxidase 1	Dao1
6817645	1.6	up	double homeobox B-like /// predicted gene, ENSMUSG00000072675 /// predicted gene, ENSMUSG00000072672	Duxbl /// ENSMUSG00000072675 /// ENSMUSG00000072672
6819883	1.5	down	PDZ binding kinase	Pbk
6849551	1.5	up	RIKEN cDNA E230001N04 gene	E230001N04Rik
7016340	1.5	down	NADH dehydrogenase (ubiquinone) 1 alpha subcomplex, 1	Ndufa1
6926166	1.5	up	complement component 1, q subcomponent, C chain	C1qc
6933812	1.5	down	Tescalcin	Tesc
6987954	1.5	down	E26 avian leukemia oncogene 1, 5' domain	Ets1
6892852	1.5	up	adenosine deaminase	Ada
6754149	1.5	up	glutamate-ammonia ligase (glutamine synthetase)	Glul
6791257	1.5	down	RIKEN cDNA 1810046J19 gene	1810046J19Rik
6963131	1.5	up	olfactory receptor 646	Olfr646
6756790	1.5	up	myeloblastosis oncogene-like 1	Mybl1
6971848	1.5	down	antigen identified by monoclonal antibody Ki 67	Mki67
6815291	1.5	up	polymerase (DNA directed), kappa	Polk
6985850	1.5	up	RIKEN cDNA 1190005I06 gene	1190005I06Rik
7023132	1.5	up	RIKEN cDNA D030013I16 gene /// phosphatidylserine decarboxylase pseudogene /// RIKEN cDNA 4933439C20 gene	D030013I16Rik /// LOC236604 /// 4933439C20Rik
6939270	1.5	down	neuromedin U	Nmu
6943310	1.5	down	heat shock 105kDa/110kDa protein 1	Hsph1
6949853	1.5	down	mitochondrial ribosomal protein L51	Mrpl51
6824940	1.5	up	gap junction protein, beta 6	Gjb6
6961912	1.5	down	Aggrecan	Acan
6957240	1.5	up	potassium voltage-gated channel, shaker-related subfamily, member 5	Kcna5
6785399	1.5	up	brain-specific angiogenesis inhibitor 1-associated protein 2	Baiap2
6949310	1.5	up	RIKEN cDNA 8430408G22 gene	8430408G22Rik
6758435	1.5	down	solute carrier family 40 (iron-regulated transporter), member 1	Slc40a1
6903558	1.5	up	carboxypeptidase B1 (tissue)	Cpb1
6925362	1.5	down	eukaryotic translation initiation factor 2C, 3	Eif2c3

6836700	1.5	up	lymphocyte antigen 6 complex, locus D	Ly6d
6976237	1.5	down	hydroxyprostaglandin dehydrogenase 15 (NAD)	Hpgd
6854760	1.5	down	glyoxalase 1	Glo1

Table A1: P13 gene level changes SMA vs control, fold change >1.5, P≤0.05

Transcripts Cluster Id	Fold change	Regulation	Gene Title	Gene Symbol
6809524	3.5	down	survival motor neuron 1	Smn1
6969997	2.6	down	hemoglobin, beta adult minor chain /// hemoglobin, beta adult major chain	Hbb-b2 /// Hbb-b1
6805381	2.2	up	histone cluster 1, H1c	Hist1h1c
6849595	2.2	up	cyclin-dependent kinase inhibitor 1A (P21)	Cdkn1a
7018366	2.1	up	ectodysplasin A2 isoform receptor	Eda2r
6961201	1.9	up	small nuclear ribonucleoprotein polypeptide A'	Snrpa1
6899760	1.9	up	thioredoxin interacting protein	Txnip
6755306	1.7	down	olfactory receptor 420	Olfr420
6842587	1.7	down	Chondrolectin	Chodl
6790294	1.7	up	chemokine (C-C motif) ligand 3	Ccl3
6764650	1.6	up	epoxide hydrolase 1, microsomal	Ephx1
6754143	1.6	up	ribonuclease L (2', 5'-oligoisoadenylate synthetase-dependent)	Rnasel
6926165	1.6	up	complement component 1, q subcomponent, beta polypeptide	C1qb
6963128	1.6	up	olfactory receptor 635	Olfr635
6873271	1.6	down	stearoyl-Coenzyme A desaturase 1	Scd1
6785114	1.6	down	RAB37, member of RAS oncogene family	Rab37
6926166	1.6	up	complement component 1, q subcomponent, C chain	C1qc
7009748	1.6	down	diacylglycerol kinase kappa	Dgkk
6788617	1.6	down	olfactory receptor 323	Olfr323
6885616	1.5	up	RIKEN cDNA 1700007K13 gene	1700007K13Rik
6939671	1.5	down	transmembrane protease, serine 11d	Tmprss11d
6870375	1.5	up	insulin I	Ins1
6783144	1.5	down	carbonic anhydrase 4	Car4

Table A2: P7 gene level changes SMA vs control, fold change >1.5, P≤0.05

Transcripts Cluster Id	Fold change	Regulation	Gene Title	Gene Symbol
6809524	3.4	down	survival motor neuron 1	Smn1
6805381	1.8	up	histone cluster 1, H1c	Hist1h1c
6805370	1.8	up	histone cluster 1, H2bc /// histone cluster 1, H2bj /// histone cluster 1, H2bk /// histone cluster 1, H2bf /// histone cluster 1, H2bl /// histone cluster 1, H2bn /// histone cluster 1, H2bb /// histone cluster 1, H2be /// histone cluster 1, H2bg /// predicted gene, OTTMUSG00000013203	Hist1h2bc /// Hist1h2bj /// Hist1h2bk /// Hist1h2bf /// Hist1h2bl /// Hist1h2bn /// Hist1h2bb /// Hist1h2be /// Hist1h2bg /// RP23-38E20.1
6767782	1.8	up	glycoprotein 49 A /// leukocyte immunoglobulin-like receptor, subfamily B, member 4	Gp49a /// Lilrb4
6780730	1.6	down	olfactory receptor 1393 /// olfactory receptor 1392	Olfr1393 /// Olfr1392
6772906	1.6	up	laminin, alpha 2	Lama2
6988353	1.6	down	olfactory receptor 978	Olfr978
6960235	1.6	up	kallikrein 1-related peptidase b21 /// kallikrein 1-related peptidase b24 /// kallikrein 1-related peptidase b11 /// kallikrein 1-related peptidase b27	Klk1b21 /// Klk1b24 /// Klk1b11 /// Klk1b27
6973490	1.6	down	---	---
6839959	1.6	down	polymerase (RNA) II (DNA directed) polypeptide H	Polr2h
6992950	1.5	down	ribosomal protein L14 /// RIKEN cDNA 5830454E08	Rpl14 ///

			gene	5830454E08Rik
6963442	1.5	down	Adrenomedullin	Adm

Table A3: P1 gene level changes SMA vs control, fold change >1.5, P≤0.05

Control		**SMA**	
P1 vs P7		**P1 vs P7**	
GOID	**GO Name**	**GOID**	**GO Name**
10456	cell proliferation in dorsal spinal cord	33269	internode region of axon
5243	gap junction channel activity	43209	myelin sheath
5452	inorganic anion exchanger activity		
33269	internode region of axon		
43209	myelin sheath		
14003	oligodendrocyte development		
5248	voltage\-gated sodium channel activity		
22829	wide pore channel activity		
P7 vs P13		**P7 vs P13**	
GOID	**GO Name**	**GOID**	**GO Name**
10456	cell proliferation in dorsal spinal cord	18198	peptidyl\-cysteine modification
6601	creatine biosynthetic process	17154	semaphorin receptor activity
6600	creatine metabolic process	48407	platelet\-derived growth factor binding
32291	ensheathment of axons in the central nervous system	5248	voltage\-gated sodium channel activity
5243	gap junction channel activity	9065	glutamine family amino acid catabolic process

5452	inorganic anion exchanger activity		
33269	internode region of axon		
43209	myelin sheath		
22010	myelination in the central nervous system		
14003	oligodendrocyte development		
33270	paranode region of axon		
19911	structural constituent of myelin sheath		
5248	voltage\-gated sodium channel activity		
22829	wide pore channel activity		
		P7 vs P13 **20-49% changed**	
		GOID	**GO Name**
		77	DNA damage checkpoint
		32508	DNA duplex unwinding
		32392	DNA geometric change
		6270	DNA replication initiation
		6268	DNA unwinding during replication

Table A4: Comparison of between time point changes in control and SMA mice using GO Elite for >50% and 3 genes changed. Only a selection of GOIDs changed 20-49% in SMA mice is shown.

	ENSE			ENSG		
lambda	P1	P7	P13	P1	P7	P13
0.01	5518 (0.43)	2024 (0.62)	9434 (0.14)	667 (0.28)	432 (0.3)	1883 (0.09)
0.005	2953 (0.4)	1113 (0.52)	6258 (0.09)	358 (0.26)	262 (0.22)	1371 (0.06)
0.001	630 (0.39)	282 (0.29)	2559 (0.03)	83 (0.23)	92 (0.09)	693 (0.02)
5.00E-04	299 (0.41)	164 (0.21)	1816 (0.02)	51 (0.22)	60 (0.05)	520 (0.01)
1.00E-04	72 (0.35)	66 (0.06)	812 (0.01)	8 (0.25)	27 (0)	269 (0)
5.00E-05	41 (0.3)	56 (0.04)	573 (0.01)	6 (0.17)	20 (0)	201 (0)
1.00E-05	22 (0.09)	36 (0)	270 (0)	3 (0)	12 (0)	104 (0)

Table A5 Permutation based analysis: Number of significant results at each time point, along with the estimated FDR, for a number of different choices of p-value cut-off, λ.

Appendix 2- List of publications derived from this thesis

Bäumer, D., Ansorge, O., Almeida, M., and Talbot, K. 2010. The role of RNA processing in the pathogenesis of motor neuron degeneration. *Expert Rev Mol Med* **12**: e21.

Bäumer, D., Hilton, D., Paine, S.M., Turner, M.R., Lowe, J., Talbot, K., and Ansorge, O. 2010. Juvenile ALS with basophilic inclusions is a FUS proteinopathy with FUS mutations. *Neurology* **75**:611-618

Bäumer, D., Lee, S., Nicholson, G., Davies, J.L., Parkinson, N.J., Murray, L.M., Gillingwater, T.H., Ansorge, O., Davies, K.E., and Talbot, K. 2009a. Alternative splicing events are a late feature of pathology in a mouse model of spinal muscular atrophy. *PLoS Genet* **5**(12): e1000773.

Bäumer, D., Parkinson, N., and Talbot, K. 2009b. TARDBP in amyotrophic lateral sclerosis: identification of a novel variant but absence of copy number variation. *J Neurol Neurosurg Psychiatry* **80**(11): 1283-1285.

Murray, L.M., Lee, S., Bäumer, D., Parson, S.H., Talbot, K., and Gillingwater, T.H. Pre-symptomatic development of lower motor neuron connectivity in a mouse model of severe spinal muscular atrophy. *Hum Mol Genet* **19**(3): 420-433.

Parkinson, N.J., Baumer, D., Rose-Morris, A., and Talbot, K. 2008. Candidate screening of the bovine and feline spinal muscular atrophy genes reveals no evidence for involvement in human motor neuron disorders. *Neuromuscul Disord* **18**(5): 394-397.

Turner, B.J., Bäumer, D., Parkinson, N.J., Scaber, J., Ansorge, O., and Talbot, K. 2008. TDP-43 expression in mouse models of amyotrophic lateral sclerosis and spinal muscular atrophy. *BMC Neurosci* **9**: 104.